Progressive Fatigue Damage Modeling of Composite Materials

by

Mahmood M. Shokrieh

Department of Mechanical Engineering
McGill University
Montréal, Canada

A thesis submitted to the Faculty of Graduate Studies and Research in partial fulfillment of the requirements for the degree of
Doctor of Philosophy

February, 1996

ISBN 0-612-12484-3

To the memory of my father

Abstract

A modeling technique for simulating the fatigue behaviour of laminated composite materials with or without stress concentrations, called *progressive fatigue damage modeling*, is established. The *model* is capable of simulating the *residual stiffness*, *residual strength* and *fatigue life* of composite laminates with arbitrary geometry and stacking sequence under complicated fatigue loading conditions.

The *model* is an integration of three major components: stress analysis, failure analysis, and material property degradation rules. A three-dimensional, nonlinear, finite element technique is developed for the stress analysis. By using a large number of elements near the edge of the hole and at layer interfaces, the edge effect has been accounted for. Each element is considered to be an orthotropic material under multiaxial state of stress. Based on the three-dimensional state of stress of each element, different failure modes of a unidirectional ply under multiaxial states of stress are detected by a set of fatigue failure criteria. An analytical technique, called the *generalized residual material property degradation technique*, is established to degrade the material properties of failed elements. This analytical technique removes the restriction of the application of failure criteria to limited applied stress ratios. Based on the *model*, a computer code is developed that simulates cycle-by-cycle behaviour of composite laminates under fatigue loading.

As the input for the *model*, the material properties (residual stiffness, residual strength and fatigue life) of unidirectional AS4/3501-6 graphite/epoxy material are fully characterized under tension and compression, for fiber and matrix directions, and under in-plane and out-of-plane shear in static and fatigue loading conditions. An extensive experimental program, by using standard experimental techniques, is performed for this purpose. Some of the existing standard testing methods are necessarily modified and improved. To validate the *generalized residual material property degradation technique*, fatigue behaviour of a 30-degrees off-axis specimen under uniaxial fatigue loading is simulated. The results of an experimental program conducted on 30-degrees off-axis specimens under uniaxial fatigue show a very good correlation with the analytical results. To evaluate the *progressive fatigue damage model*, fatigue behaviour of pin/bolt-loaded composite laminates is simulated as a very complicated example. The *model* is validated by conducting an experimental program on pin/bolt-loaded composite laminates and by experimental results from other authors. The comparison between the analytical results and the experiments shows the successful simulation capability of the *model*.

Résumé

Use technique de modélisation est développée pour faire l'analyse du comportement mécanique en fatigue des structures fabriquées de matériaux composites qui peuvent être sujettes à des concentrations de contraintes. Cette technique s'appelle le *modelage de dommages progressifs en fatigue*. Le *modèle* peut simuler et prédire la rigidité résiduelle, la résistance résiduelle et la vie totale en fatigue d'une plaque laminée en composite qui peut avoir une géométrie et une séquence de plies arbitraires, et peut être soumise à une condition complexe de chargement.

Trois modules constituent l'intégralité du *modèle*: l'analyse de contrainte, l'analyse de rupture et les règles de dégradation des propriétés des matériaux. Pour développer l'analyse de contrainte, une méthode par élément fini, non linéaire et tridimensionelle, sera utilisée. En choisissant un grand nombre d'éléments près du bord des ouvertures et de l'interface des plies, les effets de bord seront inclus. Chaque élément possède une propriété orthotropique en état de contrainte multi-axe en trois dimensions. Les contraintes, calculées pour chaque élément, sont évaluées par des critères de rupture en fatigue. Pour détériorer les propriétés des éléments endommagés, une nouvelle technique est mise au point: la *technique générale d'évaluation des propriétés résiduelles des matériaux*. Cette technique élimine une restriction importante sur l'utilisation des critères de rupture qui sont normalement limités à une seule proportion (maximum sur minimum) de contrainte appliquée. Un logiciel est développé pour simuler, cycle par cycle, le comportement en fatigue des structures en matériaux composites.

Le *modèle* nécessite que les propriétés de base (rigidité résiduelle, résistance résiduelle et vie totale en fatigue) du matériau unidirectionnel graphite/époxie AS4/3501-6 soient mesurées. Les caractéristiques du matériau seront répertoriées après qu'on ait mesuré les propriétés, en tension et en compression, dans la direction des fibres, de la matrice et du cisaillement du matériau, et tout cela en statique et en fatigue. Pour compléter tous ces essais, plusieurs techniques expérimentales standards sont utilisées. Quelques essais ont nécessités des modifications et des améliorations. Pour vérifier la *technique générale d'évaluation des propriétés résiduelles des matériaux*, des essais de fatigue utilisants des coupons d'essais avec l'angle des plies à trente degrés ont été effectués. Les résultats corroborent très bien les prédictions. Pour évaluer la technique de *modelage de dommages progressifs en fatigue*, le comportement des plaques ayant une connexion goupillée/boulonnée (exemple de chargement complexe) est simulé. Ces simulations sont comparées à des essais faits sur des plaques goupillées/boulonnées ainsi qu'à des résultats tirés de la littérature scientifique. La corroboration des résultats démontre avec succès les capacités de simulation du *modèle*.

Acknowledgments

The author would like to express his sincere gratitude and immense thanks to his thesis supervisor Prof. L. B. Lessard for his invaluable guidance, continued support and encouragement during this research. Also, his scientific ability and his sociable personality are admirable.

I would also like to thank Prof. D. R. Axelrad, Prof. J. W. Provan, Prof. B. Harris, Dr. C. Poon, Prof. G. G. Bach, Prof. J. A. Nemes, Prof. S. C. Shrivastava, Prof. P. Léger and the reviewers of my publications, for their knowledge and great discussions that they have provided to me.

I am indebted to my wife, Mojgan Mohamed, my daughter, Momeneh, and my son, Ahmad, for their kindness, love, understanding and patience. They were great supporters for me during these busy years. I also appreciate my mother and parents-in-law for their kindness and love.

The author thanks graduate students, J. H. Esbensen, A. S. Schmidt, O. P. Eilers, J. F. Milette, and P. Kotsiopriftis and numerous undergraduate students with whom the author worked during the course of this research.

Thanks goes out to the technicians in the Measurement Laboratory and the Machine Tool Laboratory of the Mechanical Engineering Department of McGill University, and the National Research Council of Canada for their help during the experimental phase of this study.

Special thanks to my officemates, fellow graduate students, F. Hassani, H. Eskandari and Dr. A. Makris, for the friendly and scientific environment provided to me during these years.

I also extend my sincere thanks to Ms. N. Daneau for translating the French language abstract and Ms. A. Cianci for the careful editing of this thesis.

Contents

List of Figures

Chapter 5

Chapter 6

Chapter 7

Chapter 8

List of Tables

Chapter 1

Introduction

The word fatigue is defined by the ASM [1] as the phenomenon leading to fracture under repeated or fluctuating stresses having a maximum value less than the ultimate static strength[†] of the material. Perhaps Poncelet in 1839 was the first person who called this phenomenon "fatigue" [2]. One of the earliest papers on fatigue of metals was published in 1867, by A. Wohler, a German engineer [3]. Since then, a great quantity of research has been performed on fatigue behaviour of homogenous materials. Despite this, research in fatigue of composite materials was virtually non-existent before 1958 [4].

Intricacy and non-homogeneity of composite materials make their fatigue behaviour very complicated in comparison with traditional materials. Although today there is a large amount of research in fatigue of composite materials, however the level of understanding of the fatigue behaviour is far less than that obtained for homogenous materials [5]. In spite of the complicated behaviour of composite materials in fatigue loading conditions and the lack of a relatively comprehensive knowledge of the fatigue behaviour, the long life, light weight, high stiffness and high strength of such materials make them attractive for design. Increasing application of composite materials in primary structures is a good example of this attraction, and one that demands a more challenging research effort. Thus the fatigue analysis of composite materials is a field of current and growing importance.

[†] The words "ultimate tensile strength" in the original definition by the ASM are replaced by "ultimate static strength" in this thesis. In this way the definition is applicable to tension, compression and shear fatigue loading conditions.

1.1 Literature review

Before beginning this section, it should be pointed out that this thesis covers numerous topics. Hence, combining a literature review of all the different topics covered by the thesis in this section would make it lengthy and confusing. Instead, this section reviews papers related only to the main subject of the thesis, i.e., fatigue modeling of composite laminates with or without stress concentrations. Papers related to specific areas covered by the thesis are reviewed and discussed in detail in relevant chapters.

Among the different types of composite materials, polymer matrices reinforced with graphite fibers are used extensively in aerospace industries. Due to the large difference between the mechanical properties of graphite fiber and epoxy matrix, the resulting composite materials show highly orthotropic behaviour. Also, the failure modes of unidirectional composites under different fatigue loading conditions, such as tension, compression, in-plane shear or out-of-plane shear in fiber or matrix directions, are all completely different. Moreover a composite laminate, consisting of plies with different orientations and different stacking sequence, has a more complicated fatigue behaviour. For instance, delamination or separation between layers is a very complicated failure mechanism which is special to composite laminates. Existence of stress concentrations multiplies the complexity of fatigue failure of composite laminates and consequently the modeling is even more difficult. It is necessary to mention here that the words "stress concentrations" are equivalent to words such as notches, slots, slits, cracks, open holes and pin/bolt-loaded holes used by authors in the literature. By considering all the aforementioned complexities, some of which are inherent to composites, the fatigue modeling of these materials is a very tedious task. Specifically, the fatigue of composite laminates with stress concentrations is one of the most complicated subjects which is still under research.

There are some remarkable efforts in the literature studying the fatigue behaviour of unidirectional plies and laminated composites (see review papers [4-9]). Three principal approaches are used for predicting the fatigue life of composite materials: residual strength, residual stiffness and empirical methodologies. In each category, phenomenological, mechanistic, statistical and mixed methods are utilized by different authors. Most of these works are devoted to the fatigue behaviour of unidirectional plies or simple laminates, while the number of research papers on fatigue of notched laminates is more limited. Unfortunately, the valuable information provided by different authors for the fatigue of simple composites without stress concentrations can not be directly used for the fatigue analysis of composite laminates with stress concentrations.

However, they can be considered as basic knowledge for understanding the mechanics of fatigue failure in order to develop suitable models for the fatigue failure analysis of composites with stress concentrations.

One of the earliest papers in fatigue of composite laminates with stress concentrations was published by Owen and Bishop [10]. Today, there are several experimental [11-22] and analytical [23-39] research papers in this field. However, the present state of knowledge is still in the stage of development and improvement. Among the existing models, the semi-empirical model of Kulkarni *et al.* [27-31], the critical element model of Reifsnider *et al.* [32-34], and the damage growth model of Spearing *et al.* [35-39] are all systematic and methodological, therefore they are worthwhile for discussion. The semi-empirical model of Kulkarni *et al.* [27,28] was developed based on a mechanistic wearout [40] framework. The wearout philosophy treats fatigue damage as the growth of pre-existing flaws or discontinuities in a material. By growing the flaws, the strength of the material decreases and reaches to the level of the state of stress and finally, catastrophic fatigue failure occurs. The semi-empirical model was evaluated by experimental techniques [29], but little correlation between the theory and experiments was found. Later, they modified [30] their model by considering the effect of interlaminar shear stress in the failure analysis. However, the experimental results still did not show any correlation with the results of the analysis. In a subsequent attempt [31], the stress analysis part of their model was modified, but unfortunately no attempt was made to correlate the results of that analysis with experimental data. Although the semi-empirical model of Kulkarni *et al.* [27-31] never showed a correlation with experimental results, there are however many interesting points and valuable information in their work. The critical element model of Reifsnider *et al.* [32-34] was developed based on a mechanistic approach. Their mechanistic approach is based on micromechanical representations of strength. Sendeckyj [6] listed some of the weaknesses of this model. In the critical model, it is assumed that failure occurs suddenly and everywhere in the lamina, which is not consistent with the experimental observations. Also in the model, the dependence of lamina failure stresses on the lamina thickness in laminates is not properly considered. Moreover, the model does not properly account for delamination between the laminae in the laminate. The damage growth model of Spearing *et al.* [35-39] is based on quantification of notch tip damage by the extent of the individual failure processes, such as splitting in the 0° plies and delamination between the 0° ply and off-axis plies. There are some limitations in the damage growth model which are listed here. The model is laminate geometry dependent, i.e., by changing the lay-up of the laminate, the model must be modified. Moreover, the existence of transverse ply cracks, which is an important failure mode, is ignored in their model. Furthermore, they assume that the damage pattern is similar in all plies and delamination shape is the same at all interfaces which is not a general assumption. Also, the shape of the notch is pre-defined. In addition, their model is only capable of considering cyclic tensile loading. Thus all existing models for fatigue analysis of composites have limitations which make them unsuitable for general use.

1.2 Motivation and Objectives

Experimental characterization of fatigue behaviour of composite materials is time consuming and expensive. Moreover, generalization by extending and extrapolating of experimental results for composite laminates is not straightforward and sometimes, not possible. Therefore, modeling is an attractive tool for saving time and expenses in the fatigue design of composite laminates. By considering the complexity of the fatigue failure of composite materials, the level of present knowledge and shortcomings of existing models, the necessity of development of more general models with less limitations is quite obvious. The main objective of this research is to establish a model to simulate the fatigue behaviour of composite laminates under general conditions (loading, geometry, etc.), using the results of various types of uniaxial fatigue experiments of unidirectional plies. The model should be capable of simulating cycle-by-cycle fatigue behaviour of composite laminates with or without stress concentrations. There are several points and parameters which should be taken into account in order to ensure the generality of the model. A general model must not be limited to a special geometry, lay-up, loading condition, boundary condition, loading ratio or loading sequence.

Progressive damage modeling, which is a widely used failure analysis technique, has been successfully utilized to study the behaviour of composite laminates under static loading [41-43]. In progressive damage modeling, stress analysis, failure analysis and material property degradation are three important components. The states of stress in the composite materials are found by a stress analysis technique, e.g., finite element method. Then the failure analysis is performed by evaluating the stresses using a set of failure criteria, capable of distinction of different failure modes. Finally, the material properties of failed regions are changed by a set of degradation rules. Progressive damage modeling allows the detailed study of damage progression from damage initiation to the final catastrophic state. However, so far this technique has been used to study composite laminates under static types of loading. In this research, the concept of progressive damage modeling is extended and the framework of *progressive fatigue damage modeling* is established and utilized for fatigue failure analysis of composite laminates with or without stress concentrations

One complicated example of a composite laminate with stress concentrations is a pin/bolt-loaded composite plate. Behaviour of pin/bolt-loaded composite laminates under static loading situation has been studied extensively (see [41] for a comprehensive review). However, after a thorough literature review in fatigue of composite laminates, it is found that fatigue behaviour of pin/bolt-loaded composite laminates has been studied much less extensively. All of the existing investigations [44-54] are primarily experimental and restricted to a special type of loading, specific laminate configuration, certain geometry, etc. Therefore the pin/bolt-loaded composite plate under fatigue loading conditions, is selected as a reasonable and sufficiently difficult example for evaluating the *model* developed in this study. Moreover, by considering the existing limited research conducted in the field of pin/bolt-loaded composite plates, the results obtained by the *model* will be a useful addition to the literature. The established *model* must be able to predict the residual strength, residual life, final failure mechanisms (direction of failure propagation) and final fatigue life of the composite laminates under general fatigue loading conditions.

Chapter 2

Problem Statement

In this chapter, a general explanation of the mechanics of fatigue failure of composite materials is presented. Available information in the literature on the mechanics of fatigue failure is reviewed and discussed. Different fatigue failure modes of unidirectional composite materials under various uniaxial fatigue loading conditions are explained. A pin/bolt-loaded composite laminate is selected as a sophisticated problem to be solved by the *model*. Furthermore, a detailed description of this problem is presented and the pertinent mechanisms of failure are discussed. The difference between two terms used in this thesis, the modes and the mechanisms of fatigue failure are elucidated. The framework of the established fatigue modeling strategy, capable of simulating the fatigue behaviour of composite materials in general conditions is explained.

2.1 Mechanics of Fatigue Failure

It is well known that the propagation of a dominant crack is responsible for final fatigue failure in metals, while accumulation of cracks causes failure in composite materials. Consider a unidirectional composite material under fatigue loading conditions. Matrix cracking is the first failure mode which occurs at the first cycles of fatigue loading of composite materials. Matrix cracks occur at the interface of fiber and matrix as well as within the matrix. By increasing the number of fatigue cycles, cracks propagate and accumulate. At higher number of cycles or stress levels, cracks initiate in fibers and finally, catastrophic failure occurs. This brief explanation is a simplified scenario of the uniaxial fatigue failure process of a unidirectional composite without considering the directions (fiber or matrix) or types (tensile, compressive, in-plane or out-of-plane shear) of fatigue loading.

A proper understanding of mechanics of initiation and propagation of damage in unidirectional composite materials under cyclic loading is an important step in fatigue modeling of laminated composites. Due to non-homogeneity of composite materials, the fatigue failure behaviour of a unidirectional ply loaded in fiber direction is different from a ply loaded in matrix direction. Moreover, the fatigue behaviour of a unidirectional ply under various types of loading such as tensile, compressive, in-plane shear and out-of-plane shear loading is also different. The fatigue behaviour of a unidirectional ply under various types of loading is called mode of failure in this study. Fatigue behaviour of unidirectional plies under longitudinal tensile [55-61], longitudinal compressive [62-63], matrix compressive [62-64] and in-plane shear loading [55, 65-76] has been studied by different authors. In most of these works, fatigue failure is explained by interpretation of experimental observations of damage modes. However, there is no attempt in the literature to fully characterize the fatigue properties of a unidirectional ply (such as, residual stiffness, residual strength and life) under various types of fatigue loading. There is also a lack of information in the literature on transverse tensile and out-of-plane shear fatigue behaviour of unidirectional plies.

By considering the differences between the failure modes of a unidirectional ply under various fatigue loading conditions, it is very easy to confirm that the fatigue behaviour of laminated composites, consisting of unidirectional plies with different orientations, is more complicated. In addition, existence of delamination which is special to laminated composites makes the fatigue analysis even more sophisticated. Also, existence of stress concentrations in the laminated composite makes the problem extraordinarily difficult. In fatigue modeling of composite materials, these difficulties can be alleviated by utilizing different strategies. The problem can be simplified by limiting the capability of the model to special cases such as specific laminates and lay-ups, pre-defined loading conditions, fixed geometries, etc. In this way, some success can be obtained in fatigue modeling [35-39], however the models are case dependent and limited to the initial assumptions. Another strategy is a localized analysis of fatigue failure events by means of a micromechanical approach and integrating these localized results into a global model. The model established in this manner could be general. However, to perform this strategy, a deep understanding of the localized fatigue failure events must be available and micromechanical models for all failure modes, such as fiber debonding, matrix cracking, fiber breakage, etc., should be established. Unfortunately, there are no comprehensive micromechanical models for the different fatigue failure modes to be incorporated into a systematic model to predict the global failure behaviour of a complicated problem. This strategy is under development [32-34], however all the essential information required by the model is not as yet available. Also by considering the state of our present knowledge, creation of such information seems to be a very tedious task. Moreover, the model established in this way would be too complicated and expensive. Instead of sacrificing the feasibility of the model because of its generality or vice versa, another strategy is adopted in this research and a modeling approach is established which satisfies both generality and feasibility. The phenomenological behaviour of unidirectional plies under different type of fatigue loading can be measured, fully characterized and incorporated into a global systematic model. The following example helps to describe the important basis of the model.

2.2 Description of the Problem

Among different examples of composite materials under fatigue loading conditions, a pin/bolt-loaded composite laminate is a complicated problem. Pinned/bolted joints are widely used in joining of components made of composite materials. The existence of stress concentrations, edge effects, different stacking sequences and selection of various load and stress ratios are some difficulties which exist in the pin/bolt-loaded composite laminate problem. Consider a composite plate with a pin/bolt-loaded hole, i.e., the plate has a circular hole filled with a rigid pin or bolt. Load is applied at one end of the plate and is resisted by the rigid pin or bolt. The coordinate axis, dimensions and nomenclatures are shown in Fig. 2.1. The existence of stress concentrations, which cause a non-uniform state of stress, as well as the existence of singular state of stress near the free edge of the hole (edge effects), make the stress analysis more cumbersome. The plate is a laminated composite made of layers of continuous fibers embedded in an organic matrix. Each layer of the laminate is called a "ply" or "unidirectional layer". The geometry (size and location of the hole, length, width, and thickness of the laminate), stacking sequence of unidirectional plies in the laminate and the applied fatigue loading ratio ($load_{min}/load_{max}$), which induces the fatigue stress ratio ($\sigma_{min}/\sigma_{max}$) in the laminate can be selected arbitrarily. Existence of all theses difficulties makes the pin/bolt-loaded composite laminate a suitable problem for examining and evaluating the *model*.

Before explaining the fatigue failure events in a pin/bolt-loaded composite laminate, it is worthwhile to explain the steps of failure initiation and propagation of this problem under static loading conditions. The composite plate is loaded with an in-plane load "P" as shown in Fig. 2.1. By increasing the load monotonically to a certain value, which is called the first ply failure load, failure initiates at a location near the edge of the hole. Experimental observations show that matrix cracking failure mode usually starts first. If after failure initiation, the load is increased, failure will

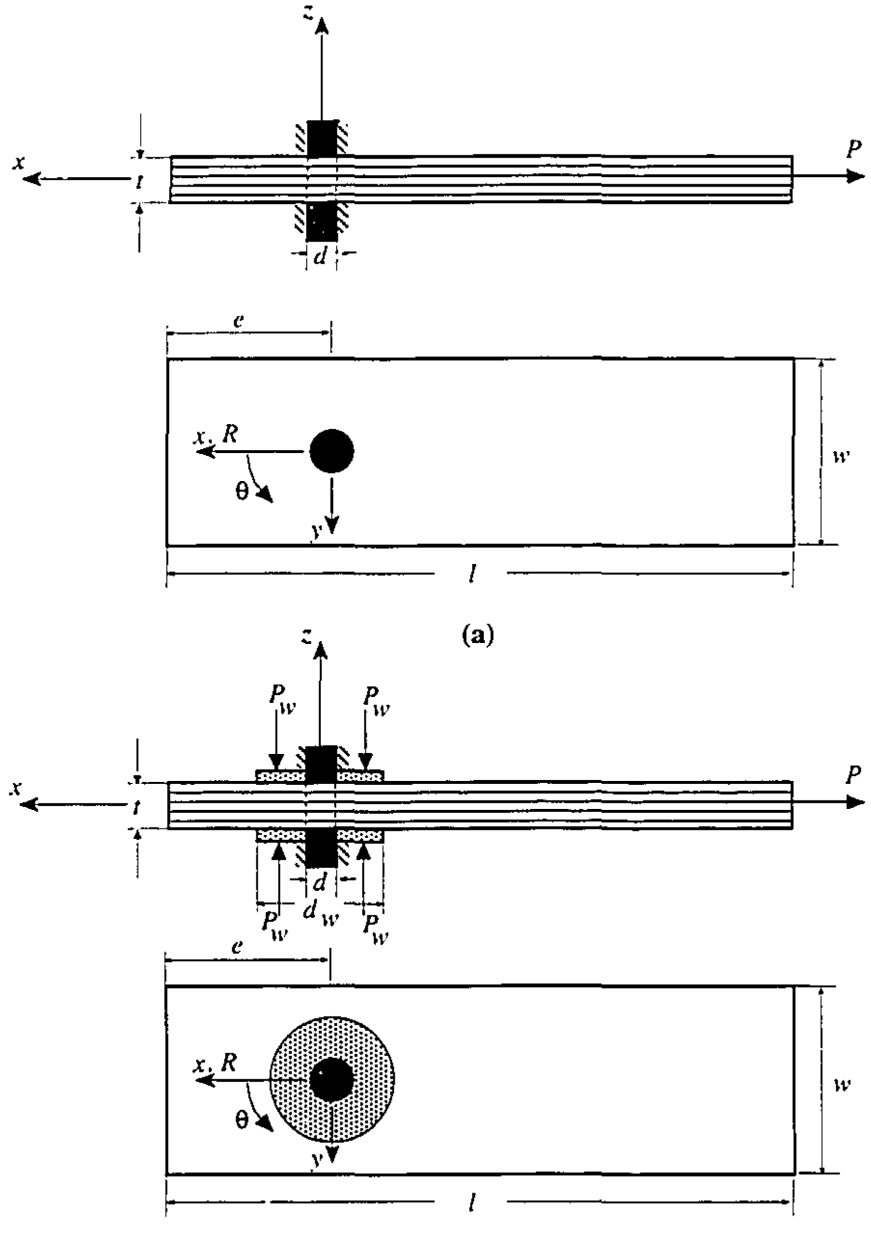

Fig. 2.1 Geometry of a laminated composite plate with a circular hole, subjected to (a) pin loading, and (b) bolt loading

propagate in different directions. By increasing the monotonic load, delamination and fiber failure occur after matrix cracking. Finally at a higher load called the ultimate strength load, damage will propagate to an extent that the plate cannot tolerate any additional load. It has been observed experimentally that mechanically fastened joints fail under three basic *mechanisms*. The mechanisms of structural failure are net tension, shear-out and bearing. Typical damage due to each mechanism is shown in Fig. 2.2. The magnitude of the first ply failure load, the position of the initial failure, the direction of the failure propagation (or mechanism of failure) and the ultimate strength load depend upon the material properties, dimensions, laminate configurations and many other parameters.

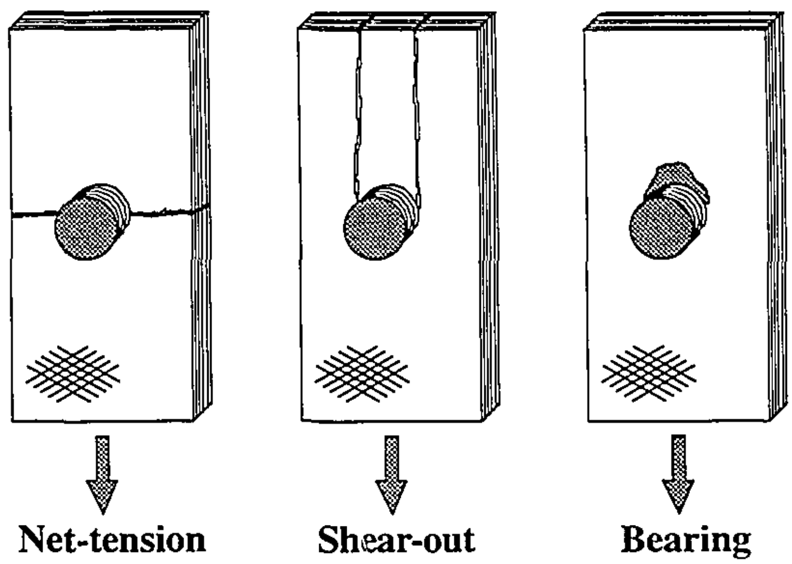

Fig. 2.2 Different failure mechanisms of pin/bolt-loaded composite laminates

By noticing the failure modes and mechanisms of a pin/bolt-loaded composite laminate under static loading conditions, the behaviour of the composite under fatigue loading conditions can be explained easier. At the start of cyclic loading, the strength of the material is greater than the stress state, therefore there is no static mode of failure anywhere on the plate. By increasing the number of cycles from zero, based on the stress states at each point of the plate, material properties (stiffness and strength) at those points are degraded as functions of number of cycles, state of stress and stress ratio. By increasing the number of cycles, which is accompanied by more degradation of the material properties and redistribution of stresses, failure begins in regions where the strength of the material falls below the stress level at that point. After failure initiation, stresses are redistributed around failed regions. By further increasing the number of cycles, failure propagates in different directions. Finally after a certain number of cycles called *fatigue life*, the laminate cannot tolerate additional cycles. At this point the maximum number of cycles is reached and the laminate has failed completely. Although material properties of all points of the pin/bolt-loaded composite plate have been degraded as functions of number of cycles, experimental observations however, show that the final mechanisms of failure in static and fatigue loading conditions are the same.

It should be pointed out that the failure modes of unidirectional composites under uniaxial fatigue loading conditions are inherent properties, while the mechanisms of failure depend upon the ply sequence and geometry of laminated composites. Since there are a limited number of failure modes for a unidirectional ply, they can be fully characterized by experimental techniques and mathematical models. However the failure mechanism is a case dependent property, therefore a variety of different mechanisms of failure can exist for laminated composites with various geometries, stacking sequence, etc. This is an important point which categorizes the fatigue models into two classes: general and case dependent.

2.3 Requirements and Modeling Strategy

It is desired to develop a model to simulate the behaviour of composite laminates under general fatigue loading conditions. For this purpose, the framework of the *progressive fatigue damage model* is established. The *model* is an integration of three major components: stress analysis, failure analysis and material property degradation rules. The *model* determines the state of damage at any load level and number of cycles, from failure initiation and propagation to catastrophic failure. The *model* is able to predict the residual strength, residual life, final failure mechanisms (direction of failure propagation) and final fatigue life of the composite laminates under general fatigue loading conditions.

In order to establish a model able to meet such requirements, a specific strategy must be followed. Realistic stress analysis, failure analysis and material property degradation rules are key points in the fatigue failure analysis of composite laminates. First, the stresses induced in the composite laminate are analyzed by utilizing a finite element method. There are some complexities which make the role of a realistic stress analysis salient, e.g., existence of bolt load, non-homogeneity of composite materials before and after failure, presence of stress concentrations, nonlinear shear stress-strain behaviour of unidirectional plies [77] and the existence of singular states of stress near the free edges of composite laminates (see [78] as a review). Achieving a realistic stress analysis for different geometries, lay-ups, loading conditions and boundary conditions in general forms, is not possible without using a three-dimensional nonlinear finite element technique. As mentioned earlier, there are different failure modes for unidirectional plies under uniaxial state of fatigue stress which must be fully characterized and used as basic information for the *model*. Also, for predicting the failure of a unidirectional ply under multiaxial states of stress, the stresses are examined by a set of stress-based failure criteria. Moreover, on the condition that failure exists, material properties of the failed regions are changed. For this purpose, the *model* should be capable of simulating the material property degradation of unidirectional plies (residual stiffness and residual strength) under uniaxial and multiaxial states of fatigue stress. Upon increasing the number of fatigue cycles, the whole process should be repeated until catastrophic failure is achieved. For this purpose, a user-friendly computer code must be developed to integrate the different components of the *model*.

2.4 Summary

Although a general description of the modeling strategy has been given in a very compacted form in this chapter, the three major components of the *model*; stress analysis, failure analysis and material degradation rules will be discussed in detail in the following three chapters. A detailed explanation of the *model*, which is an integration of the three components, will be presented in chapter six.

Chapter 3

Stress Analysis

In this chapter the first component of the *model*, the stress analysis is explained. The free edge effect (stress singularity), a very important subject in the stress analysis of composite laminates, is considered and discussed. A three-dimensional finite element algorithm is developed to analyze the three-dimensional state of stress of a pin/bolt-loaded composite laminate as a sophisticated problem. A detailed explanation of the finite element algorithm and the theoretical basis of the finite element formulation is presented. For achieving higher accuracy, a twenty-node isoparametric quadratic solid element is used. Three different configurations, namely, cross-ply $[0_4/90_4]_s$ and $[90_4/0_4]_s$, and an angle-ply $[+45_4/-45_4]_s$ are considered. By using a large number of elements near the edge of the hole and at layer interfaces, the edge effect is simulated. Also, by noting the nonlinear shear stress-strain behaviour of a unidirectional ply, the effect of material nonlinearity on the stress state near the edge of the hole, which is a critical location for failure initiation is considered. For this purpose, an existing model for the mathematical presentation of material nonlinear in-plane shear stress-strain behaviour of a unidirectional composite ply is extended to be also applicable for out-of-plane shear stress-strain. Moreover, an iterative scheme is added to the algorithm to properly account for the existence of material nonlinearity. The effect of existence of bolt load on the state of stress, near the edge of the hole is also studied and discussed.

3.1 Free Edge Effects: A Review

Delamination is a well-known out-of-plane mechanism of failure which usually occurs at the free edge of composite laminates under static and fatigue loading conditions. It should be mentioned that delamination can also exist inside of the composite laminate, far from the edge, resulting from impact loading which is not considered in this study. In order to study the fatigue behaviour of composites under general conditions, it is important to understand the three-dimensional nature of the stress distribution of composite laminates. Stress analysis which includes the third or thickness direction is required in order to understand the free edge effects. The state of stress at free edges of a simple composite plate (without any simplifying assumptions), was studied for the first time by Pipes and Pagano [79] in 1970. They used classical linear theory of elasticity to set up three coupled, elliptic, second-order, partial differential equations and applied finite difference techniques to solve for displacements and stresses. Their results revealed that there were significant magnitudes for normal and shear stresses on the free edges, between different layers of composite plates (Fig. 3.1).

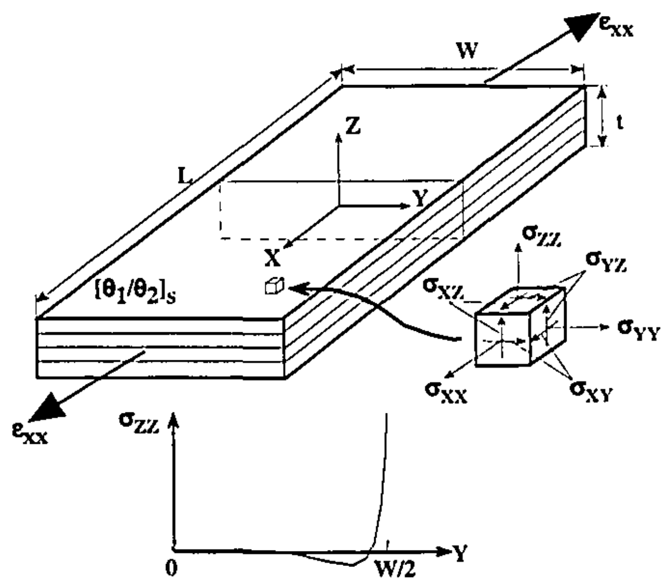

Fig. 3.1 Laminate geometry and edge effects (after Pagano and Pipes [79])

Because of the important role of normal and out-of-plane shear stresses in the creation of delamination, numerous attempts have been made to obtain an accurate stress state on the edge of a composite plate by investigators. For this purpose, different techniques like finite difference [80], finite element [81-87], closed form solutions [88-100], boundary layer theory [101], perturbation method [102,103], Galerkin method [104] and experimental methods [95,105,106] were applied by different authors. To reduce the great difficulties encountered in numerical and closed form techniques, such as computer time, satisfying all boundary conditions, existence of a mathematical singularity in the stress field, etc., approximate techniques were used by Pagano and Pipes [107]. They assumed that the normal stress is constant inside of a composite plate and varies linearly near the edges. However, with respect to the results that have been obtained by other techniques, this approximation seems coarse. There are other attempts to simplify this problem, for example, the works of Kassapoglou and Lagace [108], and Rose and Herakovich [109] must be mentioned. In 1980, Raju *et al.* [110] reviewed many previous works and showed discrepancies in the results obtained by different authors. They also investigated the reliability of displacement-formulated finite element techniques for analyzing the edge problem. A detailed review of different models for studying free edge effects is presented by Pagano and Soni [78].

Although in [85,86] it has been shown that interlaminar stress distributions converge to large but finite magnitudes, almost all investigators believe that there is a mathematical stress singularity on the free edges of composite plates, between layers of different orientations. In [111-114] different analytical studies have been conducted to prove the existence of stress singularities near the edges. However, the form, strength and power of the singularity are still open questions for further research.

Most of the work in this field has been devoted to straight free edges, however there are a few research papers related to stress analysis of curved edges. Normal and interlaminar stresses around an open hole in a composite plate have been studied by different authors [115-121]. Stacking sequence, different configurations, and size effects on normal and interlaminar stresses near the edges have been considered in their works. While in these studies [115-121] finite element techniques have been used, in [122], a simplified closed form solution was applied to compute the interlaminar stresses around a circular open hole. Three-dimensional finite element techniques have been used in [123-125] to analyze the behaviour of pin and bolt-loaded composite laminates. Nevertheless, in these works all stresses are not presented. Also, stress singularities near the edge of the hole (edge effects) are not examined. In [126], the normal stress around the hole of a pin-loaded composite laminate has been studied, however the interlaminar shear stresses have not considered by them. Recently, the author published research papers on the three-dimensional linear elastic stress analysis of simple composite plates [127,128] and pin/bolt-loaded composite laminates [129,175] with different ply lay-ups. Also, the effect of material nonlinearity [77] on the stress state of pin-loaded composite laminates near the edge of the hole has been studied by author [130]. To the best knowledge of author, no comprehensive research exists in the field of edge effects on pin/bolt-loaded composite laminates and it can be concluded that this problem is still an open field for further research. Therefore, in this chapter a detailed study of this problem is presented.

3.2 Problem Statement

Consider a composite plate with a pin/bolt-loaded hole (Fig. 2.1). The plate has width w = 25.4 mm, length l = 101.6 mm, thickness t = 2.336 mm (16 plies), edge distance e = 25.4 mm, hole diameter d = 6.35 mm and washer diameter d_w= 18.8 mm. The plate is a laminated composite with arbitrary ply orientation. The pin or bolt is fixed and the load is applied on the other end of the composite plate. Three different configurations, $[0_4/90_4]_s$, $[90_4/0_4]_s$, and $[+45_4/-45_4]_s$ are selected for studying the effect of stacking sequence. The magnitude of applied load P is 1.0 KN, which is less than the failure initiation load of all three configurations (found experimentally) and the magnitude of washer pressure is 2.48 MPa.

3.3 Finite Element Analysis

As previously mentioned, by considering edge effects, delamination and stacking sequence effects that are fully three-dimensional phenomena, applying a three-dimensional finite element technique is essential to the pin/bolt-loaded composite plate problem. Therefore, a three-dimensional finite element code is developed to analyze the stress state of the problem. To achieve high accuracy, the isoparametric quadratic 20-node brick element is used. By considering the curved boundary around the hole of a composite laminate, and in order to apply boundary conditions, mixed Cartesian-Cylindrical coordinates are used (see Fig. 2.1). In order to simulate the stress singularity between two layers of different ply orientations on the edge of the hole, a large number of elements is used at that location (Fig. 3.2).

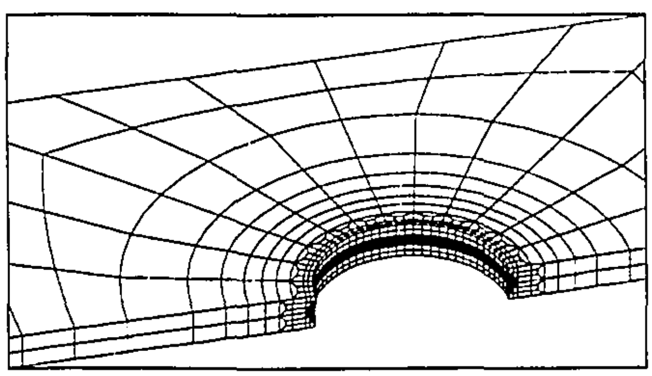

Fig. 3.2 Finite element mesh of the problem, showing large number of elements at the hole boundary

To explain the details of the finite element code developed in this research, the theoretical basis of the finite element formulation is presented in the following sections.

3.3.1 Material Properties

A unidirectional ply is shown in Fig. 3.3. The x, y and z axes are the longitudinal, transverse and normal directions, respectively. It is assumed that y-z plane is the special plane of isotropy and the behaviour of material parameters are the same in x-y and z-x planes. Therefore, the material properties of a unidirectional ply are assumed to be transversely isotropic [132]. By this assumption, in three-dimensional cases, the number of experiments required to characterize the material parameters (moduli, strengths and Poisson's ratios) are reduced drastically. In this study, AS4/3501-6 material is used with the material properties measured in Composite Materials Laboratory of McGill University, shown in Table 3.1.

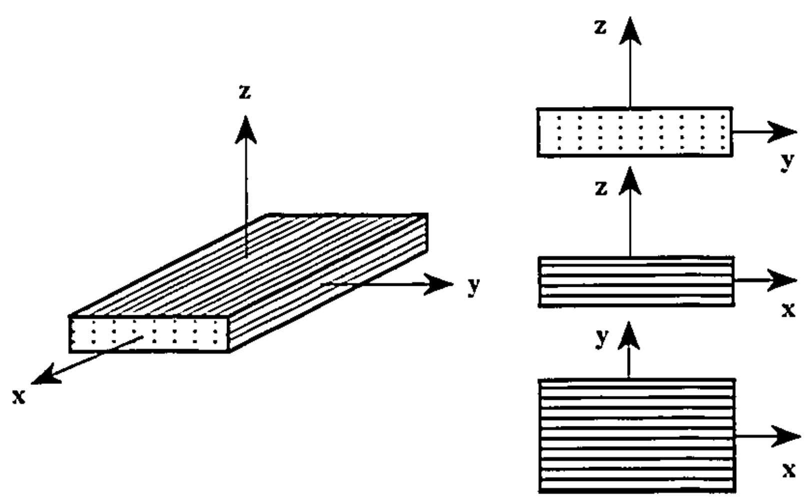

Fig. 3.3 Three-dimensional geometry of a layer of composite material

where in Table 3.1, E_{xx}, E_{yy} and E_{zz} are the longitudinal, transverse, and normal modulus, respectively. Also, E_{xy}, E_{xz} and E_{yz} are shear moduli, ν_{xy}, ν_{xz} and ν_{yz} are Poisson's ratios, and X_t, Y_t, Z_t, X_c, Y_c, Z_c, S_{xy}, S_{xz}, and S_{yz} are longitudinal tensile, matrix tensile, normal tensile, longitudinal compressive, matrix compressive, normal compressive, in-plane shear, out-of-plane shear (x-z plane), and out-of-plane shear (y-z plane) strength, respectively. The x, y and z directions are material directions as shown in Fig. 3.3. The Poisson's ratio in y-z plane (ν_{yz}) is calculated by using Christensen's formula [159].

Properties	Magnitudes
E_{xx}	147.0 GPa
$E_{yy} = E_{zz}$	9.0 GPa
$E_{xy} = E_{xz}$	5.0 GPa
E_{yz}	3.0 GPa
$\nu_{xy} = \nu_{xz}$	0.3
ν_{yz}	0.42
X_t	2004. MPa
X_c	1197. MPa
$Y_t = Z_t$	53. MPa
$Y_c = Z_c$	204.0 MPa
$S_{xy} = S_{xz}$	137.0 MPa
S_{yz}	42.0 MPa
ply thickness	0.146 mm
fiber volume	62%

Table 3.1 Material properties of AS4/3501-6

3.3.2 Constitutive Equations

By assuming transverse isotropic material properties for each unidirectional ply, the number of material parameters (moduli, Poison's ratios and strengths) are reduced from eighteen to eleven. By using this assumption, experimental costs for material characterization can be reduced drastically. The constitutive equations in terms of engineering constants are [131,132]:

$$\begin{Bmatrix} \sigma_{xx} \\ \sigma_{yy} \\ \sigma_{zz} \\ \sigma_{yz} \\ \sigma_{zx} \\ \sigma_{xy} \end{Bmatrix} = [C] \begin{Bmatrix} \varepsilon_{xx} \\ \varepsilon_{yy} \\ \varepsilon_{zz} \\ \varepsilon_{yz} \\ \varepsilon_{zx} \\ \varepsilon_{xy} \end{Bmatrix} \qquad \textbf{Eq. 3.1}$$

where,

$$[C] = \begin{bmatrix} C_{11} & C_{12} & C_{13} & 0 & 0 & 0 \\ C_{21} & C_{22} & C_{23} & 0 & 0 & 0 \\ C_{31} & C_{32} & C_{33} & 0 & 0 & 0 \\ 0 & 0 & 0 & C_{44} & 0 & 0 \\ 0 & 0 & 0 & 0 & C_{55} & 0 \\ 0 & 0 & 0 & 0 & 0 & C_{66} \end{bmatrix} \qquad \textbf{Eq. 3.2}$$

and,

$$C_{11} = (1 - \upsilon_{yz}^2)VE_{xx}$$

$$C_{12} = C_{13} = \upsilon_{yx}(1 + \upsilon_{yz})VE_{yy}$$

$$C_{23} = (\upsilon_{yz} + \upsilon_{yx}\upsilon_{xy})VE_{yy}$$

$$C_{22} = C_{33} = (1 - \upsilon_{yx}\upsilon_{xy})VE_{yy}$$

$$C_{44} = (1 - \upsilon_{yz} - 2\upsilon_{yx}\upsilon_{xy})VE_{yy} / 2$$

$$C_{55} = C_{66} = E_{xy}$$

$$V = 1 / [(1 + \upsilon_{yz})(1 - \upsilon_{yz} - 2\upsilon_{yx}\upsilon_{xy})]$$

3.3.3 Material Nonlinearities

Composite materials exhibit nonlinear behaviour to an extent that accurate results cannot always be obtained with a linear model. Inelastic stress-strain response of a composite lamina has been studied by different authors [133-143]. Petit and Waddoups [133] simulated the nonlinear stress-strain response of a lamina by using an incremental method based on a database of experimental stress-strain results. Hahn and Tsai [77], and Hashin *et al.* [134] presented appropriate constitutive equations by curve fitting of the experimental stress-strain data of a composite lamina using Ramberg-Osgood parameters. In [77], a constitutive equation for in-plane shear stress and strain is presented, and in [134] constitutive equations for in-plane transverse and shear stresses and strains are proposed. Sandhu [135], by using cubic spline interpolation functions, represented experimental shear stress-strain data. Sendeckyj *et al.* [136] experimentally showed that the method of Sandhu [135] gave excellent results for predicting nonlinear response of balanced laminates. Foye [137] and Adams [138] used finite element techniques to study the nonlinear stress-strain behaviour of a composite lamina by considering the fibers and matrix properties at the micromechanical level. Jones and Nelson [139-142] modeled nonlinear mechanical properties as functions of strain energy density. Their model converged only up to a specific strain energy value. Jones and Morgan [143] removed the mentioned limitation by using extrapolations of the available stress-strain curve and mechanical property-energy curve for strain energies above available stress-strain data. An interesting feature of their model is the ability to simulate the nonlinear behaviour of material in all principal material directions.

Experimental evidence shows that the shear stress-strain response of a graphite/epoxy lamina is clearly nonlinear (Fig. 3.4). However, the longitudinal and transverse stress-strain responses of the mentioned lamina are quite linear. Therefore, a suitable candidate model to study the nonlinear behaviour of this type of material is the Hahn and Tsai model [77]. The Hahn-Tsai model can be easily implemented into a finite element code. By considering the limitations of their model to the study of two-dimensional cases (in-plane shear stress-strain), the present research modifies this model for three-dimensional cases. The constitutive equation for in-plane shear stress-strain is [77]:

$$\varepsilon_{xy} = \frac{\sigma_{xy}}{E_{xy}} + \delta\sigma_{xy}^{3}$$ **Eq. 3.3**

where,

E_{xy} = initial lamina longitudinal-transverse shear modulus
σ_{xy} = in-plane shear stress
ε_{xy} = in-plane engineering shear strain
δ = nonlinearity parameter of the material (1.015E-8 $(MPa)^{-3}$ determined experimentally)

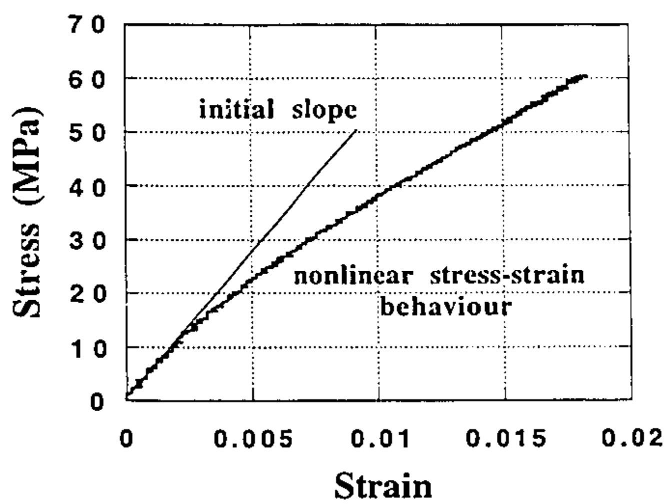

Fig. 3.4 Nonlinear elastic in-plane shear stress-strain (σ_{xy} - ε_{xy}) behaviour of AS4/3501-6

By recalling the transversely isotropic material properties assumption, it is assumed that normal-longitudinal shear modulus (E_{xz}) is equal to longitudinal-transverse shear modulus:

$$E_{xz} = E_{xy}$$ **Eq. 3.4**

Therefore, it can be assumed that there is a similar constitutive equation for interlaminar normal-longitudinal shear stress-strain (σ_{xz} - ε_{xz}):

$$\varepsilon_{xz} = \frac{\sigma_{xz}}{E_{xz}} + \delta\sigma_{xz}^{3}$$ **Eq. 3.5**

where,

σ_{xz} = interlaminar shear stress
ε_{xz} = interlaminar engineering shear strain

Also by considering that the *yz* plane is the plane of isotropy, and the lamina transverse-normal interlaminar shear modulus (E_{yz}) is not an independent function:

$$E_{yz} = \frac{E_{yy}}{2(1+\nu_{yz})}$$ **Eq. 3.6**

where,

E_{yz} = lamina transverse-normal shear modulus
E_{yy} = lamina transverse shear modulus
ν_{yz} = transverse-normal Poisson's ratio

By noticing that the tensile transverse stress-strain response (σ_{yy} - ε_{yy}) for a graphite/epoxy lamina is linear, and by using Eq. 3.6 and noticing that the ν_{yz} is assumed to be a constant, it is seen that the transverse-normal interlaminar shear stress-strain response (σ_{yz} - ε_{yz}) is also linear. This result is in very good agreement with the experimental results found by Gipple and Hoyans [160].

In order to apply the inelastic behaviour to a computer code, instantaneous (nonlinear) in-plane and interlaminar shear moduli of a lamina must be derived. By partial differentiation of both sides of Eq. 3.3, with respect to σ_{xy}:

$$\frac{\partial \varepsilon_{xy}}{\partial \sigma_{xy}} = \frac{1}{E_{xy}} + 3\delta\sigma_{xy}^2$$ **Eq. 3.7**

It is clear that

$$\overline{E}_{xy} = \frac{\partial \sigma_{xy}}{\partial \varepsilon_{xy}}$$ **Eq. 3.8**

where,

$\overline{E}_{xy}$ = instantaneous in-plane (longitudinal-transverse) shear modulus

then by considering Eqs. 3.7 and 3.8:

$$\overline{E}_{xy} = \frac{1}{\frac{1}{E_{xy}} + 3\delta\sigma_{xy}^2} \qquad \textbf{Eq. 3.9}$$

By applying the same procedure on Eq. 3.5:

$$\overline{E}_{zx} = \frac{1}{\frac{1}{E_{zx}} + 3\delta\sigma_{zx}^2} \qquad \textbf{Eq. 3.10}$$

where,

$\overline{E}_{xz}$ = instantaneous interlaminar (normal-longitudinal) shear modulus

There is limited research on the effect of material nonlinearity on the state of stress at the edge of a simple composite laminate [144-147]. To the author's best knowledge, there is no research on the effect of nonlinearity on the state of stress of a pin-loaded composite laminate. Therefore, for the first time this effect is considered in this study. For further information, the reader can refer to a paper [130] recently published by the author. It should be emphasized that the mentioned nonlinearities are due to inelastic behaviour of the material before failure initiation. Nonlinearities due to failure are completely different phenomena and they are considered by failure analysis techniques in this study.

3.3.4 Material Orientation

In the computer program it is necessary to determine the stiffness matrix of the material [E], with respect to a coordinate axis (x-y) (Fig. 3.5), when the stiffness matrix of the material [C] is known relative to a rotated coordinate system (x'-y') [132]. Suppose we have the following constitutive relation:

$$\{\sigma'\} = [C]\{\varepsilon'\} \qquad \textbf{Eq. 3.11}$$

where [C] is a known transversely isotropic stiffness matrix (Eq. 3.2). In the rotated coordinate system, we have:

$$\{\sigma\} = [E]\{\varepsilon\} \qquad \textbf{Eq. 3.12}$$

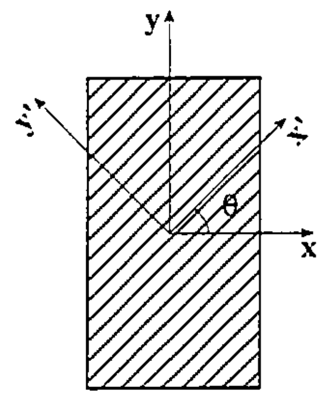

Fig. 3.5 Original and rotated coordinate systems

The transformed stresses in rotated axes are:

$$\begin{Bmatrix} \sigma'_{xx} \\ \sigma'_{yy} \\ \sigma'_{zz} \\ \sigma'_{yz} \\ \sigma'_{zx} \\ \sigma'_{xy} \end{Bmatrix} = \begin{bmatrix} m^2 & n^2 & 0 & 0 & 0 & 2mn \\ n^2 & m^2 & 0 & 0 & 0 & -2mn \\ 0 & 0 & 1 & 0 & 0 & 0 \\ 0 & 0 & 0 & m & -n & 0 \\ 0 & 0 & 0 & n & m & 0 \\ -mn & mn & 0 & 0 & 0 & m^2-n^2 \end{bmatrix} \begin{Bmatrix} \sigma_{xx} \\ \sigma_{yy} \\ \sigma_{zz} \\ \sigma_{yz} \\ \sigma_{zx} \\ \sigma_{xy} \end{Bmatrix} \qquad \textbf{Eq. 3.13}$$

where $m = \cos\theta$, and $n = \sin\theta$.

Also the transformed strains in rotated axes are:

$$\begin{Bmatrix} \varepsilon'_{xx} \\ \varepsilon'_{yy} \\ \varepsilon'_{zz} \\ \varepsilon'_{yz} \\ \varepsilon'_{zx} \\ \varepsilon'_{xy} \end{Bmatrix} = \begin{bmatrix} m^2 & n^2 & 0 & 0 & 0 & mn \\ n^2 & m^2 & 0 & 0 & 0 & -mn \\ 0 & 0 & 1 & 0 & 0 & 0 \\ 0 & 0 & 0 & m & -n & 0 \\ 0 & 0 & 0 & n & m & 0 \\ -2mn & 2mn & 0 & 0 & 0 & m^2-n^2 \end{bmatrix} \begin{Bmatrix} \varepsilon_{xx} \\ \varepsilon_{yy} \\ \varepsilon_{zz} \\ \varepsilon_{yz} \\ \varepsilon_{zx} \\ \varepsilon_{xy} \end{Bmatrix} \qquad \textbf{Eq. 3.14}$$

Substituting Eqs. 3.13 and 3.14 into Eq. 3.11, we obtain:

$$[T_\sigma]\{\sigma\} = [C][T_\varepsilon]\{\varepsilon\} \qquad \textbf{Eq. 3.15}$$

where $[T_\sigma]$ and $[T_\varepsilon]$ are the stress and strain transformations as defined by Eqs. 3.13 and 3.14. From Eq. 3.15, we have:

$$\{\sigma\} = [T_\sigma]^{-1}[C][T_\varepsilon]\{\varepsilon\} \qquad \textbf{Eq. 3.16}$$

Thus,

$$[E] = [T_\sigma]^{-1}[C][T_\varepsilon] \qquad \textbf{Eq. 3.17}$$

By substituting Eq. 3.2 into Eq. 3.17, we obtain:

$$\begin{aligned}
E_{11} &= C_{11}m^4 + 2m^2n^2(C_{12} + 2C_{66}) + C_{22}n^4 \\
E_{12} &= m^2n^2(C_{11} + C_{22} - 4C_{66}) + C_{12}(m^4 + n^4) \\
E_{13} &= C_{13}m^2 + C_{23}n^2 \\
E_{16} &= mn\left[C_{11}m^2 - C_{22}n^2 - (C_{12} + 2C_{66})(m^2 - n^2)\right] \\
E_{22} &= C_{11}n^4 + 2m^2n^2(C_{12} + 2C_{66}) + C_{22}m^4 \\
E_{23} &= C_{13}n^2 + C_{23}m^2 \\
E_{26} &= mn\left[C_{11}n^2 - C_{22}m^2 + (C_{12} + 2C_{66})(m^2 - n^2)\right] \\
E_{33} &= C_{33} \\
E_{36} &= (C_{23} - C_{13})mn \\
E_{44} &= C_{44}m^2 + C_{55}n^2 \\
E_{45} &= (C_{55} - C_{44})mn \\
E_{55} &= C_{44}n^2 + C_{55}m^2 \\
E_{66} &= m^2n^2(C_{11} + C_{22} - 2C_{12}) + C_{12}(m^2 - n^2)^2 \\
E_{14} &= E_{15} = E_{24} = E_{25} = E_{34} = E_{35} = E_{46} = E_{56} = 0
\end{aligned} \qquad \textbf{Eq. 3.18}$$

It is clear that the transformed matrix [E] is not transversely isotropic, but is monoclinic.

3.3.5 Shape Functions

The isoparametric, quadratic, 20-node, solid element has been used as shown in Fig. 3.6. The existence of stress singularities on the edges of composite laminates between layers with different orientations necessitates the utilization of this type of element in order to increase the accuracy of the results. The associated shape functions are [148]:

$$N_i = \frac{1}{8}(1+\xi_0)(1+\eta_0)(1+\zeta_0)(\xi_0+\eta_0+\zeta_0-2)$$
$$i = 1,3,5,7,13,15,17,19$$
$$N_i = \frac{1}{4}(1-\xi^2)(1+\eta_0)(1+\zeta_0)$$
$$i = 2,6,14,18$$
$$N_i = \frac{1}{4}(1+\xi_0)(1-\eta^2)(1+\zeta_0) \qquad \textbf{Eq. 3.19}$$
$$i = 4,8,16,20$$
$$N_i = \frac{1}{4}(1+\xi_0)(1+\eta_0)(1-\zeta^2)$$
$$i = 9,10,11,12$$

where $\xi_0 = \xi_i\xi \quad ,\eta_0 = \eta_i\eta \quad ,\zeta_0 = \zeta_i\zeta$ for node i

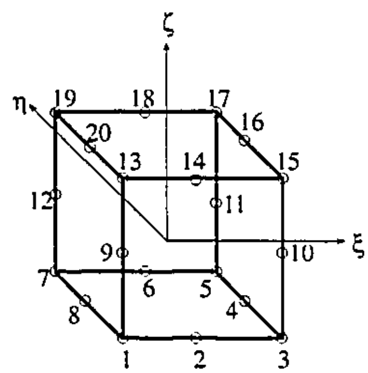

Fig. 3.6 Twenty-node quadratic isoparametric solid element

3.3.6 Derivation of Element Matrices

Using the isoparametric concept [149], displacements within an element $\{u\}$, are interpolated from element nodal degrees of freedom $\{d\}$:

$$\{u\} = [N]\{d\} \qquad \textbf{Eq. 3.20}$$

Strains $\{\varepsilon\}$ are obtained from displacements by differentiation:

$$\{\varepsilon\} = [\partial]\{u\} \quad \text{yields} \quad \{\varepsilon\} = [B]\{d\} \quad \text{where} \quad [B] = [\partial][N] \qquad \textbf{Eq. 3.21}$$

where in the three-dimensional problem:

$$[\partial] = \begin{bmatrix} \frac{\partial}{\partial x} & 0 & 0 \\ 0 & \frac{\partial}{\partial y} & 0 \\ 0 & 0 & \frac{\partial}{\partial z} \\ \frac{\partial}{\partial y} & \frac{\partial}{\partial x} & 0 \\ 0 & \frac{\partial}{\partial z} & \frac{\partial}{\partial y} \\ \frac{\partial}{\partial z} & 0 & \frac{\partial}{\partial x} \end{bmatrix} \quad \& \quad [B] = \begin{bmatrix} N_{i,x} & 0 & 0 \\ 0 & N_{i,y} & 0 \\ 0 & 0 & N_{i,z} \\ 0 & N_{i,z} & N_{i,y} \\ N_{i,z} & 0 & N_{i,x} \\ N_{i,y} & N_{i,x} & 0 \end{bmatrix} \qquad \textbf{Eq. 3.22}$$

As shown in Eq. 3.19, shape functions are calculated in the ξ, η and ζ coordinate system. To obtain the derivatives of the shape functions in Eq. 3.22 with respect to x, y and z, the shape functions must be transformed from the previous coordinate system to the x, y and z coordinate system. Again by utilizing the isoparametric concept, we have:

$$\begin{aligned} x &= \Sigma N_i x_i \\ y &= \Sigma N_i y_i \\ z &= \Sigma N_i z_i \end{aligned} \qquad \textbf{Eq. 3.23}$$

and derivatives are given by:

$$\begin{Bmatrix} N_{i,\xi} \\ N_{i,\eta} \\ N_{i,\zeta} \end{Bmatrix} = [J] \begin{Bmatrix} N_{i,x} \\ N_{i,y} \\ N_{i,z} \end{Bmatrix} \qquad \textbf{Eq. 3.24}$$

where [J] is the Jacobian matrix:

$$[J] = \begin{bmatrix} x_{,\xi} & y_{,\xi} & z_{,\xi} \\ x_{,\eta} & y_{,\eta} & z_{,\eta} \\ x_{,\zeta} & y_{,\zeta} & z_{,\zeta} \end{bmatrix} \qquad \textbf{Eq. 3.25}$$

then derivatives of shape functions with respect to x, y, and z are found from Eq. 3.24:

$$\begin{Bmatrix} N_{i,x} \\ N_{i,y} \\ N_{i,z} \end{Bmatrix} = [J]^{-1} \begin{Bmatrix} N_{i,\xi} \\ N_{i,\eta} \\ N_{i,\zeta} \end{Bmatrix} \qquad \textbf{Eq. 3.26}$$

We have the following expression for potential energy in a linearly elastic body:

$$\begin{aligned} \Pi_p = & \int_V (\frac{1}{2}\{\varepsilon\}^T[E]\{\varepsilon\} - \{\varepsilon\}^T[E]\{\varepsilon_0\} + \{\varepsilon\}^T\{\sigma_0\})dV \\ & \int_V \{u\}^T\{F\}dV - \int_S \{u\}^T\{\Phi\}dS - \{D\}^T\{P\} \end{aligned} \qquad \textbf{Eq. 3.27}$$

where,

$\{u\}$ = the displacement field
$\{\varepsilon\}$ = the strain field
$[E]$ = the material property matrix
$\{\varepsilon_0\}$ and $\{\sigma_0\}$ = initial strains and initial stresses
$\{F\}$ = body forces
$\{\Phi\}$ = surface tractions
$\{D\}$ = nodal d.o.f. of the structure
$\{P\}$ = loads applied to d.o.f. by external agencies
S and V = surface area and volume of the structure

By substituting expressions for $\{u\}$ and $\{\varepsilon\}$ (Eqs. 3.20 and 3.21) into Eq. 3.27, we obtain:

$$\Pi_p = \frac{1}{2}\sum_{n=1}^{numel} \{d\}_n^T[K]_n\{d\}_n - \sum_{n=1}^{numel} \{d\}_n^T\{r\}_n - \{D\}^T\{P\} \qquad \textbf{Eq. 3.28}$$

where summation symbols indicate that contributions from all elements of the structure are included, and we define the stiffness matrix [k] and load array $\{r\}$ of an element by:

$$[k] = \int_{V_e} [B]^T[E][B]dV \qquad \textbf{Eq. 3.29}$$

and,

$$\{r\} = \int_{V_e}[B]^T[E]\{\varepsilon_0\}dV - \int_{V_e}[B]^T\{\sigma_0\}dV + \int_{V_e}[N]^T\{F\}dV + \int_{S_e}[N]^T\{\Phi\}dS \qquad \textbf{Eq. 3.30}$$

where,

S_e and V_e = surface area and volume of the element, respectively.

It must be mentioned that the expression for the load array {r} appears more complicated than the stiffness matrix [k], but in fact, [k] contains the greater number of calculation steps. To complete the derivation, we must determine the algebraic equations to be solved for the nodal d.o.f. as follows. By considering Eq. 3.28, every local degree of freedom in an element vector {d} also appears in the vector of global degrees of freedom {D}. Therefore {D} can replace {d} in Eq. 3.28, if [k] and {r} of every element are conceptually expanded to structural size. Thus Eq. 3.28 becomes:

$$\Pi_p = \frac{1}{2}\{D\}^T[K]\{D\} - \{D\}^T\{R\} \qquad \textbf{Eq. 3.31}$$

where,

$$[K] = \sum_{n=1}^{numel}[k]_n \quad \text{and} \quad \{R\} = \{P\} + \sum_{n=1}^{numel}\{r\}_n \qquad \textbf{Eq. 3.32}$$

Now by making Π_p stationary with respect to small changes in the D_i, we have:

$$\left\{\frac{\partial \Pi_p}{\partial D}\right\} = \{0\} \quad \text{yields} \quad [K]\{D\} = \{R\} \qquad \textbf{Eq. 3.33}$$

3.3.7 Fast Formation of Element Stiffness Matrix

The number of computational operations to build the stiffness matrix of a 20-node, solid element is high. By applying an organized formulation, the number of computational operations is decreased dramatically. There are several methods to reduce the number of operations [150-152]. In this study, an efficient scheme to evaluate the stiffness matrix [152] is applied and explained in the following. By referring to Eqs. 3.18, 3.22 and 3.29, the matrix product is formed explicitly. For typical nodal pairs *i* and *j*, the element stiffness matrix is given by:

$$\left[k_{ij}\right]=\int_{V_e}\left[B_i\right]^T\left[Q_j\right]dV \qquad \textbf{Eq. 3.34}$$

where,

$$\left[Q_j\right]=[E]\left[B_j\right] \qquad \textbf{Eq. 3.35}$$

thus,

$$\left[Q_j\right]=\begin{bmatrix} E_{11}N_{j,x}+E_{16}N_{j,y} & E_{16}N_{j,x}+E_{12}N_{j,y} & E_{13}N_{j,z} \\ E_{12}N_{j,x}+E_{26}N_{j,y} & E_{26}N_{j,x}+E_{22}N_{j,y} & E_{23}N_{j,z} \\ E_{13}N_{j,x}+E_{36}N_{j,y} & E_{36}N_{j,x}+E_{23}N_{j,y} & E_{33}N_{j,z} \\ E_{45}N_{j,z} & E_{44}N_{j,z} & E_{45}N_{j,x}+E_{44}N_{j,y} \\ E_{55}N_{j,z} & E_{45}N_{j,z} & E_{55}N_{j,x}+E_{45}N_{j,y} \\ E_{16}N_{j,z}+E_{66}N_{j,y} & E_{66}N_{j,z}+E_{26}N_{j,y} & E_{36}N_{j,z} \end{bmatrix} \qquad \textbf{Eq. 3.36}$$

and

$$\left[k_{ij}\right]=\int_V\begin{bmatrix} N_{i,x}Q_{11}+N_{i,y}Q_{61}+N_{i,z}Q_{51} & N_{i,x}Q_{12}+N_{i,y}Q_{62}+N_{i,z}Q_{41} & N_{i,x}Q_{13}+N_{i,y}Q_{63}+N_{i,z}Q_{53} \\ N_{i,x}Q_{61}+N_{i,y}Q_{21}+N_{i,z}Q_{41} & N_{i,x}Q_{62}+N_{i,y}Q_{22}+N_{i,z}Q_{42} & N_{i,x}Q_{63}+N_{i,y}Q_{23}+N_{i,z}Q_{43} \\ N_{i,x}Q_{51}+N_{i,y}Q_{41}+N_{i,z}Q_{31} & N_{i,x}Q_{41}+N_{i,y}Q_{42}+N_{i,z}Q_{32} & N_{i,x}Q_{53}+N_{i,y}Q_{43}+N_{i,z}Q_{33} \end{bmatrix}dV$$

Eq. 3.37

Now the stiffness matrix for each element is in a more compact form. Also the stiffness matrix is symmetric and only half of it would be formed during numerical integration.

3.3.8 Coordinate Systems

When there are skewed boundary conditions [153] for nodes, for example, radial boundary conditions around a pin-loaded hole, coordinate system must be transformed from Cartesian to Cylindrical (Fig. 3.7).

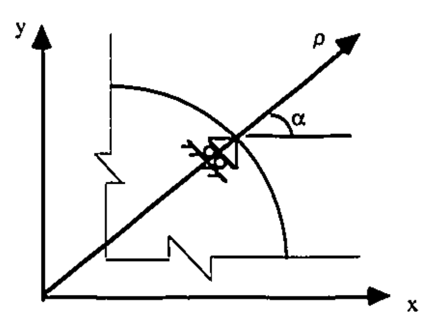

Fig. 3.7 Radial boundary condition for a node on a hole boundary

By this transformation, skewed boundary conditions may be treated as normal boundary conditions. The transformation equation for the stiffness matrix and load vector of an element that has skewed boundary conditions for some of its nodal points in Cylindrical coordinates is:

$$[k]_{p-c} = [T]^T [k]_c [T]$$
$$\{r\}_{p-c} = [T]^T \{r\}_c \qquad \textbf{Eq. 3.38}$$

where p and c mean Cylindrical and Cartesian coordinates, and

$$[T] = \begin{bmatrix} [I] & & & 0 & & \\ & [I] & & & & \\ & & \ddots & & & \\ & & & [t_i] & & \\ & & & & \ddots & \\ & 0 & & & & [I] \end{bmatrix}_{20*20} \qquad \textbf{Eq. 3.39}$$

where [I] is identity (or unit) matrix and,

$$[t_i] = \begin{bmatrix} \cos\alpha_i & \sin\alpha_i & 0 \\ -\sin\alpha_i & \cos\alpha_i & 0 \\ 0 & 0 & 1 \end{bmatrix} \qquad \textbf{Eq. 3.40}$$

where i is the number of node that is located in Cylindrical coordinates. Finally, we find $\{D\}_c$ by the following equation:

$$\{D\}_c = [T]\{D\}_{p-c} \qquad \textbf{Eq. 3.41}$$

This transformation is performed before the formation of the global stiffness matrix, thus making the method efficient.

3.3.9 Boundary Conditions

By considering the symmetry of $[0_4/90_4]_s$ and $[90_4/0_4]_s$ pin/bolt-loaded composite plates with respect to 1-2 and 3-1 planes, one quarter of the specimen is modeled in the finite element analysis (Fig. 3.8). For $[+45_4/-45_4]_s$ there is symmetry and antisymmetry with respect to 1-2 and 3-1 planes, respectively. Therefore one half of the specimen should be considered in the finite element analysis. However it was shown [123] that if one quarter of the specimen was considered, the only significant differences for stresses in some layers occurred on the $\theta = 0^\circ$ line (Fig. 2.1), and the error was less than 5%. By accepting this minor deviation, one quarter of the specimen has also been considered for the $[+45_4/-45_4]_s$.

Plane	Boundary Cond.		
	x	y	z
BCIH	0	1	0
DEKJ	0	1	0
GHKL	0	0	1

Fixed = 1
Free = 0

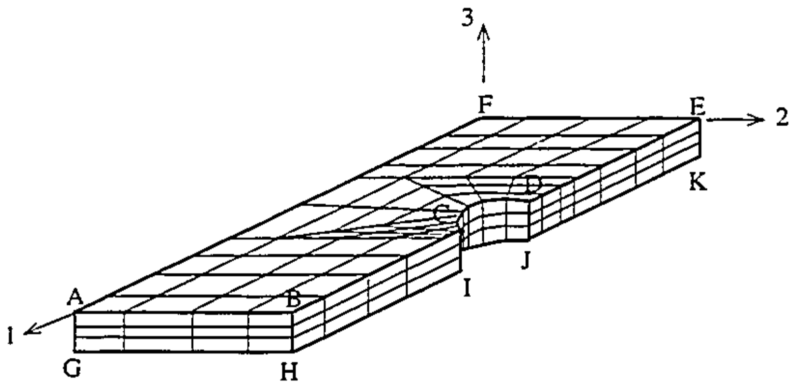

Fig. 3.8 Finite element model

To simulate the pin load, different techniques have been used in the literature. Matthews *et al.* [123] and Sperling [124] simulated a rigid pin by attaching high stiffness bar elements between the hole center and nodes on the loaded side of the hole. They applied the pin load by applying a suitable displacement to the hole center. However, in a progressive damage simulation, reducing the material properties of the failed elements on the loaded side of the hole, connected to high stiffness bar (rigid) elements, can cause a numerical instability. Marshall *et al.* [125] fixed the degrees of freedom of all nodes of the loaded region in the radial direction. Also, by applying tangential displacement boundary conditions, they simulated the friction between pin and hole. Applying a cosine distributed load on the loaded side of the hole is another method which has been shown to be inaccurate when the degree of orthotropy increases [154]. Chaudhary and Bathe [155] developed a method for applying the contact load which seems to be more realistic. However using their method is time consuming and expensive. To consider the singularity, a large number of elements must be used which makes the analysis expensive and adding the contact element to the model makes it even more costly. By considering the advantages and disadvantages of these methods, in the present study, radial displacement boundary conditions have been applied to nodes around the hole at the load region (nodes from $\theta = 0°$ to $82.5°$ restrained radially [123]). Previous experience shows that applying tangential boundary conditions to simulate the friction between the pin and the edge of the hole, induces an over constraint on the model and the results are not reliable [41]. Therefore, friction between the pin and the hole is not considered here. To simulate a fully tightened bolt, a uniform pressure is applied on the washer region. Moreover, to simulate friction between the washer and the plate, fixed displacement boundary conditions in radial and tangential directions are applied on nodes on the surface of the composite plate and under the washer region. The load "P" is applied as a uniformly distributed negative pressure on the end edge of the composite laminate (Fig. 2.1).

3.3.10 Method of Solution for a System of Nonlinear Algebraic Equations

In order to solve Eq. 3.33, different techniques can be applied. However because of the large number of degrees of freedom (d.o.f.) used in the finite element model, the stiffness matrix [K] is a large matrix (d.o.f. by d.o.f.). The costly way to store the stiffness matrix is to save it in form of an array of dimension K(i,j). However, the stiffness matrix [K] is symmetric and there are many unnecessary zero elements in it which are never needed in the calculations. A more effective method which is called the *skyline storage scheme* is used to store [K] in a compact form. Because of this special storage scheme, a modified Gauss elimination technique called *the active column solution* or *the skyline solution* [156] has been used to find the inverse of the stiffness matrix.

By considering material nonlinearity, Eq. 3.33 is a set of nonlinear equations which must be solved by a suitable nonlinear solution technique. The Newton-Raphson technique is a good candidate for this purpose. However in this technique stiffness matrix must be updated in each iteration, which is a computer-time consuming task that should be avoided. Therefore in this study, a modified Newton-Raphson technique [161] has been applied. In this technique, the stiffness matrix is updated after four iterations and at the beginning of each new load step.

The developed finite element code is evaluated by standard patch test methods [157]. The code passed the test successfully, but due to space limitations, the results of the patch test are not presented here.

3.4 Stress Analysis Results

Some of the most important and interesting results of the stress analysis are presented in this section. For more information about the three-dimensional stress analysis of simple and pin/bolt-loaded composite laminates with a detailed interpretation, the reader can refer to the results published by the author [127-130].

The fairly optimum mesh size and mesh distribution for achieving a reliable stress state of the problem were found by trial and error. By refining the meshes, smooth stress distributions for all six stresses from the edge of the hole to the far field region are achieved. It should be noted that for AS4/3501-6 with a fiber volume of 62% and a fiber diameter of 8 μm, to satisfy the orthotropic behaviour of an element, the smallest element should have a minimum dimension of 0.013 mm.

Otherwise, the dimension of the smallest element would be smaller than the fiber diameter or spacing between fibers.

To study the effects of material nonlinearity and bolt load, all six components of the stress tensor near the edge of the hole and along the interface between the two layers with different orientations are examined. Although the stresses for all different points of the composite laminate are used for failure analysis, however the stresses far from the edge of the hole are not discussed in this chapter. First the effect of material nonlinearity on the state of stress of a pin-loaded composite laminate is explained. Moreover, the effect of bolt load on the stress state near the edge of the hole is considered and discussed. As mentioned earlier, two different cross-ply laminates, $[0_4/90_4]_S$ and $[90_4/0_4]_S$, and an angle-ply laminate, $[+45_4/-45_4]_S$, are considered.

3.4.1 Effects of Material Nonlinearity

3.4.1.1 Cross-Ply $[0_4/90_4]_s$

All six stresses of a $[0_4/90_4]_s$ cross-ply laminate, along the interface between the two layers with different orientations at the hole edge, for linear and nonlinear cases, are shown in Fig. 3.9. Inducing material nonlinearity for shear stress-strain response in the x-y and x-z planes decreases σ_{xy} and σ_{xz}, respectively. As shown in Fig. 3.9, σ_{xz} is decreased between $30^o < \theta < 60^o$ for the nonlinear case, and it remains nearly the same for the linear and nonlinear cases at $0^o < \theta < 30^o$ and at $60^o < \theta < 180^o$. As shown in Fig. 3.9, σ_{xy} is reduced at $10^o < \theta < 85^o$ and at $100^o < \theta < 135^o$ for the nonlinear case, and remains nearly the same for linear and nonlinear cases elsewhere. By considering σ_{xx} in Fig. 3.9, it is evident that the material nonlinearity does not have a significant effect on the longitudinal stress. However as shown in Fig. 3.9, σ_{yy} and σ_{yz} are increased significantly for $0^o < \theta < 85^o$ for the nonlinear case. By comparing the linear and nonlinear interlaminar normal stress (σ_{zz}) curves in Fig. 3.9, it is seen that nonlinearity increases the magnitude of interlaminar normal stress (σ_{zz}) at $\theta = 0^o$ and at $\theta = 90^o$, while it decreases around $\theta = 45^o$. Increasing σ_{zz} and σ_{yz} can create delamination which is not favoured in the design of laminated composites.

3.4.1.2 Cross-Ply $[90_4/0_4]_s$

Results of the stress analysis of $[90_4/0_4]_S$ cross-ply, for linear and nonlinear cases are shown in Fig. 3.10. By comparing Figs. 3.9 and 3.10, it is clear that longitudinal and transverse stresses (σ_{xx} and σ_{yy}) for both cross-plies ($[0_4/90_4]_S$ and $[90_4/0_4]_S$) are exactly the same. Also, interlaminar shear stresses (σ_{xz} and σ_{yz}) have the same magnitudes but different signs. However, the normal stress (σ_{zz}) is different for the two cases. By comparing σ_{zz} in Figs. 3.9 and 3.10, for the linear case (solid curves) it is seen that the magnitude of normal stress (σ_{zz}) at $\theta = 0^{o}$, for $[0_4/90_4]_s$ case is higher than that of $[90_4/0_4]_s$ case. This evidence qualitatively confirms the experimental results reported in [158], where it was found that lay-ups with 90^{o} layers located at the surface, under pin-load conditions, show superior bearing strength. However, it must be emphasized that without applying a progressive damage model the difference in strength between $[0_4/90_4]_s$ and $[90_4/0_4]_s$ can not be shown quantitatively. By considering Fig. 3.10, it is seen that, like the $[0_4/90_4]_s$ case, material nonlinearity shifted σ_{zz} at $\theta = 0^{o}$, from the negative towards positive magnitudes which again is not favoured in design.

3.4.1.3 Angle-Ply $[+45_4/-45_4]_s$

The distribution of all six stresses of an angle-ply $[+45_4/-45_4]_s$ along the hole edge, for linear and nonlinear cases, are shown in Fig. 3.11. As shown in Figs. 3.11, material nonlinearity decreased the magnitudes of σ_{xz} and σ_{xy}. By examining σ_{xz} in Fig. 3.11, it is clear that this stress is decreased at $45^{o} < \theta < 120^{o}$. Also, as shown in Fig. 3.11, σ_{xy} is reduced at $0^{o} < \theta < 35^{o}$ and at $50^{o} < \theta < 130^{o}$ for the nonlinear case, and it remains nearly the same elsewhere. By considering Fig. 3.11, it is seen that the material nonlinearity increased the longitudinal stress (σ_{xx}) locally at $\theta = 45^{o}$. By considering σ_{yy} and σ_{yz} in Fig. 3.11, it is clear that, for nonlinear case, these stresses are increased at $0^{o} < \theta < 135^{o}$ and remain constant at $135^{o} < \theta < 180^{o}$. Interlaminar normal stress (σ_{zz}), in Fig. 3.11, is decreased at $0^{o} < \theta < 25^{o}$ and is increased at $25^{o} < \theta < 90^{o}$ and at $110^{o} < \theta < 160^{o}$ due to material nonlinearity, and it remains nearly the same elsewhere. It must be mentioned again that increasing σ_{zz} and σ_{yz} can create delamination which is not favoured in the design of composite laminates.

3.4.1.4 Summary of the Effects of Material Nonlinearity

In general, by inducing the material nonlinearity for shear stress-strain response of (σ_{xy} - ε_{xy} and σ_{xz} - ε_{xz}), relevant stresses (σ_{xy} and σ_{xz}) are decreased for all three different configurations (two cross-ply laminates and one angle-ply). However, by looking at the behaviour of longitudinal stress (σ_{xx}) for the three configurations, Fig. 3.9 to 3.11, it is clear that this stress is not strongly effected by inducing the mentioned material nonlinearity. Moreover, transverse stress (σ_{yy}) and one of the interlaminar stresses (σ_{yz}) are significantly increased at $0^{o} < \theta < 90^{o}$ for all three configurations. Also, interlaminar normal stress (σ_{zz}) is increased and shifted towards the positive magnitudes for all three cases. Thus, considering material nonlinearity causes significant decrease in magnitudes of some stresses while others are increased to compensate.

3.4.2 Effects of Bolt Load

As mentioned earlier, the state of stress on the edge of the hole (which is a site for failure initiation) and the effects of the bolt load on the stresses at that location are discussed here. The stress state far from the edge of the hole is also important and will be used for failure analysis later.

3.4.2.1 Cross-ply Laminates $[0_4/90_4]_s$ and $[90_4/0_4]_s$

In Figs. 3.12 and 3.13, six different stresses for $[0_4/90_4]_S$ and $[90_4/0_4]_S$ under bolt loading conditions (by considering the material nonlinearity) are shown, respectively. By comparing the results of stress analysis for a pin-loaded $[0_4/90_4]_S$ in Fig. 3.9 and a bolt-loaded $[90_4/0_4]_S$ in Fig. 3.12, it is clear that by applying bolt load, all stresses are decreased dramatically by some orders of magnitude. The decrease in the state of stress near the edge of the hole is accompanied by an increase in the magnitudes of stresses far from the edge of the hole which are certainly not as critical as the magnitudes of stresses right at the edge. By comparing normal stress, σ_{zz}, and interlaminar shear stresses, σ_{xz} and σ_{yz}, in Figs. 3.12 and 3.13, it is concluded that applying bolt load can decrease the normal and interlaminar shear stresses of the $[0_4/90_4]_S$ case more than the $[90_4/0_4]_S$ case. By comparison between the pinned and bolted $[0_4/90_4]_S$ cases in Figs. 3.9 and 3.12, it can be seen that the effect of the bolted washer decreases the interlaminar shear stresses, σ_{xz} and σ_{yz}, by a greater factor than the out-of-plane normal stress, σ_{zz}.

3.4.2.2 Angle-ply Laminate $[+45_4/-45_4]_s$

In Fig. 3.14, six different stresses for $[+45_4/-45_4]_S$ under bolt loading conditions (by considering the material nonlinearity) are shown. Similar to cross-ply laminates, by applying bolt load, all stresses are decreased dramatically. Furthermore, as in the case of cross-ply laminates, bolt loading changed the sign of all positive normal stresses, σ_{zz}, to negative which is favored in the design of composite joints.

3.5 Summary

A three-dimensional nonlinear finite element algorithm is developed in this chapter. The three-dimensional stress state of the pin/bolt-loaded composite laminate is calculated. The edge effect (stress singularity) which is one of the most important phenomenon in fatigue behaviour of composite laminates is considered. The effect of material nonlinearity and the bolt load on the states of singular stress near the edge of the hole and between layers with different ply orientations are studied. Therefore, the first component of the *progressive fatigue damage model* is established. So far, we are able to analyze the three-dimensional stress state of a complicated example such as pin/bolt-loaded composite laminates. However, to check the failure initiation and propagation, the stresses should be examined by a set of failure criteria which is the subject of the following chapter. The second component of the *model*, failure analysis, is presented and discussed in the next chapter.

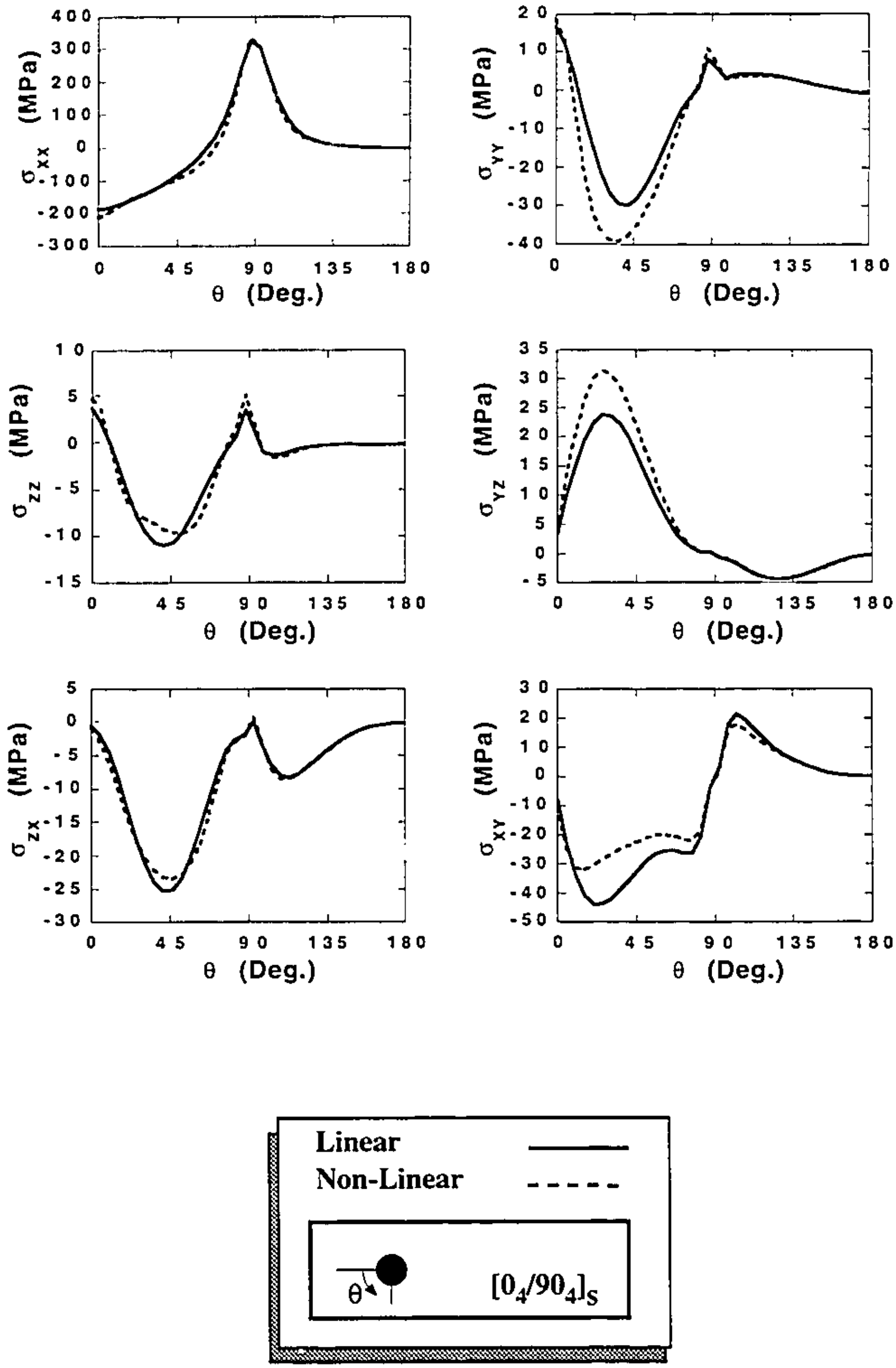

Fig. 3.9 Variation of stresses of a pin-loaded $[0_4/90_4]_s$ case along θ at the 0°/90° interface

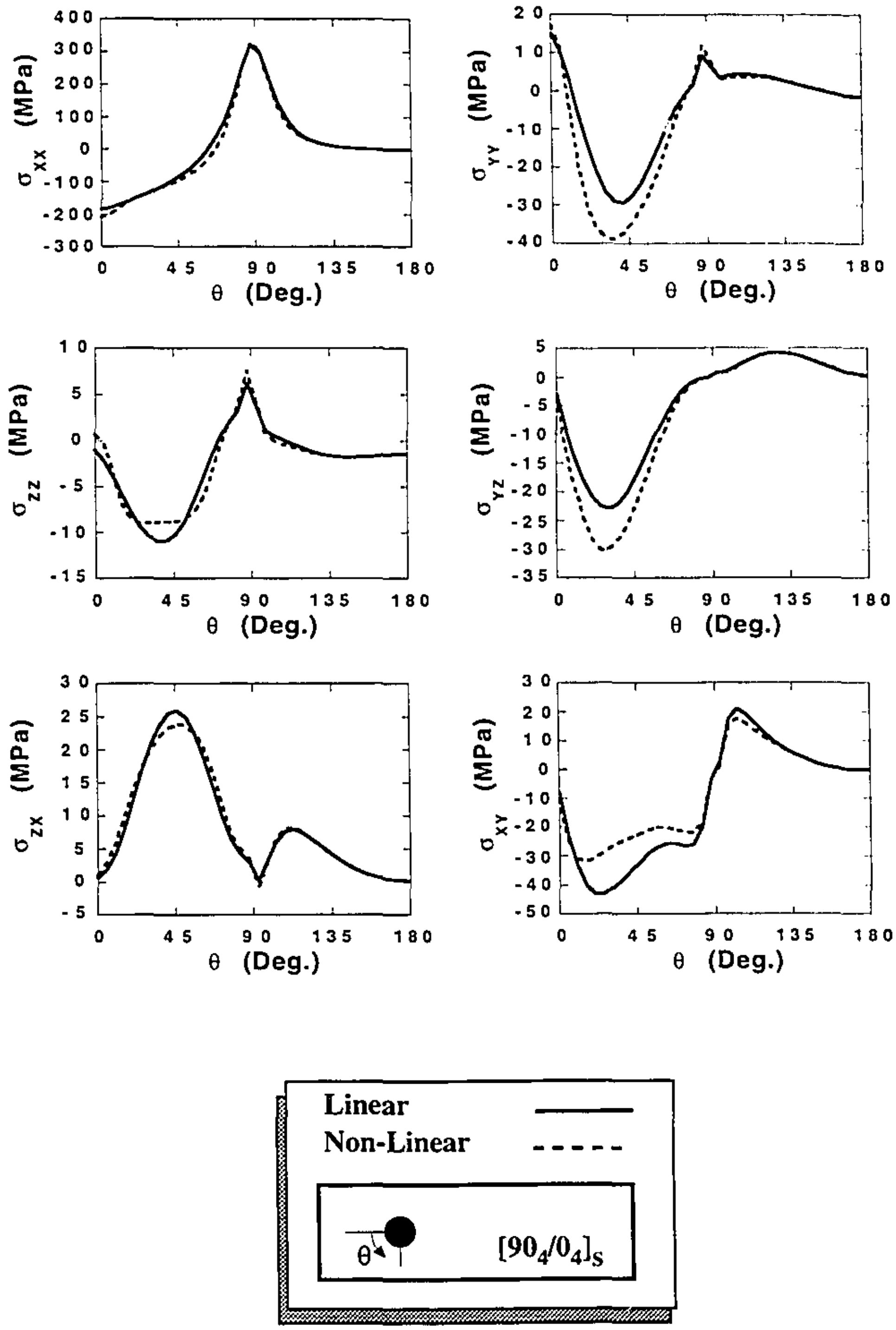

Fig. 3.10 Variation of stresses of a pin-loaded $[90_4/0_4]_s$ case along θ at the 90°/0° interface

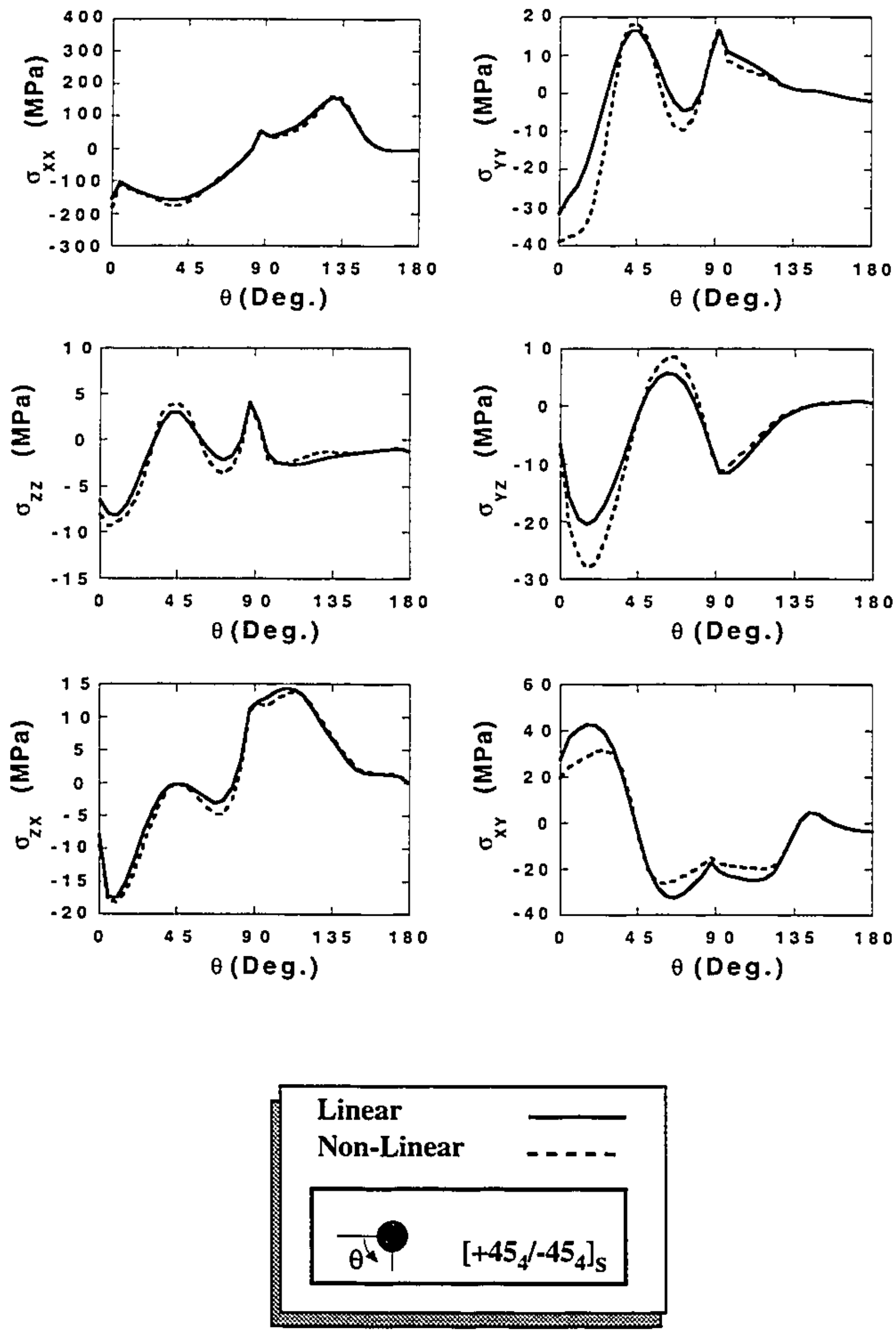

Fig. 3.11 Variation of stresses of a pin-loaded $[+45_4/-45_4]_s$ case along θ at the +45°/-45° interface

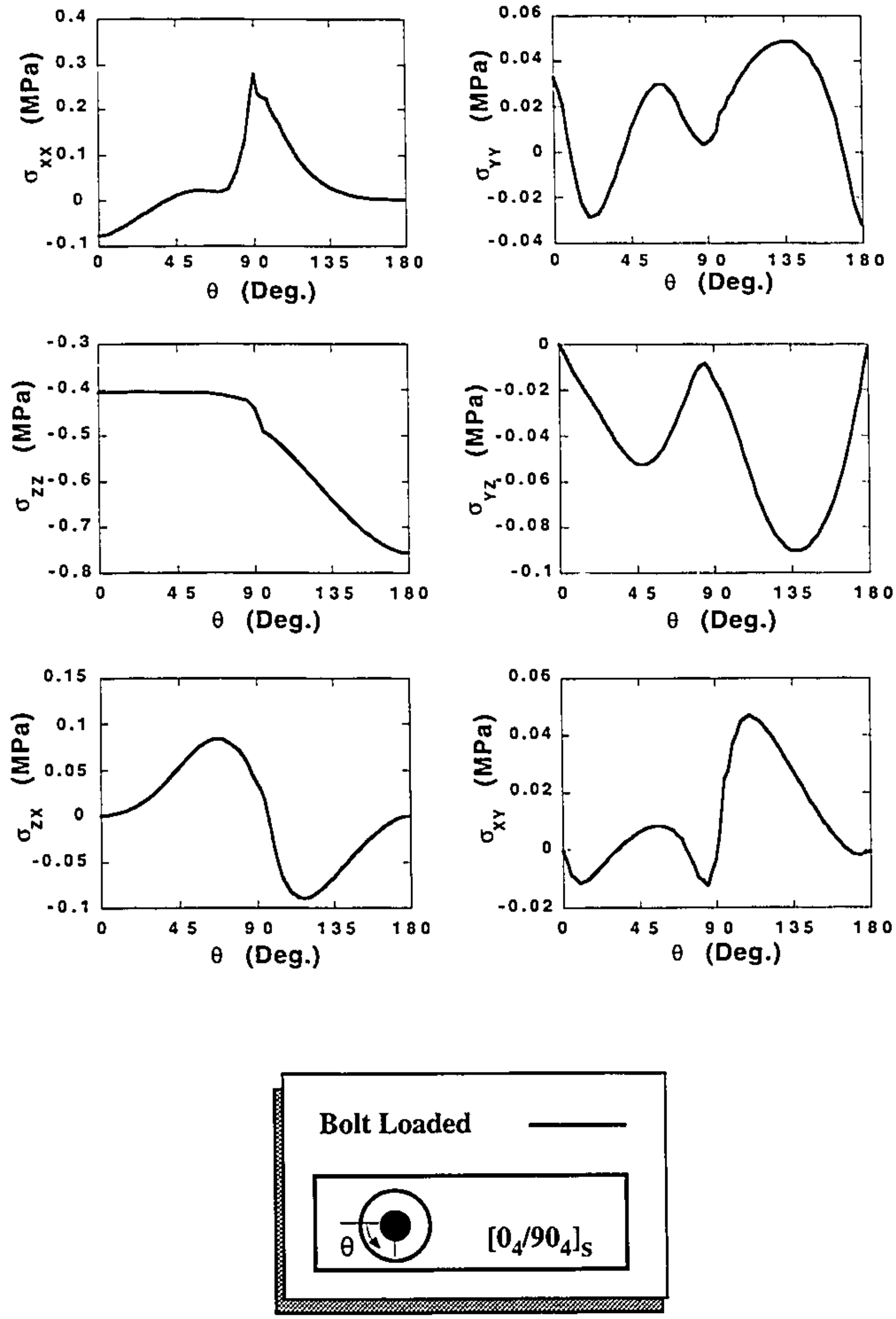

Fig. 3.12 Variation of stresses of a bolt-loaded $[0_4/90_4]_s$ case along θ at the 0°/90° interface

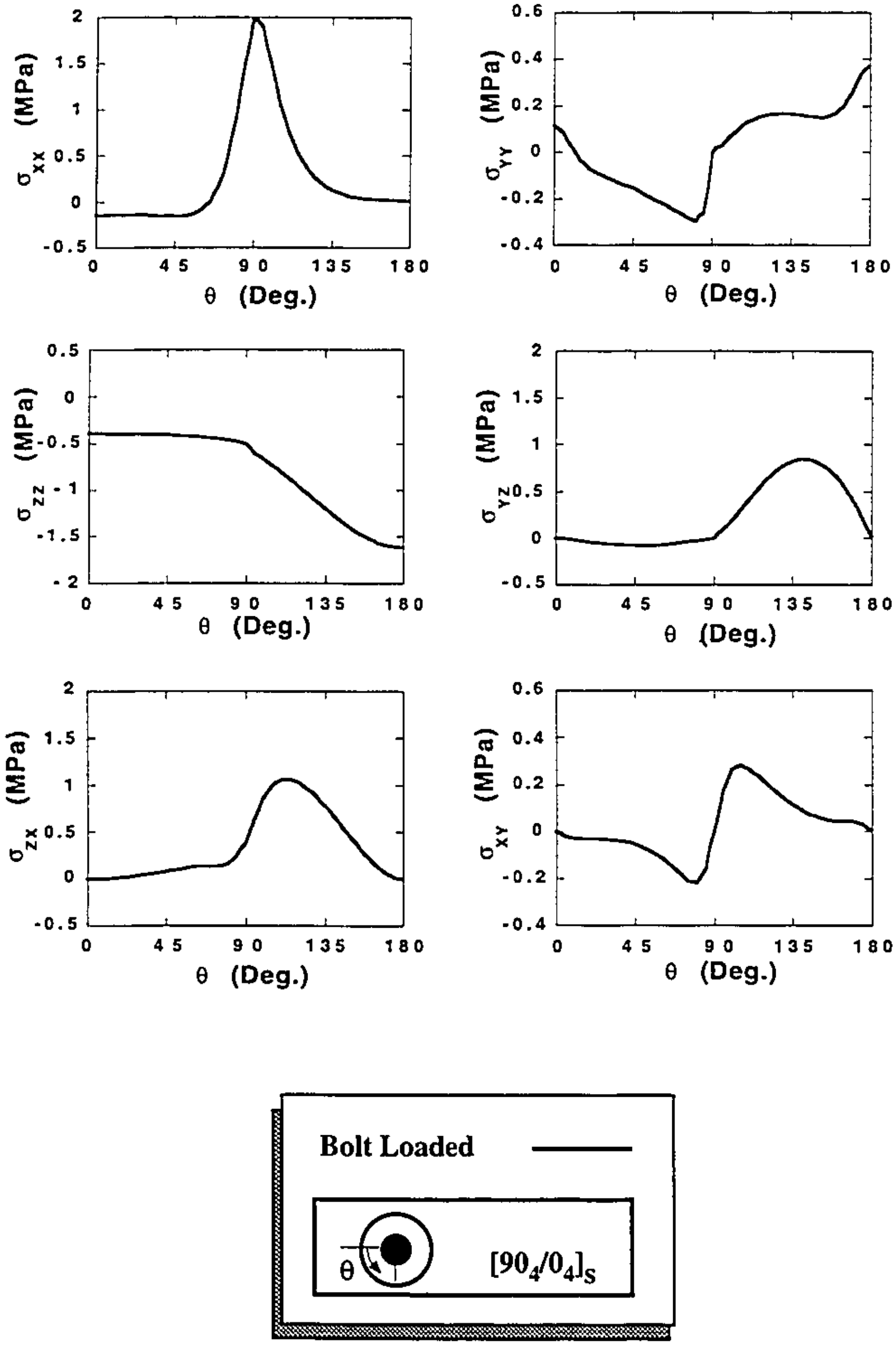

Fig. 3.13 Variation of stresses of a bolt-loaded $[90_4/0_4]_s$ case along θ at the 90°/0° interface

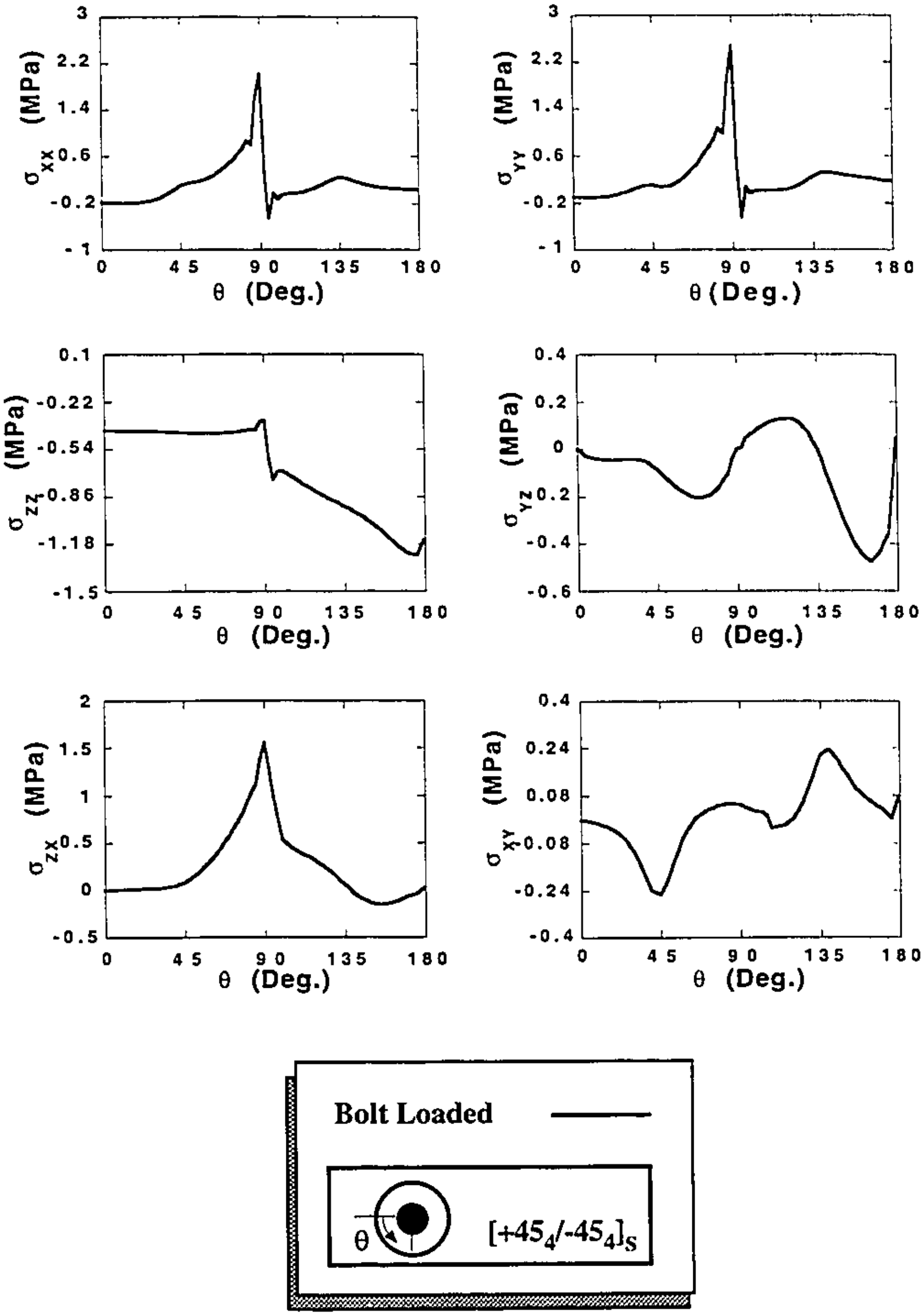

Fig. 3.14 Variation of stresses of a bolt-loaded $[+45_4/-45_4]_s$ case along θ at the +45°/-45° interface

Chapter 4

Failure Analysis

In this chapter, the second component of the *model*, failure analysis is discussed. Seven different failure modes for the unidirectional ply under multiaxial state of stress are considered which are: fiber tension, fiber compression, fiber-matrix shearing, matrix tension, matrix compression, normal tension and normal compression failure modes. Suitable stress-based failure criteria for detecting these modes of failure under static and fatigue loading conditions are derived. The effect of material nonlinearity on the mathematical form of the failure criteria is also considered. Difficulties and limitations of application of such failure criteria, in traditional forms, for unidirectional plies under multiaxial fatigue loading conditions for general stress state and stress ratios are discussed.

4.1 An Introduction to Failure Analysis

To analyze the strength of any laminated composite, it would be extremely costly and time consuming to perform static tests for all possible stacking sequences. To predict the strength of a unidirectional composite ply under multiaxial state of stress, strength theories are established by investigators. Failure analysis is a tool for predicting the strength of a laminated composite, containing several plies with different orientations, under complex loading conditions using strength data obtained from uniaxial tests of unidirectional plies and strength theories. As a direct result of the complex nature of observed failure phenomena, there are numerous strength theories in the form of different failure criteria for unidirectional composite materials under multiaxial loading conditions (see [162] as a review). A survey of the literature reveals that different types of failure criteria have been used by various authors in the design of composite laminates. A list of the various types of failure criteria used for failure analysis of pin-loaded composite laminates by different authors is given in Table 4.1.

Author(s)	**Finite Element Analysis (two-dimensional)**	**Applied Failure Criteria**
Waszczak and Cruse [165]	Linear	Distortional Energy criteria Max. Stress and Max. Strain
Humphris [166]	Linear	Hill-Tsai criteria
Agarwal [167]	Linear	Average stress criteria
Shokrieh [41] Lessard and Shokrieh [42]	Linear	Modified Hashin criteria (Progressive Damage Model)
Chang, *et al.* [168]	Linear	Yamada criteria (at characteristic distance)
Chang, *et al.* [169-171]	Linear	Yamada-Sun criteria (at characteristic distance)
Chang, *et al.* [172]	Nonlinear (material)	Yamada-Sun criteria (at characteristic distance)
Tsujimoto and Wilson [173]	Elasto-Plastic	Hill criteria
Soni [174]	Linear	Tsai-Wu
Chang and Chang [43]	Nonlinear (material and geometry)	Modified Hashin criteria (Progressive Damage Model)
Lessard and Shokrieh [175]	Nonlinear (material and geometry)	Modified Hashin criteria (Progressive Damage Model)
Tsiang and Mandell [176]	Linear, Hybrid	Tsai-Hill and criteria Max. Stress criteria
Conti [177]	Linear	Azzi-Tsai criteria
Serabian and Oplinger[178]	Nonlinear (material)	Hoffman criteria

Table 4.1 Different stress analysis techniques and failure criteria used by different authors to analyze pin-loaded composite laminates

Among the different failure criteria, the classic quadratic failure criterion by Tsai and Wu [163] is useful for predicting first ply failure, but cannot distinguish the modes of failure. Consequently, it cannot indicate how to properly degrade material properties in damaged areas. Maximum Stress or Maximum Strain criteria [131] are useful because these criteria determine the modes of failure, however the lack of interaction terms with shear stresses makes these criteria quite conservative. Hashin type failure criteria [164] are in polynomial forms similar to the quadratic failure envelope except that in the Hashin formulation, there are distinct polynomials corresponding to the different failure modes. Thus, the Hashin-type criteria combine the advantages of accuracy found in the quadratic criteria and the ability to distinguish failure modes found in the maximum stress criteria. This makes the Hashin-type failure criteria ideal for use in progressive damage models [41-43]. By noting the advantages of the Hashin-type failure criteria, quadratic polynomial stress based failure criteria capable of distinction of different modes of failure are developed for static and fatigue failure analysis in this research.

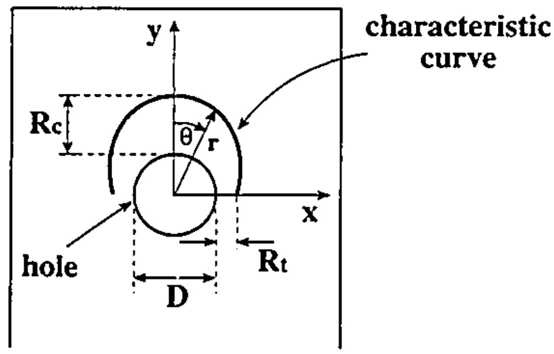

Fig. 4.1 In characteristic distance approach stresses are analyzed along a curve described by two fitting parameters, R_t and R_c

By considering the existence of singular stresses near the edge of the hole of a pin-loaded composite laminate (discussed in Chapter three), using an average stress approach [179] in the polynomial type failure criteria seems to be appropriate. In this approach, stresses are examined at a certain distance "d_0" from the stress concentration and final failure is predicted when stresses at this distance reach a critical value (Fig. 4.1). The drawbacks of the characteristic distance method are that: 1) only final failure load can be determined and the mechanism of failure is not achieved, and, 2) characteristic distance, an empirical experimental parameter, must be introduced which is material and layup dependent. By considering the aforementioned limitations, noticing the lack of a physical meaning for the characteristic distance concept, and the discrepancies found in the literature regarding the magnitude of the characteristic distance (see Table 4.2), this approach is not used in this research.

Characteristic Distance		
Reference	**Material**	**Magnitude**
Kim and Soni [180]	T300/5208	1.00 * ply thickness
Jen *et al.* [181]	T300/5208	2.00 * ply thickness
Soni and Kim [182]	T300/1034-c	1.00 * ply thickness
Ye [183]	T300/648-BF3/MEA T300/648-DDS	2.00 * ply thickness
Kim [184]	T300/934C	1.00 * ply thickness
Sun and Zhou [185]	AS4/3501-6	2.00 * ply thickness
Brewer and Lagace [186]	AS4/3501-6	1.05 * ply thickness
Joo and Sun [187]	AS4/3501-6	1.50 * ply thickness

Table 4.2 Different magnitudes of characteristic distances used in the literature

In this study, instead of using the characteristic distance approach, the magnitude of stresses are calculated and averaged at the twenty-seven Gauss points for each twenty-node quadratic isoparametric solid element in the finite element model and examined by the polynomial type failure criteria. Thus, the stresses are averaged within an element rather than over a fixed distance.

4.2 Static Failure Criteria

Before explaining the failure criteria for fatigue loading conditions, it is helpful to establish the static failure criteria for detecting the failure of a unidirectional ply under multiaxial state of stress. As previously mentioned in Chapter one, the behaviour of a unidirectional ply under various types of static loading is completely different. Experimental evidence shows that the failure behaviour of a unidirectional ply loaded in tension or compression in fiber or matrix directions or under in-plane or out-of-plane shear loading conditions are clearly different. The behaviour of a unidirectional ply under a multiaxial state of stress is even more complicated. In Fig. 4.2, a laminated composite under uniaxial loading conditions is shown. Each point of the laminated composite can be considered to be a unidirectional ply under multiaxial state of stress in the on-axis coordinate system, shown in Fig. 4.2. To establish the failure criteria, capable of detecting the modes of failure, it is assumed that the three on-axis stresses σ_{xx}, σ_{xy} and σ_{xz} are responsible for creation of failure in fiber direction. Also, the other three on-axis stresses σ_{yy}, σ_{xy} and σ_{yz} cause failure in matrix direction. Moreover, the three on-axis stresses σ_{zz}, σ_{xz} and σ_{yz} are responsible for creation of failure in normal direction. According to the sign of σ_{xx}, σ_{yy} and σ_{zz}, the failure occurs in tension or compression in the longitudinal, transverse and normal directions, respectively.

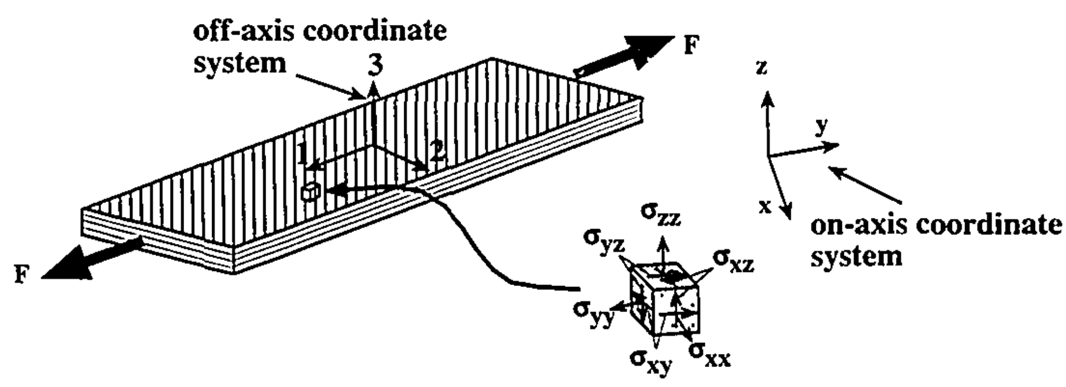

Fig. 4.2 On-axis stresses of a unidirectional ply under multiaxial stress state, responsible for causing different modes of failure

For each mode of failure, a suitable quadratic polynomial failure criteria is established. The following failure criteria are developed in this study based on the quadratic polynomial forms for detecting different modes of failure of a unidirectional ply under multiaxial state of stress. The traditional form of failure criteria for the linear cases are modified for the nonlinear situation (for detailed explanation, refer to [172]).

4.2.1 Fiber Tension Static Failure Mode

For fiber tension static failure mode ($\sigma_{xx} > 0$), of a unidirectional ply under a multiaxial state of static stress, the following criterion is used:

$$\left(\frac{\sigma_{xx}}{X_t}\right)^2 + \frac{\int_0^{\varepsilon_{xy}} \sigma_{xy} d\varepsilon_{xy}}{\int_0^{\varepsilon_{xy}^u} \sigma_{xy} d\varepsilon_{xy}} + \frac{\int_0^{\varepsilon_{xz}} \sigma_{xz} d\varepsilon_{xz}}{\int_0^{\varepsilon_{xz}^u} \sigma_{xz} d\varepsilon_{xz}} = e_{F^*}^2 \qquad \text{(if } e_{F^*} > 1\text{, then failure)} \qquad \textbf{Eq. 4.1}$$

where X_t is the longitudinal tensile strength of a unidirectional ply under uniaxial static tensile stress in the fiber direction. By considering the nonlinear shear stress-strain behaviour of the unidirectional ply in x-y plane, the second and third terms in Eq. 4.1 appear in integral forms. In the denominator of the second and third terms, the upper limits of integration are the ply ultimate in-plane and out-of-plane shear strain, respectively. By introducing the ply shear stress-strain relationship of Eq. 3.3 and 3.5, we obtain:

$$\left(\frac{\sigma_{xx}}{X_t}\right)^2 + \left(\frac{\dfrac{\sigma_{xy}^2}{2E_{xy}} + \dfrac{3}{4}\delta\sigma_{xy}^4}{\dfrac{S_{xy}^2}{2E_{xy}} + \dfrac{3}{4}\delta S_{xy}^4}\right) + \left(\frac{\dfrac{\sigma_{xz}^2}{2E_{xz}} + \dfrac{3}{4}\delta\sigma_{xz}^4}{\dfrac{S_{xz}^2}{2E_{xz}} + \dfrac{3}{4}\delta S_{xz}^4}\right) = e_{F^*}^2 \quad \text{(if } e_{F^*} > 1\text{, then failure)} \qquad \textbf{Eq. 4.2}$$

where δ, E_{xy}, S_{xy}, E_{xz} and S_{xz} are parameters of material nonlinearity, in-plane ply shear stiffness, in-plane ply shear strength, out-of-plane ply shear stiffness and out-of-plane ply shear strength, respectively. It should be mentioned that fiber tension failure is a catastrophic mode of failure. The material properties of the unidirectional ply, failed under this mode of failure degrade catastrophically, and the ply cannot tolerate any type or combination of stresses thereafter. More details on the material property degradation caused by this mode and the other modes will be explained in the next chapter. It should be added that by equating $\delta = 0$, the nonlinear failure criterion in form of Eq. 4.2 reduces to a linear failure criteria, as proposed by Hashin [164].

$$\left(\frac{\sigma_{xx}}{X_t}\right)^2 + \left(\frac{\sigma_{xy}}{S_{xy}}\right)^2 + \left(\frac{\sigma_{xz}}{S_{xz}}\right)^2 = e_{F^+} \qquad (\text{if } e_{F^+} > 1, \text{ then failure}) \qquad \textbf{Eq. 4.3}$$

4.2.2 Fiber Compression Static Failure Mode

For fiber compression static failure mode ($\sigma_{xx} < 0$), of a unidirectional ply under a multiaxial state of static stress, the following criterion is used:

$$\left(\frac{\sigma_{xx}}{X_c}\right) = e_{F^-} \qquad (\text{if } e_{F^-} > 1, \text{ then failure}) \qquad \textbf{Eq. 4.4}$$

where X_c is the longitudinal compressive strength of a unidirectional ply under uniaxial static compressive stress in the fiber direction. The effect of shear stresses on the compressive behaviour of a unidirectional ply is not well understood and more research must be performed to model this phenomenon [188]. Hence, for this mode of failure the interaction terms from shear stresses are not considered. Consequently, a conservative criterion for this mode of failure is presented. It should be added that the fiber compression failure is a catastrophic mode of failure and the failed ply under this mode of failure cannot tolerate any type or combination of stresses thereafter.

4.2.3 Fiber-Matrix Shearing Static Failure Mode

For the previous mode of failure, i.e. the fiber in compression failure mode, the contribution of shear stresses in the failure criterion is not considered which leads to a conservative type of criterion (Eq. 4.4). Lessard [189] considered the effect of the in-plane shear stress in compressive behaviour of a unidirectional ply in two-dimensional (biaxial) conditions. He presented a criterion which detects a mode of failure which is not as catastrophic as the fiber in compression failure mode. Here, the following equation is developed for detecting this mode for a unidirectional ply under a multiaxial state of static stress when $\sigma_{xx} < 0$:

$$\left(\frac{\sigma_{xx}}{X_c}\right)^2 + \frac{\int_0^{\varepsilon_{xy}} \sigma_{xy} d\varepsilon_{xy}}{\int_0^{\varepsilon_{xy}^u} \sigma_{xy} d\varepsilon_{xy}} + \frac{\int_0^{\varepsilon_{xz}} \sigma_{xz} d\varepsilon_{xz}}{\int_0^{\varepsilon_{xz}^u} \sigma_{xz} d\varepsilon_{xz}} = e_{FM}^2 \qquad (\text{if } e_{FM} > 1, \text{ then failure}) \qquad \textbf{Eq. 4.5}$$

Again, by considering the ply shear stress-shear strain relationship of Eq. 3.3 and 3.5, we obtain:

$$\left(\frac{\sigma_{xx}}{X_c}\right)^2+\left(\frac{\frac{\sigma_{xy}^2}{2E_{xy}}+\frac{3}{4}\delta\sigma_{xy}^4}{\frac{S_{xy}^2}{2E_{xy}}+\frac{3}{4}\delta S_{xy}^4}\right)+\left(\frac{\frac{\sigma_{xz}^2}{2E_{xz}}+\frac{3}{4}\delta\sigma_{xz}^4}{\frac{S_{xz}^2}{2E_{xz}}+\frac{3}{4}\delta S_{xz}^4}\right)=e_{FM}^2 \quad (\text{if } e_{FM}>1\text{, then failure}) \qquad \textbf{Eq. 4.6}$$

4.2.4 Matrix Tension Static Failure Mode

For matrix tension static failure mode ($\sigma_{yy} > 0$), of a unidirectional ply under a multiaxial state of static stress, the following criterion is used:

$$\left(\frac{\sigma_{yy}}{Y_t}\right)^2+\frac{\int_0^{\varepsilon_{xy}}\sigma_{xy}d\varepsilon_{xy}}{\int_0^{\varepsilon_{xy}^u}\sigma_{xy}d\varepsilon_{xy}}+\left(\frac{\sigma_{yz}}{S_{yz}}\right)^2=e_{M^+}^2 \qquad (\text{if } e_{M^+}>1\text{, then failure}) \qquad \textbf{Eq. 4.7}$$

where Y_t, and S_{yz} are the transverse tensile strength and shear strength in y-z plane, respectively. By using the transversely isotropic material property assumption, the stress-strain behaviour of the material in y-z plane is linear, therefore the third term in Eq. 4.7 does not appear in an integral form. Again, by considering the ply shear stress-shear strain relationship of Eq. 3.3, we obtain:

$$\left(\frac{\sigma_{yy}}{Y_t}\right)^2+\left(\frac{\frac{\sigma_{xy}^2}{2E_{xy}}+\frac{3}{4}\delta\sigma_{xy}^4}{\frac{S_{xy}^2}{2E_{xy}}+\frac{3}{4}\delta S_{xy}^4}\right)+\left(\frac{\sigma_{yz}}{S_{yz}}\right)^2=e_{M^+}^2 \quad (\text{if } e_{M^+}>1\text{, then failure}) \qquad \textbf{Eq. 4.8}$$

4.2.5 Matrix compression static failure mode

Similarly, for matrix compression static failure mode ($\sigma_{yy} < 0$), of a unidirectional ply under a multiaxial state of static stress, the following equation can be derived:

$$\left(\frac{\sigma_{yy}}{Y_c}\right)^2+\left(\frac{\frac{\sigma_{xy}^2}{2E_{xy}}+\frac{3}{4}\delta\sigma_{xy}^4}{\frac{S_{xy}^2}{2E_{xy}}+\frac{3}{4}\delta S_{xy}^4}\right)+\left(\frac{\sigma_{yz}}{S_{yz}}\right)^2=e_{M^-}^2 \quad (\text{if } e_{M^-}>1\text{, then failure}) \qquad \textbf{Eq. 4.9}$$

where Y_c is the transverse compressive strength of a unidirectional ply under uniaxial compressive static stress in the matrix direction.

4.2.6 Normal Tension Static Failure Mode

For normal tension static failure mode ($\sigma_{zz} > 0$), of a unidirectional ply under a multiaxial state of static stress, which in the literature is sometimes referred to as delamination in tension failure criterion, the following criterion is used:

$$\left(\frac{\sigma_{zz}}{Z_t}\right)^2 + \frac{\int_0^{\varepsilon_{xz}} \sigma_{xz} d\varepsilon_{xz}}{\int_0^{\varepsilon_{xz}^u} \sigma_{xz} d\varepsilon_{xz}} + \left(\frac{\sigma_{yz}}{S_{yz}}\right)^2 = e_{N^+}^2 \qquad \text{(if } e_{N^+} > 1\text{, then failure)} \qquad \textbf{Eq. 4.10}$$

where Z_t is the normal tensile strength of a unidirectional ply under uniaxial tensile static stress. In the denominator of the second term, the upper limit of integration is the ply ultimate shear strain. Again, by considering the ply shear stress-shear strain relationship of Eq. 3.5, we obtain:

$$\left(\frac{\sigma_{zz}}{Z_t}\right)^2 + \left(\frac{\frac{\sigma_{xz}^2}{2E_{xz}} + \frac{3}{4}\delta\sigma_{xz}^4}{\frac{S_{xz}^2}{2E_{xz}} + \frac{3}{4}\delta S_{xz}^4}\right) + \left(\frac{\sigma_{yz}}{S_{yz}}\right)^2 = e_{N^+}^2 \qquad \text{(if } e_{N^+} > 1\text{, then failure)} \qquad \textbf{Eq. 4.11}$$

4.2.7 Normal Compression Static Failure Mode

Similarly, for normal compression static failure mode ($\sigma_{zz} < 0$), of a unidirectional ply under a multiaxial state of static stress, which in the literature is sometimes referred to as delamination in compression failure criterion, the following equation can be derived:

$$\left(\frac{\sigma_{zz}}{Z_c}\right)^2 + \left(\frac{\frac{\sigma_{xz}^2}{2E_{xz}} + \frac{3}{4}\delta\sigma_{xz}^4}{\frac{S_{xz}^2}{2E_{xz}} + \frac{3}{4}\delta S_{xz}^4}\right) + \left(\frac{\sigma_{yz}}{S_{yz}}\right)^2 = e_{N^-}^2 \qquad \text{(if } e_{N^-} > 1\text{, then failure)} \qquad \textbf{Eq. 4.12}$$

where Z_c is the normal compressive strength of a unidirectional ply under uniaxial compressive static stress in the normal direction.

The aforementioned failure criteria are suitable for detecting the failure modes of a unidirectional ply under multiaxial static loading conditions. In order to apply the set of proposed static failure criteria, the material properties of a unidirectional ply under uniaxial static loading conditions in the fiber and matrix direction under tension and compression and under in-plane and out-of-plane shear loading conditions must be fully characterized. After failure detection by any of the failure criteria, the material properties of the failed material must be changed by suitable material property degradation rules which will be explained in the next chapter.

To predict the fatigue failure of a unidirectional ply under multiaxial fatigue loading conditions, a similar approach to that used for the static case is adopted and suitable polynomial fatigue failure criteria are developed in this research. In the following section, the strategy for developing quadratic polynomial failure criteria to predict the failure of a unidirectional ply under multiaxial fatigue loading conditions is explained and suitable fatigue failure criteria for each mode of fatigue failure are established. Similar to the static loading conditions, the effect of the material nonlinearity (nonlinear shear stress-strain behaviour of a unidirectional ply) on the mathematical forms of the fatigue failure criteria is also considered.

4.3 Fatigue Failure Criteria

Despite the existence of an extensive amount of research on biaxial/multiaxial fatigue of metals [190], research in the same field on composite materials [191-197] is less complete. Literature reviews on multiaxial and biaxial fatigue loading of composite materials presented by Found [196], and Chen and Matthews [197] state that further research in this field is needed.

Under fatigue loading conditions, the material is loaded by a stress state which is less than the maximum strength of the material, therefore there is no static mode of failure. However, by increasing the number of cycles, the material properties degrade and eventually lower to the level of the stress state and, at this point, catastrophic failure occurs. The idea of using polynomial failure criteria to predict the life of a composite ply under multiaxial fatigue loading has been utilized by many investigators [198-210]. They used the fatigue strength, as a function of number of cycles, in the denominators of failure criteria instead of the static strength of the material. This strategy is potentially beneficial, however in practice, the application of their models are restricted to very specific conditions.

To show the restriction of application of fatigue failure criteria in traditional forms, consider the following fatigue failure criterion introduced by Hashin [200] for fiber tension fatigue failure mode of a unidirectional ply under a two-dimensional state of stress (biaxial fatigue),

$$\left(\frac{\sigma_{xx}}{X_t(n,\sigma,\kappa)}\right)^2 + \left(\frac{\sigma_{xy}}{S_{xy}(n,\sigma,\kappa)}\right)^2 = g_f^2 \qquad \text{(if } g_f > 1\text{, then failure)} \qquad \textbf{Eq. 4.13}$$

where $X_t(n,\sigma,\kappa)$ is the residual longitudinal tensile strength of a unidirectional ply under uniaxial fatigue loading, and $S_{xy}(n,\sigma,\kappa)$ is the residual in-plane shear strength of a unidirectional ply under uniaxial shear fatigue loading conditions. Both X_t and S_{xy} are functions of n, σ and κ, which are number of cycles, stress state and stress ratio, respectively.

The fatigue behaviour of a composite lamina varies under different states of stress. For instance, under high level state of stress, the residual strength as a function of number of cycles is nearly constant and it decreases drastically at the number of cycles to failure (Fig. 4.3). The *sudden death model* [211,212] is a suitable technique to describe this behaviour. However at low level state of stress, the residual strength of the lamina, as a function of number of cycles, degrades gradually (Fig. 4.3). The *wear out model* [40] is a suitable technique to present this behaviour. It should be mentioned that for each state of stress, the *s-n* curve passes through the point (catastrophic failure point) of the residual strength curve, as shown in Fig. 4.3.

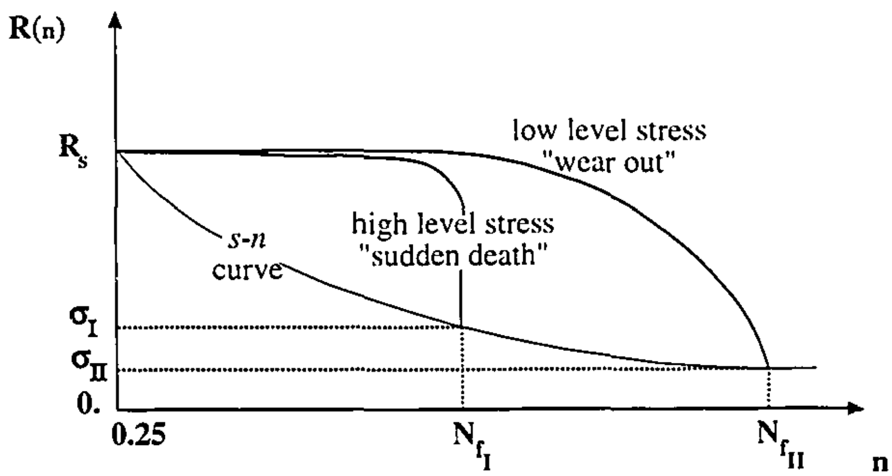

Fig. 4.3 Strength degradation under different states of stress

In practice, designers must deal with a wide range of states of stress, varying from low to high. Therefore, in order to apply Eq. 4.13, the residual longitudinal tensile fatigue strength and residual in-plane shear fatigue strength of a unidirectional ply ($X_t(n,\sigma,\kappa)$ and $S_{xy}(n,\sigma,\kappa)$) must be fully characterized under different stress levels and stress ratios. This requires a large quantity of experiments just to predict the fiber in tension fatigue failure mode of a unidirectional ply under simple biaxial fatigue loading conditions. By considering the other modes of failure and the multiaxial states of stress which are encountered in the real fatigue design of composite structures, the proposed method is faced with severe difficulties. As mentioned previously, for a multiaxial fatigue failure analysis, the material properties of the unidirectional ply in fiber and matrix directions under tension and compression and under in-plane and out-of-plane shear fatigue conditions for different stress levels and stress ratios must be fully characterized. This is an expensive and time consuming task and virtually impossible in practice.

To overcome the difficulties arising from the large quantity of experiments required at different stress states and stress ratios to characterize the material, many investigators [198-210] restricted their models to specific stress ratios. A summary of different stress ratios utilized by authors is presented in Table 4.3. This assumption is too restrictive for general cases. For example, in the analysis of a pin/bolt fatigue loaded composite laminate, using a constant stress ratio leads to incorrect results. Clearly, for this problem there are different states of stress at different points in the material. Also, after applying fatigue load on a notched composite laminate, failure initiates near the stress concentrations and the material property degrades, therefore the stress ratio and the state of stress are not constant at different points. This means that in practice, stresses redistribute during the fatigue loading. By considering the different behaviour of a unidirectional ply for each combination of the stress state and stress ratio, an infinite number of experiments would be required in order to fully characterize the residual properties of a unidirectional ply under arbitrary state of stress and stress ratio.

References	Utilized Stress Ratios (κ)
Sims and Brogdon [198]	.818, .5 and .313
Hahn [199]	0 and .1
Hashin [200,201]	-1 to establish failure criteria .1 for experiments
Rotem *et al.* [202-204,209] Ellyin and El-Kadi [205] Wu [208] Ryder and Crossman [210]	.1
Tennyson *et al.*[206,207]	.05 in tension (20 in compression)

Table 4.3 A summary of different load ratios utilized by authors

To eliminate the aforementioned obstacle of using the quadratic polynomial failure criteria for a wide range of stress state and stress ratio, a technique is established in this study which will be explained in detail in the next chapter. In the following, a set of quadratic polynomial fatigue failure criteria capable of distinction of different modes of failure of a unidirectional ply under multiaxial fatigue loading conditions are established. The fatigue failure criteria for different modes of failure are similar to static failure criteria, except that the material properties are not constants but functions of number of cycles, stress state, and stress ratios. It should be added that the effects of material nonlinearity on the fatigue failure criteria are also considered similar to the static loading conditions.

4.3.1 Fiber Tension Fatigue Failure Mode

For fiber tension fatigue failure mode ($\sigma_{xx} > 0$) of a unidirectional ply under a multiaxial state of fatigue stress, the following criterion is used:

$$\left(\frac{\sigma_{xx}}{X_t(n,\sigma,\kappa)}\right)^2+\left(\frac{\dfrac{\sigma_{xy}^2}{2E_{xy}(n,\sigma,\kappa)}+\dfrac{3}{4}\delta\sigma_{xy}^4}{\dfrac{S_{xy}^2(n,\sigma,\kappa)}{2E_{xy}(n,\sigma,\kappa)}+\dfrac{3}{4}\delta S_{xy}^4(n,\sigma,\kappa)}\right)+\left(\frac{\dfrac{\sigma_{xz}^2}{2E_{xz}(n,\sigma,\kappa)}+\dfrac{3}{4}\delta\sigma_{xz}^4}{\dfrac{S_{xz}^2(n,\sigma,\kappa)}{2E_{xz}(n,\sigma,\kappa)}+\dfrac{3}{4}\delta S_{xz}^4(n,\sigma,\kappa)}\right)=g_{F^+}^2$$

(if $g_{F^+} > 1$, then failure) **Eq. 4.14**

where $X_t(n,\sigma,\kappa)$ is the longitudinal tensile residual fatigue strength of a unidirectional ply under uniaxial fatigue loading, $S_{xy}(n,\sigma,\kappa)$ is the in-plane shear residual fatigue strength of a unidirectional ply under uniaxial shear fatigue loading, $E_{xy}(n,\sigma,\kappa)$ is the in-plane shear residual fatigue stiffness of a unidirectional ply under uniaxial shear fatigue loading, $S_{xz}(n,\sigma,\kappa)$ is the out-of-plane shear (in x-z plane) residual fatigue strength of a unidirectional ply under uniaxial shear fatigue loading and $E_{xz}(n,\sigma,\kappa)$ is the out-of-plane shear residual fatigue stiffness of a unidirectional ply under uniaxial shear fatigue loading conditions. Also n, σ, κ and δ are number of cycles, stress state, stress ratio and parameter of material nonlinearity, respectively. It should be mentioned that the parameter of material nonlinearity (δ) is assumed to be a constant, not a function of number of cycles, stress state and stress ratio. In order to express the relationship between the parameter of material nonlinearity and number of cycles for various stress states and stress ratios, further research is needed.

4.3.2 Fiber Compression Fatigue Failure Mode

For fiber compression fatigue failure mode ($\sigma_{xx} < 0$), of a unidirectional ply under a multiaxial state of fatigue stress, the following criterion is used:

$$\left(\frac{\sigma_{xx}}{X_c(n,\sigma,\kappa)}\right) = g_{F^-} \qquad \text{(if } g_{F^-} > 1\text{, then failure)} \qquad \textbf{Eq. 4.15}$$

where $X_c(n,\sigma,\kappa)$ is the longitudinal compressive residual fatigue strength of a unidirectional ply under uniaxial fatigue loading conditions. Similar to the static loading conditions, the effect of shear stresses on the compressive fatigue behaviour of a unidirectional ply is not clear. Therefore, the interaction terms of shear stresses are not considered in the proposed criterion.

4.3.3 Fiber-Matrix Shearing Fatigue Failure Mode

For fiber-matrix shearing fatigue failure mode ($\sigma_{xx} < 0$), of a unidirectional ply under a multiaxial state of fatigue stress, the following criterion is used:

$$\left(\frac{\sigma_{xx}}{X_c(n,\sigma,\kappa)}\right)^2 + \left(\frac{\dfrac{\sigma_{xy}^2}{2E_{xy}(n,\sigma,\kappa)} + \dfrac{3}{4}\delta\sigma_{xy}^4}{\dfrac{S_{xy}^2(n,\sigma,\kappa)}{2E_{xy}(n,\sigma,\kappa)} + \dfrac{3}{4}\delta S_{xy}^4(n,\sigma,\kappa)}\right) + \left(\frac{\dfrac{\sigma_{xz}^2}{2E_{xz}(n,\sigma,\kappa)} + \dfrac{3}{4}\delta\sigma_{xz}^4}{\dfrac{S_{xz}^2(n,\sigma,\kappa)}{2E_{xz}(n,\sigma,\kappa)} + \dfrac{3}{4}\delta S_{xz}^4(n,\sigma,\kappa)}\right) = g_{FM}^2$$

$$\text{(if } g_{FM} > 1\text{, then failure)} \qquad \textbf{Eq. 4.16}$$

4.3.4 Matrix Tension Fatigue Failure Mode

For matrix tension fatigue failure mode ($\sigma_{yy} > 0$), of a unidirectional ply under a multiaxial state of fatigue stress, the following criterion is used:

$$\left(\frac{\sigma_{yy}}{Y_t(n,\sigma,\kappa)}\right)^2 + \left(\frac{\dfrac{\sigma_{xy}^2}{2E_{xy}(n,\sigma,\kappa)} + \dfrac{3}{4}\delta\sigma_{xy}^4}{\dfrac{S_{xy}^2(n,\sigma,\kappa)}{2E_{xy}(n,\sigma,\kappa)} + \dfrac{3}{4}\delta S_{xy}^4(n,\sigma,\kappa)}\right) + \left(\frac{\sigma_{yz}}{S_{yz}(n,\sigma,\kappa)}\right)^2 = g_{M^+}^2.$$

$$\text{(if } g_{M^+} > 1\text{, then failure)} \qquad \textbf{Eq. 4.17}$$

where $Y_t(n,\sigma,\kappa)$ is the transverse tensile residual fatigue strength of a unidirectional ply under uniaxial fatigue loading and $S_{yz}(n,\sigma,\kappa)$ is the out-of-plane shear (in y-z plane) residual fatigue strength of a unidirectional ply under uniaxial shear fatigue loading conditions.

4.3.5 Matrix Compression Fatigue Failure Mode

Similarly, for matrix compression static failure mode ($\sigma_{yy} < 0$), of a unidirectional ply under a multiaxial state of fatigue stress, the following equation can be derived:

$$\left(\frac{\sigma_{yy}}{Y_c(n,\sigma,\kappa)}\right)^2 + \left(\frac{\dfrac{\sigma_{xy}^2}{2E_{xy}(n,\sigma,\kappa)} + \dfrac{3}{4}\delta\sigma_{xy}^4}{\dfrac{S_{xy}^2(n,\sigma,\kappa)}{2E_{xy}(n,\sigma,\kappa)} + \dfrac{3}{4}\delta S_{xy}^4(n,\sigma,\kappa)}\right) + \left(\frac{\sigma_{yz}}{S_{yz}(n,\sigma,\kappa)}\right)^2 = g_{M^-}^2$$

(if $g_M^- > 1$, then failure) **Eq. 4.18**

where $Y_c(n,\sigma,\kappa)$ is the transverse compressive residual fatigue strength of a unidirectional ply under uniaxial fatigue loading conditions.

4.3.6 Normal Tension Fatigue Failure Mode

For normal tension fatigue failure mode ($\sigma_{zz} > 0$), of a unidirectional ply under a multiaxial state of fatigue stress, the following criterion is used:

$$\left(\frac{\sigma_{zz}}{Z_t(n,\sigma,\kappa)}\right)^2 + \left(\frac{\dfrac{\sigma_{xz}^2}{2E_{xz}(n,\sigma,\kappa)} + \dfrac{3}{4}\delta\sigma_{xz}^4}{\dfrac{S_{xz}^2(n,\sigma,\kappa)}{2E_{xz}(n,\sigma,\kappa)} + \dfrac{3}{4}\delta S_{xz}^4(n,\sigma,\kappa)}\right) + \left(\frac{\sigma_{yz}}{S_{yz}(n,\sigma,\kappa)}\right)^2 = g_{N^+}^2$$

(if $g_N^+ > 1$, then failure) **Eq. 4.19**

where $Z_t(n,\sigma,\kappa)$ is the normal tensile residual fatigue strength of a unidirectional ply under uniaxial fatigue loading conditions.

4.3.7 Normal Compression Fatigue Failure Mode

For normal compression fatigue failure mode ($\sigma_{zz} < 0$), of a unidirectional ply under a multiaxial state of fatigue stress, the following criterion is used:

$$\left(\frac{\sigma_{zz}}{Z_c(n,\sigma,\kappa)}\right)^2 + \left(\frac{\dfrac{\sigma_{xz}^2}{2E_{xz}(n,\sigma,\kappa)} + \dfrac{3}{4}\delta\sigma_{xz}^4}{\dfrac{S_{xz}^2(n,\sigma,\kappa)}{2E_{xz}(n,\sigma,\kappa)} + \dfrac{3}{4}\delta S_{xz}^4(n,\sigma,\kappa)}\right) + \left(\frac{\sigma_{yz}}{S_{yz}(n,\sigma,\kappa)}\right)^2 = g_{N}^2$$

(if $g_N^- > 1$, then failure) **Eq. 4.20** where $Z_c(n,\sigma,\kappa)$ is the normal compressive residual fatigue strength of a unidirectional ply under uniaxial fatigue loading conditions.

To use the proposed set of fatigue failure criteria, the residual material properties of a unidirectional ply under uniaxial fatigue loading conditions in fiber and matrix direction under tension and compression and under in-plane and out-of-plane shear fatigue loading conditions must be fully characterized. After failure detection by any of the fatigue failure criteria, the material properties of the failed material must be changed by suitable material property degradation rules which will be explained in the next chapter.

4.4 Summary

In this chapter, a set of stress based quadratic polynomial failure criteria for static and fatigue failure detection of a unidirectional ply under multiaxial static and fatigue loading conditions is established. The proposed set of static and fatigue failure criteria are capable of distinction between different modes of failure. The effect of the material nonlinearity (nonlinear shear stress-strain behaviour of a unidirectional ply) on the mathematical forms of failure criteria is taken into account. It was explained how the proposed fatigue failure criteria in traditional forms cannot be used for a general stress state and stress ratio. To eliminate this difficulty, a technique will be established in the next chapter which allows the application of the quadratic polynomial fatigue failure criteria under a wide range of stress states and stress ratios.

Chapter 5

Material Property Degradation

In this chapter, the third component of the *model*, material property degradation is discussed. The strategy of changing material properties (stiffness, strength and Poisson's ratio) of failed material under static and fatigue loading for each mode of failure is explained. For each sudden mode of static or fatigue failure detected by the set of failure criteria, explained in the previous chapter, a suitable sudden material property degradation rule is associated. For the fatigue case, before detecting the sudden mode of failure, the material properties of the unidirectional ply gradually degrade due to fatigue loading. To simulate gradual material property degradation, normalization techniques for strength degradation, stiffness degradation and fatigue life of a unidirectional ply under uniaxial state of stress are utilized. The *normalized strength degradation* and *normalized fatigue life models* are adopted and modified from the works of other investigators, and the *normalized stiffness degradation model* is developed in this study. The limitations of application of failure criteria in traditional forms, discussed in Chapter four, are overcome in this chapter. For this purpose, the *generalized material property degradation technique* is established by the coupling of the *normalized strength degradation*, *normalized stiffness degradation* and *normalized fatigue life* models. The developed *technique* simulates the fatigue life and material property (strength and stiffness) degradation of a unidirectional ply under multiaxial state of stress and arbitrary stress ratio.

5.1 Material Property Degradation Rules

In the previous chapter, suitable failure criteria are establish to detect the sudden static and fatigue failure modes of a unidirectional ply under multiaxial state of stress. As failure occurs in a ply of a laminate, material properties of that failed ply are changed by a set of sudden material property degradation rules. Some of the failure modes are catastrophic and some of them are not. Therefore, for a unidirectional ply failed under each mode of static or fatigue failure, there exists an appropriate *sudden* material property degradation rule.

The scenario of material degradation of a unidirectional ply failed under static and fatigue loading conditions before occurrence of sudden failure is different. For a unidirectional ply under multiaxial state of static stress before sudden failure initiation, detected by the set of static failure criteria, there is no material degradation. However, for a unidirectional ply under a multiaxial state of fatigue stress before sudden failure initiation, detected by the set of fatigue failure criteria, there is a *gradual* material property degradation. To explain this difference more clearly, consider a laminated composite under static loading conditions. The load is increased monotonically and at a certain load level, failure initiation in a ply of the laminate is detected by the static failure criteria (Eqs. 4-1 to 4-12). At this stage, the mechanical properties of the failed region of the unidirectional ply of the laminate must be changed. This type of degradation is called *sudden material property degradation.* For a laminated composite under fatigue loading conditions, in the first cycles, the strength of the plies can be higher than the stress state. Therefore, during the first cycles, the proposed fatigue failure criteria (Eqs. 4-13 to 4-19) do not detect any sudden mode of fatigue failure. However, by increasing the cyclic loading of the laminate, material properties of each ply are degraded. This type of degradation is called *gradual material property degradation.* By further increasing the number of cycles, mechanical properties of the piles eventually reach to a level where different modes of failure can be detected by the proposed fatigue failure criteria (Eqs. 4-13 to 4-19). At this stage, the mechanical properties of the failed material are changed by *sudden material property degradation rules.*

The *sudden material property degradation rules* for some failure modes of a unidirectional ply under a biaxial state of static stress are available in the literature [41-43]. A complete set of sudden material property degradation rules for all the various failure modes of a unidirectional ply under a multiaxial state of static and fatigue stress is developed in this study and explained in the following section. Moreover, the *gradual material property degradation rules*, established in this research will be explained thereafter.

5.2 Sudden Material Property Degradation Rules

In the following, a complete set of sudden material property degradation rules is established for each mode of failure of a unidirectional ply under a multiaxial state of static or fatigue stress detected by the static or fatigue failure criteria. The rules must be carefully applied to avoid numerical instabilities during computation by the computer program.

Conventional finite element techniques are by definition limited to an intact continuum. Thus, after failure occurrence in a ply, instead of inducing a real crack, the failed region of the ply is replaced by an intact ply of lower material properties (Fig. 5.1). Therefore, conventional finite element techniques can be applied for stress analysis even after failure initiation.

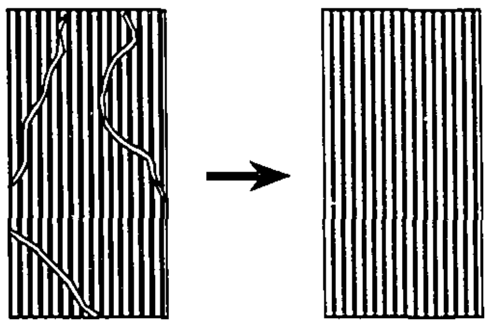

Fig. 5.1 Degraded ply is modeled by an intact ply of lower material properties

5.2.1 Fiber Tension Property Degradation

Fiber tension failure mode of a unidirectional ply (detected by Eq. 4.2 for static and Eq. 4.14 for fatigue cases) is a catastrophic mode of failure and when it occurs, the failed material cannot sustain any type or combination of stresses. Thus, all material properties of the failed ply are reduced to zero, as follows:

Stiffnesses and Poisson's ratios:

$$\begin{gathered}\left[E_{xx}, E_{yy}, E_{zz}, E_{xy}, E_{xz}, E_{yz}, \nu_{xy}, \nu_{xz}, \nu_{yz}, \nu_{yx}, \nu_{zx}, \nu_{zy}\right] \\ \downarrow \\ [0,0,0,0,0,0,0,0,0,0,0,0]\end{gathered} \qquad \textbf{Eq. 5.1 (a)}$$

Strengths:

$$\left[X_t, Y_t, Z_t, X_c, Y_c, Z_c, S_{xy}, S_{xz}, S_{yz}\right] \\ \downarrow \\ [0,0,0,0,0,0,0,0,0] \qquad \textbf{Eq. 5.1 (b)}$$

As mentioned, this mode of failure is catastrophic, therefore if it occurs, the other modes of failure do not need to also be verified. During numerical computations by the computer program, reducing material properties to zero creates numerical instabilities. To avoid this difficulty, for the case of failure, the material properties are reduced to very small values.

5.2.2 Fiber Compression Property Degradation

Fiber compression failure mode of a unidirectional ply (detected by Eq. 4.4 for static and Eq. 4.15 for fatigue cases) is a catastrophic mode of failure and when it occurs, the failed material cannot sustain any type or combination of stresses. Thus, all material properties of the failed ply are reduced to zero, as follows:

Stiffnesses and Poisson's ratios:

$$\left[E_{xx}, E_{yy}, E_{zz}, E_{xy}, E_{xz}, E_{yz}, \nu_{xy}, \nu_{xz}, \nu_{yz}, \nu_{yx}, \nu_{zx}, \nu_{zy}\right] \\ \downarrow \\ [0,0,0,0,0,0,0,0,0,0,0,0] \qquad \textbf{Eq. 5.2 (a)}$$

Strengths:

$$\left[X_t, Y_t, Z_t, X_c, Y_c, Z_c, S_{xy}, S_{xz}, S_{yz}\right] \\ \downarrow \\ [0,0,0,0,0,0,0,0,0] \qquad \textbf{Eq. 5.2 (b)}$$

As mentioned, this mode of failure is catastrophic, therefore if it occurs, the other modes of failure do not need to also be verified.

5.2.3 Fiber-Matrix Shearing Property Degradation

In fiber-matrix shearing failure mode of a unidirectional ply (detected by Eq. 4.6 for static and Eq. 4.16 for fatigue cases), the material can still carry load in the fiber, matrix and normal directions, but in-plane shear stress can no longer be carried. This is modeled by reducing the in-plane shear material properties of the failed ply to zero, as follows:

Stiffnesses and Poisson's ratios:

$$\begin{gathered}\left[E_{xx}, E_{yy}, E_{zz}, E_{xy}, E_{xz}, E_{yz}, \nu_{xy}, \nu_{xz}, \nu_{yz}, \nu_{yx}, \nu_{zx}, \nu_{zy}\right] \\ \downarrow \\ \left[E_{xx}, E_{yy}, E_{zz}, 0, E_{xz}, E_{yz}, 0, \nu_{xz}, \nu_{yz}, 0, \nu_{zx}, \nu_{zy}\right]\end{gathered} \qquad \textbf{Eq. 5.3 (a)}$$

Strengths:

$$\begin{gathered}\left[X_t, Y_t, Z_t, X_c, Y_c, Z_c, S_{xy}, S_{xz}, S_{yz}\right] \\ \downarrow \\ \left[X_t, Y_t, Z_t, X_c, Y_c, Z_c, 0, S_{xz}, S_{yz}\right]\end{gathered} \qquad \textbf{Eq. 5.3 (b)}$$

After detecting this mode of failure, which is not catastrophic, the other modes of failure must be verified. After this mode of failure occurs, in order to check the other modes of failure by relevant failure criteria, the terms containing S_{xy} must not be further considered.

5.2.4 Matrix Tension Property Degradation

For matrix tension failure mode of a unidirectional ply (detected by Eq. 4.8 for static and Eq. 4.17 for fatigue cases), the transverse modulus, E_{yy}, the transverse tensile strength Y_t, and Poisson's ratios ν_{yx} and ν_{yz} are reduced to zero. This mode of failure is not catastrophic, and affects only matrix direction properties, therefore other material properties are left unchanged.

Stiffnesses and Poisson's ratios:

$$\begin{gathered}\left[E_{xx}, E_{yy}, E_{zz}, E_{xy}, E_{xz}, E_{yz}, \nu_{xy}, \nu_{xz}, \nu_{yz}, \nu_{yx}, \nu_{zx}, \nu_{zy}\right] \\ \downarrow \\ \left[E_{xx}, 0, E_{zz}, E_{xy}, E_{xz}, E_{yz}, \nu_{xy}, \nu_{xz}, 0, 0, \nu_{zx}, \nu_{zy}\right]\end{gathered} \qquad \textbf{Eq. 5.4 (a)}$$

Strengths:

$$\begin{gathered}[X_t, Y_t, Z_t, X_c, Y_c, Z_c, S_{xy}, S_{xz}, S_{yz}] \\ \downarrow \\ [X_t, 0, Z_t, X_c, Y_c, Z_c, S_{xy}, S_{xz}, S_{yz}]\end{gathered} \qquad \textbf{Eq. 5.4 (b)}$$

After detecting this mode of failure, which is not catastrophic, the other modes of failure must be verified.

5.2.5 Matrix Compression Property Degradation

Matrix compression failure mode (detected by Eq. 4.9 for static and Eq. 4.18 for fatigue cases) results in the same type of damage to the composite ply as the matrix tension failure mode. Thus, the transverse modulus E_{yy}, the transverse compressive strength Y_c, and Poisson's ratios ν_{yz} and ν_{yx} are reduced to zero. This mode of failure is not catastrophic, therefore, other material properties are left unchanged.

Stiffnesses and Poisson's ratios:

$$\begin{gathered}[E_{xx}, E_{yy}, E_{zz}, E_{xy}, E_{xz}, E_{yz}, \nu_{xy}, \nu_{xz}, \nu_{yz}, \nu_{yx}, \nu_{zx}, \nu_{zy}] \\ \downarrow \\ [E_{xx}, 0, E_{zz}, E_{xy}, E_{xz}, E_{yz}, \nu_{xy}, \nu_{xz}, 0, 0, \nu_{zx}, \nu_{zy}]\end{gathered} \qquad \textbf{Eq. 5.5 (a)}$$

Strengths:

$$\begin{gathered}[X_t, Y_t, Z_t, X_c, Y_c, Z_c, S_{xy}, S_{xz}, S_{yz}] \\ \downarrow \\ [X_t, Y_t, Z_t, X_c, 0, Z_c, S_{xy}, S_{xz}, S_{yz}]\end{gathered} \qquad \textbf{Eq. 5.5 (b)}$$

Similar to matrix tension failure mode, matrix compression is not a catastrophic mode of failure. Thus, after detecting this failure mode, the other modes of failure must be verified.

5.2.6 Normal Tension Property Degradation

For normal tension failure mode of a unidirectional ply (detected by Eq. 4.11 for static and Eq. 4.19 for fatigue cases), the normal modulus E_{zz}, the normal tensile strength Z_t, and Poisson's ratios ν_{zx} and ν_{zy} are reduced to zero. This mode of failure is not catastrophic, therefore, other material properties are left unchanged. This is essentially the same type of failure as matrix tension failure mode.

Stiffnesses and Poisson's ratios:

$$\left[E_{xx}, E_{yy}, E_{zz}, E_{xy}, E_{xz}, E_{yz}, \nu_{xy}, \nu_{xz}, \nu_{yz}, \nu_{yx}, \nu_{zx}, \nu_{zy}\right]$$
$$\downarrow \qquad \textbf{Eq. 5.6 (a)}$$
$$\left[E_{xx}, E_{yy}, 0, E_{xy}, E_{xz}, E_{yz}, \nu_{xy}, \nu_{xz}, \nu_{yz}, \nu_{yx}, 0, 0\right]$$

Strengths:

$$\left[X_t, Y_t, Z_t, X_c, Y_c, Z_c, S_{xy}, S_{xz}, S_{yz}\right]$$
$$\downarrow \qquad \textbf{Eq. 5.6 (b)}$$
$$\left[X_t, Y_t, 0, X_c, Y_c, Z_c, S_{xy}, S_{xz}, S_{yz}\right]$$

After detecting this mode of failure, which is not catastrophic, the other modes of failure must be verified.

5.2.7 Normal Compression Property Degradation

For normal compression failure mode of a unidirectional ply (detected by Eq. 4.12 for static and Eq. 4.20 for fatigue cases), the normal modulus E_{zz}, the normal compressive strength Z_c, and Poisson's ratios ν_{zx} and ν_{zy} are reduced to zero. This mode of failure is not catastrophic, therefore, other material properties are left unchanged. This is essentially the same type of failure as matrix compression failure mode.

Stiffnesses and Poisson's ratios:

$$\left[E_{xx}, E_{yy}, E_{zz}, E_{xy}, E_{xz}, E_{yz}, \nu_{xy}, \nu_{xz}, \nu_{yz}, \nu_{yx}, \nu_{zx}, \nu_{zy}\right]$$
$$\downarrow \qquad \textbf{Eq. 5.7 (a)}$$
$$\left[E_{xx}, E_{yy}, 0, E_{xy}, E_{xz}, E_{yz}, \nu_{xy}, \nu_{xz}, \nu_{yz}, \nu_{yx}, 0, 0\right]$$

Strengths:

$$\left[X_t, Y_t, Z_t, X_c, Y_c, Z_c, S_{xy}, S_{xz}, S_{yz}\right]$$
$$\downarrow \qquad \textbf{Eq. 5.7 (b)}$$
$$\left[X_t, Y_t, Z_t, X_c, Y_c, 0, S_{xy}, S_{xz}, S_{yz}\right]$$

After detecting this mode of failure, which is not catastrophic, the other modes of failure must be verified.

5.2.8 Summary of Sudden Material Degradation Rules

This complete set of sudden material degradation rules (Eqs. 5.1 to 5.7) for all various failure modes of a unidirectional ply under a multiaxial state of static (detected by Eqs. 4-1 to 4-12) and fatigue stress (detected by Eqs. 4.14 to 4-20) will be used in *the progressive fatigue damage model* explained in the next chapter. However, the material properties of a unidirectional ply before sudden failure (detected by Eqs. 4.13 to 4-19) degrade due to fatigue loading. In order to simulate this phenomenon, the *gradual material property degradation rules* are established in this research and explained in the following section.

5.3 Gradual Material Property Degradation Rules

To apply the fatigue failure criteria (Eqs. 4-14 to 4-20), the residual material properties of a unidirectional ply under arbitrary multiaxial state of fatigue stress and stress ratio must be modeled. For this purpose, the *generalized material property degradation technique* is established which simulates the fatigue behaviour of a unidirectional ply under multiaxial state of fatigue stress and arbitrary stress ratio by using the results of uniaxial fatigue experiments. In this way, the severe limitation of application of the fatigue failure criteria in traditional forms, mentioned in the previous chapter, is overcome. In the following, after a review of different residual strength models proposed in the literature, a suitable model to simulate the behaviour of a unidirectional lamina under a uniaxial state of fatigue stress is selected. Then, the normalization technique for stiffness degradation is established. Subsequently, a procedure to find the fatigue life of a unidirectional lamina under a uniaxial state of fatigue stress, with an arbitrary stress ratio, is explained. Finally, to simulate the behaviour of a unidirectional ply under multiaxial fatigue loading, with arbitrary state of stress and stress ratio, the *generalized material property degradation technique* is established.

5.3.1 Normalized Strength Degradation Model

There are two major approaches to simulate the residual strength of laminated composites under uniaxial fatigue loading [210], which are called the statistical (probability-based damage) and mechanistic (emphasis on damage mechanics) approaches. Works of Halpin *et al.* [40,213] and Broutman and Sahu [214] are the two earliest examples of statistical and mechanistic approaches, respectively. Investigations by Hahn and Kim [215], Chou and Croman [211,212], Whitney [216], Sendeckyj [217], Radhakrishnan [218], and works of Yang and his co-workers [219-226] are other examples in the statistical category. On the other hand, Reifsnider and Stinchcomb [32], Reifsnider [33,34], Ryder and Crossman [210], Daniel and Charewicz [227,228], Rotem [229], Whitworth [230], Spearing and Beaumont [38], and Harris and his co-workers [231-232] presented different mechanistic models. In both categories, statistical and mechanistic, no comprehensive study of the behaviour of unidirectional plies under multiaxial fatigue loading has been conducted.

Consider a unidirectional lamina under a constant uniaxial fatigue loading. Under static loading, or equivalently at n=0.25 cycles (quarter of a cycle) in fatigue, the strength of the unidirectional lamina is R_s (Fig. 5.2). It should be mentioned that the character "R" is used as a representative symbol for the strength of a unidirectional ply which has different magnitudes in different directions such as, X_t, Y_t, etc. By increasing the number of cycles, under a constant applied stress (σ), fatigue strength (R(n)) decreases. Finally, after a certain number of cycles which is called number of cycles to failure (N_f), the magnitude of the strength decreases to the magnitude of the applied stress. At this point, the composite lamina fails catastrophically. In Fig. 5.2, the residual strength and *s-n* curves are shown in one graph. As shown, it is clear that for a particular state of stress (σ) the *s-n* curve passes through the end point (catastrophic failure point) of the residual strength curve.

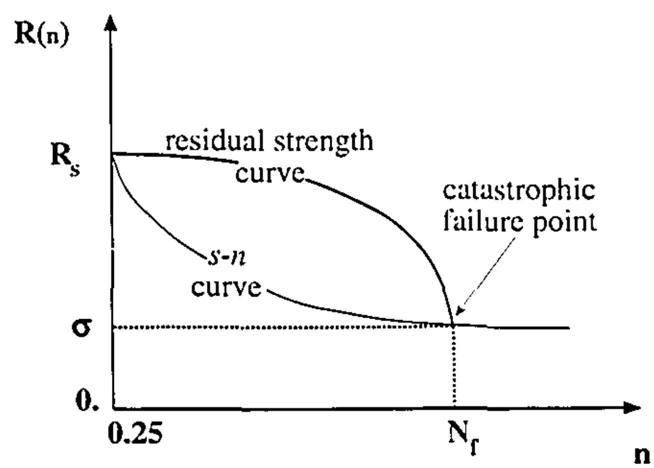

Fig. 5.2 Strength degradation of a unidirectional lamina under a constant uniaxial fatigue loading

As mentioned in the previous chapter and repeated here, the fatigue behaviour of a composite lamina varies under different states of stress. For instance, under high level state of stress, the residual strength as a function of number of cycles is nearly constant and it decreases drastically at the number of cycles to failure (Fig. 5.3). The *sudden death model* [211,212] is a suitable technique to describe this behaviour. However at low level state of stress, the residual strength of the lamina, as a function of number of cycles, degrades gradually (Fig. 5.3). The *wear out model* [40] is a suitable technique to present this behaviour. In practice, designers must deal with a wide range of states of stress varying from low to high, therefore a model to present the behaviour of composite materials under a general state of stress is essential.

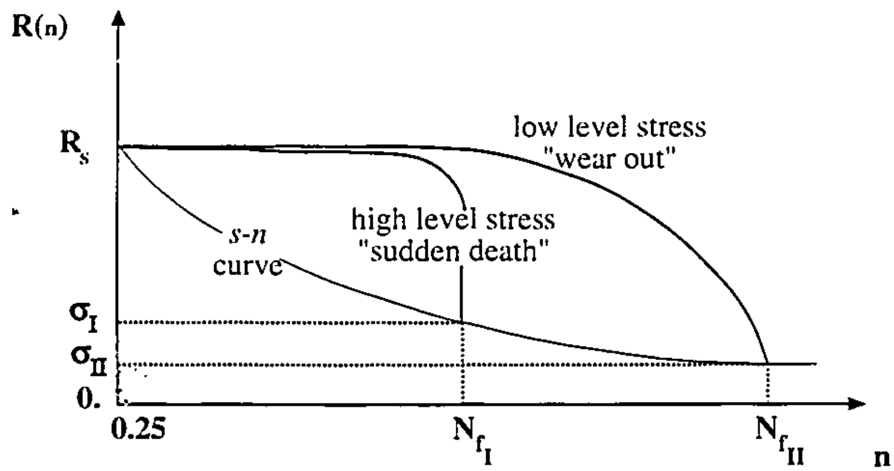

Fig. 5.3 Strength degradation under different states of stress

Different models have been presented in the literature to simulate the residual strength of composite laminates under fatigue loading. In the following, a comparison between different models is made. It should be mentioned that there are many details in these models which are not discussed here. Therefore in the following, the models and equations used by other authors are only considered from our point of view. Realizing that various notations have been used by different authors, for simplicity, a unified notation has been applied here in order to present the models of other authors in an informative manner. It must be mentioned that in this thesis, there is no attempt to study the probabilistic features of the residual strength of composite materials; only the mechanistic characteristics are considered here.

The *sudden death model* [211,212] is very simple and straightforward. The strength of the composite lamina is constant until the number of cycles to failure (N_f), where the composite lamina fails catastrophically. In the *wear out model*, which was initially presented by Halpin *et al.*[40], it is assumed that the residual strength R(n) is a monotonically decreasing function of number of cycles (n), and the change of the residual strength is approximated by a power-law growth equation,

$$\frac{dR(n)}{dn} = -A(\sigma)/m[R(n)]^{m-1} \qquad \textbf{Eq. 5.8}$$

in which $A(\sigma)$ is a function of the maximum cyclic stress (σ), and m is a constant. This model has been used by many authors [215-226] in probabilistic and mechanistic models.

By integrating Eq. 5.8 from n_0 to n_1 cycles,

$$R^m(n_1) = R^m(n_0) - A(\sigma)(n_1 - n_0) \qquad \textbf{Eq. 5.9}$$

with $n_0 = 0$ and $n_1 = n$, Eq. 5.9 reduces to:

$$R^m(n) = R_s^m - A(\sigma)n \qquad \textbf{Eq. 5.10}$$

where R_s is the static strength.

By considering that at the number of cycles to failure (N_f), the residual strength (R(n)) is equal to the applied stress (σ), Eq. 5.10 reduces to:

$$R^m(n) = R_s^m - \frac{R_s^m - \sigma^m}{N_f} n \qquad \textbf{Eq. 5.11}$$

Eq. 5.11 expresses the residual strength (R(n)), as a function of static strength (R_s), number of cycles (n), and number of cycles to failure (N_f). Also, m is a constant which is found experimentally. For different states of stress, "m" has different values, therefore to fully characterize a material, large number of experiments should be performed.

For comparing between different models proposed by different authors, Eq. 5.11 can be rewritten in the following form,

$$\frac{R^m(n) - R_s^m}{R_s^m - \sigma^m} = -\frac{n}{N_f} \qquad \textbf{Eq. 5.12}$$

and by the following algebraic operation,

$$\frac{R^m(n) - R_s^m - \sigma^m + \sigma^m}{R_s^m - \sigma^m} = -\frac{n}{N_f} \qquad \textbf{Eq. 5.13}$$

Eq. 5.12 reduces to:

$$\frac{R^m(n) - \sigma^m}{R_s^m - \sigma^m} = 1 - \frac{n}{N_f} \qquad \textbf{Eq. 5.14}$$

Eq. 5.14 is a normalized form of Eq. 5.11 which can be used for the purpose of comparing different models. By using a unified notation and applying similar algebraic operations to the other models proposed in the literature, a list of the residual strength models is presented in Table 5.1.

References	Models	Explanations
Halpin *et al.* [40] Hahn and Kim [215] Yang *et al.* [219-226] Chou and Croman [211,212] Sendeckyj [217]	$\frac{R^m(n) - \sigma^m}{R_s^m - \sigma^m} = 1 - \frac{n}{N_f}$	"m" is a curve fitting parameter, found experimentally
Broutman and Sahu [214]	$\frac{R(n) - \sigma}{R_s - \sigma} = 1 - \frac{n}{N_f}$	linear strength degradation
Daniel *et al.* [227,228]	$\frac{R(n) - \sigma}{R_s - \sigma} = g\left(\frac{n}{N_f}\right)$	$g\left(\frac{n}{N_f}\right)$ is undefined function
Reifsnider and Stinchcomb [32] Reifsnider [33,34]	$\frac{R(n) - \sigma}{R_s - \sigma} = 1 - \left(\frac{n}{N_f}\right)^k$	"k" is a curve fitting parameter, found experimentally
Harris *et al.* [231,232]	$\left(\frac{R(n) - \sigma}{R_s - \sigma}\right)^\alpha = 1 - \left(\frac{\log(n) - \log(.5)}{\log(N_f) - \log(.5)}\right)^\beta$	"α" and "β" are two curve fitting parameters, found experimentally

Notes:

Hahn and Kim [215] use F=R(n), t=n, R(0)= R_s

Yang *et al.* [219] use m=c, s=σ, N=N_f, R(0)= R_s

Chou and Croman [211,212] use S=σ, N=N_f, R(0)= R_s

Sendeckyj [217] uses $\sigma_a=\sigma$, σ_r=R(n), $\sigma_e=R_s$, 1/S=m, $C=\left(\frac{R_s^m}{\sigma^m}-1\right)/N_f$ (not derived by him)

Broutman and Sahu [214] use σ_i^*=R(n), $f_i=\frac{n}{N_f}$, $\sigma_{ults}^{i-1}=\sigma_{ults}^0= R_s$ (for one state of stress)

Daniel *et al.* [227,228] use f_r=R(n), s=σ, N=N_f, R(0)= R_s

Reifsnider and Stinchcomb [32] use S_r(n)=R(n), $S_u= R_s$, $S_a=\sigma$, N=N_f, i=k (critical element model)

Harris *et al.* [231,232] use f_r=R(n), s=σ, N=N_f, R(0)= R_s

Table 5.1 A summary of different strength degradation models

As shown in Table 5.1, Hahn and Kim [215], Yang *et al.* [219-226], Chou and Croman [211,212], and Sendeckyj [217] applied exactly the same model proposed by Halpin *et al.* [40]. Broutman and Sahu [214] assumed a linear relationship between the fatigue strength and number of cycles. This assumption is not consistent with the experimental evidence of strength degradation at low level state of stress nor at high level state of stress. In a model presented by Daniel *et al.* [227], an undefined function of normalized number of cycles "g" is introduced. There is no effort in their paper [227] to define this function (Table 5.1). In Table 5.1, in the equation proposed by Reifsnider and Stinchcomb [32] and Reifsnider [33,34], "k" is a curve fitting parameter which must be found experimentally. Harris *et al.* [231-232] presented a normalized equation consisting of two curve fitting parameters (Table 5.1). They showed that "α" and "β" are stress independent curve fitting parameters which must be found experimentally. They emphasized that stress-independent models, like the model proposed by Fong [233], which is based on the assumption that the fatigue process is controlled by a single primary damage mechanism, is not realistic. They postulated that their model permitted the incorporation of all modes of damage accumulation, from *wear out* to *sudden death*, by the adjustment of the curve fitting parameters α and β. In their studies, the equivalent number of fatigue cycles for a static loading condition is assumed to be 0.5, however by considering that a static loading is really a quarter of a cycle, the equivalent number of cycles should be changed to 0.25.

By using the normalization technique, all different curves for different states of stress, in Fig. 5.3 collapse to a single curve (Fig. 5.4). For use in this research, the equation presented by Harris *et al.* [231,232] is changed to the following form (with the equivalent number of fatigue cycles for a static loading condition changed from 0.5 to 0.25):

$$R(n,\sigma) = \left[1 - \left(\frac{\log(n) - \log(.25)}{\log(N_f) - \log(.25)}\right)^{\beta}\right]^{\frac{1}{\alpha}} (R_s - \sigma) + \sigma \qquad \textbf{Eq. 5.15}$$

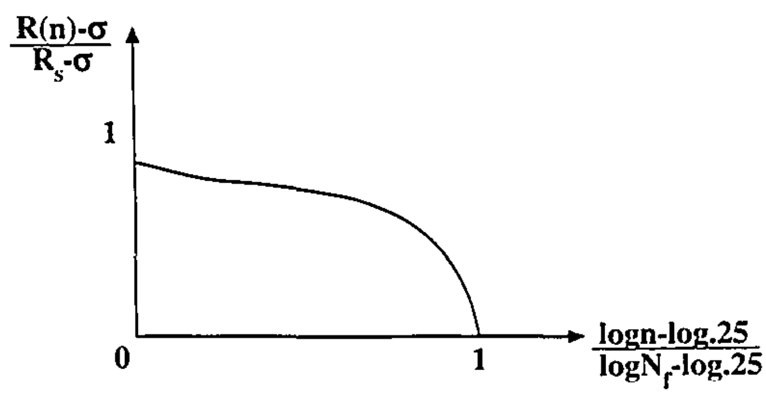

Fig. 5.4 Normalized strength degradation curve

By having static strength (R_s), state of stress (σ), number of cycles to failure (N_f) related to the state of stress, and the curve fitting parameters (α and β), residual strength ($R(n,\sigma)$), as a function of number of cycles (n) and the state of stress (σ), is found.

Since in Eq. 5.15, α and β are stress independent parameters, this model is called the *normalized strength degradation model.* However, number of cycles to failure (N_f) is a function of the state of stress (σ) and the stress ratio ($\kappa = \sigma_{min}/\sigma_{max}$). Therefore, to simulate the residual strength of a unidirectional ply under a general uniaxial fatigue loading (arbitrary state of stress and stress ratio), a suitable relationship between the fatigue life (N_f), state of stress and stress ratio is needed. For the general case, i.e. arbitrary stress ratio, Eq. 5.15 is changed to the following form:

$$R(n,\sigma,\kappa) = \left[1 - \left(\frac{\log(n) - \log(.25)}{\log(N_f) - \log(.25)}\right)^{\beta}\right]^{\frac{1}{\alpha}} (R_s - \sigma) + \sigma \qquad \textbf{Eq. 5.16}$$

By considering that for each combination of the state of stress and stress ratio there is a fatigue life for a unidirectional ply, to characterize the residual strength of a unidirectional ply under arbitrary state of stress and stress ratio, an infinite number of experiments must still be performed. As mentioned in the previous chapter, many authors restricted their failure criteria to a certain stress ratio to overcome this difficulty. However, as previously discussed, assuming a certain stress ratio for the fatigue analysis of composite laminates is not always a realistic assumption. Before removing this obstacle by introducing the *normalized fatigue life model*, the *normalized stiffness degradation model* for a unidirectional ply in a normalized form is explained in the following.

5.3.2 Normalized Stiffness Degradation Model

The residual stiffness of the material is also a function of state of stress and number of cycles. As discussed in the previous section, there are various number of strength degradation models. Similarly, there is much research in stiffness degradation [234-245] of composite materials. The stiffness degradation models are attractive to many investigators, because the residual stiffness can be used as a nondestructive measure for damage evaluation. By performing a similar procedure used as that for normalizing the residual strength, a suitable equation for residual stiffness of a unidirectional ply can be obtained. By using the normalization technique, all different curves for different states of stress can be shown by a single master curve. The idea of normalizing the residual stiffness curves and establishing a master curve has been used by many authors [9,15,247]. In this study, a new method of normalization is developed.

Consider a unidirectional lamina under a constant uniaxial fatigue loading. Under static loading, or equivalently at n=0.25 cycles (quarter of a cycle) in fatigue, the static stiffness of the unidirectional lamina is E_s (Fig. 5.5). It should be mentioned that the character "E" is used as a representative symbol for the stiffness of a unidirectional ply which has different magnitudes in different directions such as, E_{xx}, E_{yy}, etc.

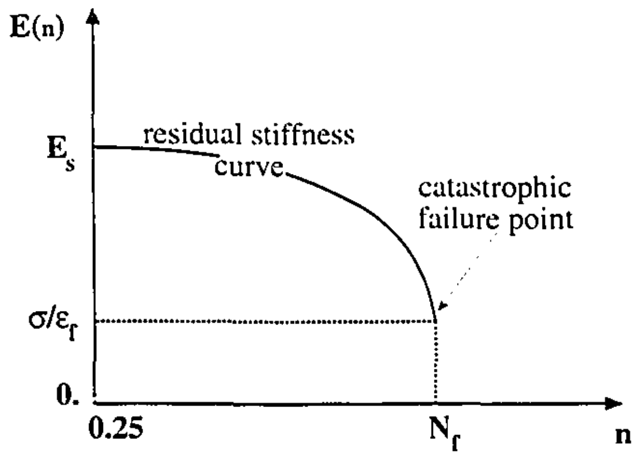

Fig. 5.5 Stiffness degradation of a unidirectional lamina under a constant uniaxial fatigue loading

By increasing the number of cycles, under a constant applied stress (σ), the fatigue stiffness (E(n)) decreases. Finally, after a certain number of cycles which is called number of cycles to failure (N_f), the magnitude of the stiffness decreases to a critical magnitude (E_f). At this point, the composite lamina fails catastrophically. The stiffness degradation of a unidirectional ply is shown in Fig. 5.5. The aforementioned critical value for stiffness (E_f) can be expressed by the following equation,

$$E_f = \frac{\sigma}{\varepsilon_f} \qquad \textbf{Eq. 5.17}$$

where,

ε_f = average strain to failure

The average strain to failure (ε_f) is assumed to be a constant and independent on the state of stress and number of cycles. This assumption is used by many authors [234-237] and verified experimentally in this study. It should be mentioned that for different states of stress, the stiffness degradation of the unidirectional ply is different. The same as for the residual strength case, under high level state of stress, the residual stiffness as a function of number of cycles is nearly constant and it decreases drastically at the number of cycles to failure (Fig. 5.6). However at low level state of stress the residual stiffness of the lamina, as a function of number of cycles, degrades gradually. In practice, designers must deal with a wide range of states of stress varying from low to high. Therefore similar to strength degradation case, a model to present the residual stiffness behaviour of composite materials under a general state of stress is essential.

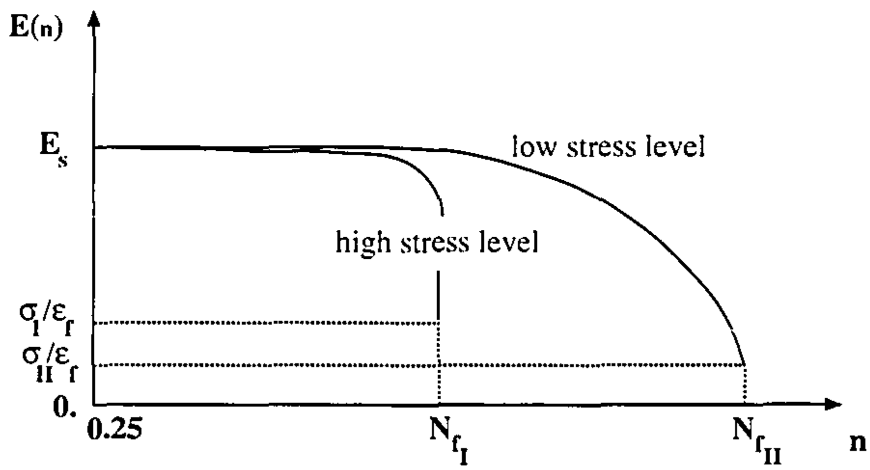

Fig. 5.6 Stiffness degradation under different states of stress

To present the residual stiffness as a function of number of cycles in a normalized form, the following equation is developed, based on a similar idea to that used for residual strength,

$$E(n,\sigma,\kappa) = \left[1-\left(\frac{\log(n)-\log(.25)}{\log(N_f)-\log(.25)}\right)^{\lambda}\right]^{\frac{1}{\gamma}}\left(E_s-\frac{\sigma}{\varepsilon_f}\right)+\frac{\sigma}{\varepsilon_f} \qquad \textbf{Eq. 5.18}$$

where,

$E(n,\sigma,\kappa)$ = residual stiffness
E_s = static stiffness
σ = magnitude of applied maximum stress
ε_f = average strain to failure
n = number of applied cycles
N_f = fatigue life at σ
γ and λ = experimental curve fitting parameters

By using this normalization technique, all different curves for different states of stress in Fig. 5.6, collapse to a single curve (Fig. 5.7).

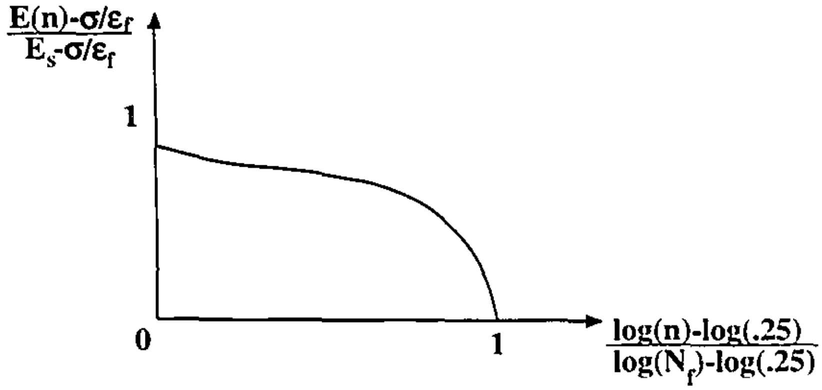

Fig. 5.7 Normalized stiffness degradation curve

As mentioned, for the normalized strength degradation equation (Eq. 5.16), since the number of cycles to failure (N_f) is a function of the state of stress (σ) and the stress ratio ($\kappa=\sigma_{min}/\sigma_{max}$), then the residual stiffness in normalized form (Eq. 5.18) is also a function of stress ratio. Therefore, the same obstacle for the normalized strength degradation model exists for the stiffness degradation in normalized form.

In the following section, a model to simulate the fatigue life for arbitrary stress ratios is explained. Then, by coupling the following procedure and the normalized strength and stiffness degradation models (Eqs. 5.16 and 5.18), the severe restriction of the using a specific stress ratio in fatigue analysis of composite laminates is avoided.

5.4 Normalized Fatigue Life Model

The effect of mean stress ($(\sigma_{max}+\sigma_{min})/2$) on fatigue life, can be presented efficiently by using constant life (Goodman-type) diagrams [247]. Establishing and interpolation of constant life diagram data in traditional form is a tedious task. However, there are some analytical methods [248-252] for predicting the effect of mean stress on fatigue life based on a limited number of experiments. In a paper by Adam *et al.* [248], an analytical method has been proposed to convert and present all data from a constant life diagram in a single two-parameter fatigue curve, which can reduce the number of needed experiments drastically. In this study, this model is called the *normalized fatigue life model.* Recently, the normalized fatigue life model was modified by Harris and his co-workers [251-252] for more general cases. In the following, this model is explained in detail.

Introducing non-dimensional stresses by division of the mean stress (σ_m), the alternating stress (σ_a) and the compressive strength (σ_c) by the tensile strength (σ_t), where $q=\sigma_m/\sigma_t$, $a=\sigma_a/\sigma_t$, and $c=\sigma_c/\sigma_t$, an empirical interaction curve may be derived [251-252]:

$$a = f(1-q)^u(c+q)^v \qquad \textbf{Eq. 5.19}$$

where,

f, u, and v = curve fitting constants
$\sigma_a = (\sigma_{max} - \sigma_{min})/2$ = alternating stress
$\sigma_m = (\sigma_{max} + \sigma_{min})/2$ = mean stress
$q = \sigma_m/\sigma_t$
$a = \sigma_a/\sigma_t$
$c = \sigma_c/\sigma_t$

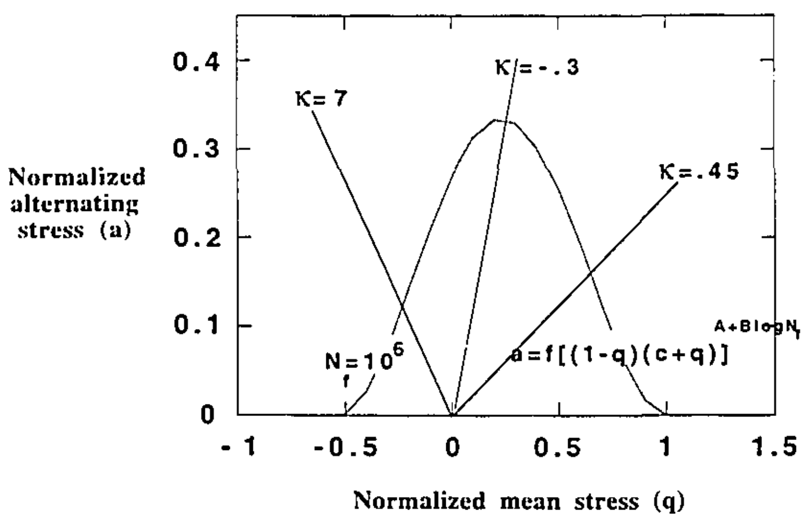

Fig. 5.8 Typical constant life diagram

A typical curve for a fatigue life of 10^6 cycles is shown in Fig. 5.8. The bell-shaped curve is the fatigue life curve. Experimental results by Gathercole *et al.* [252], showed that their previous quadratic model [249] is inappropriate for the constant life curve especially in both low and high mean stress regions (Fig. 5.8). Therefore, they introduced a power law model (Eq. 5.19) that produces a bell-shaped curve, which corresponds closer to the material behaviour under fatigue loading. In a paper by Gathercole *et al.* [252], it was shown that the exponents u and v determine the shapes of the left end right wings of the bell-shaped curve. However, it was also shown [252] that the degree of curve-shape asymmetry was not very great, therefore they assumed u and v are equal and are linear functions of fatigue life (N_f).

$$u = v = A + B\log N_f \qquad \textbf{Eq. 5.20}$$

where A and B are the curve fitting constants. By substituting Eq. 5.20 into Eq. 5.19, the following equation is obtained:

$$a = f[(1-q)(c+q)]^{A+B\log N_f} \qquad \textbf{Eq. 5.21}$$

The following example helps to explain the *normalized fatigue life model*. To predict the fatigue life, the following steps must be performed. First, a σ-logN_f curve for different stress ratios ($\kappa=\sigma_{min}/\sigma_{max}$) should be established experimentally (Fig. 5.9). Different symbols in Fig. 5.9 represent different applied stress ratios. It is obvious that testing at more states of stress will result in more accuracy. Then by rearranging Eq. 5.21, the following equation is derived and shown graphically in Fig. 5.10.

$$u = \frac{\ln(a/f)}{\ln[(1-q)(c+q)]} = A + B\log N_f \qquad \textbf{Eq. 5.22}$$

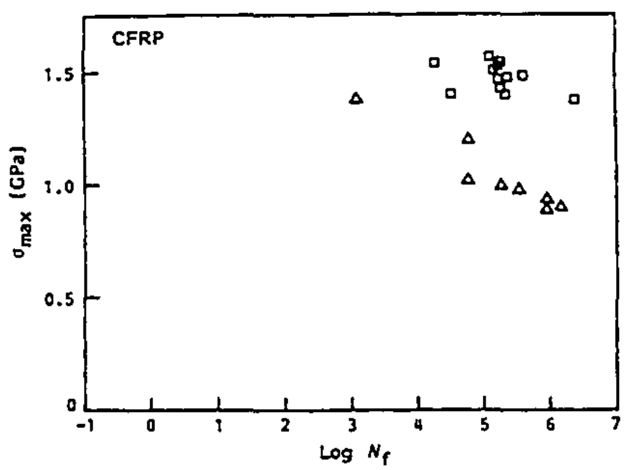

Fig. 5.9 S-logN_f curve, σ_t=1.91 (GPa), and σ_c=1.08 (GPa), Reference [248]

In Figs. (5.9 to 5.11), this procedure has been applied to numerical data from the paper by Adam *et al.* [248]. In Fig. 5.9, original fatigue data is presented. Then, based on the data from Fig. 5.9, setting f = 1.06 (suggested by Gathercole *et al.* [252]) and Eq. 5.22, the u = ln(a/f)/ln[1-q)(c+q) versus logN_f curve is extracted (Fig. 5.10), from which A and B are found. In Fig. 5.11, based on all previous information, the constant life diagram for different number of cycles to failure is predicted. Fig. 5.11 is generated by knowing A, B and f, three constants which can be determined from a relatively small quantity of tests, as demonstrated in this example. Thus, the method is very useful for reducing the number of experiments for characterization of materials.

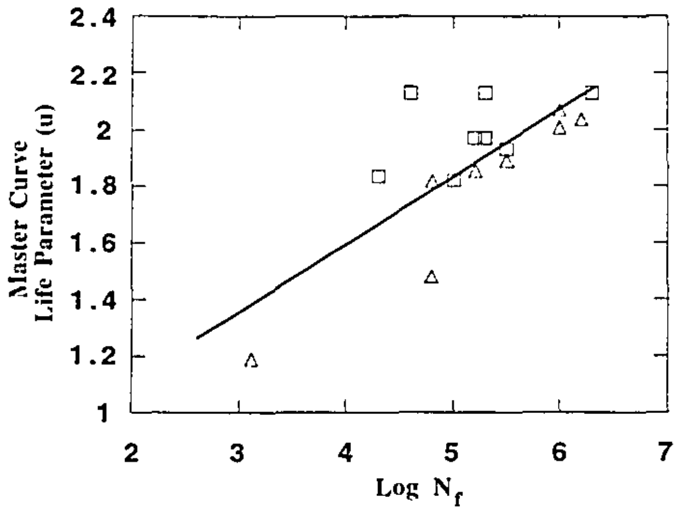

Fig. 5.10 u versus logNf curve

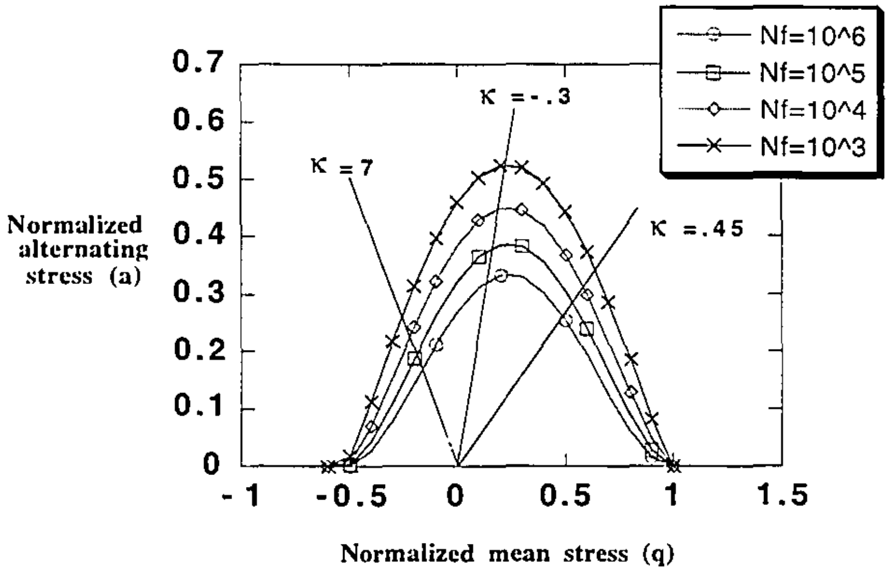

Fig. 5.11 Predicted constant life diagram

5.4.1 Modification of the Life Model for Shear Fatigue Conditions

For the simulation of the fatigue life of the unidirectional ply under shear fatigue loading conditions, the method explained by Eqs. 5.19 to 5.22 must be modified. For a unidirectional ply under shear, the definitions of tensile strength and compression strength are meaningless, i.e., there is no difference between positive and negative shear. Therefore, the word strength is used instead. By considering this, the parameter "c" in Eq. 5.22 is equal to one (c=1) for shear fatigue conditions. Also, the experimental results for unidirectional plies under in-plane shear loading conditions to be presented in Chapter 7, show that a better curve fitting is achieved by adding a "$\log_{10}$" to the left-hand side of Eq 5.22. Therefore, Eq. 5.22 is changed to the following form for the simulation of fatigue life of the unidirectional ply under shear loading conditions. The left-hand side of Eq. 5.23 is still denoted by "u" for briefness.

$$u = \log_{10}\left(\frac{\ln(a/f)}{\ln[(1-q)(1+q)]}\right) = A + B\log N_f \qquad \textbf{Eq. 5.23}$$

5.5 Generalized Material Property Degradation Technique

At this stage, the *normalized strength degradation* (Eq. 5.16), *the normalized residual stiffness* (Eq. 5.17), and the *normalized fatigue life models* in form of Eq. 5.22 (and 5.23 for shear), are established and available. By coupling these models, the *generalized material property degradation technique* is established. By using this *technique*, polynomial fatigue failure criteria can be applied for failure analysis of unidirectional plies under arbitrary stress state and stress ratios. This *technique* is explained by the flowchart shown in Fig. 5.12.

To explain the model, consider a unidirectional ply under a multiaxial state of stress. Also, suppose that one of the modes of fatigue failure, e.g., the fiber tension fatigue failure mode (Eq. 4.14) is to be verified. As shown in the flowchart (Fig. 5.12), the state of stress (σ), stress ratio (κ), number of applied cycles (n) and the static material properties must be defined at the beginning. For the aforementioned mode of failure, the static properties of the unidirectional ply in fiber direction (X_t) and in-plane shear (S_{xy} and E_{xy}) and out-of-plane shear (S_{xz} and E_{xz}) loading conditions must be known (see Eq. 4.14). Then by using the *normalized fatigue life model* (Eqs. 5.22 and 5.23), the number of cycles to failure for each stress state (N_{fxx}, N_{fxy} and N_{fxz}) is calculated. By having this information and using the residual stiffness and strength degradation models (Eqs. 5.16 and 5.18), the residual material properties of the unidirectional ply under longitudinal stress, in-plane and out-of-plane shear stresses can be calculated. It should be mentioned here that the experimental parameters (α, β, γ, λ, A, B and f) must be fully characterized in advance for each of the three states of stress in this example. At this stage, all previous results are substituted into Eq. 4.14 to detect the fiber failure mode for the unidirectional ply under multiaxial state of stress. If sudden fiber tension failure is detected, the material properties of the failed region of the unidirectional ply must be changed by sudden material property degradation rule (Eq. 5.1). This simple example shows that the model is capable of considering arbitrary state of stress and stress ratio. Therefore, by establishing the *generalized material property degradation technique*, the severe obstacle of application of quadratic failure criteria for arbitrary stress ratios is overcome.

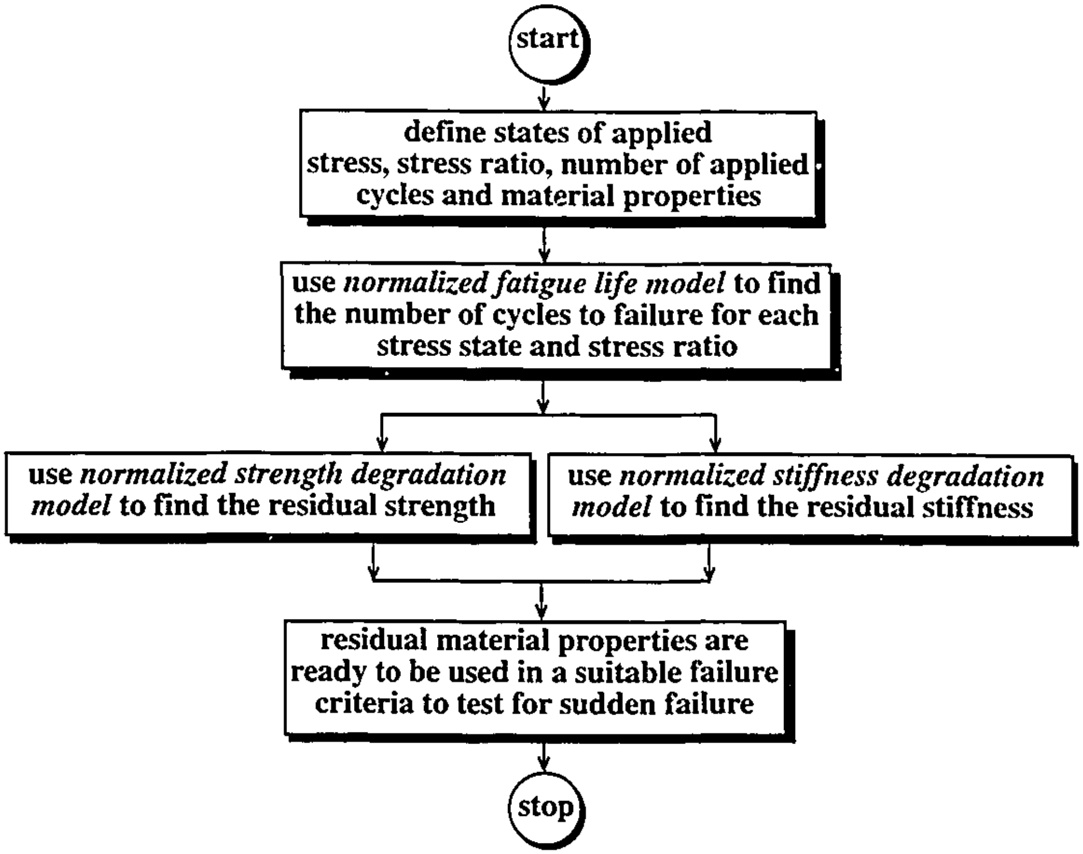

Fig. 5.12 Flowchart of *generalized material property degradation technique* at the ply level

5.6 Summary

After sudden failure detection for a unidirectional ply under a multiaxial state of static or fatigue stress, detected by static or fatigue failure criteria, the material properties of the failed region are changed by sudden material property degradation rules. For the fatigue case, before detecting the sudden mode of failure, the material properties of the unidirectional ply gradually degrade due to fatigue loading. To simulate the gradual material property degradation of a unidirectional ply under multiaxial state of fatigue stress, the *generalized material property degradation technique* is established. For this purpose, the *normalized strength degradation*, *normalized stiffness degradation* and *normalized fatigue life* models are coupled. The established *technique* is capable of simulating the residual material properties of a unidirectional ply under arbitrary stress states and stress ratios. This eliminates the restriction of application of the quadratic fatigue failure criteria for general states of stress and stress ratios.

Chapter 6

Progressive Fatigue Damage Modeling

In this chapter, the framework of *progressive fatigue damage model* is established and explained in detail. The *model* is an integration of the three important components: stress analysis, failure analysis and material property degradation. The *model* is capable of simulating the residual strength, fatigue life and final failure mechanism of composite laminates with arbitrary geometry, stress ratio and stacking sequence under complicated fatigue loading conditions using the results of various types of uniaxial fatigue experiments on unidirectional plies. The generality and capabilities of the *model* are discussed in detail. Based on the *model*, a computer code is developed which simulates the cycle-by-cycle behaviour of composite laminates under fatigue loading conditions.

6.1 Introduction to Progressive Damage Modeling

The idea of progressive damage modeling of laminated composites under static loading conditions was initially proposed by Chou *et al.* [254,255]. They did not utilize a set of failure criteria capable of distinction of different failure modes. Therefore after failure detection, they had to delete all material properties of the failed region. This procedure is a very conservative and primitive type of damage modeling which results in a very low magnitude of the final failure load compared to experimental results. The idea of detection of different failure modes (fiber and matrix directions) by a set of discrete failure criteria was initially proposed by Hashin [164]. This type of discrete failure criteria was successfully utilized by investigators in a progressive damage modeling approach for two-dimensional [41-43] and three-dimensional [130] failure simulation of pin-loaded composite laminates under static loading conditions.

To describe *progressive fatigue damage modeling*, it is helpful to explain the traditional progressive damage modeling technique used in static failure analysis of composite laminates. As previously mentioned, the progressive damage model is an integration of stress analysis, failure analysis and material degradation rules. The model can be clearly described by means of the flowchart shown in Fig. 6.1.

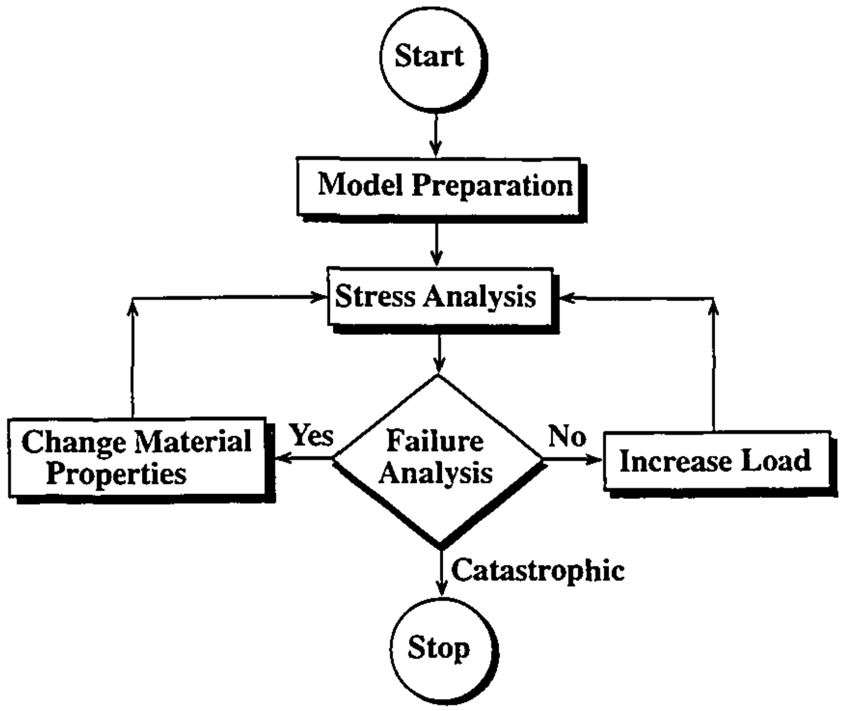

Fig. 6.1 Flowchart of traditional progressive damage model used for static failure analysis

As shown in Fig. 6.1, the finite element model must be prepared at the beginning. In this step the physical properties, material properties, and appropriate boundary conditions of the problem are provided and a load increment is selected. In the next step, a finite element stress analysis at a selected load increment is performed. In this step, on-axis stresses for each element (averaged at twenty seven Gauss points) are calculated and utilized for failure analysis. By using the static failure criteria (Eqs. 4.1 to 4.11), failure analysis is performed and the existence of sudden modes of failure for all elements is checked. If the failure criteria are not met, there is no failure at this load increment. At this stage, more load increments are applied and the stress analysis is performed. These new on-axis stresses must be added to the previously obtained on-axis stresses. Subsequently, failure analysis is performed for all elements and if there is failure in certain plies of certain elements, based the mode of failure, the material properties of the those failed plies are changed by using Eqs 5.1 to 5.7. The first instance of failure is called the failure initiation load. After changing the material properties, a new stiffness matrix is rebuilt and assigned to the finite element model. Thereafter, the stress analysis step is repeated and whole loop in the algorithm is continued. Thus if an element undergoes failure, not only are appropriate material properties reduced, but the stress state is also relaxed in that element by the fact that the stress state has been recalculated for the whole model. As the load level increases, more and more elements will fail until ultimate failure is reached. This situation (catastrophic failure) occurs when the laminated composite cannot tolerate any more load increments and a large deflection occurs. At this stage, the final failure load and failure mechanism are achieved.

The progressive damage model in traditional form cannot be used for the fatigue modeling of laminated composites. For instance, if the maximum load level in fatigue loading conditions is selected below the failure initiation load, then the sudden failure criteria will not detect any sudden mode of failure. Therefore, the progressive damage modeling strategy used for static loading must be modified to be used for fatigue loading conditions. In this study, the idea of the *progressive fatigue damage modeling* is extended from the traditional progressive damage modeling approach, used for static failure analysis of laminated composites. The three major components of the model were explained in the previous chapters. In the following section, the framework of the *progressive fatigue damage model* is explained in detail.

6.2 Progressive Fatigue Damage Modeling

The major difference between the *progressive fatigue damage model* and the traditional progressive damage model used for static loading conditions is the existence of the gradual material property degradation which occurs during fatigue loading. In the previous chapter, the *generalized material property degradation technique* is established. This technique simulates the material property (stiffness and strength) degradation and fatigue life of a unidirectional ply under a multiaxial state of stress and arbitrary stress ratio. By adding this technique to the traditional progressive damage model and necessary modification of the algorithm, the *progressive fatigue damage model* is established and explained by means of the flowchart shown in Fig. 6.2.

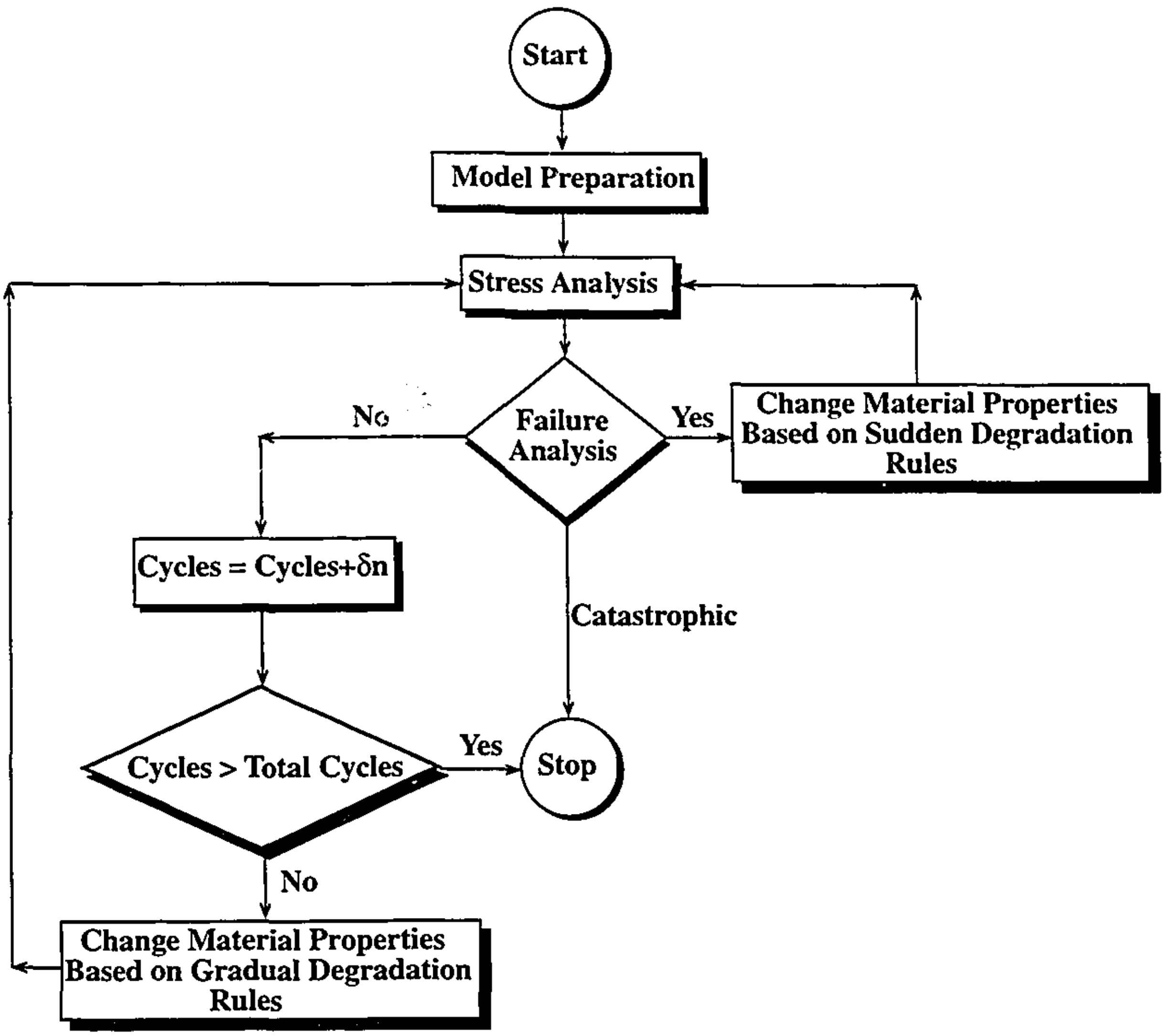

Fig. 6.2 Flowchart of ***progressive fatigue damage model***

As shown in Fig. 6.2, the finite element model must first be prepared. In this step, material properties, geometry, boundary conditions, maximum and minimum fatigue load, maximum number of cycles, incremental number of cycles, etc., are defined. Then the stress analysis, based on the maximum and minimum fatigue load, is performed. Consequently, the maximum and minimum induced on-axis stresses of all elements are calculated. It should be emphasized that on-axis stresses for each ply of each laminate of each element at Gauss points are calculated and averaged. Therefore, the stress ratio ($\kappa = \sigma_{min}/\sigma_{max}$) for each element is determined. In the next step, failure analysis is performed and the maximum stresses are examined by the set of fatigue failure criteria (Eqs. 4.13 To 4.19). If there is a sudden mode of failure, then the material properties of the failed plies are changed according to appropriate *sudden* material property degradation rules (Eqs. 5.1 To 5.7). The stiffness matrix of the finite element model is rebuilt and the stress analysis is performed again. New stresses are examined by the set of fatigue failure criteria. In this step, if there is no sudden mode of failure, an incremental number of cycles are applied (e.g., $\delta n = 100$). If the number of cycles is greater than a preset total number of cycles, then the computer program stops. Otherwise, material properties of all plies of all elements are changed according to *gradual* material property degradation rules using the *generalized material property degradation technique* (see Fig. 5.16). Then stress analysis is performed again and the above loop is repeated until catastrophic failure occurs, or the maximum number of cycles (pre-defined by the user) is reached. If catastrophic failure is reached, then fatigue life and the mechanisms of failure due to fatigue loading have been achieved. It should be noted that if the maximum number of cycles is selected as a large number, such as 10^9, then the fatigue life of the problem can be obtained by the algorithm. If the computer program stops because the user-chosen maximum number of cycles is reached, then the mechanisms of failure due to fatigue loading are found by examining the final state of damage. Furthermore, in the latter case, residual strength of the composite laminate is obtainable by performing a progressive static damage modeling on the final results of *progressive fatigue damage model.*

Based on the algorithm explained by the flowchart shown in Fig. 6.2, a user-friendly computer code is developed. The computer code developed in this study is published by the author elsewhere [276]. The computer code is able to simulate the cycle-by-cycle behaviour of a laminated composite under general fatigue loading conditions and predicts the residual strength and the fatigue life of the problem.

6.3 Requirements

In order to apply *fatigue progressive damage modeling* to study the fatigue behaviour of composite materials, a complete knowledge of material properties (stiffness, strength, and fatigue life) of a unidirectional ply under static and fatigue loading conditions is required. Hence, to run the computer program developed for *progressive fatigue modeling* of laminated composites, the mechanical behaviour of a unidirectional ply under uniaxial static and fatigue loading conditions must be fully characterized. For this purpose, the material properties of a unidirectional composite laminate in static and fatigue loading conditions; in the fiber and matrix directions; under tensile, compressive, in-plane-shear and out-of-plane-shear loading are required. Also, the experimental parameters mentioned in the previous chapter for a unidirectional ply must be obtained. To prepare this complete set of input data for the computer program, a unidirectional ply under static and fatigue loading conditions must be fully characterized which is the subject of the next chapter.

Chapter 7

Experimental Characterization of Basic Material Properties

This chapter is devoted to experimental characterization of the material properties of a unidirectional ply under static and fatigue loading conditions. The material properties (strength, stiffness, residual strength, residual stiffness and fatigue life) of unidirectional AS4/3501-6 graphite/epoxy material are fully characterized under tension and compression, for fiber and matrix directions, and under in-plane and out-of-plane shear, in static and fatigue loading conditions. The information provided by this series of experiments is used as input data for the *progressive fatigue damage model.* To avoid performing infinite numbers of experiments under various stress states and stress ratios in fatigue loading conditions, the normalization techniques explained in the previous chapter are utilized here. Some of the existing testing methods for characterization of composites are necessarily modified and improved during the experimental studies in this research.

7.1 Introduction

Experimental characterization refers to the determination of the material properties through tests conducted on suitably designed specimens [255]. The anisotropic nature of composite materials presents several difficulties which make the experimental characterization of such materials a tedious task. There are various testing techniques for determination of the mechanical properties of composite materials. Nevertheless, sometimes quite different magnitudes for the same mechanical property of a composite material measured by different testing techniques are reported in the literature (as a critical review see [256]). There are few standard testing methods for experimental characterization of some mechanical properties of unidirectional plies under static and fatigue loading conditions. However, after many years of using these testing methods for measuring the material properties of composite laminates in research centers and industries, more improvements are still needed. Therefore, selection of the best testing methods to find reliable results is time consuming and expensive and depends upon the experience of the investigator.

7.2 Required Experiments

In order to apply the *progressive fatigue damage model* to study the fatigue behaviour of composite materials, a complete knowledge of material properties (stiffness, strength and fatigue life) of a unidirectional ply under static and fatigue loading conditions is needed. For this purpose, the material properties of a unidirectional composite laminate in static and fatigue loading, in the fiber and matrix directions, under tensile, compressive, in-plane-shear and out-of-plane-shear loading, are determined experimentally. The experiments are designed to determine the experimental parameters needed by the model explained in previous chapters. As a first step, all material properties of a unidirectional ply (stiffness and strength) under static loading conditions are measured to establish initial strengths and stiffnesses. Using the results from static tests as normalizing parameters, material properties of a unidirectional ply (stiffness, strength, and life) under fatigue loading are characterized experimentally. From the experiments conducted in fatigue, residual strength, residual stiffness and fatigue life of the unidirectional ply under uniaxial loading are fully determined. The static and fatigue tests, required for full characterization of the material properties of a unidirectional ply are shown in Fig. 7.1.

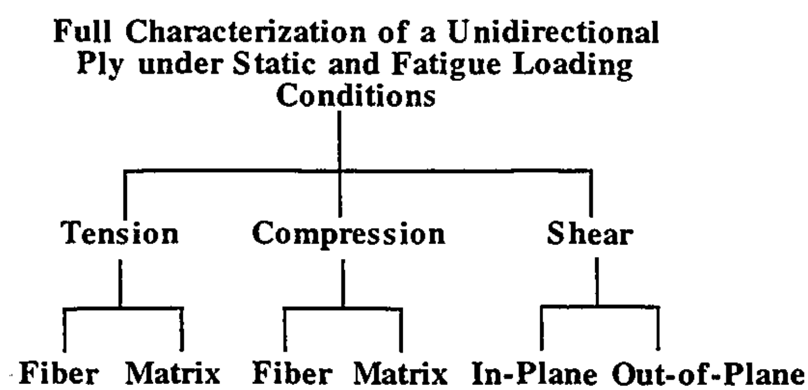

Fig. 7.1 Tests needed to fully characterize material properties of a unidirectional ply under static and fatigue loading

It must be noted that the series of tests are designed based on the transversely isotropic material property assumption, explained in Chapter 3. Consequently, the material properties of the unidirectional ply in normal and transverse directions are assumed to be the same. This assumption decreases the number of required experiments. Also to avoid the infinite number of fatigue experiments under arbitrary stresses and stress ratios, three normalization techniques (explained in Chapter 5) for stiffness degradation, strength degradation and fatigue life are used.

7.3 Experimental Setup

Tests are performed using the Material Testing System (MTS 810) equipped with hydraulic grips (Fig. 7.2). A personal computer is connected to the MTS for data acquisition. Displacement, load and strain are monitored for static experiments. In fatigue tests, maximum and minimum displacement, load and strain as well as number of cycles, are monitored. The strain is measured by using an extensometer or strain gages. To transfer the results from the strain gages to the controller and the computer, an accurate Wheatstone bridge is made and calibrated. Static tests are performed under displacement control, while the fatigue tests are carried out under load control conditions. To avoid temperature effects, which could degrade the material properties, fatigue tests are performed at frequencies less than 10 Hz. All tests are performed in ambient temperature.

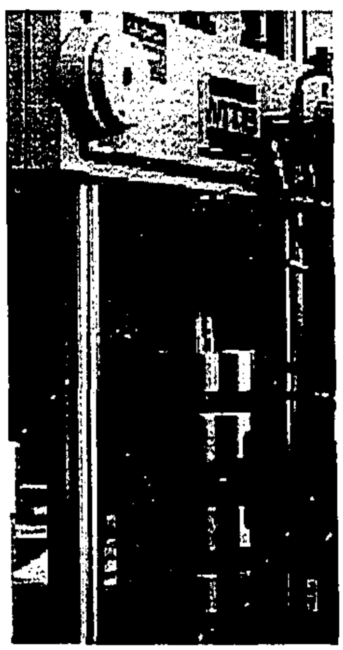

Fig. 7.2 MTS 810 equipped with hydraulic grips

7.4 Specifications of Test Specimens

The specifications (dimensions, standards, and modifications) of the test specimens in static and fatigue loading conditions, for full characterization of unidirectional plies, are explained in Table 7.1.

Type of test (Static or Fatigue)	Test Specimens	Standards	Notes
Fiber Tension	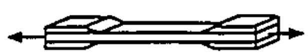	D 3039-76 D 3479-76	With Hydraulic Grips
Fiber Compression		———	With Hydraulic Grips
Matrix Tension		D 3039-76 D 3479-76	With Hydraulic Grips
Matrix Compression		D 3410-87	With Hydraulic Grips
In-Plane Shear	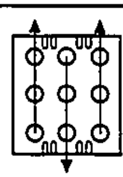	D 4255-83	Modified Notched Specimen
Out-of-Plane Shear		D 2733-70 D 2344-84	With Clamp

Table 7.1 Specifications of test specimens

7.5 Test Procedures

Tests are designed based on the required information and data for the *progressive fatigue damage model* (explained in previous chapters). First, static tests are performed to find the static strengths and stiffnesses. For all six cases, except for the out-of-plane shear case, mentioned in Table 7.1, the static strengths and moduli are measured. For the out-of-plane shear case, the static strength is measured while the stiffness is calculated by the transversely isotropic material property assumption (Eq. 3.6). Then the fatigue tests are performed to measure the residual stiffness, residual strength and fatigue life. The fatigue load is applied in a sinusoidal form. For the fatigue life experiments, the maximum applied stress is selected based on some percentage of static strength (e.g., 50%, 60%, etc.). Different stress ratios ($\kappa=\sigma_{min}/\sigma_{max}$) are applied and tests are continued until catastrophic failure is achieved. To determine the residual properties, two stress levels (low and high) are selected and fatigue load is stopped after some number of cycles (e.g., 10^2, 10^3, etc.). Static load is then applied to measure the residual moduli and strengths.

7.6 Test Results

As mentioned earlier, fatigue behaviour of unidirectional plies under longitudinal tensile [55-61], longitudinal compressive [62,63], matrix compressive [62-64] and in-plane shear loading [55,65-76] has been studied by different authors. In most of these works, fatigue failure is explained by interpretation of experimental observations of damage modes. However, there is no attempt in the aforementioned references to fully characterize the fatigue properties of a unidirectional ply (such as, residual stiffness, residual strength and fatigue life) under various types of fatigue loading. Also, there is a lack of information in the literature, on transverse tensile and out-of-plane shear fatigue behaviour of unidirectional plies. Unfortunately, the existing results in the literature cannot be used in the established model. Therefore, an extensive experimental program is conducted in this research to fully characterize the material properties of unidirectional AS4/3501-6 graphite/epoxy. The material is used in prepreg form and processed in an autoclave by the method suggested by the supplier. The specimens are manufactured and machined using available techniques.

7.6.1 Longitudinal Tensile Tests

In this section, the results of static and fatigue experiments for characterizing the material properties of a unidirectional ply $[0]_{16}$, in the fiber direction under tensile loading are summarized. The specimens for fiber in tension tests are manufactured based on ASTM D 3039-76 [258] and ASTM D 3479-76 [259] standards. The specimen and the dimensions are shown in Fig. 7.3. Among different tabbing methods examined in this study, the fiberglass tabs have the best performance. Therefore, specimens are equipped with fiberglass tabs to reduce the gripping effects.

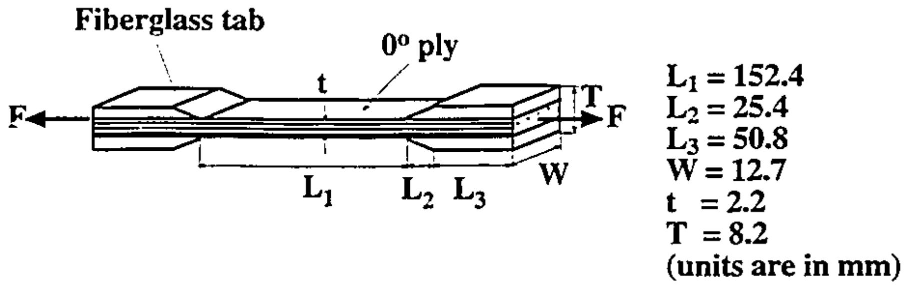

Fig. 7.3 Fiber in tension specimen

7.6.1.1 Static Stiffness and Strength

The results of static experiments for measuring the stiffness and strength of the material in fiber direction under tensile loading are summarized in this section. Typical stress-strain behaviour of a unidirectional 0° ply under static tensile loading in the fiber direction is shown in Fig. 7.4. As shown, the stress-strain behaviour is linear and final failure occurs catastrophically.

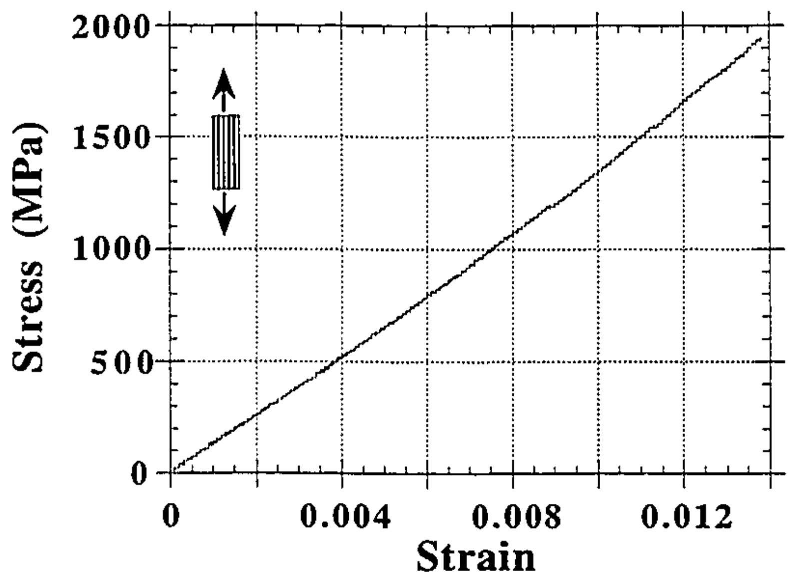

Fig. 7.4 Typical stress-strain behaviour of a unidirectional 0° ply under static tensile loading in the fiber direction

The results of static experiments for measuring the static stiffness and strength of the unidirectional 0° ply under longitudinal tensile loading conditions (average values and standard deviations) are shown in Figs. 7.5 and 7.6, respectively.

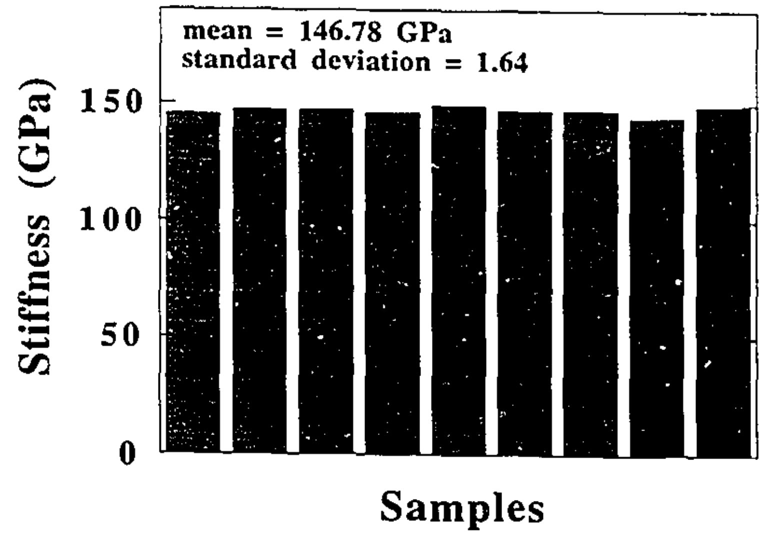

Fig. 7.5 Static stiffness of unidirectional 0° ply under longitudinal tensile stress

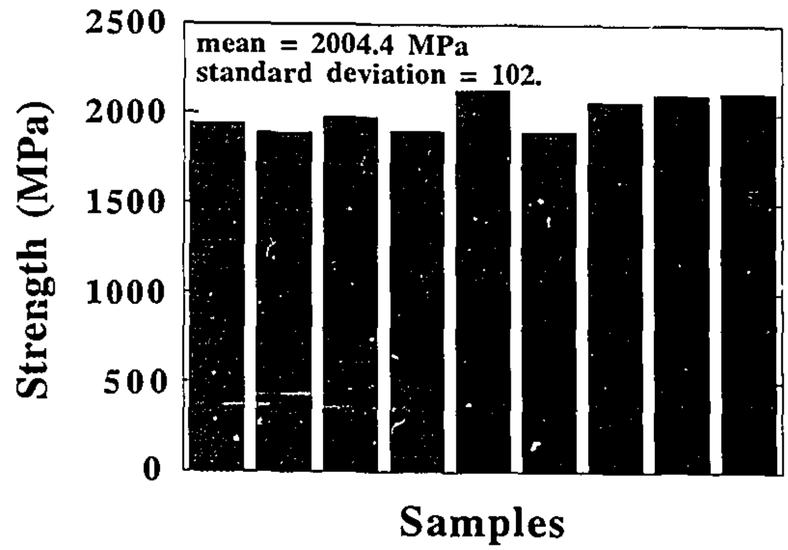

Fig. 7.6 Static strength of unidirectional 0° ply under longitudinal tensile stress

The mean ($\overline{x}$) and standard deviation (S) are calculated by the following standard equations:

$$\overline{x} = \frac{\sum_{i=1}^{n} x_i}{n}$$

and **Eq. 7.1**

$$S = \sqrt{\frac{\sum_{i=1}^{n} (x_i - \overline{x})^2}{n-1}}$$

where x and n are the test value and number of samples.

7.6.1.2 Normalized Residual Stiffness and Strength

The results of experiments for measuring the residual stiffness and residual strength of unidirectional 0° plies under tension-tension fatigue are presented here. To measure the residual stiffness and residual strength, two different states of stress (80% and 60% of the longitudinal tensile static strength) are selected. By selecting these two different states of stress, the high and low stress levels are applied. A stress ratio equal to 0.1 and a frequency below 10 Hz are applied. The results of residual stiffness and strength experiments are shown in Figs. 7.7 and 7.8, respectively. A least square curve fitting method is used and the curve fitting parameters using Eqs. 5.16 and 5.18 are also calculated and mentioned in Figs. 7.7 and 7.8. An interesting increase in residual stiffness and in residual strength (about 8 to 13% of the static stiffness and strength) for the first few cycles, is observed experimentally. The increase in residual stiffness is perhaps due to realignment of some of the 0° fibers. The phenomenon of increasing of residual fatigue stiffness and strength for unidirectional plies has also been observed by Awerbuch and Hahn [257]. As clearly shown in Figs. 7.7 and 7.8, while the curve fitting using Eqs. 5.16 and 5.18 is able to fit the decreasing parts of the curves very well, it is not able to consider the increase in residual stiffness and strength in the first few cycles. As will be shown in the next chapter, these results in the present forms can be used for simulation of decreasing of the residual strength of notched composite laminates. However, by ignoring the increasing parts of the residual stiffness and strength curves of the unidirectional ply, simulation of increasing of the residual strength of notched composites for the first few fatigue cycles, which is a frequently observed phenomenon [4, 9, 11, 13, 17-20, 25, 27, 33, 38, 44, 257, 282-287], is not possible. A new strategy for curve fitting and more details about this subject will be discussed in the next chapter.

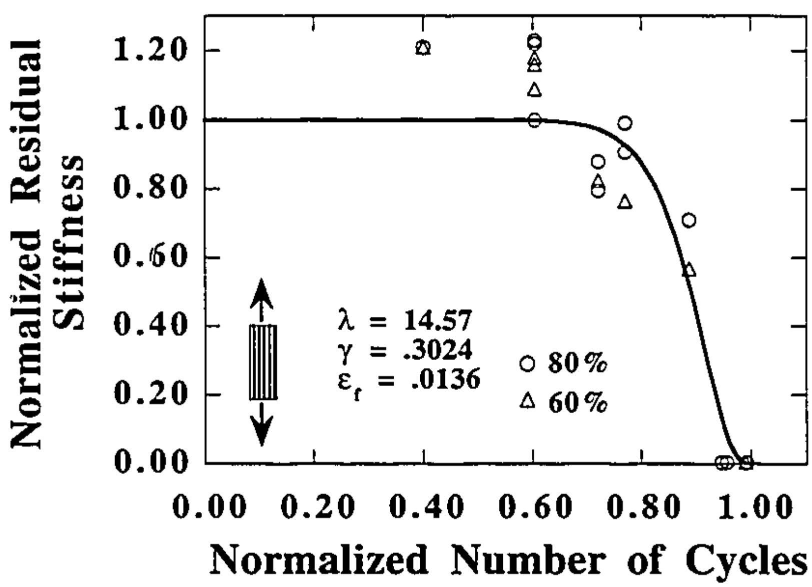

Fig. 7.7 Normalized residual stiffness of a unidirectional 0° ply under longitudinal tensile fatigue loading conditions (using Eq. 5.18)

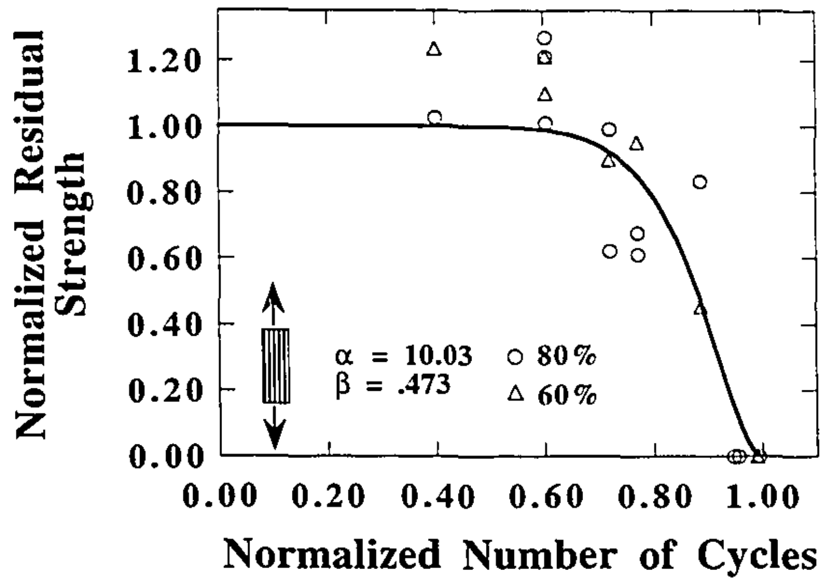

Fig. 7.8 Normalized residual strength of a unidirectional 0° ply under longitudinal tensile fatigue loading conditions (using Eq. 5.16)

7.6.1.3 Static and Fatigue Modes of Failure

The final failure mode of the tension-tension fatigue tests for the unidirectional 0° plies loaded in fiber direction is the same as the final failure mode from static experiments. There is a small amount of tab debonding near the gage area for the specimen under static loading, and for fatigue experiments this phenomena is more visible. A picture of unidirectional 0° plies, failed in tensile static and fatigue loading in the fiber direction, is shown in Fig. 7.9.

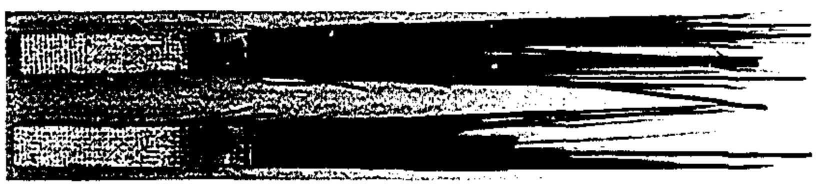

(a) static failure

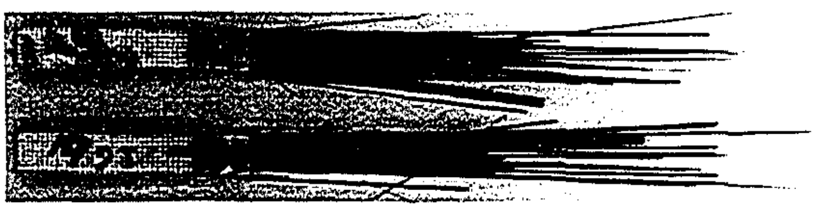

(b) fatigue failure

Fig. 7.9 Unidirectional 0° plies, failed under tensile static and fatigue loading in the fiber direction

In the following, the results of static and fatigue experiments for a unidirectional 0° ply under uniaxial compressive loading are presented. Thereafter, the results of fatigue life experiments for a unidirectional 0° ply under uniaxial tensile and compressive loading will be combined and presented in a normalized form.

7.6.2 Longitudinal Compressive Tests

In this section, the results of static and fatigue experiments for characterizing the material properties of a unidirectional ply $[0]_{24}$, in the fiber direction under compressive loading are summarized. The compression test is one of the most difficult types of test to perform. There are various testing methods for performing compression experiments and they are categorized based on the type of loading (end load, shear load, mixed end/shear load and bending load) of the compression specimen. A list of some of these methods is given in Table 7.2. Many of these methods need to use fixtures which reduce their simplicity.

Type of Loading	Compression Testing Method	References
End load	ASTM D-695 Modified ASTM D-695 RAE Northrop	[264] [265] [266] [267]
Shear load	Celanese IITRI Wyoming modified IITRI Hydraulic grips	[260] [260] [268] [269,270,271]
Mixed end/shear load	Atmure ICSTM RAE modified Celanese	[272] [273] [274]
Bending load	Four point bend Sandwich beam	[260] [275]

Table 7.2 Compression testing methods

Most of the aforementioned testing methods are not suitable for fatigue experiments. Therefore, a new test specimen (Fig. 7.10) has been developed during this research which is suitable for both static and fatigue testing. No fixture is required to perform the static and fatigue tests which is an important advantage of the new specimen. Hydraulic grips are used for experiments and to improve the traction of the wedges, they were plasma projected by an electric arc procedure. To decrease the gripping effects, the specimen is equipped with flat fiberglass tabs and Teflon inserts. The catastophic failure of the developed specimen consistently occurs in the gage area, and its performance shows great improvement in both static and fatigue loading conditions. The analytical and experimental study of the developed specimen and its advantages are published elsewhere [270,271], and due to space limitations, are not presented here.

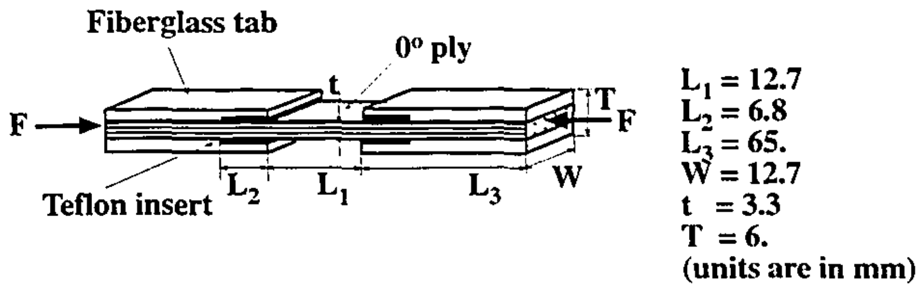

Fig. 7.10 Fiber compression specimen

7.6.2.1 Static Stiffness and Strength

The results of static experiments for measuring the static stiffness and strength of the material in the fiber direction under compressive loading are summarized here. Typical stress-strain behaviour of a unidirectional 0° ply under static compressive loading in the fiber direction, using back to back strain gages, is shown in Fig. 7.11. As shown, the stress-strain behaviour is slightly nonlinear and final failure occurs catastrophically.

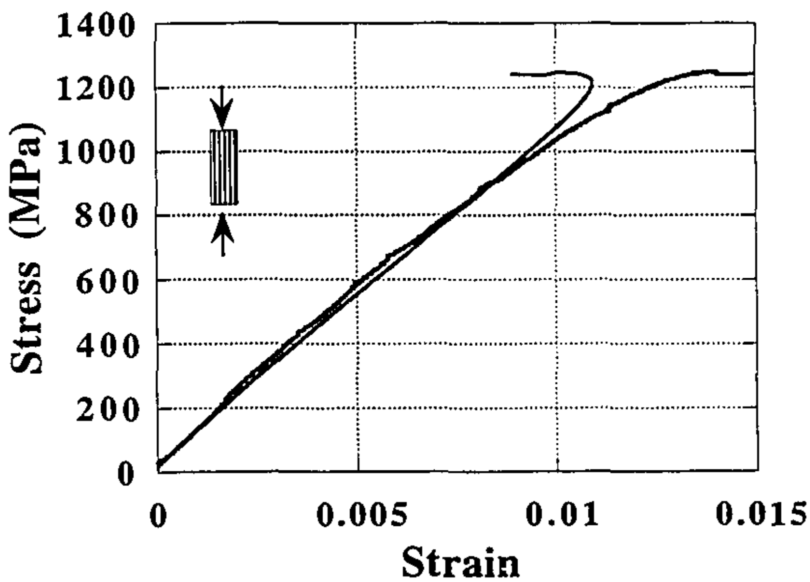

Fig. 7.11 Typical stress-strain behaviour of a unidirectional 0° ply under static compressive loading in the fiber direction (using back to back strain gages)

The results of static experiments for measuring the static stiffness and strength of the unidirectional 0° ply under longitudinal compressive loading conditions (average values and standard deviations) are shown in Figs. 7.12 and 7.13, respectively.

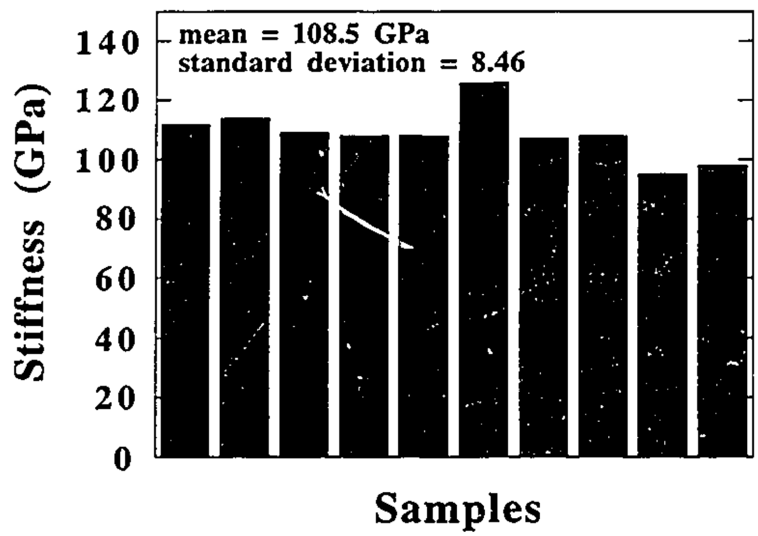

Fig. 7.12 Static stiffness of unidirectional 0° ply under longitudinal compressive stress

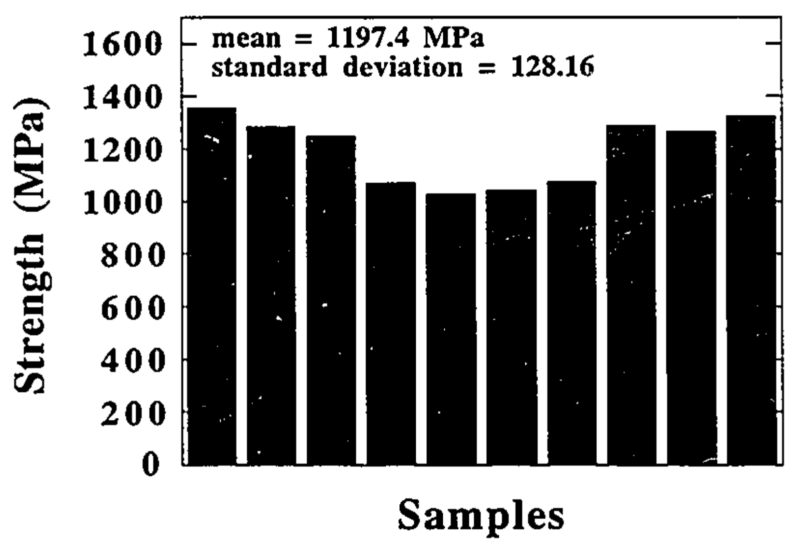

Fig. 7.13 Static strength of unidirectional 0° ply under longitudinal compressive stress

Although the static stiffness of unidirectional 0° ply under compressive loading is characterized experimentally, in the finite element modeling the tensile stiffness is utilized. The difference between the longitudinal static stiffness of a unidirectional 0° ply under tensile and compressive loading is about 26%. By modification of the constitutive equation and using an iterative scheme in the finite element model, different modulus of elasticity for tensile and compressive regions could be considered. However, adding such a scheme to the finite element code makes it more complicated and is avoided in this study.

7.6.2.2 Normalized Residual Strength

The results of experiments for measuring the residual strength of unidirectional 0° plies under compression-compression fatigue are presented here. To measure residual strength under fatigue loading, two different states of stress (80% and 60% of the longitudinal compressive static strength) are selected. Again, by selecting these two different states of stress, high and low stress levels are applied. A stress ratio equal to 10 and a frequency below 10 Hz are applied. The results of residual strength experiments are shown in Fig. 7.14. The residual stiffness of the unidirectional 0° ply under compressive fatigue loading is also experimentally characterized in this study but published by the author elsewhere [276]. However, similar to the static case, the residual stiffness under tension and compression fatigue loading conditions are assumed to be equal. Also, similar to the fiber in tension case, an increase in residual strength of 8 to 10% of the static strength is observed experimentally. As clearly shown in Fig. 7.14, Eq. 5.16 is not able to account for the increase in the residual strength. This subject was explained for fiber in tension case in section 7.6.1.2 and is valid here, and will be discussed further in the next chapter.

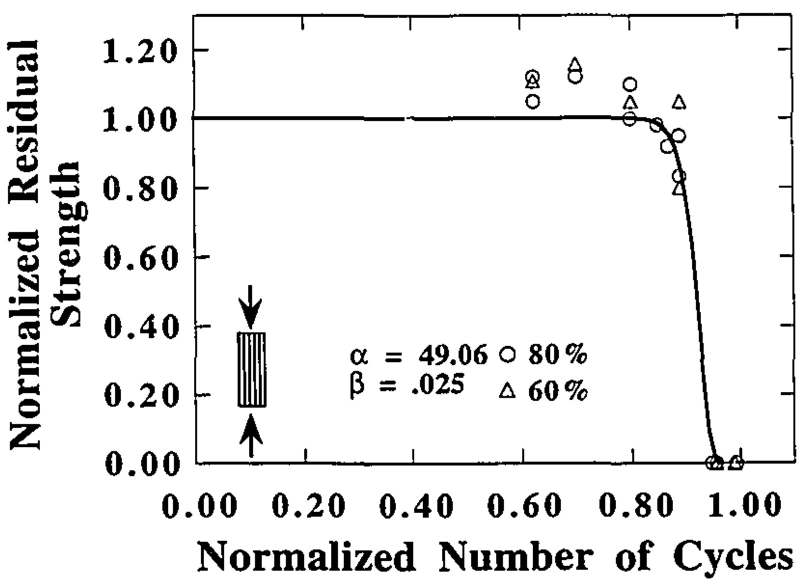

Fig. 7.14 Normalized residual strength of a unidirectional 0° ply under longitudinal compressive fatigue loading conditions (using Eq. 5.16)

7.6.2.3 Static and Fatigue Modes of Failure

The final failure mode of the compression-compression fatigue tests of the unidirectional 0° plies loaded in fiber direction is the same as the final failure mode from static experiments. Also, there is a small amount of tab debonding near the gage area for the specimen under static loading, and for fatigue experiments, this phenomena is more visible. Pictures of unidirectional 0° plies, failed in compressive static and fatigue loading in the fiber direction, are shown in Fig. 7.15.

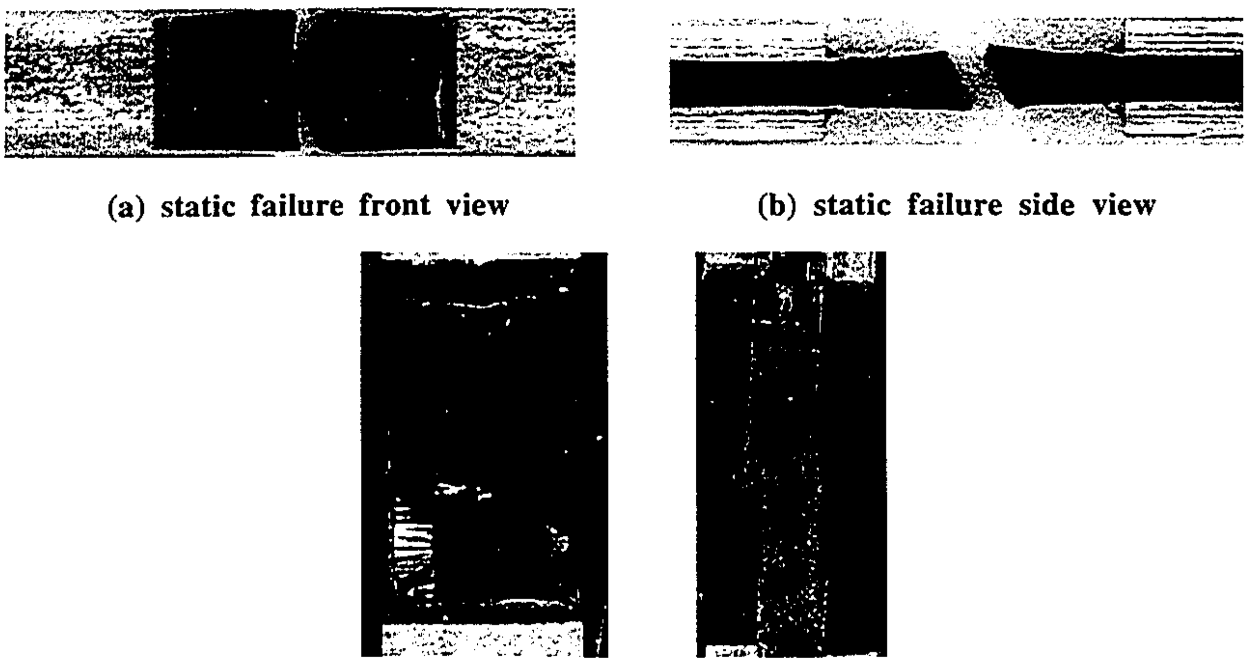

(a) static failure front view **(b) static failure side view**

(c) fatigue failure front view **(d) fatigue failure side view**

Fig. 7.15 Unidirectional 0° plies, failed in compressive static and fatigue loading

7.6.3 Normalized Fatigue Life of Longitudinal Tensile and Compressive Tests

As mentioned earlier, in this section the results of fatigue life experiments for the unidirectional 0° ply under longitudinal tensile and compressive fatigue loading conditions are coupled and presented in a normalized form. Two different stress ratios ($\kappa=\sigma_{min}/\sigma_{max}$ = 0.1 and 10) and different percentages of the static strength (selected as the maximum stress) are applied to find the fatigue life of a unidirectional 0° ply under longitudinal tension-tension and compression-compression fatigue loading conditions. In Fig. 7.16, the master curve for the fatigue life of the unidirectional 0° ply under longitudinal tensile and compressive fatigue loading conditions is presented in a normalized form. By using Eq. 5.22, the curve fitting parameters (A and B) are found and mentioned in Fig. 7.16. Although the parameter "*f*" (in Eq. 5.22) seems to be a function of the strength of laminated composite materials [277], however in this study, a constant magnitude for this parameter (f = 1.06) appears to provide a proper curve fit.

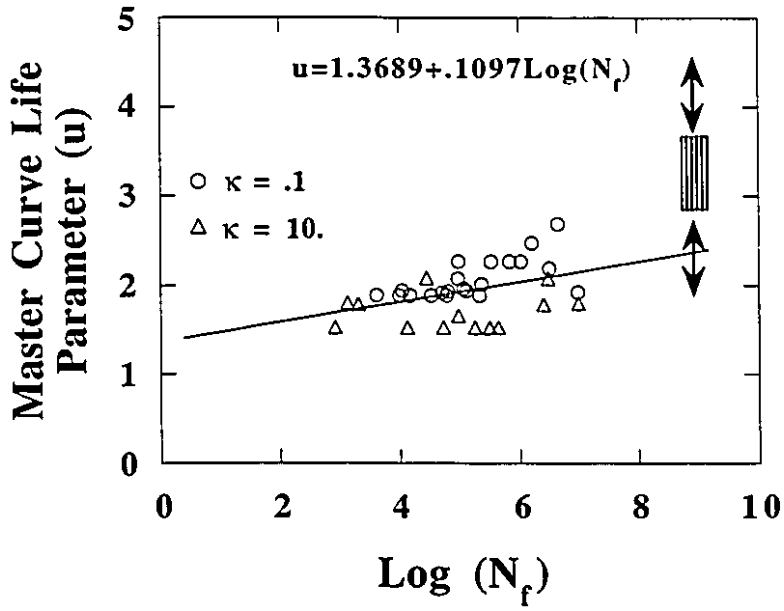

Fig. 7.16 Master curve for fatigue life of unidirectional 0° ply under longitudinal tensile and compressive fatigue loading conditions (using Eq. 5.22)

7.6.4 Transverse Tensile Tests

In the following, the results of static and fatigue experiments for characterizing the material properties of a unidirectional ply $[90]_{16}$, in the matrix direction under tensile loading are summarized. The specimens for matrix in tension tests are manufactured based on ASTM D 3039-76 [258] and ASTM D 3479-76 [259] standards. The specimen and the dimensions are shown in Fig. 7.17. The specimen is equipped with flat metallic tabs.

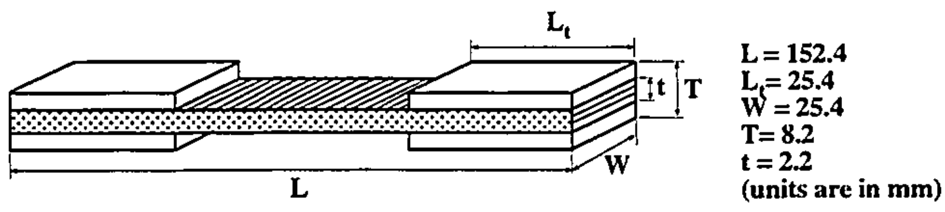

Fig. 7.17 Matrix tensile specimen

7.6.4.1 Static Stiffness and Strength Tests

The results of static experiments for measuring the stiffness and strength of the material in the matrix direction under tensile loading are summarized in this section. Typical stress-strain behaviour of a unidirectional 90° ply under static tensile loading in the matrix direction is shown in Fig. 7.18. As shown, the stress-strain behaviour is linear and final failure occurs catastrophically.

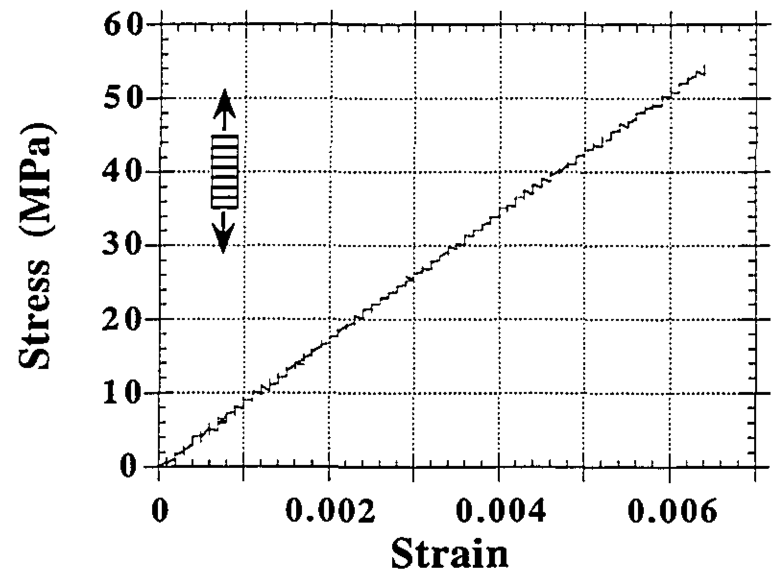

Fig. 7.18 Typical stress-strain behaviour of a unidirectional 90° ply under static tensile loading in the matrix direction

The results of static experiments for measuring the static stiffness and strength of the unidirectional 90° ply under transverse tensile loading conditions (average values and standard deviations) are shown in Figs. 7.19 and 7.20, respectively.

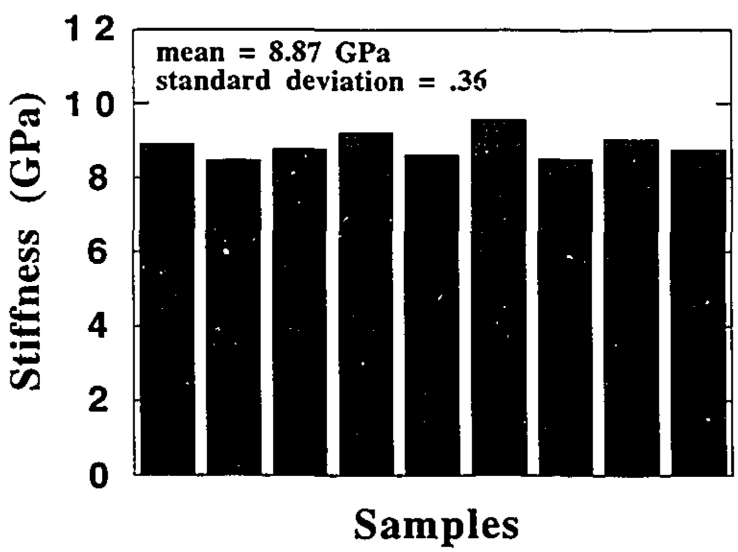

Fig. 7.19 Static stiffness of unidirectional 90° ply under transverse tensile stress

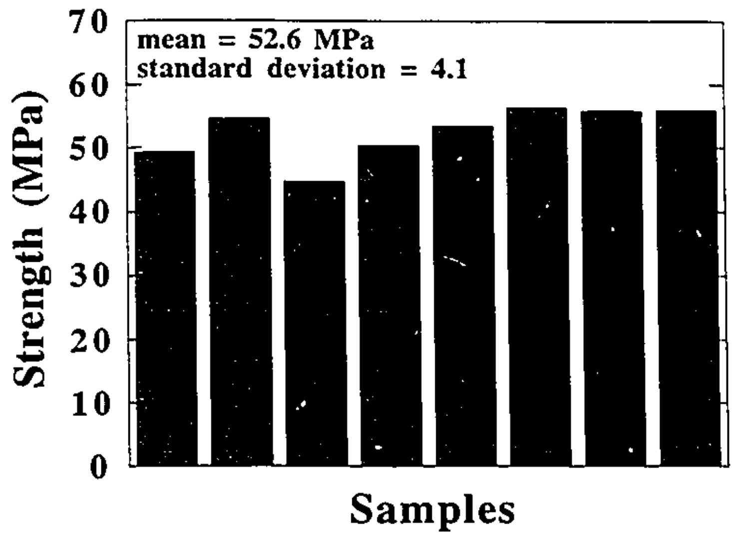

Fig. 7.20 Static strength of unidirectional 90° ply under transverse tensile stress

7.6.4.2 Normalized Residual Stiffness and Strength

The results of experiments for measuring the residual stiffness and residual strength of a unidirectional 90° ply under tension-tension fatigue are presented in this section. To measure the residual stiffness and strength under fatigue loading, two different states of stress (60% and 40% of the tensile transverse static strength) are selected. By selecting these two different states of stress, high and low stress levels are applied. A stress ratio equal to 0.1 and a frequency below 10 Hz are applied. The results of residual stiffness and strength experiments of a unidirectional 90° ply under tension-tension fatigue are shown in Figs. 7.21 and 7.22, respectively.

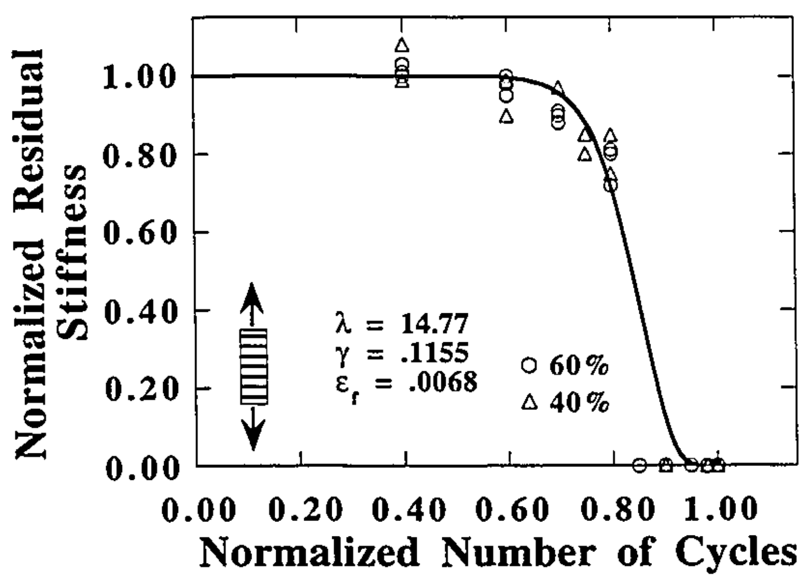

Fig. 7.21 Normalized residual stiffness of a unidirectional 90° ply under transverse tensile fatigue loading conditions (using Eq. 5.18)

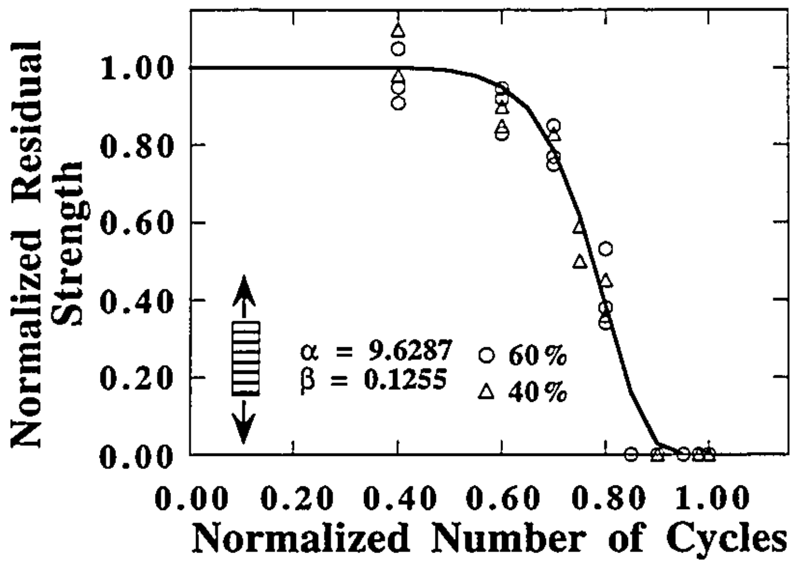

Fig. 7.22 Normalized residual strength of a unidirectional 90° ply under transverse tensile fatigue loading conditions (using Eq. 5.16)

7.6.4.3 Static and Fatigue Modes of Failure

The final failure mode of the tension-tension fatigue tests of the unidirectional 90° plies loaded in matrix direction is the same as the final failure mode from static experiments. A picture of unidirectional 90° plies, failed in tensile static and fatigue loading in the matrix direction, is shown in Fig. 7.23.

Fig. 7.23 Unidirectional 90° plies, failed in tensile static (top) and fatigue (below) loading in the matrix direction

In the following, the results of static and fatigue experiments for a unidirectional 90° ply under uniaxial compressive loading are presented first. Thereafter, the results of fatigue life experiments for a unidirectional 90° ply under uniaxial tensile and compressive loading will be combined and presented in a normalized form.

7.6.5 Transverse Compressive Tests

In this section, the results of static and fatigue experiments for characterizing the material properties of a unidirectional ply $[90]_{24}$, in the matrix direction under compressive loading are summarized. The specimens for matrix in compression tests are manufactured based on ASTM D 3410-87 [260] standard. The specimen and the dimensions are shown in Fig. 7.24. The specimen is equipped with flat metallic tabs and no fixture is required to perform the static and fatigue tests.

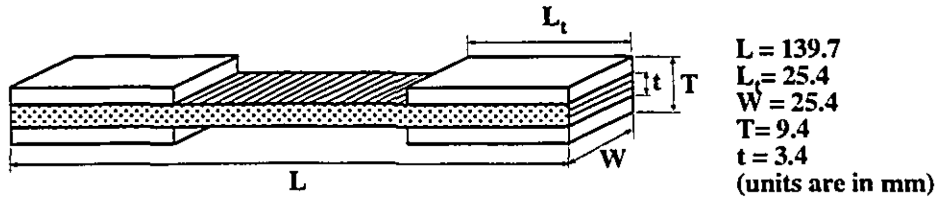

Fig. 7.24 Matrix in compression specimen

7.6.5.1 Static Stiffness and Strength

The results of static experiments for measuring the stiffness and strength of the material in the matrix direction under compressive loading are summarized here. Typical stress-strain behaviour of a unidirectional 90° ply under static compressive loading in the matrix direction is shown in Fig. 7.25. As shown, the stress-strain behaviour is slightly nonlinear and final failure occurs catastrophically.

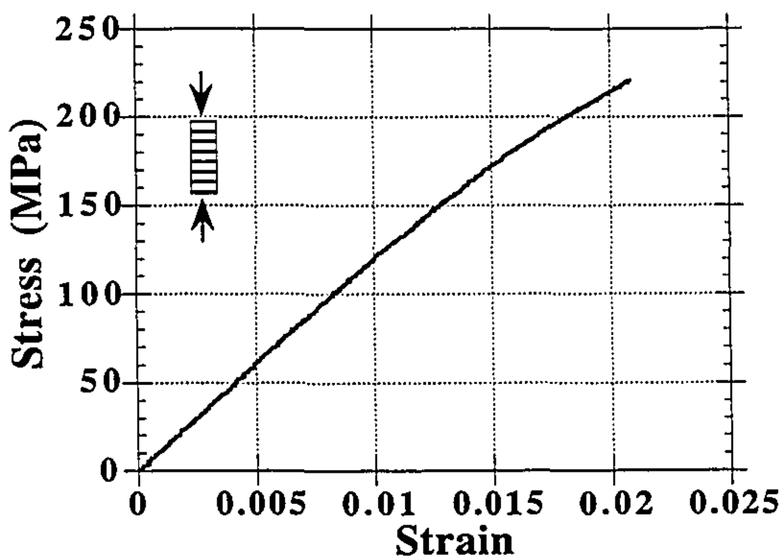

Fig. 7.25 Typical stress-strain behaviour of a unidirectional 90° ply under static compressive loading in the matrix direction

The results of static experiments for measuring the static stiffness and strength of the unidirectional 90° ply under transverse compressive loading conditions (average values and standard deviations) are shown in Figs. 7.26 and 7.27, respectively.

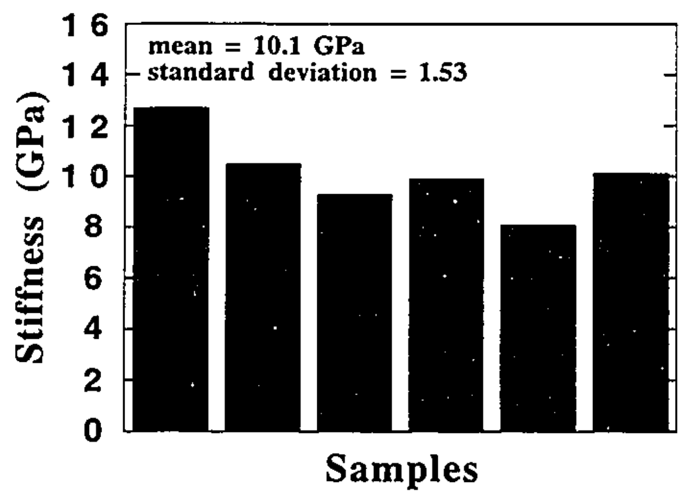

Fig. 7.26 Static stiffness of unidirectional 90° ply under transverse compressive stress

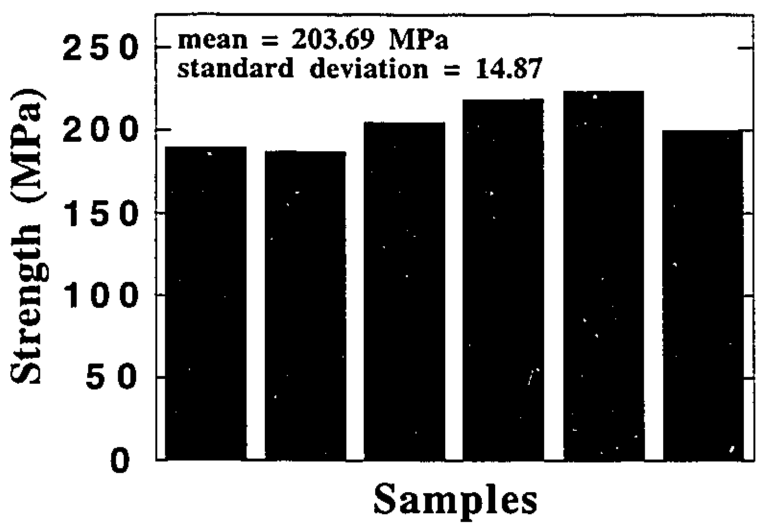

Fig. 7.27 Static strength of unidirectional 90° ply under transverse compressive stress

Similar to the longitudinal tensile and compressive cases, although the static stiffness unidirectional 90° ply under compressive loading is characterized experimentally, in the finite element modeling the tensile stiffness is utilized. The difference between the longitudinal static stiffness of a unidirectional 90° ply under tensile and compressive loading is about 12%.

7.6.5.2 Normalized Residual Strength

The results of experiments for measuring the residual strength of a unidirectional 90° ply under compression-compression fatigue are presented here. To measure the residual strength of the material under fatigue loading, two different states of stress (70% and 50% of the compressive transverse static strength) are selected. Again, by selecting these two different states of stress, high and low stress levels are applied. A stress ratio equal to 10 and a frequency below 10 Hz are applied. The residual stiffness of unidirectional 90° plies under compressive fatigue loading is also experimentally characterized in this study but published by the author elsewhere [276]. However, similar to the static case, the residual stiffness under tension and compression fatigue loading conditions are assumed to be equal. The results of residual strength experiments of a unidirectional 90° ply under compression-compression fatigue are shown in Fig. 7.28.

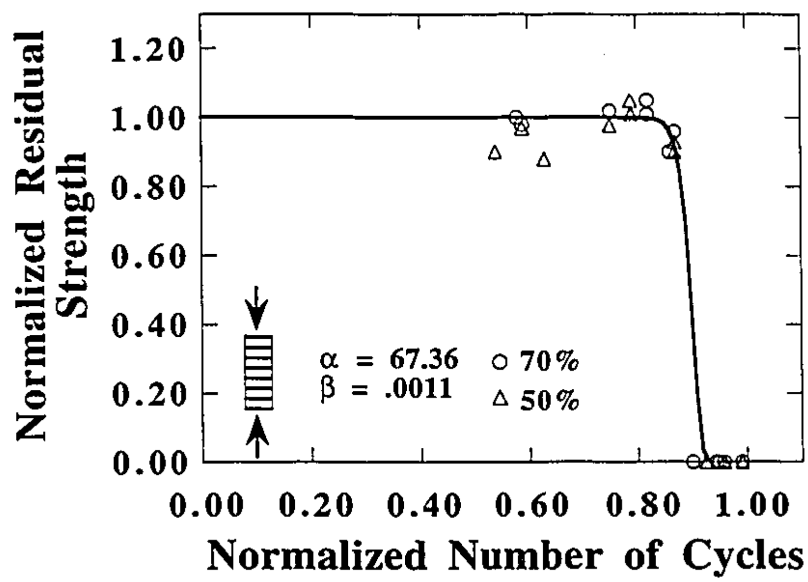

Fig. 7.28 Normalized residual strength of a unidirectional 90° ply under transverse compressive fatigue loading conditions (using Eq. 5.16)

7.6.5.3 Static and Fatigue Modes of Failure

The final failure mode of the compression-compression fatigue tests is the same as the final failure mode from static experiments. A picture of unidirectional 90° plies, failed in compressive static and fatigue loading in the matrix direction, is shown in Fig. 7.29.

Fig. 7.29 Side views of unidirectional 90° plies, failed in compressive static (top) and fatigue (bottom) loading in the matrix direction

7.6.6 Normalized Fatigue Life of Transverse Tensile and Compressive Tests

As mentioned earlier, in this section the results of fatigue life experiments for the unidirectional 90° ply under transverse tensile and compressive fatigue loading conditions are coupled and presented in a normalized form. Two different stress ratios ($\kappa = \sigma_{min}/\sigma_{max}$ = 0.1 and 10) and different percentages of the static strength (selected as the maximum stress) are applied to find the fatigue life of a unidirectional 90° ply under transverse tension-tension and compression-compression fatigue loading conditions. In Fig. 7.30, the master curve for the fatigue life of the unidirectional 90° ply under transverse tensile and compressive fatigue loading conditions is presented in a normalized form. By using Eq. 5.22, the curve fitting parameters (A and B) are found and mentioned in Fig. 7.30.

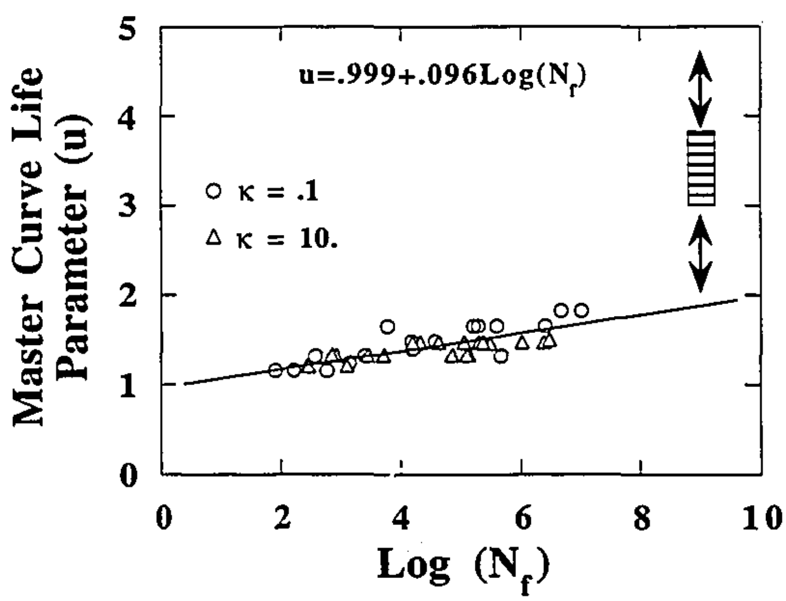

Fig. 7.30 Master curve for fatigue life of unidirectional 90° ply under transverse tensile and compressive fatigue loading conditions (using Eq. 5.22)

7.6.7 In-Plane Shear Tests

In the following, the results of static and fatigue experiments for characterizing the material properties under in-plane shear loading are summarized. There are numerous testing methods for performing the in-plane shear experiments [278-280]. Among these methods, the three-rail shear test method, described by the ASTM D 4255-83 [261] is a fairly reliable technique for characterizing the in-plane shear properties of the material. This method is modified and utilized in this study. The lower part of the standard fixture is redesigned for fatigue experiments (Fig. 7.31). A new specimen is developed by inserting notches into the edges of the specimen. This modification improves the performance of the specimen in both static and fatigue loading conditions. The philosophy behind the insertion of notches at the locations of stress concentrations is to replace a very sharp crack with a blunt crack with much lower stress concentration factor. The analytical and experimental study of the modified specimen is published by the author elsewhere [279,280], and due to space limitations, is not repeated here. To increase the stability of the specimen during the test, a $[0/90]_s$ configuration is selected instead of $0°$ ply. It is clear that theoretically, a $[0/90]_s$ behaves the same as a unidirectional $0°$ ply under in-plane shear loading conditions. The specimen configuration and the dimensions are shown in Fig. 7.32.

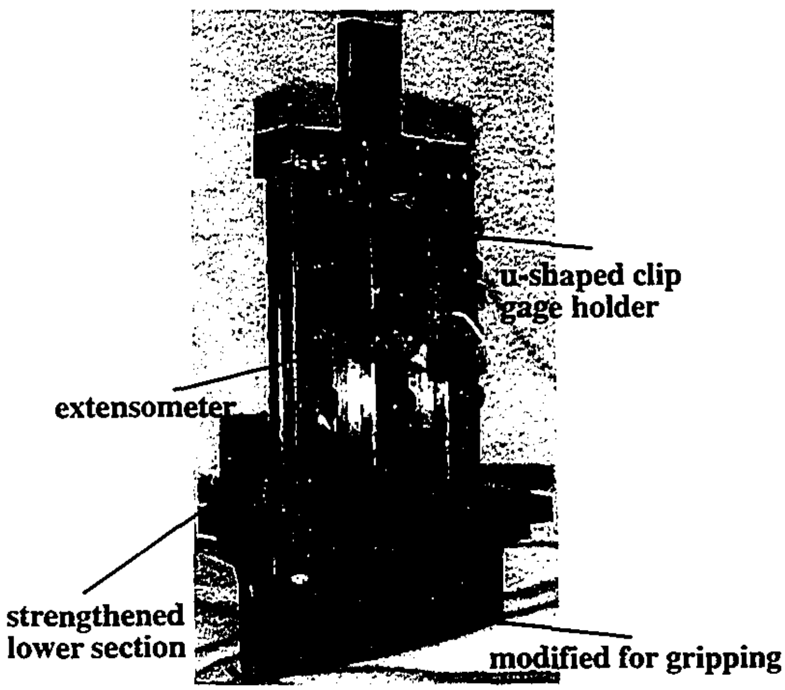

Fig. 7.31 Three-rail shear fixture modified for gripping and equipped with extensometer

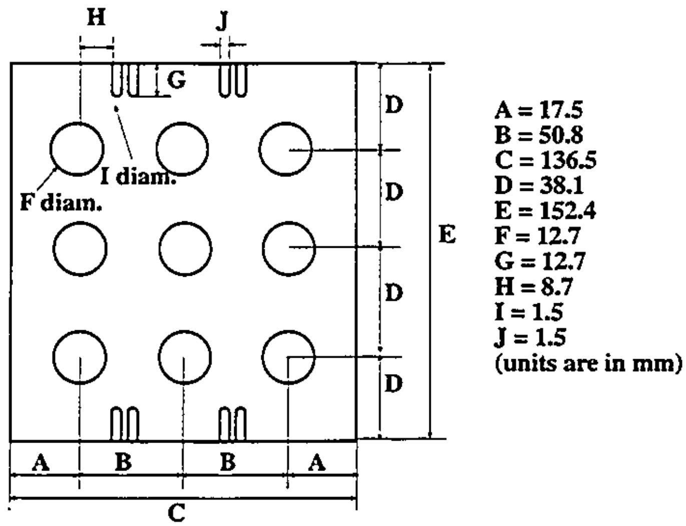

Fig. 7.32 Modified in-plane shear specimen

7.6.7.1 Static Stiffness and Strength

The results of static experiments for measuring the in-plane shear stiffness and strength of are summarized here. Typical stress-strain behaviour of modified specimen (notched) and standard specimen (un-notched) under static in-plane shear loading is shown in Fig. 7.33. As shown, the stress-strain behaviour is highly nonlinear for both notched and un-notched specimens, however, the un-notched specimen fails at a lower load level. It shows that inserting notches improves the performance of the three-rail shear sample. Also, the experimental results of un-notched samples show higher scatter than that of the notched samples (for more details, refer to [279,280]).

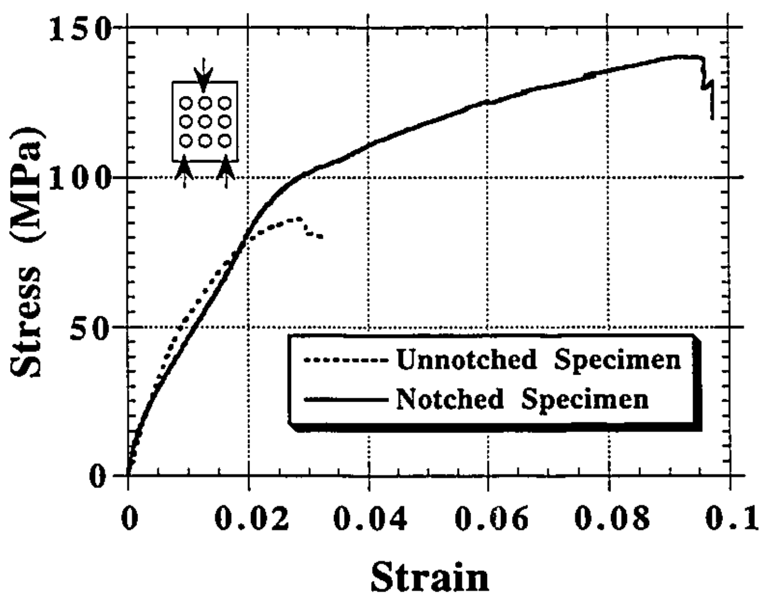

Fig. 7.33 Typical shear stress-strain behaviour of the unidirectional material

The results of static experiments for measuring the static stiffness, parameter of material nonlinearity (δ, Eq. 3.3) and strength of the notched specimens under in-plane shear loading conditions (average values and standard deviations) are shown in Figs. 7.34, 7.35 and 7.36, respectively. The linear elastic part of the stress-strain curves are used to measure the parameter of material nonlinearity (δ, Eq. 3.3).

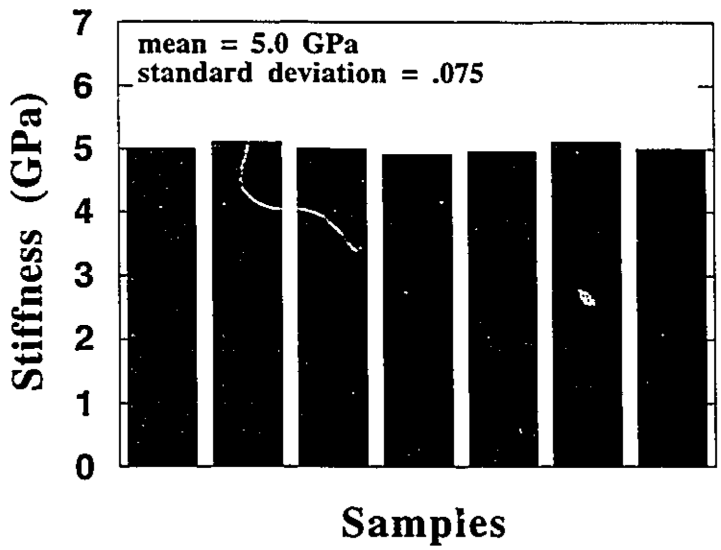

Fig. 7.34 Static stiffness of notched specimens under in-plane shear stress

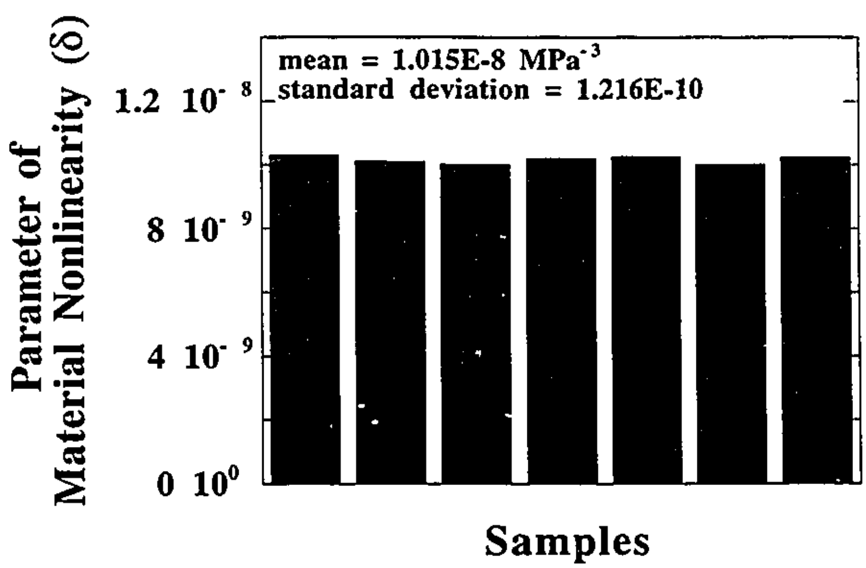

Fig. 7.35 Parameter of material nonlinearity (δ) of notched specimens under in-plane shear stress

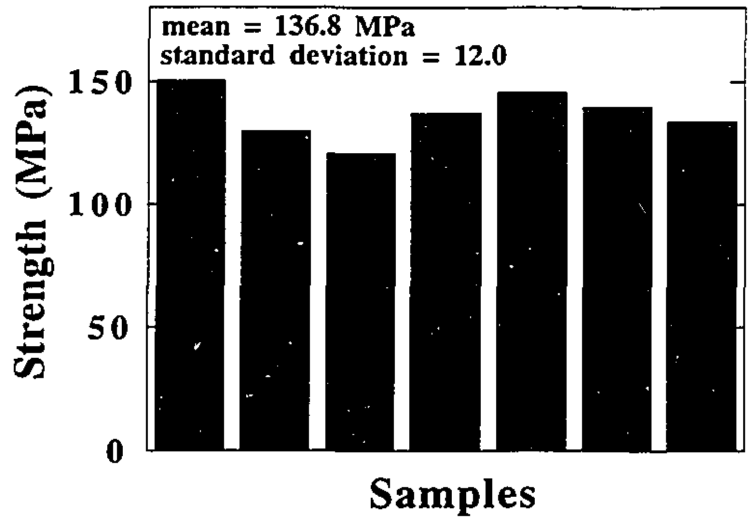

Fig. 7.36 Static strength of notched specimens under in-plane shear stress

7.6.7.2 Normalized Residual Stiffness and Strength

The results of the experiments for measuring the residual stiffness and residual strength of the notched samples under in-plane shear fatigue are presented in this section. To measure the residual stiffness and residual strength of the material, two different states of stress (59% and 40% of the in-plane shear static strength of the material) are selected. By selecting these two different states of stress, high and low stress levels are applied. A stress ratio equal to 0.1 and a frequency equal to 2 Hz are applied. The results of residual stiffness and strength experiments of the notched samples under in-plane shear fatigue are shown in Figs. 7.37 and 7.38, respectively. The curve fitting parameters for Eqs. 5.16 and 5.18 and are also mentioned in the figures.

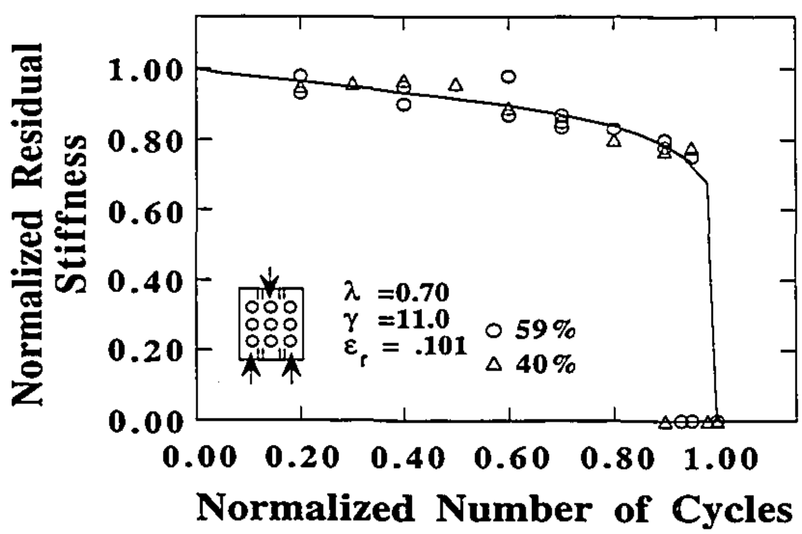

Fig. 7.37 Normalized residual stiffness of a unidirectional material under in-plane shear fatigue loading conditions (using Eq. 5.18)

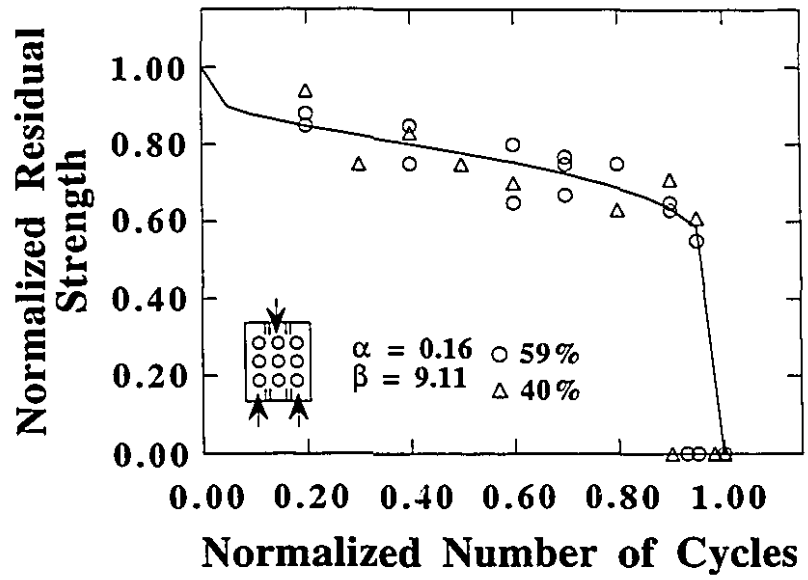

Fig. 7.38 Normalized residual strength of a unidirectional material under in-plane shear fatigue loading conditions (using Eq. 5.16)

Although the parameter of material nonlinearity (δ) seems to be a function of number of fatigue cycles (for more details refer to [279,280]), however in this study, this parameter is assumed to be a constant.

7.6.7.3 Static and Fatigue Modes of Failure

The final failure mode of the in-plane shear fatigue tests is the same as the final failure mode from static experiments. A picture of notched samples, failed under in-plane shear static and fatigue loading conditions, is shown in Fig. 7.39.

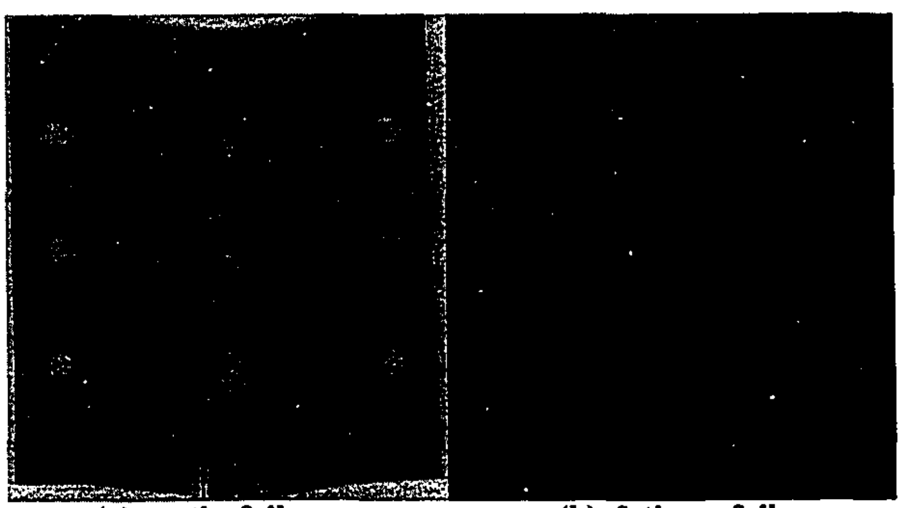

(a) static failure (b) fatigue failure

Fig. 7.39 Notched samples failed under static and fatigue in-plane shear loading conditions

After crack initiation in un-notched shear specimen under static loading conditions, by increasing the load level, cracks propagate very rapidly along the rails. The final failure mode of the un-notched sample under static loading is shown in Fig. 7.40. As shown, instead of having shear failure in the gage areas, the final failure mode is a combination of a small amount of shear in gage areas and crack propagation along the rails. It is clear that the specimen does not absorb the applied load by failing under shear in the gage areas and it seems that the failure along the rails is more dominant. Therefore, using un-notched samples for material characterization of composites under in-plane shear loading conditions may lead to incorrect results.

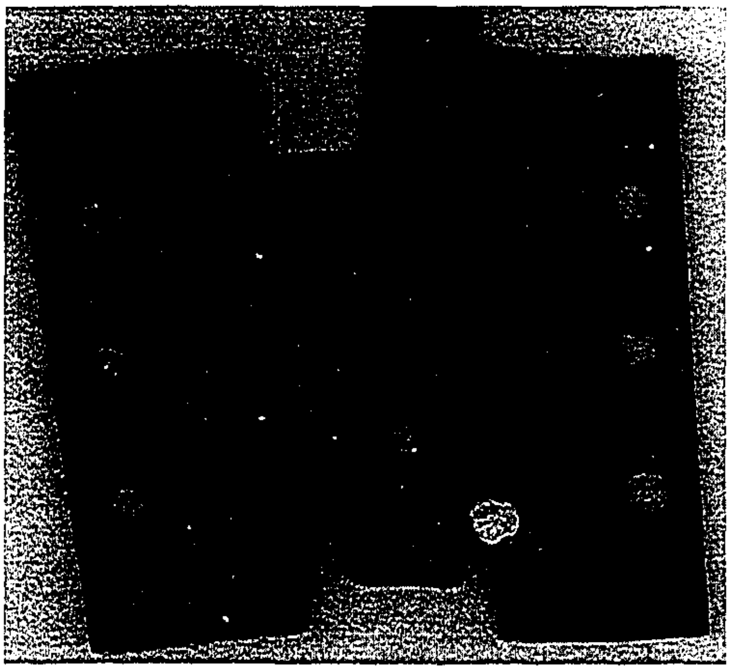

Fig. 7.40 Un-notched sample failed under static in-plane shear loading

7.6.8 Normalized Fatigue Life of In-Plane shear Tests

In this section, the results of fatigue life experiments for the notched samples under in-plane shear fatigue loading conditions are presented in a normalized form. Two different stress ratios ($\kappa = \sigma_{min}/\sigma_{max} = 0.1$ and 0.0) and different percentages of the static strength (selected as the maximum stress) are applied to find the fatigue life of the notched samples under in-plane shear fatigue loading conditions. In Fig. 7.41, the master curve for the fatigue life of the notched samples under in-plane shear fatigue loading conditions is presented in a normalized form. By using Eq. 5.23, the curve fitting parameters (A and B) are found and mentioned in Fig. 7.41.

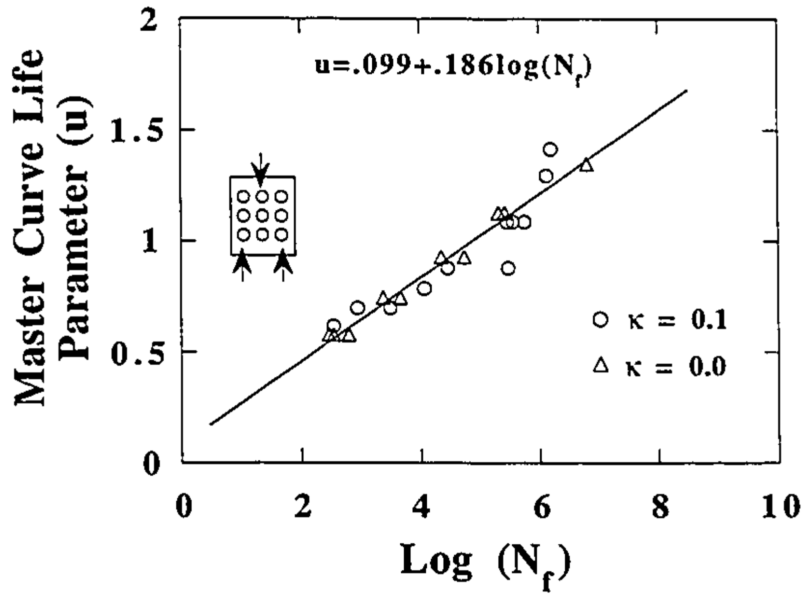

Fig. 7.41 Master curve for fatigue life of notched samples under in-plane shear fatigue loading conditions (using Eq. 5.23)

7.6.9 Out-of-Plane Shear Tests

In this section, the results of static and fatigue experiments for characterizing the material properties of a unidirectional ply loaded under out-of-plane shear loading conditions are summarized. The double-notch specimen test method, as described by the ASTM D 2733-70 [262] and ASTM D 3846-93 [263] standards, was used for characterizing the out-of-plane shear properties of the material. The specimen configuration and the dimensions are shown in Fig. 7.42. The analytical and experimental study of the modified specimen is published by the author elsewhere [281], and due to space limitations, is not repeated here. The out-of-plane shear strength of the unidirectional ply can be measured by the present method. The method is not capable of measuring the out-of-plane modulus of the unidirectional ply, however it can be easily calculated by transversely isotropic assumption (Eq. 3.6).

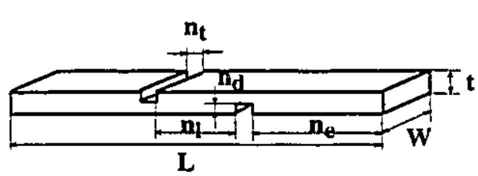

L = 152.4
W = 25.4
t = 3.4
n_t = 2.54
n_d = 1.27
n_l = 6.35
n_e = 70.5
(units are in mm)

Fig. 7.42 Out-of-plane double-notched shear specimen

In order to induce interlaminar shear (σ_{yz}) in the gage area of a double notched specimen, a 90-degree lay-up must be used. Since the material is weaker in matrix tension than in interlaminar shear loading, a tensile load applied to a double notch specimen with 90-degree lay-up results in a matrix failure prior to failure in interlaminar shear. There are two solutions to this problem. The first solution is to use $[0/90]_s$ laminate instead of a 90-degree lay-up. Also, it is known that the strength of the material in matrix compression loading is higher than in matrix tension. Therefore, the second solution is to apply a compressive load instead of a tensile load on a 90-degree lay-up. Improbability of failure between the 0 and 90-degree plies is the disadvantage of using $[0/90]_s$ laminate (first method). The disadvantage of the second method is the possibility of buckling, which can be avoided by using anti-bucking clamps. In this study, the second solution is selected. The clamp and dimensions are shown in Fig. 7.43.

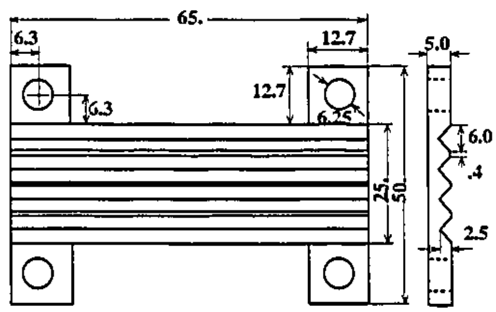

Fig. 7.43 Clamp used to eliminate the out-of-plane buckling (all units are in mm)

7.6.9.1 Static Stiffness and Strength

The results of static experiments for measuring the strength of the unidirectional ply under out-of-plane shear loading are summarized here. The results of static experiments for measuring the static strength of the unidirectional ply under out-of-plane shear loading conditions (average values and standard deviation) are shown in Fig. 7.44. As mentioned earlier, the transversely isotropic assumption (Eq. 3.6) can be used to calculate the out-of-plane shear stiffness of the unidirectional ply. Using this equation, the out-of-plane shear stiffness is calculated and is equal to 3.1 GPa. Gipple and Hoyans [160] measured the out-of-plane shear stiffness of an AS4/3501-6 unidirectional ply using the Iosipescu method. Their results show a magnitude of 2.8 GPa for the out-of-plane shear stiffness, which is 11% lower than the magnitude calculated by the transversely isotropic assumption (Eq. 3.6) in this study.

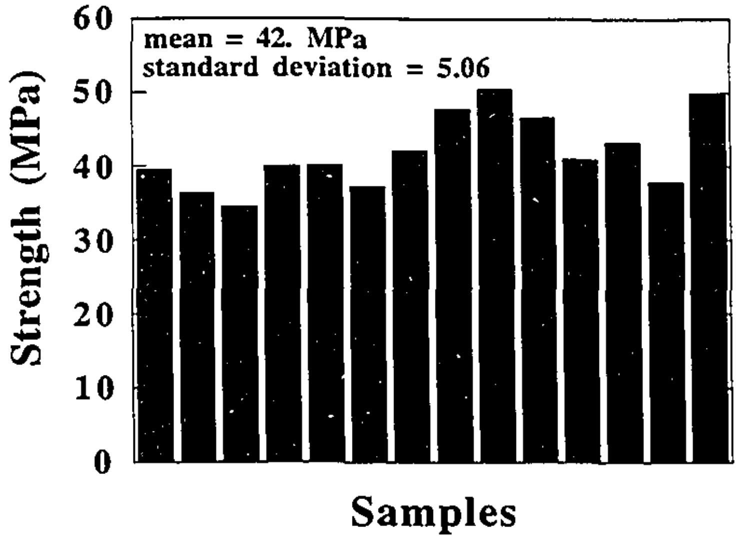

Fig. 7.44 Static strength of double-notched samples under out-of-plane shear stress

7.6.9.2 Normalized Residual Strength

The results of experiments for measuring the residual strength of a unidirectional ply under out-of-plane shear fatigue are presented in this section. To measure the residual strength of the material, two different states of stress (80% and 60% of the out-of-plane shear static strength of the material) are selected. By selecting these two different states of stress, high and low stress levels are applied. A stress ratio equal to 0.1 and a frequency below 10 Hz are applied. The results of residual strength experiments of a unidirectional ply under out-of-plane shear fatigue are shown in Fig. 7.45. The curve fitting parameters for Eq. 5.18 are also mentioned in the figure.

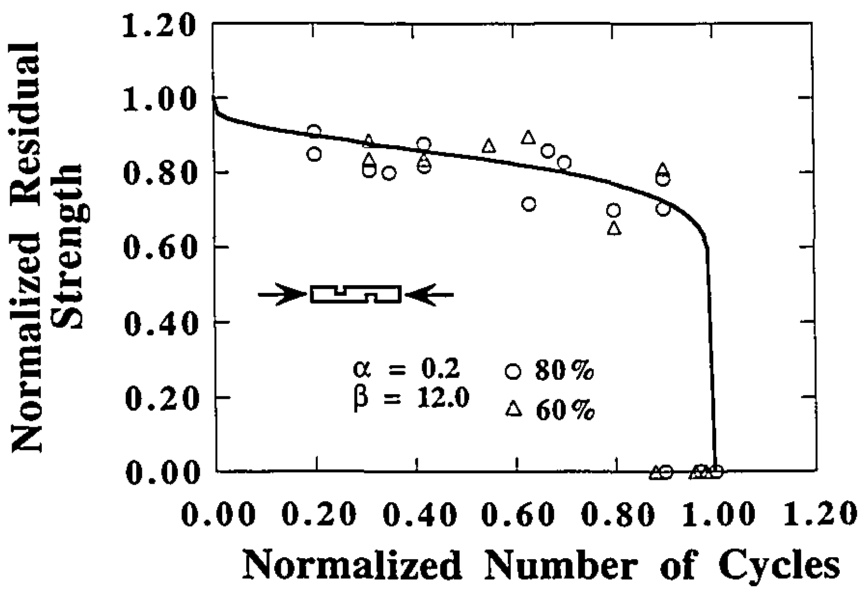

Fig. 7.45 Normalized residual strength of double-notched samples under out-of-plane shear fatigue loading conditions (using Eq. 5.18)

Furthermore, to calculate the residual out-of-plane shear stiffness of the unidirectional ply under fatigue loading conditions, the transversely isotropic assumption (Eq. 3.6) must be used.

7.6.9.3 Static and Fatigue Modes of Failure

A picture of unidirectional plies, failed under out-of-plane shear static and fatigue loading conditions, is shown in Fig. 7.46. As shown, the final failure occurs in the gage area for both static and fatigue loading conditions, although the picture for fatigue failure is slightly less clear.

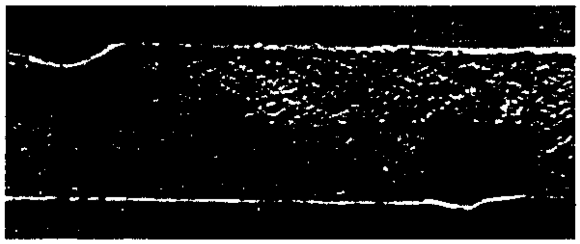

(a) static failure

(b) fatigue failure

Fig. 7.46 Out-of-plane double-notched shear specimens, failed under static and fatigue loading

7.6.10 Normalized Fatigue Life of Out-of-Plane Shear Tests

In this section, the results of fatigue life experiments for the double-notched samples under out-of-plane shear fatigue loading conditions are presented in a normalized form. Two different stress ratios ($\kappa = \sigma_{min}/\sigma_{max} = 0.1$ and 0.0) and different percentages of the static strength (selected as the maximum stress) are applied to find the fatigue life of double-notched samples under out-of-plane shear fatigue loading conditions. In Fig. 7.47, the master curve for the fatigue life of the double-notched samples under out-of-plane shear is presented in a normalized form. By using Eq. 5.23, the curve fitting parameters (A and B) are found and mentioned in Fig. 7.47.

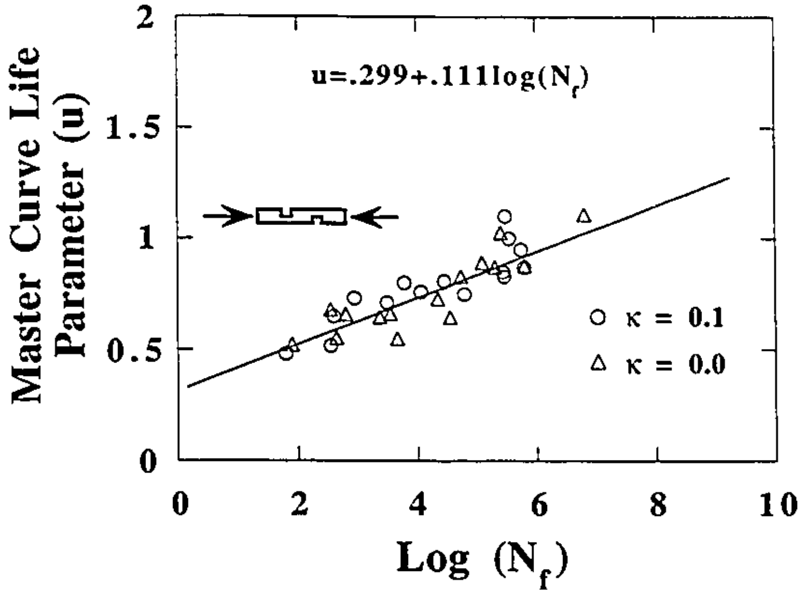

Fig. 7.47 Master curve for fatigue life of double-notched samples under out-of-plane shear fatigue loading conditions (using Eq. 5.23)

7.7 Summary

In this chapter by using different testing techniques, the material properties of unidirectional AS4/3501-6 graphite/epoxy ply are fully characterized in fiber and matrix directions, in tension and compression and under in-plane and out-of-plane shear static and fatigue loading conditions. In general, the results obtained are consistent and reliable. The test methods yielded very low scatter, even for fatigue experiments. The test fixtures performed well, which was evident by the fact that the static and fatigue experiments showed identical modes of failure for each type of test. Thus, the results provided a good experimental data base for AS4/3501-6 graphite/epoxy material.

The results obtained are used as input for the *progressive fatigue damage model.* By increasing the number of tests for static and fatigue loading conditions, more reliable experimental results and curve fitting parameters could be obtained which is also time consuming and costly. An extensive and expensive experimental program is performed for fully characterization of the material, however fatigue behaviour of laminated composites with different lay-ups and geometries under various stress states and stress ratios, can be predicted by using the aforementioned model and the results obtained in this chapter. This can save a large amount of time and expense for testing of different lay-ups and geometries.

Chapter 8

Final Experimental Evaluation

This chapter is devoted to experimental evaluation of the *progressive fatigue damage model* and some of its components. Firstly, to evaluate the *generalized residual material property degradation technique*, which is an important component of the *model*, a series of static and fatigue experiments are conducted on 30° off-axis specimens. This set of experiments is in fact a method used to study a unidirectional ply under biaxial loading conditions. A very good agreement between the results obtained from the aforementioned *technique* and the experimental results is achieved. Secondly, a series of static and fatigue experiments are performed on pin/bolt-loaded composite laminates to verify the *progressive fatigue damage model*. An excellent agreement between the results of progressive static damage model simulation and the experimental results is obtained. Fatigue life and residual strength of different pin/bolt-loaded composite laminates with different ply lay-ups are predicted by the *model* and evaluated by the experiments. Also, the results of the *progressive fatigue damage model* are compared to experimental results of other authors. A good agreement between the results of experiments (performed in this study and also from the other authors) and the *model* is achieved which shows the successful simulation capability of the *model*. Finally, the fatigue behaviour of pin-loaded composite laminates under two consecutive load levels (low and high) is predicted by the *model*. By changing the sequence of the applied load level (high-to-low or low-to-high), it is shown that the traditional Miner's Rule is not able to simulate this problem. As an improvement, a fairly good agreement between the results of the two consecutive load level experiments and the simulated results by the *model* is achieved.

8.1 Introduction

In the previous chapter, material properties of unidirectional AS4/3501-6 graphite/epoxy under static and fatigue loading conditions are fully characterized by conducting an extensive experimental program. The comprehensive data base provided by those experiments, for the material at the ply level, is used by the *model*, to simulate the static and fatigue behaviour of pin/bolt-loaded composite laminates as an example of a sophisticated problem. As explained in the previous chapters, the *progressive fatigue damage model* contains several important parts which can be considered as the basic components of the *model*. To evaluate the *model*, it is important to also verify the performance of its components. Among several components of the *model*, the *generalized residual material property degradation technique* and the static progressive damage model are of special importance. Therefore, these two components are evaluated experimentally. Moreover, the fatigue life and residual strength simulation capabilities of the *model* are evaluated experimentally. Also, the fatigue life simulation capability of the *model* is evaluated by using independent sets of available experimental results by other authors in the literature. Furthermore, another outcome of the *model* which is the residual fatigue life simulation capability is evaluated experimentally. In the following, each set of experiments is explained in detail.

To validate the *generalized residual material property degradation technique*, which is an important part of the *model*, a series of uniaxial static and tension-tension fatigue tests are performed on a unidirectional off-axis $[30_{16}]$ laminate. For this purpose, a series of static tests are performed to measure the static strength of the specimen and based on those results, fatigue tests are performed to find the fatigue life of the specimen under different stress levels (Fig. 8.1).

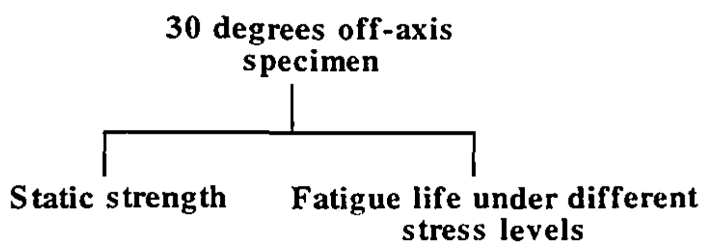

Fig. 8.1 Tests needed to verify the *generalized material property degradation technique*

In the next step, in order to verify the results obtained from the *progressive fatigue damage model* (simulation of progressive failure of pin/bolt-loaded composite laminates), a series of static and fatigue experiments are performed on different pin/bolt-loaded composite laminates (Fig. 8.2).

To verify the capability of the progressive static damage model for predicting the static strength (failure initiation and catastrophic load) of pin/bolt-loaded composite laminates, various experiments are performed for different ply lay-ups and geometries. To verify the fatigue simulation capability of the *model*, fatigue life and residual strength tests are also performed for different ply configurations and load levels. To show the generality of the *model*, simulated results for fatigue life of the pin/bolt-loaded composite laminates are also compared with independent experimental results available in the literature. Also, the residual fatigue life of the pin-loaded composite laminates under two consecutive load levels (low and high) is measured experimentally and the results are compared with simulated results by the *model*.

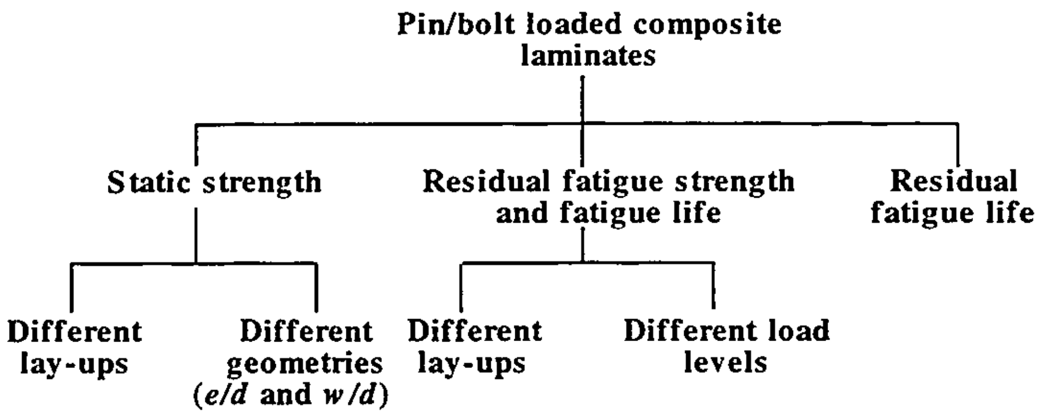

Fig. 8.2 Tests needed to evaluate the *progressive fatigue damage model*

The specimens used for experimental studies are made from AS4/3501-6 graphite/epoxy material in prepreg form. The specimens are manufactured and machined using standard techniques. The AS4/3501-6 graphite/epoxy material is fully characterized experimentally and the results were presented in Chapter 7.

8.2 Evaluation of *Generalized Residual Material Property Degradation Technique*

The theoretical bases of the *technique* were explained in Chapter 5. As mentioned, the main advantage of this *technique* is that it can simulate the fatigue behaviour of a unidirectional ply under multiaxial state of stress and arbitrary stress ratio by using the results of uniaxial fatigue experiments. This *technique* plays a very important role in the *progressive fatigue damage model*, therefore, special attention should be paid to evaluate it. Performing a multiaxial fatigue test on a unidirectional ply is a cumbersome task requiring special machines and fixtures. However, simple biaxial testing of a unidirectional ply under static and fatigue loading conditions is essential. Therefore, the first step in the experimental program is to find a suitable and feasible method for testing a unidirectional ply under a biaxial state of stress. There are several different ways for inducing biaxial stress conditions in a unidirectional ply. A cylinder under a combination of axial tension or compression, internal pressure and tangential torsion; a plate under bilateral bending loading; a flat cruciform specimen under biaxial loading applied to the arms; an off-axis unidirectional specimen under uniaxial tension or compression loading, etc., are examples of different techniques for creating biaxial stress conditions (see [197] as a review paper). Difficulties in manufacturing of the specimen, costs of manufacturing, special fixtures, and complicated machine requirements are difficulties associated with these methods. A list of the major biaxial testing methods and some of their difficulties are summarized in Table 8.1. There are various advantages and disadvantages for each of these testing methods, however among them, the off-axis unidirectional specimen under uniaxial tensile or compressive loading is special to composites and is the simplest way of creating biaxial loading conditions. No special fixture is needed and manufacturing of the samples is simple. Therefore, the off-axis specimen test method is selected for performing the experimental program in this study.

	Testing Difficulties					
Test Methods	manufacturing difficulties	high cost	complicated fixture	special or complicated machine	pressure leakage	tab required
cylindrical specimen	✓	✓	✓	✓	✓	
bilateral bending plate		✓	✓			
cruciform plate	✓	✓	✓	✓		
off-axis specimen						✓

Table 8.1 Different biaxial test methods and their inherent difficulties

Because of its simplicity, the off-axis specimen test method is used by many authors for experimental evaluation of polynomial failure criteria [288-294] for characterization of in-plane-shear properties of composites [295-297] and for fatigue analysis of off-axis composites [298]. Along with the advantages of the off-axis specimen testing method, there are some difficulties, such as end constraint and uniformity of stress state in the specimen, which should be considered and avoided. To overcome the aforementioned difficulties, the test method has received much attention from different researchers [299-307]. The first attempt to study the behaviour of the off-axis specimen under uniaxial type of loading was accomplished by Pagano and Halpin [299]. Specifically, they showed [299] that increasing the length of the specimen provided more uniformity of the stress state in the gage area. They [299] also showed that the bending effects and nonuniform stress state resulting from end constraint can produce serious consequences in the experimental results. To reduce the constraints transferred from the machine to the specimen, special fixtures which allow rotation at the ends were developed and modified by many authors [300-302]. The performance of the rotating fixture was criticized by Rizzo [303], who showed that this method could not eliminate stress concentrations. Long tapered tabs, as suggested by Pipes and Cole [304] and by Richards *et al.* [305], are difficult to manufacture. A special tab was designed [306] by using fiberglass fabrics embedded in a silicon rubber matrix. Although this tab allows the use of rigid grips available on most material testing machines, it cannot sustain load in high temperature and tab manufacturing is time consuming. Then an oblique end tab was designed by Sun and Chung [307] which creates a uniform state of stress in the off-axis specimen and is very simple to fabricate. Among different techniques for reducing the nonuniformity of the stress state in the gage area of the off-axis specimen, the latest method [307], because of its simplicity, is selected in this study.

8.2.1 Theoretical Background

In Fig. 8.3, an off-axis unidirectional specimen under uniaxial tension is shown. The off-axis and on-axis coordinate systems are denoted by 1-2 and x-y axes, respectively.

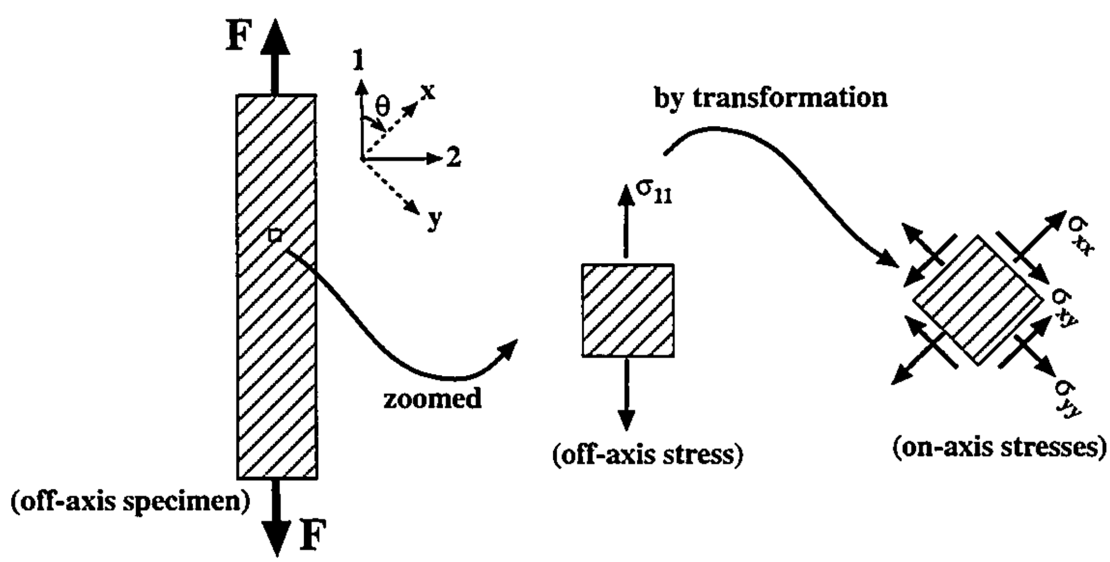

Fig. 8.3 Off-axis specimen under uniaxial tensile loading

The on-axis stresses are found by transforming the off-axis stresses from the off-axis to on-axis directions using a suitable transformation operator [308].

$$\begin{aligned}\sigma_{xx} &= \sigma_{11} * \cos^2\theta \\ \sigma_{yy} &= \sigma_{11} * \sin^2\theta \\ \sigma_{xy} &= -\sigma_{11} * \sin\theta * \cos\theta\end{aligned} \qquad \textbf{Eq. 8.1}$$

As shown in Fig. 8.3, by applying a uniaxial loading on the off-axis specimen, a biaxial state of stress in the on-axis direction is induced. By changing the fiber angle (θ) from 0 to 90 degrees, the mode of failure changes from fiber to matrix failure. To detect the failure of an off-axis specimen, which in fact is a unidirectional ply under biaxial state of stress, polynomial failure criteria capable of detecting modes of failure can be utilized. The Hashin-type polynomial failure criteria [164], capable of distinction of the modes of failure (Eqs. 4.2 and 4.8 from Chapter 4), are used to detect the static failure. By considering the biaxial state of stress, the third terms in those equations are dropped. For simplicity and for presenting the results as closed form equations, the material nonlinearity is ignored. By knowing that the in-plane shear stress induced in a $[30_{16}]$ laminate is not dominant in comparison with the matrix stress, ignoring material nonlinearity does not induce a large percentage of error in the results. It should be added that the following procedure can also be performed by considering the material nonlinearity, however the resultant equations should be solved numerically. Therefore, Eqs. 4.2 and 4.8 are rewritten to the following forms:

$$\left(\frac{\sigma_{xx}}{X_t}\right)^2 + \left(\frac{\sigma_{xy}}{S_{xy}}\right)^2 = 1 \quad \textit{for static fiber failure mode} \qquad \textbf{Eq. 8.2}$$

$$\left(\frac{\sigma_{yy}}{Y_t}\right)^2 + \left(\frac{\sigma_{xy}}{S_{xy}}\right)^2 = 1 \quad \textit{for static matrix failure mode} \qquad \textbf{Eq. 8.3}$$

As mentioned, by changing the fiber angle (θ) from 0 to 90 degrees, the mode of failure changes from fiber to matrix failure. The transition angle (θ_t) is defined as the angle where the mode of failure changes from fiber to matrix mode. To find the transition angle, Eq. 8.1 is inserted into Eqs. 8.2 and 8.3.

$$\sigma_{11} = \sigma_f = \frac{1}{\cos\theta \left(\dfrac{\cos^2\theta}{X_t^2} + \dfrac{\sin^2\theta}{S_{xy}^2}\right)^{\frac{1}{2}}} \qquad \textbf{Eq. 8.4}$$

$$\sigma_{11} = \sigma_m = \frac{1}{\sin\theta \left(\frac{\sin^2\theta}{Y_t^2} + \frac{\cos^2\theta}{S_{xy}^2} \right)^{\frac{1}{2}}} \qquad \text{Eq. 8.5}$$

where subscripts "f" and "m" denote the fiber and matrix. These two equations are plotted in Fig. 8.4 for graphite/epoxy AS4/3501-6 with the material properties mentioned in Table 3.1. The transition angle, the intersection of these two equations, is equal to 9.3 degrees. Therefore to achieve the matrix failure mode, the off-axis angle for the specimen must be greater than 9.3 degrees. In this study, an off-axis angle equal to 30 degrees is selected. The stress analysis for the 30-degrees off-axis specimen shows that the transverse and in-plane shear stresses are dominant. Therefore, the matrix cracking failure mode is dominant for this specimen and Eq. 8.3 can be used to predict the static failure.

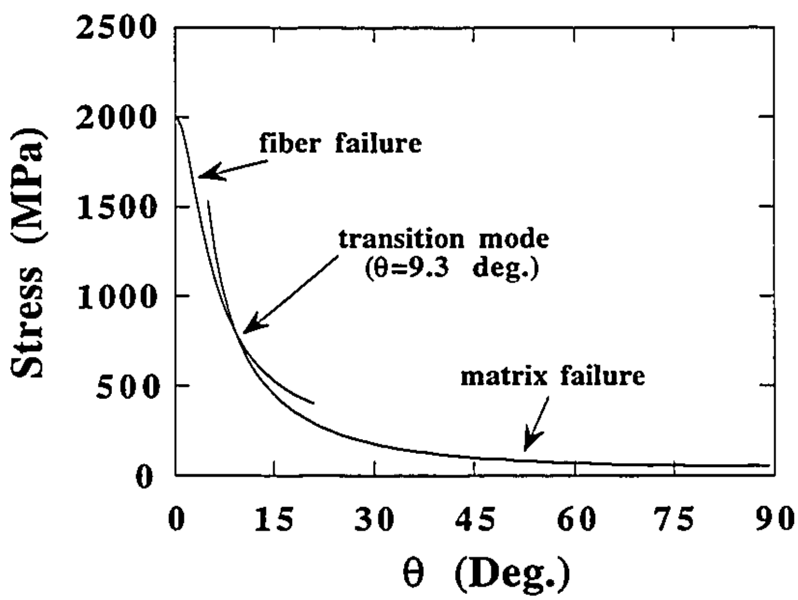

Fig. 8.4 Transition angle from fiber to matrix failure for AS4/3501-6

As explained in Chapter 5, in order to apply the *generalized residual material property degradation technique* to study the fatigue behaviour of a unidirectional ply under biaxial state of stress, a complete knowledge of material properties (fatigue life and strength) of a unidirectional ply under uniaxial static and fatigue loading conditions is needed. The problem of failure prediction in the static case is simpler than in fatigue, because for the static cases the magnitudes of the required static strengths are experimental constants. For instance, to check the matrix failure mode in static condition, Eq. 8.3 can be used. Knowing the state of stress along with the matrix and in-plane shear static strengths, the matrix failure mode can be examined. However, since the strength of the material under fatigue loading is not an experimental constant, but rather a function of the number of cycles, stress state, and stress ratio, the problem in fatigue is more complicated. For instance, for the 30-degrees off-axis specimen where matrix failure mode is dominant, to examine the failure in fatigue (Eq. 4.17) can be used. Again, by considering the biaxial state of stress the third term is dropped and the material nonlinearity is ignored for simplicity. Therefore, Eq. 4.17 is rewritten to the following form:

$$\left(\frac{\sigma_{yy}}{Y_t(n,\sigma,\kappa)}\right)^2+\left(\frac{\sigma_{xy}}{S_{xy}(n,\sigma,\kappa)}\right)^2=1 \quad \textit{for fatigue matrix failure mode} \qquad \textbf{Eq. 8.6}$$

It should be noted that the residual matrix and in-plane shear strength in fatigue are functions of n, σ and κ (number of cycles, stress state, and stress ratio). By using Eqs. 5.16 instead of Y_t and S_{xy}, Eq. 8.6 is changed to the following form.

$$\left(\frac{\sigma_{yy}}{\left[1-\left(\frac{\log(n)-\log(.25)}{\log\left(N_{f_{yy}}\right)-\log(.25)}\right)^{\beta_{yy}}\right]^{\frac{1}{\alpha_{yy}}}\left(Y_t-\sigma_{yy}\right)+\sigma_{yy}}\right)^2+$$

$$\left(\frac{\sigma_{xy}}{\left[1-\left(\frac{\log(n)-\log(.25)}{\log\left(N_{f_{xy}}\right)-\log(.25)}\right)^{\beta_{xy}}\right]^{\frac{1}{\alpha_{xy}}}\left(S_{xy}-\sigma_{xy}\right)+\sigma_{xy}}\right)^2=1$$

for fatigue matrix failure mode **Eq. 8.7**

where α and β are experimental parameters found by curve fitting of residual matrix and in-plane shear strength curves (experiments are performed in Chapter 7). Also subscripts "yy" and "xy" refer to matrix and in-plane shear. Moreover, N_f is the number of cycles to failure for the relevant state of stress, for instance $N_{f_{yy}}$ is the number of cycles to failure for the matrix direction under uniaxial transverse stress σ_{yy}, and arbitrary stress ratio, which have been found experimentally in Chapter 7. Also "n" is the number of cycles that the unidirectional ply fails under biaxial state of stress which is found by solving of the Eq. 8.7, numerically. For more details, the reader should refer to papers recently published by author [309, 310].

8.2.2 Off-Axis Specimen Experiments and Results

Tests are performed using an MTS 810 material testing system, equipped with hydraulic grips. A computer was connected to the MTS for data acquisition. Displacement and load are monitored for static experiments. During fatigue tests, maximum and minimum displacements and loads as well as number of cycles are monitored. Static tests are performed under displacement control, while the fatigue tests are carried out under load control conditions. The fatigue load is applied in a sinusoidal form. To avoid temperature effects, which could degrade the material properties, fatigue tests are performed at frequencies less than 10 Hz. All tests are performed in ambient temperature. The specimens are manufactured, cut and polished using standard techniques. To reduce the gripping effects, oblique Aluminum tabs [307] are used. A diagram of the off-axis specimen with the oblique tabs is shown in Fig. 8.5.

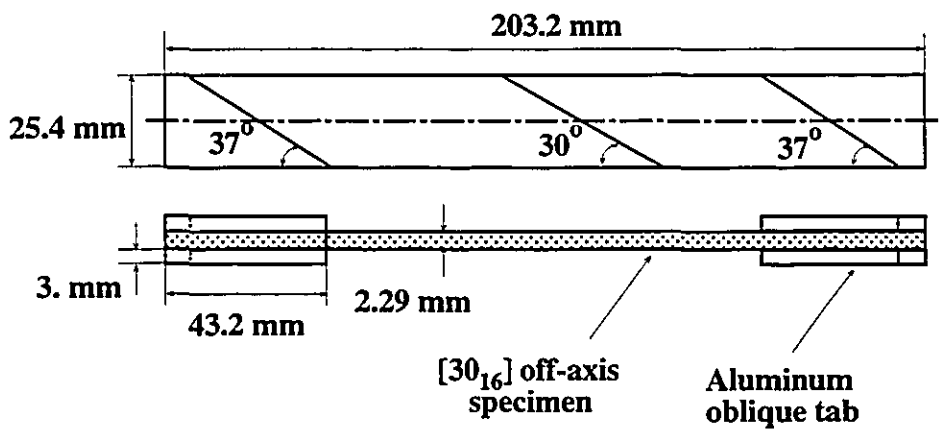

Fig. 8.5 Diagram of the off-axis specimen with oblique tabs

At first, a series of static experiments are performed to measure the magnitude of static strength of the off-axis specimen and to evaluate the static failure criteria (Eq. 8.3). The results of static experiments are summarized in Fig. 8.6. Using Eqs. 8.1 and 8.3, the magnitude of the off-axis failure stress for the $[30_{16}]$ off-axis specimen is calculated and compared with the experimental results in Fig. 8.6. As shown, the static failure load calculated by polynomial failure criterion overestimates the static strength of off-axis specimen by about 5%, which is quite satisfactory.

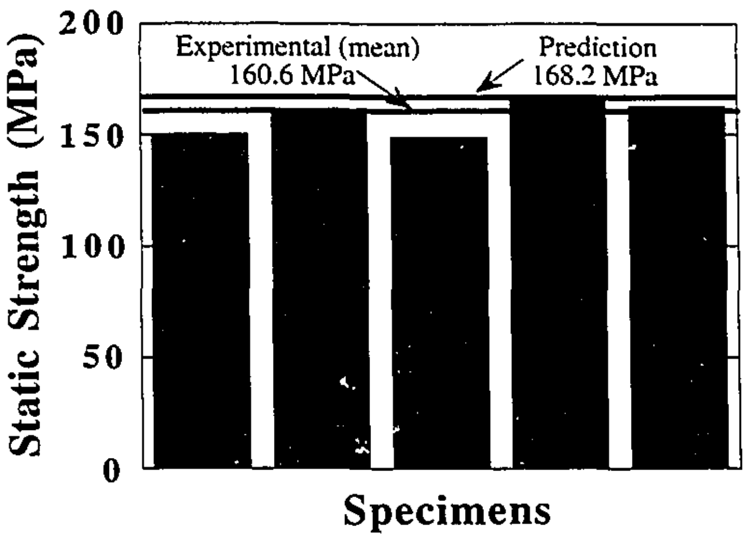

Fig. 8.6 Comparison of calculated static failure load with experimental results for $[30_{16}]$ off-axis specimens

Tension-tension fatigue tests are performed under load control conditions and the load ratio (F_{min}/F_{max}) equal to 0.1 is applied to off-axis specimens. Different percentages of the maximum static failure load, such as 40, 50, 60, 70 and 80% are selected as the maximum load. The fatigue tests are continued until catastrophic failure is achieved and the maximum number of cycles to failure is monitored. The experimental results of fatigue life of the $[30_{16}]$ off-axis specimen is shown in Fig. 8.7. A linear curve fitting approach is utilized and the experimental S-N curve is shown by a solid line in Fig. 8.7.

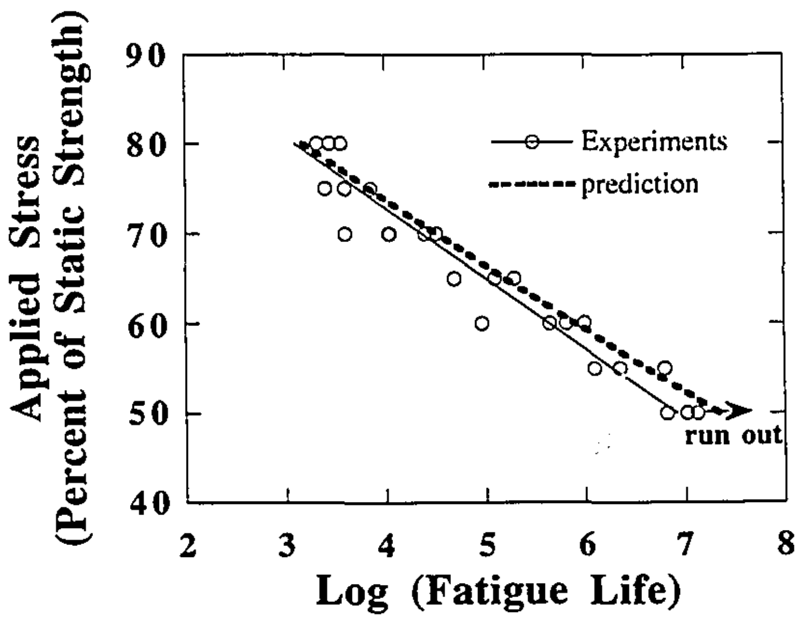

Fig. 8.7 Fatigue life (S-N) curve of the $[30_{16}]$ off-axis specimens (experiments and prediction)

The final failure mode of the tension-tension fatigue tests is the same as the final failure mode from static experiments. A close-up view of 30-degrees off-axis specimens, failed in static and fatigue loading, are presented in Fig. 8.8 to show the similarity of the failure modes.

Fig. 8.8 Off-axis $[30_{16}]$ specimens, failed under tensile static (top) and fatigue (below) loading

Now, by inserting the experimental curve fitting parameters found in Chapter 7, into Eq. 8.7, the number of cycles to failure for the $[30_{16}]$ off-axis specimen under various applied stress conditions and stress ratios are calculated by using the Newton-Raphson technique. The results calculated by the *technique* are compared with the experimental results and are shown in Fig. 8.7. By comparing the S-N curves (experimental data points curve-fitted mathematically and simulated by the *technique*), it seems the S-N curve simulated by the *technique* overestimates the fatigue life of the 30-degrees off-axis specimen. However, as shown in Fig. 8.7, the simulated S-N curve is located inside of the experimental scatter range. Therefore, it can be concluded that the deterministic *technique* is reasonably simulating the behaviour of the unidirectional ply under biaxial state of stress.

A summary of selected fatigue life results from the experiments and the *technique* is presented in numerical form in Table 8.2. In fatigue loading conditions, applying the biaxial load decreases the fatigue life of the unidirectional ply drastically. For instance, consider the $[30_{16}]$ off-axis specimen under uniaxial tensile fatigue loading conditions, with the maximum stress equal to 80% of its maximum static strength as shown in Table 8.2. By using Eq. 8.1 and ignoring the longitudinal stress (σ_{xx}), it is clear that this case is equivalent to a unidirectional ply under transverse loading combined with in-plane shear loading, where the σ_{yy} (maximum transverse stress) is equal to 66.0% of Y_t (maximum transverse tensile static strength) and the σ_{xy} (maximum in-plane shear stress) is equal to 45.3% of S_{xy} (maximum in-plane static shear strength). The fatigue life of the unidirectional ply under uniaxial transverse tensile loading with 66.0% of Y_t as the maximum stress is about 11,380 cycles. Moreover, the fatigue life of the unidirectional ply under uniaxial in-plane shear loading with 45.3% of S_{xy} as the maximum stress, is about

10,920,000 cycles. By coupling the two states of stress ($[30_{16}]$ off-axis specimen under 80% of its maximum strength) the fatigue life of the unidirectional ply, found experimentally, is decreased to about 1,202 cycles and the *technique* simulated 1,494 cycles. It shows that the fatigue life of the off-axis specimen measured experimentally and simulated by the *technique* are in a very good agreement. For the other stress levels, the difference between the experimental and simulated results seems to be considerable, however on a logarithmic scale (Fig. 8.7) very good agreement is achieved. The effect of the interaction of the transverse and in-plane shear stresses is apparent from the results.

applied stress (off-axis specimen)	induced stress (σ_{yy}/Y_t)	uniaxial life $N_{f_{yy}}$ (cycles)	induced stress (σ_{xy}/S_{xy})	uniaxial life $N_{f_{xy}}$ (cycles)	experimental biaxial life (cycles)	simulated biaxial life (cycles)
80%	66.0%	11,380	45.3%	10,920,000	1,202	1,494
75%	61.8%	57,507	42.4%	27,393,000	5,012	6,972
70%	57.7%	292,630	39.6%	72,361,000	23,422	33,060
65%	53.6%	1,502,400	36.8%	203,000,000	104,713	160,000
60%	49.5%	7,818,100	33.9%	610,850,000	441,570	794,700
55%	43.3%	41,584,000	31.1%	1,996,500,000	1,995,292	4,085,000

Table 8.2 Fatigue life results from the experiments and the *technique*

Before ending this section, there are some critical points which should be mentioned. As shown in Table 8.2, by decreasing the applied stress level, the difference between the results simulated by the *technique* and the experimental results increases. It should be mentioned that by decreasing the applied fatigue stress level for the off-axis specimen, the unidirectional material is under very low level states of stress. From the previous chapter, remember that the unidirectional material was characterized at high and low states of stress but not at very low stress levels. Therefore, the material properties of the unidirectional ply under very low level states of stress are extrapolated from the real experimental results. This is the main reason for the increased difference between the fatigue life simulated by the *technique* and measured experimentally at very low levels of applied stress. By increasing the number of experiments for characterization of unidirectional material at the very low level states of stress, which is not impossible but expensive and time consuming, this difference could be reduced.

Moreover, the magnitudes and proportions of the on-axis stresses induced in the off-axis specimen cannot be selected arbitrarily. According to Eq. 8.1, the magnitudes of these stresses depend on the off-axis applied stress and the angle of orientation of fibers. This should be noted as a limitation of the off-axis specimen method as a biaxial testing technique. Nonetheless, the simplicity of this method makes it attractive as a biaxial loading technique.

Also, it is clear that by using the *generalized residual material property degradation technique* which is a deterministic method, a single curve is simulated as the fatigue life curve of the off-axis specimen. It is well-known that experimental scatter is inherent to the fatigue properties of the material. Therefore, instead of having a single curve for the fatigue life of the off-axis specimen, a range of scattered data points are found by the experimental techniques in the laboratory. This limitation could be eliminated by coupling a probabilistic model to the *technique* which is not considered in this study.

In spite of all explained limitations, the results obtained by the 30° off-axis experiments show that the *generalized residual material property degradation technique* is fairly capable of simulating of the fatigue behaviour of a unidirectional ply under biaxial state of stress and arbitrary stress ratio by using the results of uniaxial fatigue experiments. Experimental evaluation of the established *technique* for the multiaxial fatigue loading conditions is not simple as the biaxial case and therefore, left for future work. Instead, the verification of the *technique* for the multiaxial fatigue loading conditions will be performed indirectly by evaluating of its performance in the *progressive fatigue damage model.*

The *generalized residual material property degradation technique* has passed the experimental evaluation successfully. Hence, it can be used in the *progressive fatigue damage model* reliably. In the following sections, the *progressive fatigue damage model* and its components are evaluated experimentally.

8.3 Evaluation of Progressive Static Damage Model

To develop a model to predict the fatigue behaviour of composite materials, it is essential to be able to first predict the static behaviour of such materials. As explained in Chapter 6, the progressive static damage model, which simulates the static behaviour of laminated composites, is an important part of the *progressive fatigue damage model.* Therefore, it is important to show the validity of the progressive static damage model adopted in this research. By using the code developed in this study, a static progressive failure analysis (see Fig. 6.1 in Chapter 6) is performed on three different pin/bolt-loaded composite plates with different ply configurations ($[0_4/90_4]_s$, $[90_4/0_4]_s$ and $[+45_4/-45_4]_s$). The stress analysis is performed using the three-dimensional finite element code developed in this study and the edge effects are considered by refining the elements near the edge of the hole between different plies with different orientations. Also, the effects of material nonlinearity on the prediction of the failure initiation and final failure loads are studied. To the best knowledge of the author, the effect of material nonlinearity on the edge effects for pin/bolt-loaded composite laminates is not comprehensively studied in the literature.

To evaluate the results of the analysis, a series of experiments was performed on different pin/bolt-loaded composite laminates with different configurations. Consider a composite plate with a pin/bolt-loaded hole as shown in Fig. 2.1 (in Chapter 2). The plate is a laminated composite with arbitrary ply orientation. The plate has width w = 25.4 mm, length l = 101.6 mm, thickness t = 2.336 mm (16 plies), edge distance e = 25.4 mm, hole diameter d = 6.35 mm, washer diameter d_w = 18.8 mm and the inside diameter of the washer to bolt diameter ratio is 1.224. The specimens were manufactured, cut, drilled and polished using standard techniques. A suitable fixture is used for the experiments (shown in Fig. 8.9). The pin/bolt is fixed and load is applied on the other end of the composite plate and static tests are performed under stroke control conditions. For the bolt-loaded conditions, a torque equal 4.02 N-m (higher than finger tight) is applied for all cases.

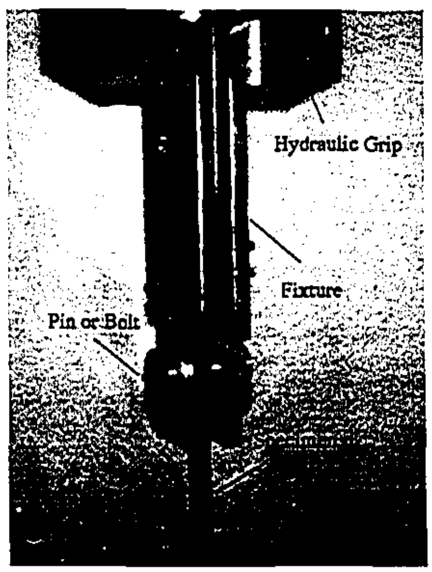

Fig. 8.9 Fixture for pin/bolt-loaded composite laminates

To find the failure initiation load, each specimen was loaded up to a certain limit, then unloaded and inspected by X-ray. If no failure was detected, the specimen was reloaded and the previous procedure repeated until failure initiation was achieved. It is understood that other techniques, such as C-Scan and ultrasonic methods may also be used for non-destructive testing, but equipment was not available to the author. To measure the final failure load, the specimen was loaded until the catastrophic failure was achieved. The results of analysis and experiments for failure initiation and final failure loads for pin/bolt-loaded composite laminates are summarized in Tables 8.3 and 8.4, respectively. For all cross-ply laminates ($[0_4/90_4]_s$ and $[90_4/0_4]_s$) the final failure mechanism was shear-out failure with dominant delamination failure, which corresponds to the results simulated by the model. Moreover, for all angle-ply laminates ($[+45_4/-45_4]_s$), the final failure mechanism was net-tension failure with dominant delamination failure which also corresponds to the results simulated by the model.

		Failure Initiation Load (kN)		
Layup	**Type of Loading**	**Linear Theory** *(error %)*	**Nonlinear Theory** *(error %)*	**Experimental Results** *(standard deviation)*
$[0_4/90_4]_s$	**Pin**	1.30 *(17.%)*	1.50 *(4.4%)*	1.57 *(.132)*
	Bolt	2.13 *(14.%)*	2.45 *(1.2%)*	2.48 *(.112)*
$[90_4/0_4]_s$	**Pin**	1.31 *(21.%)*	1.56 *(5.4%)*	1.65 *(.141)*
	Bolt	2.21 *(16.%)*	2.59 *(1.5%)*	2.63 *(.151)*
$[+45_4/-45_4]_s$	**Pin**	1.91 *(32.%)*	2.61 *(6.8%)*	2.80 *(.122)*
	Bolt	2.68 *(30.%)*	3.64 *(4.5%)*	3.81 *(.137)*

Table 8.3 Comparison of failure initiation load by linear theory, nonlinear theory and experimental results

		Final Failure Load (kN)		
Layup	**Type of Loading**	**Linear Theory** *(error %)*	**Nonlinear Theory** *(error %)*	**Experimental Results** *(standard deviation)*
$[0_4/90_4]_s$	**Pin**	4.68 *(19.%)*	5.31 *(8.1%)*	5.78 *(.335)*
	Bolt	7.38 *(17.%)*	8.71 *(2.3%)*	8.92 *(1.56)*
$[90_4/0_4]_s$	**Pin**	5.11 *(22.%)*	5.98 *(8.7%)*	6.55 *(.231)*
	Bolt	8.60 *(18.%)*	10.1 *(3.8%)*	10.5 *(.523)*
$[+45_4/-45_4]_s$	**Pin**	2.31 *(37.%)*	3.32 *(9.5%)*	3.67 *(.290)*
	Bolt	3.01 *(34.%)*	4.32 *(5.3%)*	4.56 *(.281)*

Table 8.4 Comparison of final failure load by linear theory, nonlinear theory and experimental results

By comparing the results of the failure analysis for linear and nonlinear cases and the experimental results (Tables 8.3 and 8.4), the following points are concluded:

- By ignoring material nonlinearity, the stress based failure criteria underpredicts the failure initiation load. The difference between failure initiation loads for $[0_4/90_4]_s$ and $[90_4/0_4]_s$ is negligible by linear theory, whereas the difference is more clear by introducing material nonlinearity. Also, the predicted final failure loads by considering material nonlinearity are in better agreement with the experimental results, showing the importance of considering the nonlinearity.

- The percentage of error for prediction of failure initiation and final failure loads for the angle-ply $[+45_4/-45_4]_s$ case by linear theory is more than the other two configurations, and this is due to the high magnitude of in-plane shear stress induced for this case. The predicted failure initiation and final failure loads by considering material nonlinearity are in very good agreement with the experimental results.

- Experimental results show that the existence of bolt load decreases the edge effects and increases the failure initiation and final failure loads. This phenomenon is also simulated by the model successfully.

A picture of the progressive failure of a pin-loaded cross-ply, $[0_4/90_4]_s$, under static loading conditions is shown in Fig. 8.10. The final failure mechanisms of a pin-loaded cross-ply, $[90_4/0_4]_s$, and an angle-ply, $[+45_4/-45_4]_s$, under static loading conditions are shown in Fig. 8.11.

intact specimen

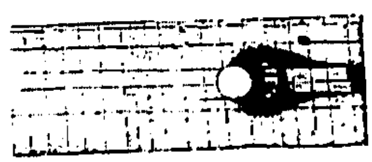

before final failure (X-ray)

final failure

Fig. 8.10 Progressive static failure of a pin-loaded $[0_4/90_4]_s$ cross-ply laminate

Fig. 8.11 Final static failure mechanisms of the pin-loaded $[+45_4/-45_4]_s$ angle-ply laminate (top), and $[90_4/0_4]_s$ cross-ply laminate (below)

Although the final static failure loads of a bolt-loaded composite laminate is higher than that of a pin-loaded case, the final failure mechanisms are similar. A picture of a typical final static failure mechanism of a bolt-loaded $[0_4/90_4]_s$ cross-ply composite laminate is shown in Fig. 8.12.

Fig. 8.12 Final static failure mechanisms of the bolt-loaded $[0_4/90_4]_s$ cross-ply laminate

Moreover, to validate the capability of the progressive static damage model to simulate the behaviour of different pin-loaded composite laminates with various geometries, two different *e/d* and *w/d* (see Fig. 2.1 in Chapter 2) are examined. The results of experiments and model simulation of final failure load for different cases are summarized and compared in Table 8.5. It should be mentioned that material nonlinearity is considered for all cases. As shown, a very good agreement is achieved between the model and the experimental results. The final failure mechanisms of different pin-loaded cases with various geometries are shown in Fig. 8.13.

			Final Failure Load (kN)	
Configuration	***e/d***	***w/d***	**Model (*error %*)**	**Experiments (*standard deviation*)**
$[0_4/90_4]_s$	2	4	2.63 (*2.95%*)	2.71 (*.085*)
	5	2	4.53 (*5.62%*)	4.80 (*.550*)
$[90_4/0_4]_s$	2	4	3.47 (*4.93%*)	3.65 (*.250*)
	5	2	4.66 (*5.86%*)	4.95 (*.010*)
$[+45_4/-45_4]_s$	2	4	1.98 (*6.60%*)	2.12 (*.010*)
	5	2	1.01 (*5.60%*)	1.07 (*.017*)

Table 8.5 Final failure load for different pin-loaded composite laminates with different geometries, simulated by model and measured by experiments

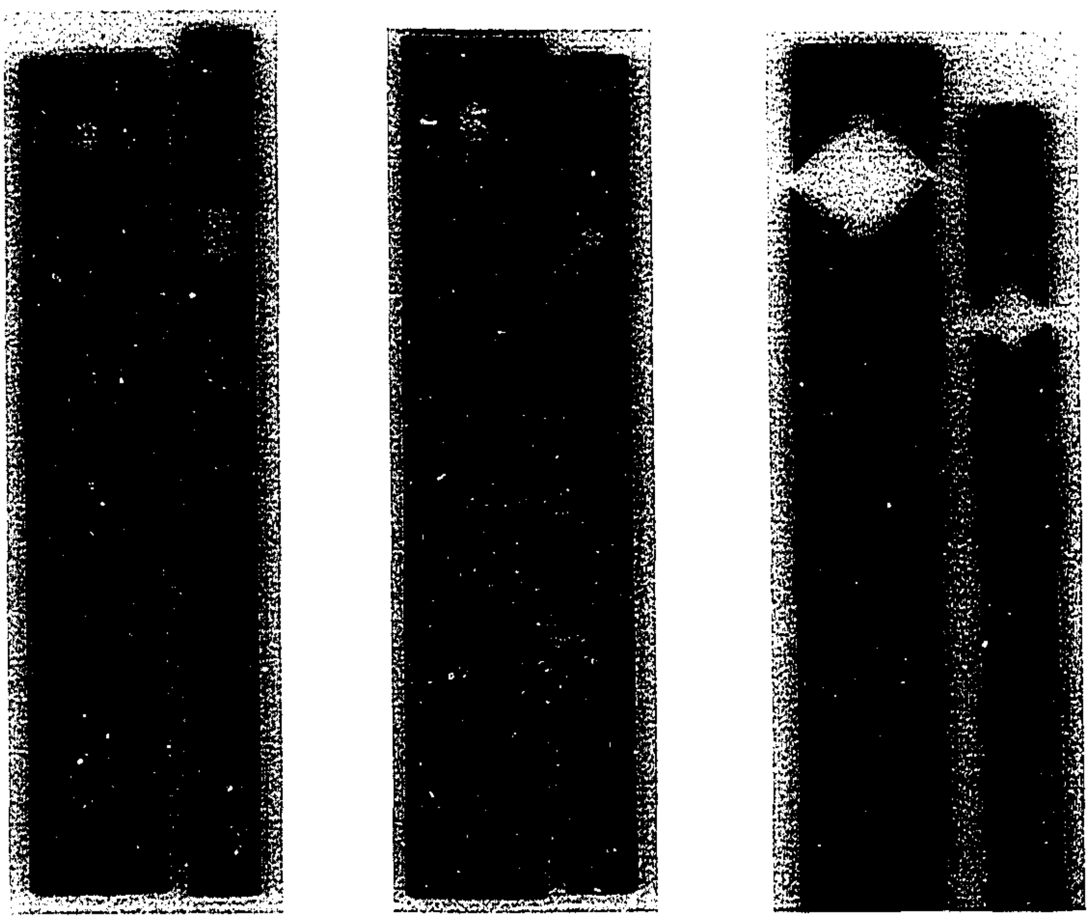

$[0_4/90_4]_s$ $[90_4/0_4]_s$ $[+45_4/-45_4]_s$

Fig. 8.13 Final static failure mechanisms of the pin-loaded laminates with different geometries (*e/d* and *w/d*)

The results presented in this section confirm that the traditional progressive static damage model developed in this study, which is a part of the *progressive fatigue damage model* has passed the experimental evaluation successfully. The reliable prediction of the static failure loads (initiation and final) is an essential capability to establish the *progressive fatigue damage model*. In the following section, the *progressive fatigue damage model* is evaluated experimentally.

8.4 Evaluation of *Progressive Fatigue Damage Model*

The evaluation of the *progressive fatigue damage model* is performed in different ways. The capabilities of the *model* to simulate the fatigue life and the residual strength of composite laminates are examined. To study the stacking sequence, three different ply configurations ($[0_4/90_4]_s$, $[90_4/0_4]_s$ and $[+45_4/-45_4]_s$) are utilized. For the purpose of comparing results, all tests are performed at load ratio (F_{min}/F_{max}) equal to 0.1 and a frequency less than 10 Hz. It is clear that although the load ratio is kept constant, the stress ratio for different points of the pin/bolt-loaded problem is not constant and also varies with the number of cycles.

8.4.1 Fatigue Life Simulation

A series of fatigue tests is performed to measure the fatigue life of the pin or bolt-loaded composite laminates with different lay-ups. Based on the maximum static strength of each case, presented in the previous section, the fatigue experiments were accomplished under load control conditions. In the following, the results of fatigue life simulation and experiments for different cases are summarized.

8.4.1.1 Cross-ply $[0_4/90_4]_s$

A series of fatigue life tests is performed at different percentages of the maximum strength of the pin-loaded cross-ply $[0_4/90_4]_s$ laminate with *e/d=w/d*=4. The maximum applied load versus number of cycles for the pin-loaded cross-ply $[0_4/90_4]_s$ laminate is shown in Fig. 8.14. The solid line shows that the experimental fatigue life curve, fitted by using a least square method. Also, the dotted line shows the simulated fatigue life using the *progressive fatigue damage model*. As shown in Fig. 8.14, very good agreement between the experimental and simulated results is achieved which shows that the model is performing successfully. For instance, at 4.335 kN which is 80% of the maximum static strength of the pin-loaded cross-ply $[0_4/90_4]_s$ laminate, the experimental fatigue life is about 9,910 cycles and the fatigue life simulated by the *model* is 15,400 cycles, which is in the scatter range of the experimental results. As explained earlier, the main reason for greater difference between the fatigue life prediction and the experiments in Fig. 8.14, at very low load levels is that material characterization of the unidirectional ply is performed at high and low states of stress but not at very low stress levels.

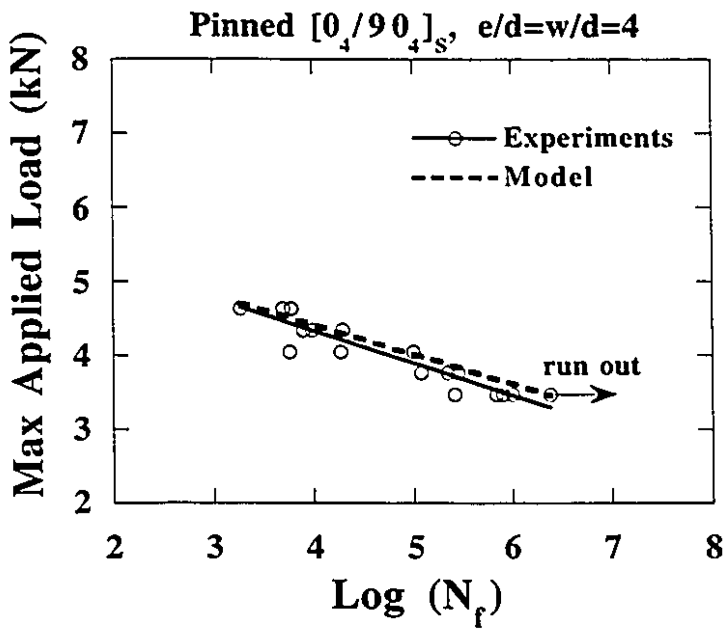

Fig. 8.14 Fatigue life curve of pin-loaded cross-ply $[0_4/90_4]_s$ laminates

A series of fatigue life tests is performed at different percentages of the maximum strength of the bolt-loaded cross-ply $[0_4/90_4]_s$ laminate with *e/d=w/d*=4. The maximum applied load versus number of cycles for the bolt-loaded $[0_4/90_4]_s$ laminate is shown in Fig. 8.15. Again, the solid line shows the experimental fatigue life curve, fitted by using a least square method. Also, the dotted line shows the simulated fatigue life using the *progressive fatigue damage model*. As shown in Fig. 8.15, very good agreement between the experimental and simulated results is achieved.

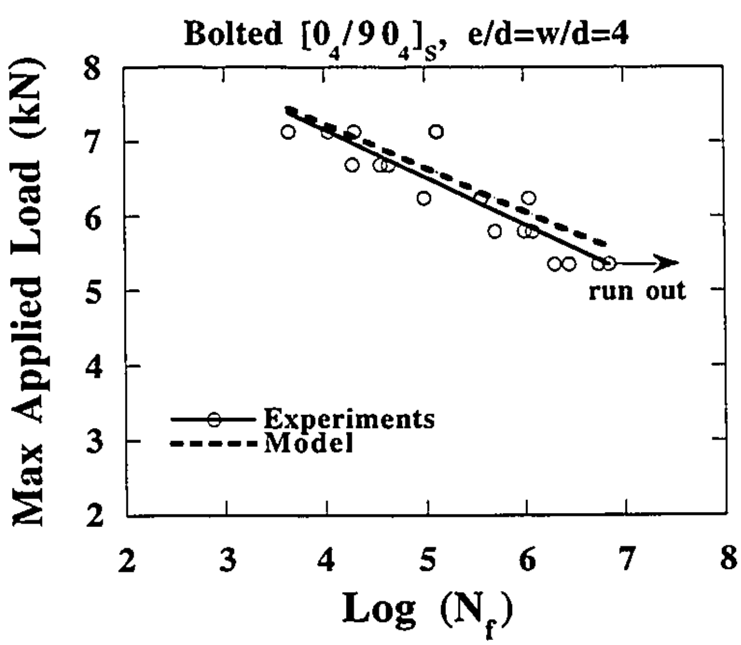

Fig. 8.15 Fatigue life curve of bolt-loaded cross-ply $[0_4/90_4]_s$ laminates

By comparing the pin and bolt-loaded cases for the cross-ply $[0_4/90_4]_s$ laminate (Figs. 8.14 and 8.15), it is clear that the bolt load increases the fatigue life by decreasing the edge effects. The effects of bolt load on the states of stress near the edge of the hole between plies with different orientations, which is the location of stress singularity was studied in Chapter 3. The predicted results show that the *model* is clearly capable of simulating this behaviour.

8.4.1.2 Cross-ply $[90_4/0_4]_s$

Another series of fatigue life tests is performed at different percentages of the maximum strength of the pin-loaded cross-ply $[90_4/0_4]_s$ laminate with e/d=w/d=4. The maximum applied load versus number of cycles for the pin-loaded cross-ply $[90_4/0_4]_s$ laminate is shown in Fig. 8.16. Again, the solid line shows the experimental fatigue life curve, fitted by using a least square method. Also, the dotted line shows the simulated fatigue life using the *progressive fatigue damage model*. As shown in Fig. 8.16, very good agreement between the experimental and simulated results is also achieved for this case.

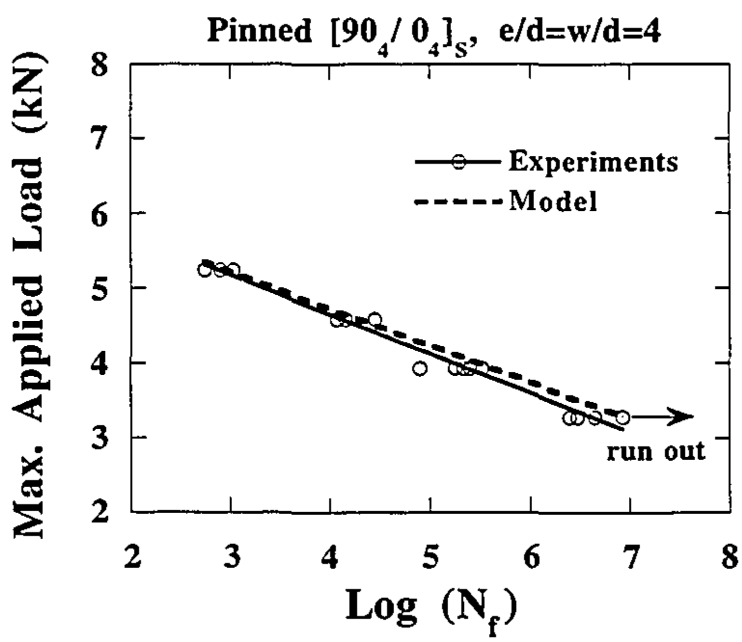

Fig. 8.16 Fatigue life curve of pin-loaded cross-ply $[90_4/0_4]_s$ laminates

In order to compare the results of the fatigue life of pin-loaded $[0_4/90_4]_s$ and $[90_4/0_4]_s$ cross-ply laminates, Figs. 8.14 and 8.16 are shown in one graph (Fig. 8.17). As shown, similar to the static strength behaviour, the pin-loaded $[90_4/0_4]_s$ laminate shows a higher fatigue life than the $[0_4/90_4]_s$ cross-ply laminate for the same fatigue loading conditions. The main reason for this behaviour is explained by the lower singular stress state for the $[90_4/0_4]_s$ cross-ply laminate near the edge of the hole, as studied in Chapter 3.

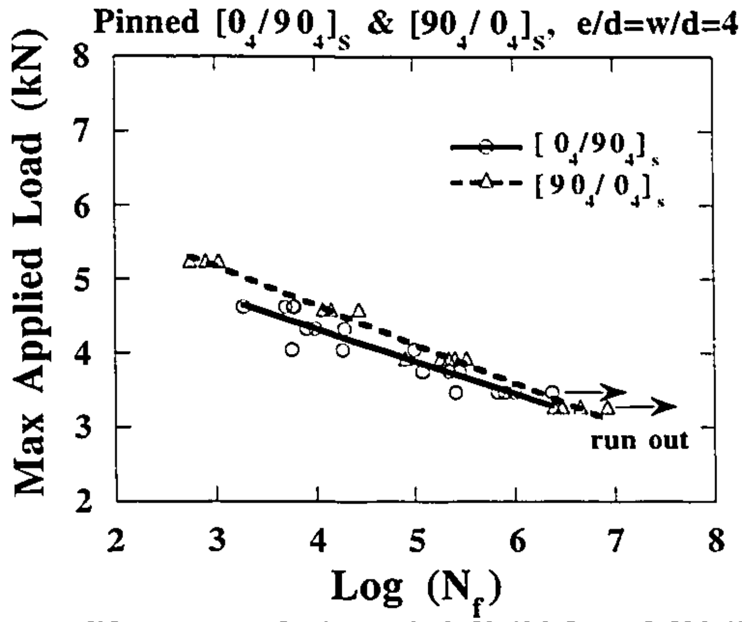

Fig. 8.17 Fatigue life curves of pin-loaded $[0_4/90_4]_s$ and $[90_4/0_4]_s$ laminates

8.4.1.3 Angle-ply $[+45_4/-45_4]_s$

Another series of fatigue life tests is performed at different percentages of the maximum strength of the pin-loaded angle-ply $[+45_4/-45_4]_s$ laminate with *e/d=w/d*=4. The maximum applied load versus number of cycles for the pin-loaded angle-ply $[+45_4/-45_4]_s$ laminate is shown in Fig. 8.18. Again, the solid line shows the experimental fatigue life curve, fitted by using a least square method. Also, the dotted line shows the simulated fatigue life using the *progressive fatigue damage model*. As shown in Fig. 8.18, good agreement between the experimental and simulated results is also achieved for this case.

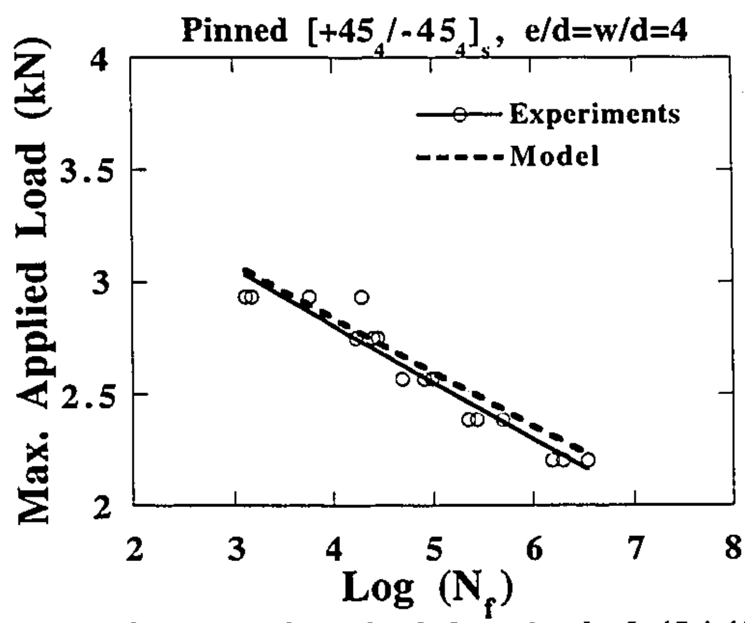

Fig. 8.18 Fatigue life curve of pin-loaded angle-ply $[+45_4/-45_4]_s$ laminates

It should be mentioned that the final failure mechanisms of the mechanical joints under static and fatigue loading conditions are similar. Typical final failure mechanisms of the pin-loaded $[0_4/90_4]_s$ and $[90_4/0_4]_s$ cross-ply laminates and $[+45_4/-45_4]_s$ angle-ply laminate are shown in Fig. 8.19.

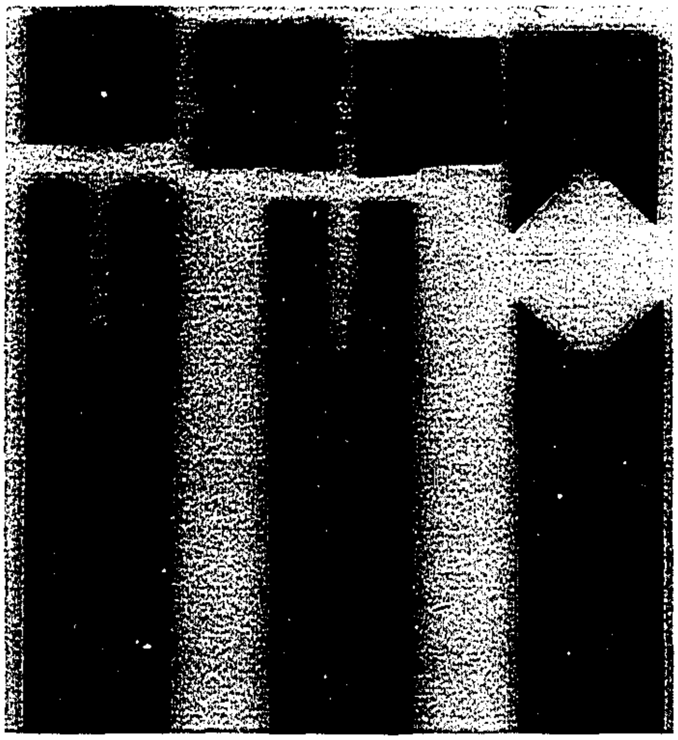

$[0_4/90_4]_s$ $[90_4/0_4]_s$ $[+45_4/-45_4]_s$

Fig. 8.19 Typical final failure mechanisms of the pin-loaded $[0_4/90_4]_s$ and $[90_4/0_4]_s$ cross-ply and $[+45_4/-45_4]_s$ angle-ply laminates

8.4.2 Residual Strength Simulation

To evaluate the residual strength simulation capability of the *progressive fatigue damage model*, a pin-loaded $[90_4/0_4]_s$ cross-ply laminate is selected as an example. The maximum fatigue load is selected as 80% of the maximum static strength of the pin-loaded $[90_4/0_4]_s$ cross-ply composite laminate measured by experiments and the load ratio is chosen to be equal 0.1. Although the load ratio is constant, the stress ratio at different points of the pin-loaded $[90_4/0_4]_s$ cross-ply laminate and at different number of cycles is obviously not constant. The specimens, after being subjected to a certain number of cycles, (e.g., 10^2, 10^3, etc.) under fatigue loading conditions, are tested under static loading conditions to measure the residual strength. For modeling purposes, first the fatigue behaviour of the specimen is simulated by the *progressive fatigue damage model* (flowchart in Fig. 6.2 in Chapter 6) and after a certain number of cycles the computer program is stopped. Thereafter, the behaviour of the specimen, with the new residual stiffness and strength properties, is simulated under static loading by the progressive static damage model (flowchart in Fig. 6.1 in Chapter 6). The results of experiments and simulation of the residual strength of the pin-loaded $[90_4/0_4]_s$ cross-ply laminate with e/d=w/d=4 as a function of number of cycles are shown in Fig. 8.20.

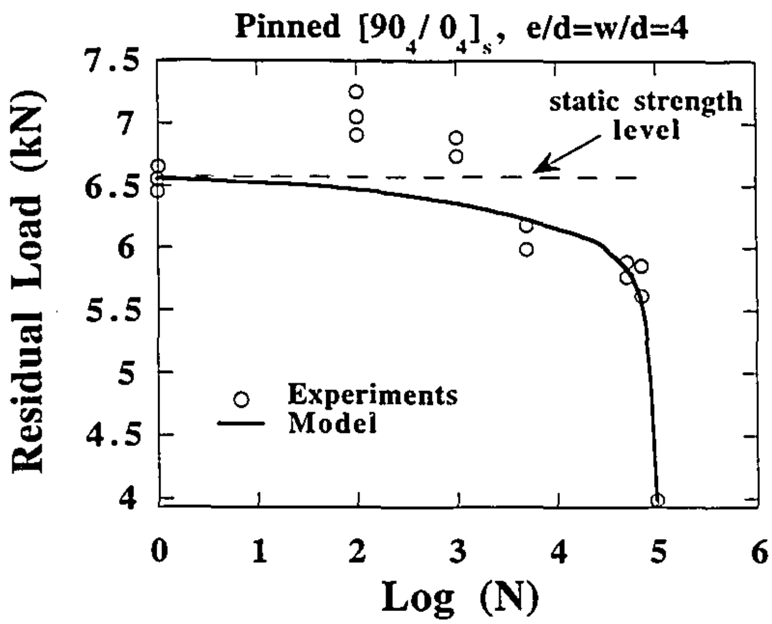

Fig. 8.20 Residual fatigue strength curve of pin-loaded cross-ply $[90_4/0_4]_s$ laminates (simulation and experiments)

As shown in Fig. 8.20, an increase in the residual strength at 10^2 and 10^3 cycles is observed experimentally. However, as shown in Fig. 8.20, while the *model* is simulating the decreasing part of the residual strength curve very well, it is not able to simulate the initial increase. As explained in Chapter 7, the increase in the residual fatigue strength of notched composites, which sometimes is referred to as *wear-in*, has been frequently observed by various authors [4, 9, 11, 13, 17-20, 25, 27, 33, 38, 44, 257, 282-287]. Some of the authors [9, 25, 33, 284, 285] postulated that the redistribution and relaxation of the stresses around the notch area are the responsible mechanisms for causing such a phenomenon.

By referring to the basic concepts of the *progressive fatigue damage model*, it is clear that the redistribution and relaxation of the stresses have been considered and the *model* is able to simulate the stress distribution at different points of the specimen as a function of number of cycles. However, the *model* is still not able to simulate the increasing part of the residual fatigue strength curve shown in Fig. 8.20. Therefore, this observation shows that only by redistribution and relaxation of stresses, it is not possible to simulate this phenomenon. The main reason for this deficiency lies in the existence of experimentally observed increases in residual stiffness and strength of the unidirectional ply under uniaxial tension and compression in the first cycles (Figs. 7.7, 7.8 and 7.14 in Chapter 7). The increase is ignored intentionally so far by the utilized curve fitting strategy explained in Chapters 5 and 7. Hence, to establish a model capable of simulating this interesting phenomenon, the realistic fatigue degradation of the material properties of a unidirectional ply as well as the ability of considering the redistribution of stresses should be considered. To eliminate this problem, a new strategy is established for curve fitting and explained in the following.

The typical residual fatigue property (stiffness or strength) of a unidirectional ply with and without considering the initial increase, under uniaxial fatigue loading conditions in a normalized form is shown in Fig. 8.21. For the simplicity the x-axis (normalized number of cycles) and the y-axis (normalized residual fatigue property) are denoted by $\mathcal{N}$ and $\mathcal{F}$, respectively.

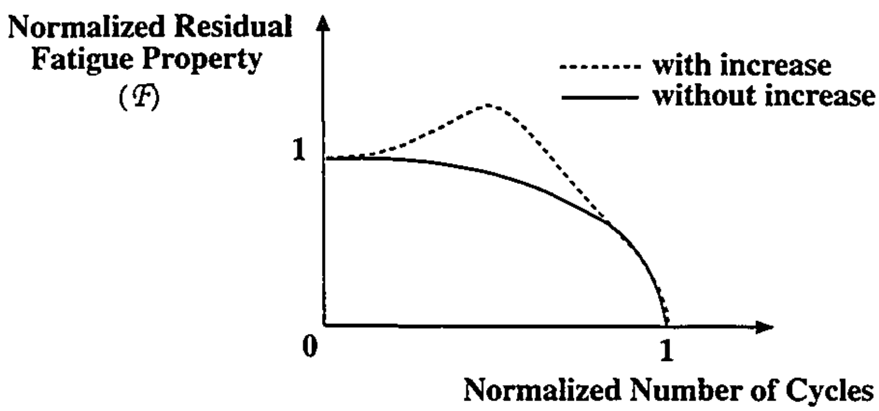

Fig. 8.21 Typical normalized residual fatigue property (stiffness or strength) of a unidirectional ply under uniaxial fatigue loading conditions (not to scale)

As defined earlier in Chapters 5 and 7, the normalized number of cycles (the x-axis in Fig. 8.21) and the normalized residual property (the y-axis in Fig. 8.21) were related by the following equation:

$$\mathcal{F} = \left(1 - \mathcal{N}^{a}\right)^{\frac{1}{b}} \qquad \textbf{Eq. 8.7}$$

which for the residual fatigue strength, $\mathcal{F}$ is,

$$\mathcal{F} = \frac{R(n,\sigma,\kappa) - \sigma}{R_s - \sigma} \qquad \textbf{Eq. 8.8}$$

and for the residual fatigue stiffness, $\mathcal{F}$ is,

$$\mathcal{F} = \frac{E(n,\sigma,\kappa) - \frac{\sigma}{\varepsilon_f}}{E_s - \frac{\sigma}{\varepsilon_f}} \qquad \textbf{Eq. 8.9}$$

and $\mathcal{N}$ denotes,

$$\mathcal{N} = \frac{\log(n) - \log(.25)}{\log(N_f) - \log(.25)} \qquad \textbf{Eq. 8.10}$$

Eq. 8.7, using two curve fitting parameters a and b, is able to curve fit the solid line in Fig. 8.21. However, this strategy cannot show the initial increase in the residual fatigue property (dotted line). To curve fit the dotted line, the following equation is a good candidate.

$$\mathcal{F} = \left[1 - \mathcal{N}^a + c\mathcal{N}^d(1-\mathcal{N})^e\right]^{\frac{1}{b}} \qquad \textbf{Eq. 8.11}$$

This equation (Eq. 8.11) contains five curve fitting parameters (a, b, c, d and e) which must be found experimentally, therefore is not simple as Eq. 8.7.

As explained in Chapter 7, during the characterization of the unidirectional ply, an increase in the residual fatigue stiffness and strength of fiber direction in tension and compression is observed. Using this newly developed curve fitting strategy (Eq. 8.11), residual fatigue properties of the unidirectional ply under tension and compression fatigue loading (Figs. 7.7, 7.8 and 7.14 in Chapter 7), are characterized and shown in Figs. 8.22, 8.23 and 8.24). As shown, the new strategy for curve fitting is able to simulate the residual fatigue behaviour very well.

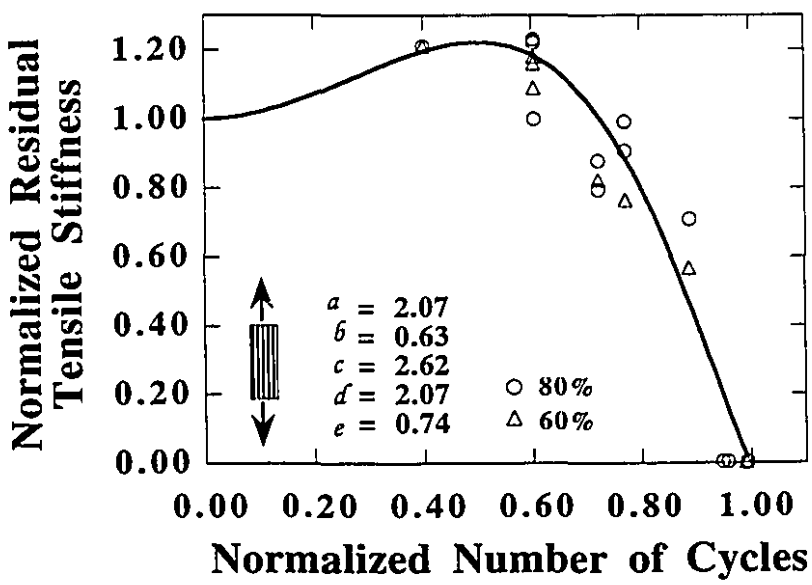

Fig. 8.22 Normalized residual stiffness of a unidirectional 0° ply under longitudinal tensile fatigue loading conditions (using Eq. 8.5)

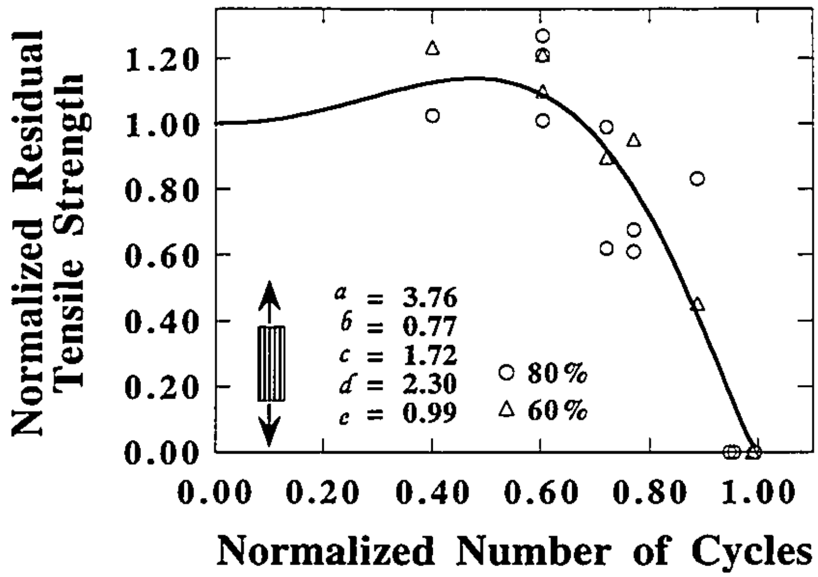

Fig. 8.23 Normalized residual strength of a unidirectional 0° ply under longitudinal tensile fatigue loading conditions (using Eq. 8.5)

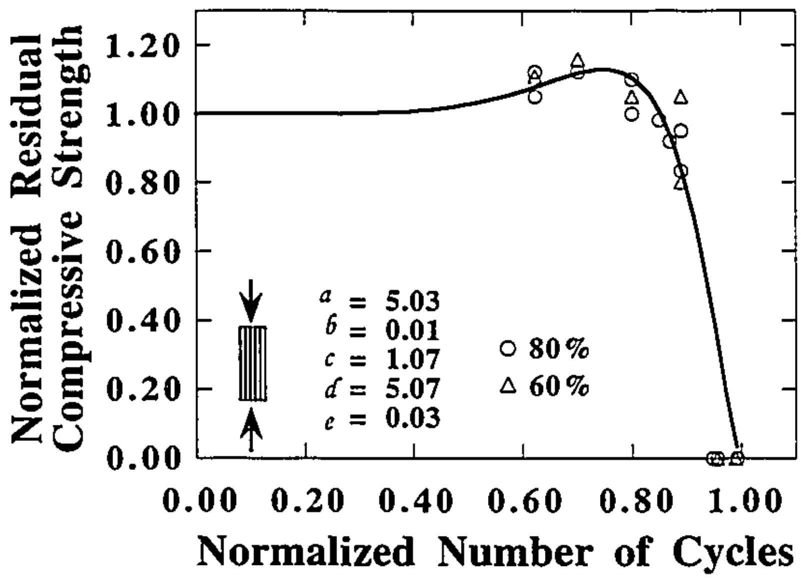

Fig. 8.24 Normalized residual strength of a unidirectional 0° ply under longitudinal compressive fatigue loading conditions (using Eq. 8.5)

In this step, the effect of increase in the residual fatigue properties of the unidirectional ply on the fatigue behaviour of notched composites is studied. Using the new experimental curve fitting parameters in the *progressive fatigue damage model*, the residual fatigue strength of the pin-loaded $[90_4/0_4]_s$ cross-ply with *e/d*=*w/d*=4 as a function of number of cycles is simulated by the *model* and compared with the experimental results (Fig. 8.25).

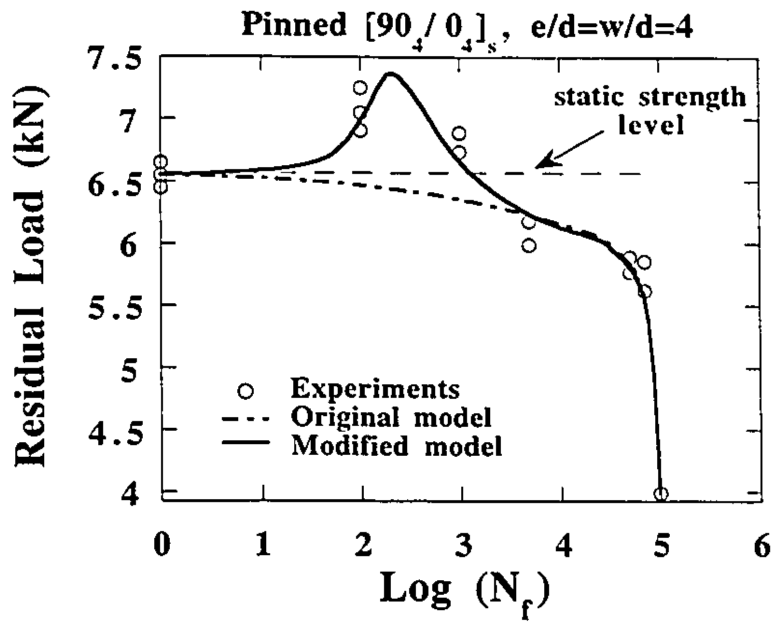

Fig. 8.25 Residual fatigue strength curve of pin-loaded cross-ply $[90_4/0_4]_s$ laminates (modified simulation and experiments)

As shown in Fig. 8.25, the new strategy of curve fitting enables the *progressive fatigue damage model* to simulate the residual fatigue strength of the pin-loaded $[90_4/0_4]_s$ cross-ply laminate at low and high number of cycles (less than 10^3 cycles). A comparison between the simulated residual fatigue strength curves by modified and original models in Fig. 8.25 reveals that while the original *model* is not able to simulate the behaviour in the first cycles (less than 10^3 cycles), it is able to simulate the residual fatigue behaviour of the notched composites at high number of cycles (bigger than 10^3 cycles). To perform a better simulation, more experiments are needed for the material characterization of the unidirectional 0° ply in tension and compression which of course demands more time and expense.

8.4.3 Fatigue Life Simulation (Experiments Performed by Other Authors)

To evaluate the *progressive fatigue damage model* by independent experimental data, the fatigue life of a pin and bolt-loaded quasi-isotropic $[0/90/\pm45]_s$ laminate made of AS4/3501-6 is simulated and compared with the experimental results of Herrington and Sabbaghian [52]. The composite plate has a width w = 38.1 mm, length l = 177.8 mm, thickness t = 1.21 mm (8 plies), edge distance e = 38.1 mm, hole diameter d = 6.35 mm and washer diameter d_w = 18.8 mm and the inside diameter of the washer to bolt diameter ratio is 1.024. They [52] selected large values for *e/d* and *w/d* equal to 6.0, therefore the final failure mechanism is expected to occur mostly in bearing (see Fig. 2.2). All tests are performed at load ratio (F_{min}/F_{max}) equal to 0.1 and a frequency equal to 10 Hz. They performed their experiments based on the definition that the final failure occurs when the hole elongation was equal to 4% of the original hole diameter. While the final failure, in the modeling strategy utilized in this study, is defined as the catastrophic failure in which the pin/bolt-loaded composite laminate cannot tolerate any more load. Therefore, due to these different definitions, some discrepancies should be expected between results of the present *model* and their experiments.

It should be mentioned that there was no direct access to the experimental results of Herrington and Sabbaghian [52], therefore, the magnitudes used in this study are interpreted from the graphs reported in their paper. In the first step, the static strength of the pin-loaded quasi-isotropic laminate is simulated by the progressive static damage model and compared with the experimental result. The simulated maximum static load, which can be carried by the specimen, is equal to 2.36 kN which is 7.3% different from the experimental result which is about 2.20 kN. In the next step, the fatigue life of the pin-loaded quasi-isotropic laminate is simulated by the *progressive fatigue damage model* and compared with the experimental results (Fig. 8.26). A reasonable agreement between the simulated and experimental results is achieved. For instance at 1.94 kN, which is 88% of the maximum static strength of the pin-loaded quasi-isotropic laminate, the experimental fatigue life is about 1,202 cycles (average of three data points) and the fatigue life simulated by the *model* is 4,800 cycles. By considering the existence of experimental scatter which is inherent to fatigue behaviour of the material, the result obtained by the *model* is quite satisfactory. Moreover, as mentioned earlier, the difference between the simulated and experimental results is also attributed to different definitions of the final failure used in this study and by the other authors [52].

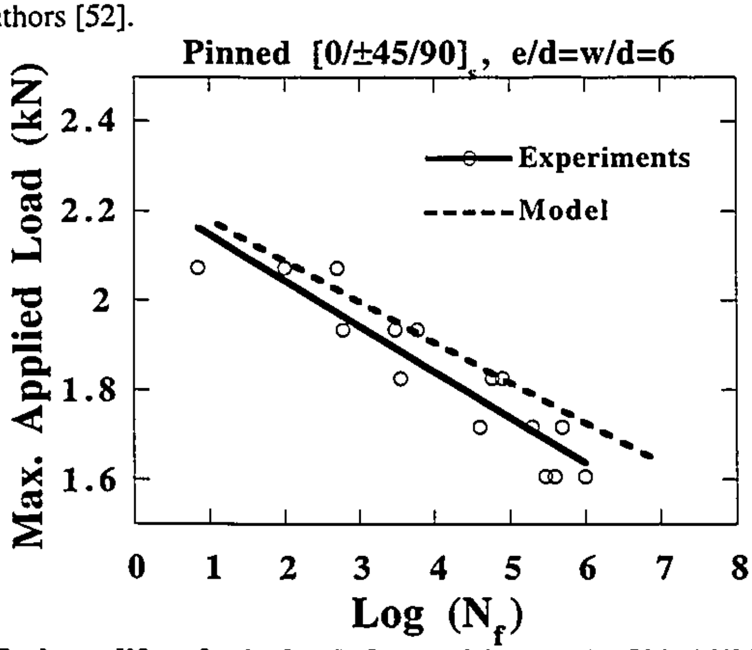

Fig. 8.26 Fatigue life of pin-loaded quasi-isotropic $[0/\pm45/90]_s$ laminates (simulation by the *model* and experiments by Herrington and Sabbaghian [52])

Additional experimental results of Herrington and Sabbaghian [52] on bolt-loaded quasi-isotropic $[0/90/\pm45]_s$ laminates are compared with the results simulated by the *model*. The clamping torque on the bolt is equal to 3.76 N-m. Again, as a first step, the static strength of the bolt-loaded quasi-isotropic $[0/90/\pm45]_s$ laminate is simulated by the progressive static damage model and compared with the experimental result. The simulated maximum static load is equal to 4.02 kN which is 5.85% different from the experimental result which is 4.27 kN. In the next step, the fatigue life of the bolt-loaded quasi-isotropic $[0/90/\pm45]_s$ laminate is simulated by the *progressive fatigue damage model* and compared with the experimental results shown in Fig. 8.27. As shown, the *model* highly overestimates the fatigue life of the bolt-loaded $[0/90/\pm45]_s$ quasi-isotropic laminate and the difference between the simulated and experimental results is very clear. As a numerical example, at 3.59 kN which is 84% of the maximum static strength of the bolt-loaded $[0/90/\pm45]_s$ quasi-isotropic laminate, the experimental fatigue life is about 7,943 cycles while the fatigue life simulated by the *model* is 125,900 cycles. As mentioned earlier, Herrington and Sabbaghian [52] stop the fatigue cycling when the hole elongation reaches to a value of 4% and they define the fatigue life of the specimen as the number of cycles at that point. However, the *model* shows that the specimen, after reaching that level of deformation, still can carry more fatigue cycles. Therefore, the different definitions of the final failure used in this study and by Herrington and Sabbaghian [52] could be the source of the large difference between the *model* and experimental results.

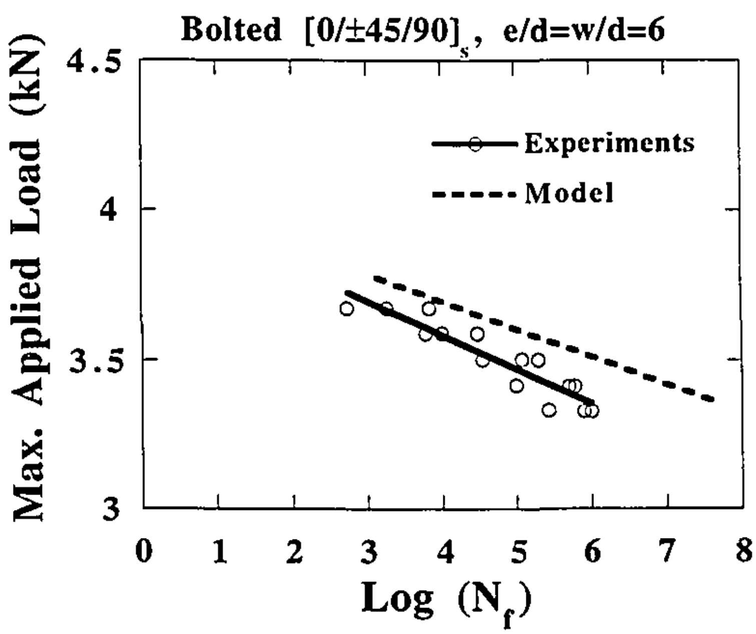

Fig. 8.27 Fatigue life of bolt-loaded quasi-isotropic $[0/\pm45/90]_s$ laminates (simulation by the *model* and experiments by Herrington and Sabbaghian [52])

The comparison of the fatigue life of the pin-loaded $[0/\pm45/90]_s$ laminate simulated by the *model* and the experiments by other authors [52] shows a fairly good agreement. The large difference observed for the fatigue life of the bolt-loaded $[0/\pm45/90]_s$ laminate, simulated by the *model* and the experiments, is probably due to two different definitions for the final failure used by other authors [52] and in this study. However, in general, it can be concluded that the *model* is successfully verified by the available independent data provided by other authors. In the next section, the fatigue behaviour of pin-loaded composite laminates under two consecutive load levels (low and high) is studied.

8.4.4 Residual Life Simulation

Another interesting outcome of the *model* is its ability to simulate the fatigue behaviour of composite laminates under two or more consecutive load levels. Although the *model* is not limited to the number of the consecutive load levels, for simplicity, the study is performed in two stages. A traditional method of predicting this behaviour is by using the Palmgren-Miner's Rule [311] (sometimes called the Miner's Rule). The main procedure is that the composite laminate is under a fatigue load level for a certain number of cycles and then the load level is changed and the composite laminate is fatigue loaded under the second load level until final failure is achieved. The load levels for both cases and the number of fatigue cycles under the first load level are known and the number of cycles under the second load level (residual life) must be calculated. As an example, consider the behaviour of a composite laminate under two different stress levels as shown in Fig. 8.28. Suppose the composite laminate is under n_1 number of cycles at σ_1 state of stress and then the stress level is changed to σ_2 and the composite laminate is fatigued until catastrophic failure is achieved.

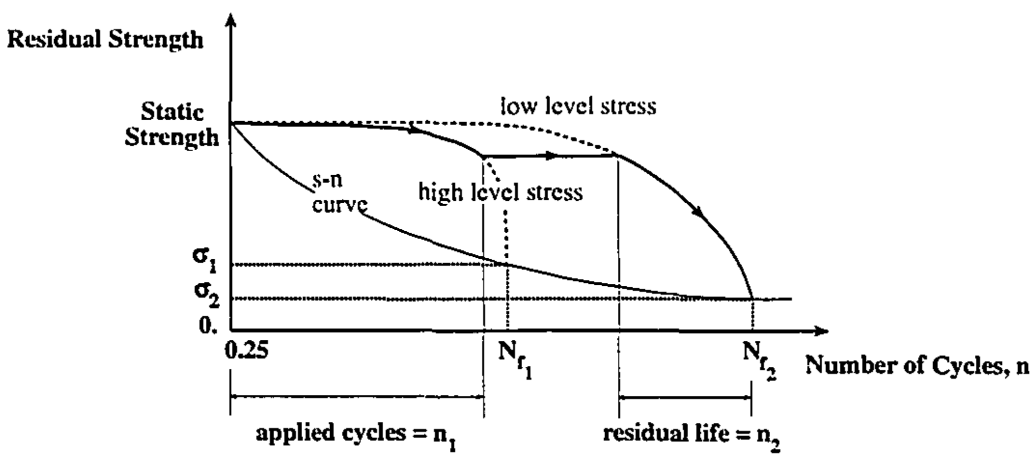

Fig. 8.28 Behaviour of a composite laminate under two different stress levels

The simple Miner's Rule (for two consecutive stress levels) states that the following equation can be used to calculate the residual life. By knowing the σ_1, σ_2, n_1, N_{f_1} and N_{f_2}, the residual life (n_2) under σ_2 is calculated using Eq. 8.12 [311].

$$\sum \frac{n}{N_f} = \frac{n_1}{N_{f_1}} + \frac{n_2}{N_{f_2}} = 1 \qquad \textbf{Eq. 8.12}$$

where,

n_1 = applied number of cycles at σ_1
N_{f_1} = fatigue life at σ_1
n_2 = residual number of cycles at σ_2
N_{f_2} = fatigue life at σ_2

Although the Miner's Rule is a simple and useful method, however, experimental evidence [312-316] reveals that it is not able to predict residual life in general. Also, experimental evidence shows that the sequence of applying stress levels (high-to-low or low-to-high) is important, while the Miner's Rule is not able to distinguish the difference. For instance, consider that the n_1 number of cycles under σ_1 stress level is applied first, and then the stress level is changed to σ_2 and the residual life (n_2) is calculated by Eq. 8.6. Now, suppose if the n_2 number of cycles under σ_2 state of stress is applied first (n_2 is calculated previously), and then the stress level is changed to σ_1. Then, the residual life (n_1) under σ_1 as calculated by Miner's Rule is the same as before, while experimental evidence does not confirm this result. This is another shortcoming of Miner's Rule which the *model* should be also checked for. From Fig. 8.28, it can be inferred that changing the loading sequence effects the residual fatigue life of the composite laminate. Therefore, considering the mechanics of the residual fatigue strength is a vital step in fatigue modeling which is considered by the *model*, while the Miner's Rule does not account for it.

To evaluate the *model* under two consecutive load levels, the pin-loaded $[+45_4/-45_4]_s$ angle-ply laminate with *e/d*=*w/d*=4 under two consecutive load levels (80% and 60% of the maximum static strength) is selected as an experiment. The load ratio of 0.1 and frequency equal to 10 Hz are selected. From Fig. 8.18, the average number of cycles to failure for the pin-loaded $[+45_4/-45_4]_s$ angle-ply laminate at the load level equal to 80% and 60% of its maximum static strength is 3,100 and 2,400,000 cycles, respectively. Two sets of tests are performed at the two consecutive stress levels (high-to-low and low-to-high) and for each set of experiments, three samples are tested. The results of the experiments, the prediction by Miner's Rule and the *model* are summarized in Table 8.6.

Applied Stresses at σ_1	Applied Cycles (n_1)	Residual Fatigue Life (n_2) Miner's Rule (*error %*)	*Model* (*error %*)	Experiment
High to Low	1,000	1,626,000 (*124%*)	910,000 (*25%*)	725,000
Low to High	1,626,000	1,000 (*54%*)	1,700 (*23%*)	2,200

Table 8.6 Residual fatigue life of pin-loaded $[+45_4/-45_4]_s$ angle-ply laminates, measured by experiments and predicted by Miner's Rule and *model*

For the first set of experiments (high-to-low), 1,000 cycles are applied at the load level equal to 80% of the maximum static strength of the pin-loaded $[+45_4/-45_4]_s$ angle-ply laminate. Thereafter, the load level is changed to 60% of the maximum static strength and the residual fatigue life is measured experimentally. The average residual fatigue life for three specimens, tested under the same conditions, is 725,000 cycles. The residual fatigue life predicted by Miner's Rule is 1,626,000 cycles which shows 124% error with respect to the experimental results. The predicted residual fatigue life by the *model* is 910,000 cycles which is 25% different from the experimental results. The Miner's Rule and the *model* both overestimate the residual fatigue life, however, the acceptable percentage of error produced by the *model* shows a fairly good agreement between the simulation and the experiments. The next set of experiments (high-to-low) is performed by applying 1,626,000 cycles (calculated for the previous set of experiments by Miner's Rule) at the load level equal to 60% of the maximum static strength. Thereafter, the load level is changed to 80% of the maximum static strength and the residual fatigue life is measured experimentally. The average residual fatigue life for three specimens, tested under the same conditions, is 2,200 cycles. While the Miner's Rule cannot distinguish the changing of the loading sequence, the *model* predicts the residual fatigue life equal to 1,700 cycles, which is 23% different from the experimental results. Clearly, from Eq. 8.6, the mechanics of failure are not considered by the simple Miner's Rule, therefore it is not surprising that the prediction of the residual life by this equation for the examined cases is not accurate. The more successful simulation of the residual fatigue life results from the progressive nature of the *model* and considering the mechanics of failure.

This limited number of experiments shows the capability of the *model* to predict the residual fatigue life of a notched specimen under two consecutive load levels. As mentioned earlier, the *model* is not confined to the special case of two consecutive load levels. To show this capability under general conditions, more experiments must be performed.

8.5 Summary

By performing several different series of experiments and using available independent experimental results by other authors, the validity of the *progressive fatigue damage model* and some of its capabilities are examined.

Although the *generalized residual material property degradation technique* is capable of simulating the fatigue behaviour of a unidirectional ply under multiaxial state of stress, experimental evaluation of the established technique under multiaxial state of fatigue stress is not a simple task. Therefore, the technique is evaluated under biaxial state of fatigue stress, using the 30° off-axis specimen. A very good agreement between the experimental and simulated results is achieved which validates the *generalized residual material property degradation technique.*

Before evaluating the fatigue simulation capability of the *model*, the progressive static damage model, which is another important part of the *progressive fatigue damage model*, is verified. Different ply configurations ($[0_4/90_4]_s$, $[90_4/0_4]_s$ and $[+45_4/-45_4]_s$) with different geometries (*e/d* and *w/d*) under static pin and bolt loading conditions are studied. The failure initiation and final failure load for different cases are simulated and compared with the experimental results. Excellent agreement between the experimental and simulated results are obtained.

To evaluate the capabilities of *the progressive fatigue damage model* for simulating the fatigue life and residual strength of the notched composites laminates, a series of experiments is performed. To show the fatigue life simulation capability of notched composites by the *model*, different pin/bolt-loaded composite laminates with different ply lay-ups ($[0_4/90_4]_s$, $[90_4/0_4]_s$ and $[+45_4/-45_4]_s$) are studied. A good agreement between the results of experiments and simulation is obtained which shows the successful fatigue life simulation capability of the *model*. Moreover, the residual strength simulation capability of the *model* is evaluated by performing experiments on the pin-loaded $[90_4/0_4]_s$ cross-ply laminates. The experimental results of the residual fatigue strength of the pin-loaded $[90_4/0_4]_s$ cross-ply laminates show an increase for the first few cycles followed by a subsequent decrease. The *model*, using the experimental curve fitting parameter in the previous chapter, is able to simulate the decreasing part of the residual fatigue strength curve as a function of number of cycles very well. However, to simulate the increasing part of the residual fatigue strength of the notched composite, the experimentally observed increase in the residual fatigue strength of the unidirectional ply in fiber direction under tension and compression fatigue loading must be considered. It should be mentioned that this behaviour was ignored intentionally in the previous chapter to show the effect on the residual fatigue strength prediction of the notched composite laminates. By using a new curve fitting strategy and considering the initial increase of the residual fatigue properties of the unidirectional ply in the fiber direction under tension and compression, a successful simulation of the residual fatigue strength of the pin-loaded $[90_4/0_4]_s$ cross-ply laminate is achieved. It is concluded that, although the redistribution and relaxation of the stress field around the notch area are important factors, however without considering the proper behaviour of the unidirectional ply under fatigue loading, the simulation of the residual fatigue strength behaviour of notched composites is difficult.

To verify the *model* by the independent experimental data available in the literature, the fatigue life of a pin and bolt-loaded quasi-isotropic $[0/90/\pm45]_s$ laminate is studied. For the pin-loaded case, fairly good agreement between the *model* and the experiments are achieved. However, for the bolt-loaded case, large differences between the simulated and experimental results are observed. The main reason for this discrepancy is stated to be the different definition of final failure utilized in the experimental study by other authors and the *model* in this study.

To evaluate another capability of the *model*, which is the fatigue behaviour simulation of composite laminates under two or more consecutive load levels, the pin-loaded $[+45_4/-45_4]_s$ angle-ply laminate with *e/d*=*w/d*=4 under two consecutive load levels (80% and 60% of the maximum static strength) is selected as an example. The shortcoming of the Miner's Rule to simulate this problem is shown and discussed. A very good agreement between the simulated and experimental results is achieved.

Chapter 9

Summary and Conclusions

The present research establishes a new modeling approach to simulate the behaviour of composite laminates under general fatigue loading conditions. Using the idea of the traditional progressive damage model which is capable of simulating of static behaviour of composite laminates, the *progressive fatigue damage model* is developed. The *model* consists of three major components: stress analysis, failure analysis and material property degradation rules. The *model* determines the state of damage at any load level and number of cycles, from failure initiation and propagation to catastrophic failure. The *model* is able to predict the residual strength, residual life, final failure mechanisms (direction of failure propagation) and final fatigue life of composite laminates under general fatigue loading conditions. Based on the *model*, a computer code is developed which simulates the cycle-by-cycle behaviour of composite laminates under fatigue loading conditions. The capabilities of the model are examined by simulation of a pin/bolt-loaded composite laminates as a complicated example.

A three-dimensional nonlinear finite element algorithm is developed for the stress analysis. By using a large number of elements near the edge of the hole and at layer interfaces, the edge effect (stress singularity) is simulated. Also, by noting the nonlinear shear stress-strain behaviour of a unidirectional ply, the effect of material nonlinearity on the stress state near the edge of the composite laminate, which is a critical location for failure initiation, is considered. An existing model for the mathematical presentation of nonlinear in-plane shear stress-strain behaviour of a unidirectional composite ply is extended to be also applicable for out-of-plane shear stress-strain. Considering material nonlinearity causes significant decreases in magnitudes of some stresses while others are increased to compensate. The effect of existence of bolt load on the state of stress, near the edge of the hole is also studied and discussed.

For the failure analysis, seven different failure modes for the unidirectional ply under multiaxial state of stress are considered which are: fiber tension, fiber compression, fiber-matrix shearing, matrix tension, matrix compression, normal tension and normal compression failure modes. Suitable stress-based failure criteria for detecting these modes of failure under static and fatigue loading conditions are derived. The effect of material nonlinearity on the mathematical form of the failure criteria is also considered. Difficulties and limitations of application of such failure criteria, in traditional forms, for unidirectional plies under multiaxial fatigue loading conditions for general stress state and stress ratios are discussed.

A strategy for changing material properties (stiffness, strength and Poisson's ratio) of failed material under static and fatigue loading for each mode of failure is established. For each sudden mode of static or fatigue failure, detected by the set of failure criteria, a suitable sudden material property degradation rule is associated. For the fatigue case, to simulate gradual material property degradation, normalization techniques for strength degradation, stiffness degradation and fatigue life of a unidirectional ply under uniaxial state of stress are utilized. The *generalized material property degradation technique* is established by using the *normalized strength degradation, normalized stiffness degradation*, and *normalized fatigue life models*. Using the established *technique*, the limitations of application of polynomial failure criteria in traditional forms are successfully overcome.

The material properties (strength, stiffness, residual strength, residual stiffness and fatigue life) of unidirectional AS4/3501-6 graphite/epoxy material are fully characterized under tension and compression, for fiber and matrix directions, and under in-plane and out-of-plane shear, in static and fatigue loading conditions. For this purpose, an extensive experimental program is performed. The information provided by this series of experiments is used as input data for the *progressive fatigue damage model*. Some of the existing testing methods for characterization of composites are necessarily modified and improved during the experimental studies in this research.

To examine the *model* and some of its important components, different sets of experiments are conducted. To evaluate the *generalized residual material property degradation technique*, which is an important basis of the *model*, a series of static and fatigue experiments are performed on 30° off-axis specimens. A very good agreement between the results obtained from the aforementioned *technique* and the experimental results is achieved. A series of static and fatigue experiments is performed on pin/bolt-loaded composite laminates to verify the *progressive fatigue damage model*. An excellent agreement between the results of progressive static damage model simulation, which is an important component of the *model*, and the experimental results is obtained. The fatigue life simulation capability of the *model* is examined by the experiments and good agreement between the results is achieved. The fatigue life simulation capability of the *model* is also verified by independent experimental results provided by other authors. For the pin-loaded case, fairly good agreement is achieved between the results, while for the bolt-loaded case a large difference is observed. The residual strength of a pin-loaded composite laminate is simulated by the *model* and measured experimentally. An initial increase in the residual strength of the pin-loaded composite laminate is observed experimentally. It was shown that although the redistribution and relaxation of the stresses are important factors, the *model* is not able to simulate this phenomenon without considering the initial increase in the residual fatigue properties of the unidirectional ply under tension and compression in the fiber direction. A modified strategy for curve fitting of the residual fatigue properties of the unidirectional ply under tension and compression in fiber direction is adopted and a successful simulation of the residual fatigue strength of the pin-loaded composite laminate with initial increase is achieved. Finally, the fatigue behaviour of the pin-loaded composite laminates under two separate consecutive load levels (low and high) is predicted by the *model*. By changing the priority of the applied load level (high-to-low or low-to-high), it was shown that the traditional Miner's Rule is not able to simulate this problem. A fairly good agreement between the results of two separate consecutive load level experiments and the simulated results by the *model* is achieved.

In summary, the established *model* can predict several aspects of fatigue behaviour of laminated composites. All experiments, performed in this study and provided by other authors, confirm the capabilities of the *model*. A survey of the literature reveals that no other existing model has been so heavily supported by experimental results. It can be concluded that the established *model* represents a major development in the fatigue analysis of composite materials.

Originality and Contribution to Knowledge

The present research contains the following original contributions:

- A new modeling approach, called the *progressive fatigue damage modeling*, for simulation of the behaviour of laminated composites under general fatigue loading conditions is established.

- Fatigue behaviour of pin/bolt-loaded composite laminates is simulated by the *model* as a sophisticated problem. For the selected problem, the effects of material nonlinearity and bolt load on the three-dimensional singular states of stress near the edge of the hole and at layer interfaces are studied.

- An existing material nonlinear model, suitable for in-plane shear stress-strain behaviour of a unidirectional ply is extended to be applicable for the out-of-plane nonlinear shear stress-strain conditions.

- A complete set of three-dimensional stress-based polynomial failure criteria capable of detecting seven different sudden modes of static and fatigue failure of a unidirectional ply under multiaxial state of stress is developed. The effect of material nonlinearity on the mathematical forms of the failure criteria is also studied. Difficulties and limitations of application of such failure criteria, in traditional forms for general stress state and stress ratios are discussed.

- A complete set of material property degradation rules for sudden modes of static and fatigue failure for a unidirectional ply under multiaxial state of stress is developed.

- To simulate the gradual material property degradation of a unidirectional ply under multiaxial state of fatigue stress, the *generalized material property degradation technique* is established. For this purpose, the normalized strength degradation, normalized stiffness degradation and normalized fatigue life models are established and coupled. Using the established *technique*, the limitations of application of polynomial failure criteria in traditional forms are successfully overcome.

- The material properties (strength, stiffness, residual strength, residual stiffness and fatigue life) of unidirectional AS4/3501-6 graphite/epoxy material are fully characterized under tension and compression, for fiber and matrix directions, and under in-plane and out-of-plane shear, in static and fatigue loading conditions. Some of the existing testing methods for characterization of composites are necessarily modified and improved.

- Static strength, residual strength, fatigue life and residual fatigue life of the selected problem (pin/bolt-loaded composite laminates) with various geometries, ply configurations and load levels are simulated by the proposed *model* and successfully compared with the experimental results.

- Increase in residual fatigue strength of the notched composites is successfully simulated by the *model.* It is shown that the initial increase in the residual fatigue properties of the unidirectional ply under tension and compression in the fiber direction, as well as the redistribution and relaxation of the stresses, are responsible factors for causing this interesting phenomenon.

- The fatigue behaviour of composite laminates under two separate consecutive load levels (high and low) is simulated by the *model.* Considering the mechanics of failure of unidirectional plies under uniaxial fatigue loading conditions and the progressive nature of the *model* enables it to distinguish the effect of the sequence of the applied load.

- The material presented in this research is partially published by the author in six journal papers [127, 130, 175, 279, 309, 310], five conference papers [128, 129, 270, 280, 281] and one technical report [276].

Recommendation For Future Work

The following recommendations should be considered to extend and improve the present research:

- The ply configurations investigated in this study are suitable for research, but not necessarily of practical use in structural applications. Therefore, for design proposes, more practical ply configurations should be studied. Furthermore, the *model* is not limited to pin/bolt loaded cases. Analysis of any useful structure would be a good application of the current *model.*

- In this research, to simulate the edge effect (stress singularity) a large number of elements is utilized near the singularity location in the finite element model. To reduce computational time, the use of singular elements may be beneficial.

- In the present work, the effect of the friction between the pin/bolt and the edge of the hole is ignored. Adding a frictional contact formulation in the finite element technique is time consuming and expensive. However, by inducing the effect of friction, the static and fatigue behaviour of pin/bolt loaded composite laminates can be studied in more detail.

- In this study, to simulate the delamination failure mode, the material properties of failed material in the normal direction are decreased. To perform a better structural simulation, a node releasing approach for delaminated elements in the finite element model should be utilized.

- Experimental evaluation of the polynomial fatigue failure criteria is performed using the off-axis 30° specimen as a biaxial testing method. To show the generality of the failure criteria, experimental evaluation by using other biaxial and multiaxial testing techniques are recommended.

- The fatigue modeling approach established in this research does not consider frequency effects. Therefore, all fatigue experiments for material characterization and model evaluation in this study are performed at frequency less than 10 Hz. Theoretical investigation should be performed to make the *model* capable of considering the frequency effects. Also, considering the viscoelastic behaviour of the composite laminates under fatigue loading conditions is suggested.

- All fatigue experiments for material characterization of the unidirectional ply are performed at high and low level states of stress. To improve the capability of the *model* to predict the behaviour of laminated composites under low level fatigue loading conditions, the unidirectional material should also be characterized at very low level states of stress.

- Some of the fatigue experiments under low level state of stress take several days to be performed. Therefore, consideration of the creep effect for these type of tests is recommended.

- The AS4/3501-6 graphite/epoxy material is fully characterized for the purpose of modeling in this investigation. Other material systems should be studied to show the generality of the *model.*

- Experimental scatter is inherent to composite materials under static and fatigue loading conditions, while the *model* established in this research is only able to simulate a deterministic fatigue behaviour for composites. A stochastic model should be coupled to the present deterministic *model* to make it capable of considering the probabilistic behaviour.

References

1. **American Society for Metals (ASM)**, *Metals Handbook*, Ninth Edition, Vol. 11, Failure Analysis and Prevention, 1986.

2. **B. B. Muvdi and J. W. McNabb**, *Engineering Mechanics of Materials*, Third Edition, Springer-Verlag, New York, 1991.

3. **A. Wohler**, "Wohler's Experiments on the Strength of the Materials," Engineering, 1867.

4. **W. W. Stinchcomb and K. L. Reifsnider**, "Fatigue Damage Mechanisms in Composite Materials: A Review," Fatigue Mechanisms, Proceedings of an ASTM-NBS-NSF Symposium, J. T. Fong, Ed., ASTM STP 675, (1979), pp. 762-787.

5. **K. L. Reifsnider**, "Introduction," Fatigue of Composite Materials, Ed. by K. L. Reifsnider, (1990), pp. 1-9.

6. **G. P. Sendeckyj**, "Life Prediction for Resin-Matrix Composite Materials," Fatigue of Composite Materials, Ed. by K. L. Reifsnider, (1990), pp. 431-483.

7. **G. M. Goetchius**, "Fatigue of Composite Materials," Advanced Composite III, Expanding the Technology, Proceedings of the Third Annual Conference on Advanced Composites, (15-17 Sept. 1987), pp. 289-298.

8. **D. S. Saunders and G. Clark**, "Fatigue Damage in Composite Laminates," Materials Forum, 17, (1993), pp. 309-331.

9. **W. W. Stinchcomb and C. B. Bakis**, "Fatigue Behavior of Composite Laminates," Fatigue of Composite Materials, Ed. by K. L. Reifsnider, (1990), pp. 105-180.

10. **M. J. Owen and P. T. Bishop**, "Fatigue Properties of Glass-Reinforced Plastics Containing a Stress Concentrator," Journal of Physics - D: Applied Physics, Vol. 6, (1973), pp. 2057-2069.

11. **F. H. Chang, D. E. Gordon, B. T. Rodini and R. H. McDaneil**, "Real Time Characterization of Damage Growth in Graphite/Epoxy Laminates," Journal of Composite Materials, Vol. 10, (July 1976), pp. 182-192.

12. **G. L. Roderick and J. D. Whitcomb**, "Fatigue Damage of Notched Boron/Epoxy Laminates under Constant Amplitude Loading," Fatigue of Filamentary Materials, ASTM STP 636, K. L. Reifsnider and K. N. Lauraitis, Eds., (1977), pp. 73-88.

13. **G. P. Sendeckyj, H. D. Stalnaker and R. A. Kleismit**, "Effect of Temperature on Fatigue Response of Surface-Notches $[(0/\pm45/0)_s]_3$ Graphite/Epoxy Laminate," Fatigue of Filamentary Materials, ASTM STP 636, K. L. Reifsnider and K. N. Lauraitis, Eds., (1977), pp. 73-88.

14. **M. N. Gibbins and W. W. Stinchcomb**, "Fatigue Response of Composite Laminates with Internal Flaws," Composite Materials: Testing and Design (Sixth Conference), ASTM STP 787, I. M. Daniel, Ed., (1982), pp. 305-322.

15. **T. Shimokawa and Y. Hamaguchi**, "Distributions of Fatigue Life and Fatigue Strength in Notched Specimens of a Carbon Eight-Harness-Stain Laminate," Journal of Composite Materials, Vol. 17, (Jan. 1983), pp. 64-76.

16. **N. F. Black and W. W. Stinchcomb**, "Compression Fatigue Damage in Thick, Notched Graphite/Epoxy Laminates," Long-Term Behavior of Composites, ASTM, STP 813, T. K. O'Brien, Ed., (1983), pp. 95-115.

17. **S. Kellas, J. Morton and S. M. Bishop**, "Fatigue Damage Development in a Notched Carbon Fiber Composite," Composites Science and Technology, Vol. 25, (1986), pp. 311-323.

18. **C. E. Bakis and W. W. Stinchcomb**, "Response of Thick, Notched Laminates Subjected to Tension-Compression Cyclic Loads," Composite Materials: Fatigue and Fracture, ASTM STP 907, H. T. Hahn, Ed., (1986), pp. 314-334.

19. **R. A. Simonds and W. W. Stinchcomb**, "Response of Notched AS4/PEEK Laminates to Tension/Compression Loading," Advances in Thermoplastic Matrix Composite Materials, ASTM STP 1044, G. M. Newaz, Ed., (1989), pp. 133-145.

20. **C. E. Bakis, R. A. Simonds and W. W. Stinchcomb**, "A Test Method to Measure the Response of Composite Materials Under Reversed Cyclic Loads," Test Methods for Design Allowables for Fibrous Composites, ASTM STP 1003, C. C. Chamis and K. L. Reifsnider, Eds., (1989), pp. 93-110.

21. **J. Xiao and C. Bathias**, "Fatigue Behaviour of Unnotched and Notched Woven Glass/Epoxy Laminates," Composites Science and Technology, 50, (1994), pp. 141-148.

22. **J. Xiao and C. Bathias**, "Fatigue Damage and Fracture Mechanism of Notched Woven Laminates," Journal of composite Materials, Vol. 28, No. 12, (1994), pp. 1127-1139.

23. **S. Kellas, J. Morton and P. T. Curtis**, "A Characteristic Fatigue Parameter for Notched Composites," International Journal of Fatigue, 13, No. 1, (1991), pp. 35-43.

24. **A. Poursartip and N. Chinatambi**, "Fatigue Damage Development in Notched $[0_2/\pm45]_s$ Laminates," Composite Materials: Fatigue and Fracture, Second Volume, ASTM STP 1012, P. A. Lagace, Ed., (1989), pp. 45-65.

25. **J. D. Whitcomb**, "Experimental and Analytical Study of Fatigue Damage in Notched Graphite/Epoxy Laminates," Fatigue of Fibrous Composite Materials, ASTM STP 723, (1981), pp. 46-63.

26. **G. Shen, G. Glinka and A. Plumtree**, "Fatigue Life Prediction of Notched Composite Components," Fatigue & Fracture of Engineering Materials & Structures, Vol. 17, No. 1, (1994), pp. 77-91.

27. **S. V. Kulkarni, P. V. McLaughlin, Jr., R. B. Pipes and B. W. Rosen**, "Fatigue of Notched Fiber Composite Laminates: Analytical and Experimental Evaluation," Composite Materials: Testing and Design (Fourth Conference), ASTM STP 617, (1977), pp. 70-92.

28. **P. V. McLaughlin, Jr., S. V. Kulkarni, S. N. Huang and B. W. Rosen**, "Fatigue of Notched Fiber Composite Laminates, Part I: Analytical Model," Technical Report, NASA CR-132747, National Aeronautics and Space Administration, Langley Research Center, Hampton, Va., March 1975.

29. **S. V. Kulkarni, P. V. McLaughlin, Jr. and R. B. Pipes**, "Fatigue of Notched Fiber Composite Laminates, Part I: Analytical and Experimental Evaluation," Technical Report, NASA CR-145039, National Aeronautics and Space Administration, Langley Research Center, Hampton, Va., 1976.

30. **R. L. Ramkumar, S. V. Kulkarni and R. B. Pipes**, "Evaluation and Expansion of an Analytical Model for Fatigue of Notched Composite Laminates," Technical Report, NASA CR-132747, National Aeronautics and Space Administration, Langley Research Center, Hampton, Va., March 1978.

31. **E. A. Humphreys and B. W. Rosen**, "Development of a Realistic Stress Analysis for Fatigue Analysis of Notched Composite Laminates," Technical Report, NASA CR-159119, National Aeronautics and Space Administration, Langley Research Center, Hampton, Va., May 1979.

32. **K. L. Reifsnider and W. W. Stinchcomb**, "A Critical-Element Model of The Residual Strength and Life of Fatigue-Loaded Composite Coupons," Composite Materials: Fatigue and Fracture, ASTM STP 907, H. T. Hahn, Ed., (1986), pp. 298-313.

33. **K. L. Reifsnider**, "The Critical Element Model: A Modeling Philosophy," Engineering Fracture Mechanics, Vol. 25, Nos. 5/6, (1986), pp. 739-749.

34. **K. L. Reifsnider**, "Damage and Damage Mechanics," Fatigue of Composite Materials, Ed. by K. L. Reifsnider, (1990), pp. 11-77.

35. **S. M. Sprearing, P. W. R. Beaumont and M. T. Kortschot**, "The Fatigue Damage Mechanics of Notched Carbon Fibre/PEEK Laminates," Composites, Vol. 23, No. 5, (September 1992), pp. 305-311.

36. **S. M. Spearing and P. W. R. Beaumont**, "Fatigue Damage Mechanics of Composite Materials. I: Experimental Measurement of Damage and Post-Fatigue Properties," Composites Science and Technology, No. 44, (1992), pp. 159-168.

37. **S. M. Spearing and P. W. R. Beaumont**, "Fatigue Damage Mechanics of Composite Materials. I: A Damage Growth Model," Composites Science and Technology, No. 44, (1992), pp. 169-177.

38. **S. M. Spearing and P. W. R. Beaumont**, "Fatigue Damage Mechanics of Composite Materials. III: Prediction of Post Fatigue Strength," Composites Science and Technology, No. 44, (1992), pp. 299-307.

39. **S. M. Spearing and P. W. R. Beaumont**, "Fatigue Damage Mechanics of Composite Materials. IV: Prediction of Post Fatigue Stiffness," Composites Science and Technology, No. 44, (1992), pp. 309-317.

40. **J. C. Halpin, K. L. Jerina and T. A. Johnson**, "Characterization of Composites for the Purpose of Reliability Evaluation," Analysis of the Test Methods for High Modulus Fibers and Composites, ASTM STP 521, (1973), pp. 5-64.

41. **M. M. Shokrieh**, *Failure of Laminated Composites Pinned Connections*, Masters Thesis, Department of Mechanical Engineering, McGill University, Montreal, Canada, 1991.

42. **L. B. Lessard and M. M. Shokrieh**, "Pinned Joint Failure Mechanisms, Part I - Two Dimensional Modeling," CANCOM 91, First Canadian International Composites Conference and Exhibition, Montréal, Québec, Canada, (September 4-6, 1991), pp. 1D51-1D58.

43. **F. K. Chang and K. Y. Chang**, "Post-Failure Analysis of Bolted Composite Joints in Tension or Shear-Out Mode Failure," Journal of Composite Materials, (1987), pp. 809-833.

44. **J. N. Webb and W. A. Smith**, "The Fatigue and Residual Tensile Strength of a Multi-Bolt Joint Between Metal and Carbon Fiber Composite," Symposium: Joining in Fiber Reinforced Plastics, (4-5 September, 1978), pp. 116-126.

45. **J. H. Crews, Jr.**, "Bolt-Bearing Fatigue of a Graphite/Epoxy Laminate," Joining of Composite Materials, ASTM STP 749, K. T. Kedwards, Ed., (1981), pp. 131-144.

46. **R. L. Ramkumar**, "Bolted Joint Design," Test Methods and Design Allowables for Fibrous Composites, C. C. Chamis, Ed., ASTM STP 734, (1981), pp. 376-395.

47. **D. Schutz, J. J. Gerharz and E. Alschwieg**, "Fatigue Properties of Unnotched, Notched and Jointed Specimens of a Graphite/Epoxy Composite," Fatigue of Fibrous Composite Materials, ASTM STP 723, (1981), pp. 31-47.

48. **R. L. Ramkumar and W. Tossavainen**, "Strength and Lifetime of Bolted Laminate," Fatigue in Mechanically Fastened Composite and Metallic Joints, ASTM STP 927, (1986), pp. 251-273.

49. **P. K. Mallick, R. E. Little and J. W. Dunham**, "Fatigue of Bolted Continuous Fiber Sheet Molding Compound Composite-Metal Joints," Fatigue in Mechanically Fastened Composite and Metallic Joints, ASTM STP 927, (1986), pp. 274-288.

50. **P. A. Smith and K. J. Pascoe**, "Fatigue of Bolted Joints in [0/90] CFRP Laminates," Composites Science and Technology, Vol. 29, (1987), pp. 45-69.

51. **R. E. Little and P. K. Mallick**, "Fatigue of Bolted Joints in SMC-R18 Sheet Molding Compound Composites," Journal of Composite Technology & Research, JCTRER, Vol. 12, No. 3, (1990), pp. 155-163.

52. **P. D. Herrington and M. Sabbaghian**, "Fatigue Failure of Composite Bolted Joints," Journal of Composite Materials, Vol. 27, No. 5, (1993), pp. 491-512.

53. **D. Liu, W. G. Gau, K. D. Zhang and B. Z. Ying**, "Empirical Damage Evaluation of Graphite/Epoxy Laminate Bolt Joint in Fatigue," Theoretical and Applied Fracture Mechanics, 19, (1993), pp. 145-150.

54. **D. S. Saunders, S. C. Galea and G. K. Deirmendjian**, "The Development of Fatigue Damage Around Fastener Holes in Thick Graphite/Epoxy Composite Laminates," Composites, Vol. 24, No. 4, (1993), pp. 309-321.

55. **E. Jarosch and A. Stepan**, "Fatigue Properties and Test Procedure of Glass Reinforced Plastic Rotor Blades," Journal of the American Helicopter Society, (Jan. 1970), pp. 33-41.

56. **A. K. Green and P. L. Pratt**, "The Axial Fatigue Behavior of Unidirectional Type IIIS Carbon Fiber-Epoxy Resin Composites," Composites, (1974), pp. 63-66.

57. **C. K. H. Dharan**, "Fatigue Failure Mechanisms in a Unidirectionally Reinforced Composite Material," Fatigue of Composite Materials, ASTM STP 569, (1975), pp. 171-188.

58. **B. D. Agarwal and J. W. Dally**, "Prediction of Low-Cycle Fatigue Behaviour of GFRP: an Experimental Approach," Journal of Materials Science, Vol. 10, (1975), pp. 193-199.

59. **C. K. H. Dharan**, "Fatigue Failure in Fiber-Reinforced Materials," ICCM, Proceedings of the International Conference on Composite Materials, Vol. 1, (1975), pp. 830-839.

60. **H. C. Kim and L. J. Ebert**, "Axial Fatigue Failure Sequence and Mechanisms in Unidirectional Fiberglass Composites," Journal of Composite Materials, Vol. 12, (1978), pp. 139-152.

61. **L. Lorenzo and H. T. Hahn**, "Fatigue Failure Mechanisms in Unidirectional Composites," Composite Materials : Fatigue and Fracture, ASTM STP 907, H. T. Hahn, Ed., (1986), pp. 210-232.

62. **G. C. Grimes**, "Experimental Study of Compression-Compression Fatigue of Graphite/Epoxy Composites," Test Methods and Design Allowables for Fibrous Composites, ASTM STP 734, C. C. Chamis, Ed., (1981), pp. 281-337.

63. **K. Schulte**, "Compressive Static and Fatigue Loading of Continuous Fiber-reinforced Composites," Compression response of Composite Materials, ASTM STP 1185, S. E. Groves and L. A. Highsmith, Eds., (1994), pp. 278-305.

64. **T. A. Collings**, "Transverse Compressive Behavior of Unidirectional Carbon Fiber Reinforced Plastics," Composites, (1974), pp. 108-116.

65. **A. G. Bader and M. Johnson**, "Fatigue Strength and Failure Mechanisms in Uniaxial Carbon Fiber Reinforced Epoxy Resin Composite Systems," Composites, (1974), pp. 58-62.

66. **D. C. Phillips and J. M. Scott**, "The Shear Fatigue of Unidirectional Fibre Composite," Composites, (Oct. 1977), pp. 233-236.

67. **E. M. Smith and K. J. Pascoe**, "The Role of Shear Deformation in the Fatigue Failure of a Glass Fiber-Reinforced Composite," Composites, (Oct. 1977), pp. 237-243.

68. **D. C. Philips and J. M. Scott**, "Shear Fatigue of CFRP Under Low Frequency Torsion," Fiber Science and Technology, No. 11, (1978), pp. 23-54.

69. **J. B. Sturgeon, Creep**, "Repeated Loading, fatigue and Crack Growth in ±45 Oriented Carbon Fiber Reinforced Plastics," Journal of Materials Science, No. 13, (1978), pp. 1490-1498.

70. **B. D. Agarwal and S. K. Joneja**, "Flexural Fatigue Properties of Unidirectional GRP in the Transverse Direction," Composites, (Oct. 1979), pp. 28-30.

71. **D. Purls**, "Some Fundamental Aspects of Composite Fractography," Composites, (Oct. 1981), pp. 241-247.

72. **J. P. Farve and G. Vidal**, "In-Plane and Interlaminar Shear Fatigue Characterization of Unidirectional GFRP and CFRP, Including Moisture Effects," TEQC83, Proceedings of the International Conference on Testing, Evaluation and Quality Control of Composites, Surrey University, Guildford, England, (Sept. 1983), pp. 57-65.

73. **R. B. Freeman**, "Shear Fatigue Evaluation of SMC," Modern Plastics, (1987), pp. 96, 98 and 100.

74. **R. J. Butler, P. M. Barnard and P. T. Curtis**, "The Development of a Satisfactory, Simple, Shear Fatigue Test for Unidirectional E-Glass Epoxy," Composite Materials: Testing and Design (Eighth Conference), ASTM STP 972, J. D. Whitcomb, Ed., (1988), pp. 227-240.

75. **G. Yaniv, I. M. Daniel and J. W. Lee**, "Method for Monitoring In-Plane Shear Modulus in Fatigue Testing of Composites," Test Methods for Design Allowables for Fibrous Composites: 2nd Volume, ASTM STP 1003, ASTM STP 1003, C. C. Chamis, Ed., (1989), pp. 276-284.

76. **J. Aronhime, H. Harel, A. Gilbert and G. Marom**, "The Rate Dependence of Flexural Shear Fatigue and Uniaxial Compression of Carbon- and Aramid-Fibre Composites and Hybrids," Composites Science and Technology, 43, (1992), pp. 105-116.

77. **H. T. Hahn and S. W. Tsai**, "Nonlinear Elastic Behavior of Unidirectional Composite Laminae," Journal of Composite Materials, Vol. 7, (1973), pp. 102-118.

78. **N. J. Pagano and S. R. Soni**, "Models for Studying Free-Edge Effects," Interlaminar Response of Composite Materials, Ed. by N. J. Pagano, (1989), pp. 1-68.

79. **R. B. Pipes and N. J. Pagano**, "Interlaminar Stresses in Composite Laminates Under Uniform Axial Extension," Journal of Composite Materials, Vol. 4, (1970), pp. 538-548.

80. **E. Altus, A. Rotem and M. Shmueli**, "Free Edge Effect in Angle Ply Laminates - A new Three Dimensional Finite Difference Solution," Journal of Composite Materials, Vol. 14, (1980), pp. 21-30.

81. **E. F. Rybicki**, "Interlaminar Shear in Laminated Composites Under Generalized Plane Stress," Journal of Composite Materials, Vol. 5, (1971), pp. 354-360.

82. **G. Isakson and A. Levy**, "Finite-Element Analysis of Interlaminar Shear in Fibrous Composites," Journal of Composite Materials, Vol. 5, (1971), pp. 273-276.

83. **T. H. H. Pian and S. T. Mau**, "Some Recent Studies in Assumed Stress Hybrid Models," Advances in Computational Methods in Structural Mechanics and Design, J. T. Oden, R. W. Clough and Y. Yamamoto, Eds., (1972), pp. 87-105.

84. **A. S. D. Wang and F. W. Crossman**, "Some New Results on Edge Effect in Symmetric Composite Laminates," Journal of Composite Materials, Vol. 11, (1977), pp. 92-106.

85. **R. L. Spilker**, "Edge Effects in Symmetric Composite Laminates: Importance of Satisfying Traction-Free-Edge Condition," Journal of Composite Materials, Vol. 14, (1980), pp. 2-20.

86. **R. L. Spilker**, "A Traction-Free-Edge Hybrid-Stress Element for the Analysis of Edge Effects in Cross-Ply Laminates," Computers and Structures, Vol. 12, (1980), pp. 167-179.

87. **C. C. Chang, R. S. Sandhu, R. L. Sierakowski and W. E. Wolfe**, "Continuous Strain Finite-Element Analysis of Free-Edge Effect in Laminated Composite Specimens," Journal of Composites Technology & Research, Vol. 10, No. 2, (1988), pp. 54-64.

88. **R. L. Sierakowski and I. K. Ebicoglu**, "On Interlaminar Shear Stresses in Composites," Journal of Composite Materials, Vol. 4, (1970), pp. 144-149.

89. **N. J. Pagano**, "Exact Solutions for Rectangular Bidirectional Composites and Sandwich Plates," Journal of Composite Materials, Vol. 4, (1970), pp. 20-35.

90. **E. P. Chen and G. G. Sih**, "Interfacial Delamination of a Layered Composite Under Anti-Plane Strain," Journal of Composite Materials, Vol. 5, (1971), pp. 12-23.

91. **V. L. Hein and F. Erdogan**, "Stress Singularities in a Two-Material Wedge," International Journal of Fracture Mechanics, Vol. 7, No. 3, (Sept. 1971), pp. 317-330.

92. **N. J. Pagano**, "On the Calculation of Interlaminar Normal Stress in Composite Laminate," Journal of Composite Materials, Vol. 8, (1974), pp. 65-81.

93. **R. B. Pipes and N. J. Pagano**, "Interlaminar Stresses in Composite Laminates - An Approximate Elasticity Solution," Journal of Applied Mechanics, Vol. 41, (1974), pp. 668-672.

94. **S. Tang**, "Interlaminar Stresses of Uniformly Loaded Rectangular Composite Plates," Journal of Composite Materials, Vol. 10, (1976), pp. 69-78.

95. **B. T. Rodini, Jr. and J. R. Eisenmann**, "An Analytical and Experimental Investigation of Edge Delamination in Composite Laminates," Fibrous Composite in Structural Design, E. M. Lenone, D. W. Oplinger and, J. J. Burke, Eds., Plenum Press, New York & London, Proceedings of the Fourth Conference on Fibrous Composites in Structural Design, San Diego, Calif., (Nov. 1978), pp. 441-457.

96. **N. J. Pagano**, "Stress Fields in Composite Laminates," International Journal of Solids and Structures, Vol. 14, (1978), pp. 385-400.

97. **A. S. D. Wang and F. W. Crossman**, "Calculation of Edge Stresses in Multi-Layer Laminates by Sub-Structuring," Journal of Composite Materials, Vol. 12, (1978), pp. 76-83.

98. **S. S. Wang and I. Choi**, "The Interface Crack Between Dissimilar Anisotropic Composite Materials," Journal of Applied Mechanics, Vol. 50, (1983), pp. 169-178.

99. **S. S. Wang and I. Choi**, "The Interface Crack Between Dissimilar Anisotropic Composites under Mixed-Mode Loading," Journal of Applied Mechanics, Vol. 50, (1983), pp. 179-183.

100. **W. Becker**, "Closed-Form Solution for the Free-Edge Effect in Cross-Ply Laminates," Composite Structures, 26, (1993), pp. 39-45.

101. **S. Tan and A. Levy**, "A Boundary Layer Theory - Part II: Extension of Laminated Finite Strip," Journal of Composite Materials, Vol. 9, (1975), pp. 42-52.

102. **P. W. Hsu and C. T. Herakovich**, "Edge Effects in Angle-Ply Composite Laminates," Journal of Composite Materials, Vol. 11, (1977), pp. 422-428.

103. **P. W. Hsu and C. T. Herakovich**, "A Perturbation Solution for Interlaminar Stresses in Bidirectional Laminates," Composite Materials: Testing and Design (Fourth Conference), ASTM STP 617, (1977), pp. 296-316.

104. **J. T. S. Wang and J. N. Dickson**, "Interlaminar Stresses in Symmetric Composite Laminates," Journal of Composite Materials, Vol. 12, (1978), pp. 390-401.

105. **R. B. Pipes and I. M. Daniel**, "Moiré Analysis of the Interlaminar Shear Edge Effect in Laminated Composites," Journal of Composite Materials, Vol. 5, (1971), pp. 255-259.

106. **R. Y. Kim**, "Experimental Observations of Free-Edge Delamination," Interlaminar Response of Composite Materials, Ed. by N. J. Pagano, 1989, pp. 111-160.

107. **N. J. Pagano and R. B. Pipes**, "Some Observation on the Laminar Strength of Composite Laminates," International Journal of Mechanical Science, Vol. 15, (1973), pp. 679-688.

108. **C. Kassapoglou and P. A. Lagace**, "An Efficient Method for the Calculation of Interlaminar Stresses in Composite Materials," Journal of Applied Mechanics, Vol. 53, (Dec. 1986), pp. 744-750.

109. **C. A. Rose and C. T. Herakovich**, "An Approximate Analytical Solution for Interlaminar Stresses in Angle-Ply Laminates," ICCM/VIII, International Conference on Composite Materials, Honolulu, Hawaii, (1991), pp. 28-W-1--13.

110. **I. S. Raju, J. D. Whitcomb and J. G. Goree**, "A New Look at Numerical Analysis of Free-Edge Stresses in Composite Laminates," NASA Technical Paper 1751, National Aeronautics and Space Administration, 1981.

111. **R. I. Zwiers, T. C. T. Ting and R. L. Spilker**, "On the Logarithmic Singularity of Free-Edge Stress in Laminated Composites under Uniform Extension," Journal of Applied Mechanics, Vol. 49, (1982), pp. 561-569.

112. **S. S. Wang and I. Choi**, "Boundary Layer Effects in Composite Laminates: Part 1- Free Edge Stress Singularities," Journal of Applied Mechanics, Vol. 49, (1982), pp. 541-548.

113. **S. S. Wang and I. Choi**, "Boundary Layer Effects in Composite Laminates: Part 2- Free Edge Stress Solutions and Basic Characteristics," Journal of Applied Mechanics, Vol. 49, (1982), pp. 549-560.

114. **D. J. Wilkins, J. R. Eisenmann, R. A. Camin, W. S. Margolis and R. A. Benson**, "Characterizing Delamination Growth in Graphite-Epoxy," Damage in Composite Materials, ASTM STP 775, K. L. Reifsnider, Ed., (1982), pp. 168-183.

115. **E. D. Rybicki and D. W. Schmueser**, "Effect of Stacking Sequence and Lay-Up Angle on Free Edge Stresses Around a Hole in a Laminated Plate Under Tension," Journal of Composite Materials, Vol. 12, (1978), pp. 300-313.

116. **Y. Yamaha and H. Okumura**, "Analysis of Local Stress in Composite Materials by 3D Finite Element," Composite Materials, K. Kawata and T. Akasaka, Ed., Proc. Japan-U.S. Conference, Tokyo, (1981), pp. 55-64.

117. **L. Carlsson**, "Interlaminar Stresses at a Hole in a Composite Member Subjected to In-Plane Loading," Journal of Composite Materials, Vol. 17, (1983), pp. 238-249.

118. **M. W. Lucking, S. V. Hoa and T. S. Sankar**, "The Effect of Geometry on Interlaminar Stresses of $[0/90]_s$ Composite Laminates with Circular Holes," Journal of Composite Materials, Vol. 17, (1984), pp. 188-198.

119. **K. Ericson, M. Persson, L. Carlsson and A. Gustavsson**, "On the Prediction of the Initiation of Delamination in a $[0/90]_s$ Laminate with a Circular Hole," Journal of Composite Materials, Vol. 18, (1984), pp. 495-506.

120. **W. H. Chen and T. F. Huang**, "Three Dimensional Interlaminar Stress Analysis at Free Edges of Composite Laminates," Computers and Structures, Vol. 32, No. 6, (1989), pp. 1275-1286

121. **J. Y. Kim and C. S. Hong**," Three-Dimensional Finite Element Analysis of Interlaminar Stresses in Thick Composite Laminates," Computers and Structures, Vol. 41, No. 4, (1991), pp. 1395-1404.

122. **K. D. Zhang and C. E. S. Ueng**, "A Simplified Approach for Interlaminar Stresses Around a Hole in $[0/90]_s$ Laminates," Journal of Composite Materials, Vol. 22, (1988), pp. 192-202.

123. **F. L. Matthews, C. M. Wang and S. Chryssafitis**, "Stress Distribution Around a Single Bolt in Fiber-Reinforced Plastic," Composites, (1982), pp. 316-322.

124. **U. O. Sperling**, "Three -Dimensional Stress Distribution Around Pin Loaded Holes in Composite Laminates," AIAA / ASME / ASCE / AHS 26th Structures, Structural Dynamics and Materials Conference, 85-0826, (1985), pp. 743-750.

125. **I. H. Marshall, W. S. Arnold and J. Wood**, "Observation on Bolted Connections in Composite Structures," Composite Structures, 13, (1989), pp. 133-151.

126. **R. Barboni, P. Gaudenzi and S. Carlini**, "A Three-Dimensional Analysis of Edge Effects in Composite Laminates with Circular Holes," Composite Structures, 15, (1990). pp. 115-136.

127. **L. B. Lessard, A. S. Schmidt and M. M. Shokrieh**, "Three Dimensional Stress Analysis of Free-Edge Effects in a Simple Composite Cross-Ply Laminate," International Journal of Solids and Structures, (1995), Submitted and Accepted.

128. **L. B. Lessard, M. M. Shokrieh and A. S. Schmidt**, "Three Dimensional Stress Analysis of Composite Plates with or without Stress Concentrations," International Conference on Composite Materials, ICCM 9, (12-16 July, 1993), Madrid, Spain, pp. 243-250.

129. **L. B. Lessard, M. M. Shokrieh and J. H. Esbensen**, "Analysis of Stress Singularities in Laminated Composite Pinned/Bolted Joints," 38th International SAMPE Symposium, Anaheim, California, (1993), pp. 53-60.

130. **M. M. Shokrieh and L. B. Lessard**, "Effects of Material Nonlinearity on the Three-Dimensional Stress State of Pin-Loaded Composite Laminates," Journal of Composite Materials, (1995), Submitted and Accepted.

131. **S. W. Tsai**, *Composite Design*, 4th Edition, Think Composites, Dayton, 1988.

132. **J. M. Whitney**, *Structural Analysis of Laminated Anisotropic Plates*, Technomic Publishing Company, Lancaster, Pennsylvania, 1987.

133. **P. H. Petit and M. E. Waddoups**, "A Method of Predicting the Nonlinear Behavior of Laminated Composites," Journal of Composite Materials, Vol. 3, (1969), pp. 2-19.

134. **Z. Hashin, D. Bagchi and W. Rosen**, "Non-linear Behavior of Fiber Composite Laminates," NASA Contractor Report 2313, National Aeronautics and Space Administration, 1974.

135. **R. S. Sandhu**, "Nonlinear Behavior of Unidirectional and Angle Ply Laminates," Journal of Aircraft, Vol. 13, No. 2, (Feb. 1976), pp. 104-111.

136. **G. P. Sendeckyj, M. D. Richardson and J. E. Pappas**, "Fracture Behavior of Thornel 300/5208 Graphite-Epoxy Laminates - Part 1: Unnotched Laminates," Composite Reliability, ASTM STP 580, (1975), pp. 528-546.

137. **R. L. Foye**, "Theoretical Post-Yielding Behavior of Composite Laminates, Part I- Inelastic Micromechanics," Journal of Composite Materials, Vol. 7, (1973), pp. 178-193.

138. **D. F. Adams**, "Inelastic Analysis of a Unidirectional Composite Subjected to Transverse Normal Loading," Journal of Composite Materials, Vol. 4, (1970), pp. 310-328.

139. **R. M. Jones and D. A. R. Nelson Jr.**, "A New Material Model for the Nonlinear Biaxial Behavior of ATJ-S Graphite," Journal of Composite Materials, Vol. 9, (1975), pp. 10-27.

140. **R. M. Jones and D. A. R. Nelson Jr.**, "Further Characteristics of a Nonlinear Material Model for STJ-S Graphite," Journal of Composite Materials, Vol. 9, (1975), pp. 251-265.

141. **R. M. Jones and D. A. R. Nelson Jr.**, "Material Models for Nonlinear Deformation of Graphite," AIAA, Journal, Vol. 14, No. 10, (June 1976), pp. 709-717.

142. **R. M. Jones and D. A. R. Nelson Jr.**, "Theoretical-Experimental Correlation of Material Models for Nonlinear Deformation of Graphite," AIAA, Journal, Vol. 14, No. 10, (Oct. 1976), pp. 1427-1435.

143. **R. M. Jones and H. S. Morgan**, "Analysis of Nonlinear Stress-Strain Behavior of Fiber-Reinforced Composite Materials," AIAA Journal, Vol. 15, No. 12, (Dec. 1977), pp. 1669-1676.

144. **P. Bar-Yoseph and G. Siton**, "The Effect of Material Non-Linearity on the Interlaminar Stress Field in Composite Laminates," Computers and Structures, Vol. 21, No. 6, (1985), pp. 1105-1118.

145. **J. K. Chen and C. T. Sun**, "Nonlinear Analysis of Interlaminar Stress in Graphite/Epoxy Laminates with and without Delamination Cracks," Composite Structures, Vol. 8, (1987), pp. 271-285.

146. **C. M. L. Wu**, "Nonlinear Analysis of Edge Effects in Angle-Ply Laminates," Computers and Structures, Vol. 25, No. 5, (1987), pp. 787-798.

147. **C. M. L. Wu**, "Nonlinear Thermal and Mechanical Analysis of Edge Effects in Angle-Ply Laminates," Computers and Structures, Vol. 35, No. 6, (1990), pp. 705-717.

148. **H. Kardestuncer**, *Finite Element Handbook*, McGraw-Hill Book Company, New York, 1987.

149. **R. D. Cook, D. S. Malkus and M. E. Plesha**, *Concepts and Applications of Finite Element Analysis*, Third Edition, John Wiley & Sons, New York, 1989.

150. **A. K. Gupta and B. Mohraz**, "A Method of Computing Numerically Integrated Stiffness Matrices," International Journal for Numerical Methods in Engineering, Vol. 5, (1972), pp. 83-89.

151. **A. K. Gupta**, "Efficient Numerical Integration of Element Stiffness Matrices," Short Communications, International Journal for Numerical Methods in Engineering, Vol. 19, (1983), pp. 1410-1413.

152. **O. C. Zienkiewicz**, *The Finite Element Method*, Third Edition, McGraw-Hill Book Company, New York, 1977.

153. **C. S. Desai and J. F. Abel**, *Introduction to the Finite Element Method, A Numerical Method for Engineering Analysis*, Van Nostrand Reinhold Company, New York, 1972.

154. **T. DeJong**, "Stresses Around a Pin Loaded Hole in Elastically Orthotropic or Isotropic Plates," Journal of Composite Materials, Vol. 11, (1977), pp. 313-331.

155. **A. B. Chaudhary and K. J. Bathe**, "A Solution Method for Static and Dynamic Analysis of Three-Dimensional Contact Problems with Friction," Computers and Structures, Vol. 24, No. 6, (1986), pp. 855-873.

156. **K. J. Bathe**, *Finite Element Procedures in Engineering Analysis*, Prentice-Hall, New Jersey, 1982.

157. **R. H. MacNeal and R. L. Harder**, "A Proposed Set of Problems to Test Finite Element Accuracy," Finite Element in Analysis and Design, Vol. 1, (1985), pp. 3-20.

158. **W. J. Quinn and F. L. Matthews**, "The Effect of the Stacking Sequence on the Pin Bearing Strength of Glass Fiber Reinforced Plastic," Journal of Composite Materials, Vol. 11, (1977), pp. 139-145.

159. **R. M. Christensen**, "Tensor Transformations and Failure Criteria for the Analysis of Fiber Composite Materials," Journal of Composite Materials, Vol. 22, (1988), pp. 874-897.

160. **K. L. Gipple and D. Hoyans**, "Measurement of the Out-of-Plane Shear Response of Thick Section Composite Materials using V-Notched Beam Specimen," Journal of Composite Materials, Vol. 28, No. 6, (1994), pp. 543-572.

161. **R. Kao**, "A Comparison of Newton-Raphson Methods and Incremental Procedures for Geometrically Nonlinear Analysis," Computers and Structures, Vol. 4, (1974), pp. 1091-1097.

162. **M. N. Nahas**, "Survey of Failure and Post-Failure Theories of Laminated Fiber-Reinforced Composites," Journal of Composites Technology & Research, Vol. 8, No. 4, (1986), pp. 138-153.

163. **S. W. Tsai and E. M. Wu**, "A General Theory of Strength for Anisotropic Materials," Journal of Composite Materials, Vol. 5, (1971), pp. 58-80.

164. **Z. Hashin**, "Failure Criteria for Unidirectional Fiber Composites," Journal of Applied Mechanics, Vol. 47, (1980), pp. 329-334.

165. **J. P. Waszczak and T. A. Cruse**, "Failure Mode and Strength Prediction of Anisotropic Bolt Bearing Specimens," Journal of Composite Materials, Vol. 5, (1971), pp. 421-425.

166. **N. P. Humphris**, "Migration of the Point of Maximum Stress in a Laminated Composite Lug Structure - A Stepwise Approach," Symposium: Joining in Fibre Reinforced Plastics, Imperial College, London, (Sept. 1978), pp. 79-86.

167. **B. L. Agarwal**, "Static Strength Prediction of Bolted Joints in Composite Material," AIAA Journal, Vol. 18, No. 11, (Nov. 1980), pp. 1371-1375.

168. **F. K. Chang, R. A. Scott and G. S. Springer**, "Strength of Mechanically Fastened Composite Joints," Journal of Composite Materials, Vol. 16, (1982), pp. 470-494.

169. **F. K. Chang, R. A. Scott and G. S. Springer**, "Failure of Composite Laminates Containing Pin Loaded Holes - Method of Solution," Journal of Composite Materials, Vol. 18, (1984), pp. 255-278.

170. **F. K. Chang, R. A. Scott and G. S. Springer**, "Design of Composite Laminates Containing Pin Loaded Holes," Journal of Composite Materials, Vol. 18, (1984), pp. 279-289.

171. **F. K. Chang**, "The Effect of Pin Load Distribution on the Strength of Pin Loaded Holes in Laminated Composites," Journal of Composite Materials, Vol. 20, (1986), pp. 401-408.

172. **F. K. Chang, R. A. Scott and G. S. Springer**, "Failure Strength of Nonlinearly Elastic Composite Laminates Containing a Pin Loaded Hole," Journal of Composite Materials, Vol. 18, (1984), pp. 464-477.

173. **Y. Tsujimoto and D. Wilson**, "Elasto-Plastic Failure Analysis of Composite Bolted Joints," Journal of Composite Materials, Vol. 20, (1986), pp. 236-252.

174. **S. R. Soni**, "Failure Analysis of Composite Laminated With a Fastener Hole," Joining of Composite Materials, ASTM STP 749, K. T. Kedward, Ed., (1981), pp. 145-164.

175. **L. B. Lessard and M. M. Shokrieh**, "Two-Dimensional Modeling of Composite Pinned Joint Failure," Journal of Composite Materials, Vol. 29, No. 5, (1995), pp. 671-697.

176. **T. H. Tsiang and J. F. Mandell**, "Damage Development in Bolt Bearing of Composite Laminates," AIAA Journal, Vol. 23, No. 10, (1985), pp. 1570-1577.

177. **P. Conti**, "Influence of Geometric Parameters on the Stress Distribution Around a Pin-Loaded Hole in a Composite Laminate," Composite Science and Technology, Vol. 25, (1986) pp. 83-101.

178. **S. M. Serabian and D. W. Oplinger**, "An Experimental and Finite Element Investigation into the Mechanical Response of 0/90 Pin-Loaded Laminates," Journal of Composite Materials, Vol. 21, (1987) pp. 631-649.

179. **J. M. Whitney and R. J. Nuismer**, "Stress Fracture Criteria for Laminated Composites Containing Stress Concentrations," Journal of Composite Materials, Vol. 8, (1974), pp. 253-265.

180. **R. Y. Kim and S. R. Soni**, "Experimental and Analytical Studies on the Onset of Delamination in Laminated composites," Journal of Composite Materials, Vol. 18, (1984), pp. 70-80.

181. **M. H. R. Jen, Y. S. Kau and J. M. Hsu**, "Initiation and Propagation of Delamination in a Centrally Notched Composite Laminate," Journal of Composite Materials, Vol. 27, No. 3, (1993), pp. 272-302.

182. **S. R. Soni and R. Y. Kim**, "Delamination of Composite Laminates Stimulated by Interlaminar Shear," Composite Materials: Testing and Design (Seventh Conference), ASTM STP 893, J. M. Whitney, Ed., (1986), pp. 286-307.

183. **L. Ye**, "Role of Matrix Resin in Delamination Onset and Growth in Composite Laminates," Composite Science and Technology, Vol. 33, (1988), pp. 257-277.

184. **R. Y. Kim**, "Initiation of Free-Edge Delamination in Composite Laminates," Key Engineering Materials, Vol. 37, (1989), pp. 103-136.

185. **C. T. Sun and S. G. Zhou**, "Failure of Quasi-Isotropic Composite Laminates with Free Edges," Journal of Reinforced Plastics and Composites, Vol. 7, (1988), pp. 515-557.

186. **J. C. Brewer and P. A. Lagace**, "Quadratic Stress Criterion for Initiation of Delamination," Journal of Composite Materials, Vol. 22, (1988), pp. 1141-1155.

187. **J. W. Joo and C. T. Sun**, "A Failure Criterion for Laminates Governed by Free Edge Interlaminar Shear Stress," Journal of Composite Materials, Vol. 26, No. 10, (1992), pp. 1510-1522.

188. **E. C. Edge**, "Does Transverse and Shear Loading Effect the Compression Strength of Unidirectional CFC? A Reply to Dr. Hart Smith," Composites, Vol. 25, No. 2, (1994), pp. 159-161.

189. **L. B. Lessard**, *Compression Failure in Laminated Composites Containing an Open Hole*, Ph.D. Thesis, Stanford University, March 1989.

190. **Y. S. Garud**, "Multiaxial Fatigue: A Survey of the State of the Art," Journal of Testing and Evaluation, JTEVA, Vol. 9, No. 3, (May 1981), pp. 165-178.

191 **P. H. Francis, D. E. Walrath, D. F. Sims and D. N. Weed**, "Biaxial Fatigue Loading of Notched Composites," Journal of Composite Materials, Vol. 11, (1977), pp. 488-501.

192. **M. J. Owen and D. J. Rice**, "Biaxial Strength Behaviour of Glass Fabric Reinforced Polyester Resins," Composites, (Jan. 1981), pp. 13-25.

193. **E. Krempi, D. M. Elzey, B. Z. Hong, T. Ayar and R. G. Loewy**, "Uniaxial and Biaxial Fatigue Properties of Thin-Walled Composite Tubes," Journal of the American Helicopter Society, (July 1988), pp. 3-10.

194. **A. Makinde and K. W. Neale**, "A General Criterion for Low-Cycle Multiaxial Fatigue Failure," Journal of Engineering Materials and Technology, Vol. 111, (1989), pp. 263-269.

195. **Z. Fawaz and K. W. Neale**, "A Parametric Criterion for Biaxial Fatigue Failure of Fiber-Reinforced Composite Laminae," Transaction of CSME, Vol. 14, No. 4, (1990), pp. 93-99.

196. **M. S. Found**, "A Review of the Multiaxial Fatigue Testing of Fiber Reinforced Plastics," Multiaxial Fatigue, ASTM STP 853, K. J. Miller and M. W. Brown, Eds., (1985), pp. 381-395.

197. **A. S. Chen and F. L. Matthews**, "A Review of Multiaxial Biaxial Loading Tests for Composite Materials," Composites, Vol. 24, No. 5, (1993), pp. 395-406.

198. **D. F. Sims and V. H. Brogdon**, "Fatigue Behavior of Composites under Different Loading Modes," Fatigue of Filamentary Materials, ASTM STP 636, K. L. Reifsnider and K. N. Lauraitis, Eds., (1977), pp. 185-205.

199. **H. T. Hahn**, "Fatigue Behavior and Life Prediction of Composite Laminates," Composite Materials: Testing and Design (Fifth Conference), ASTM STP 674, S. W. Tsai, Ed., (1979), pp. 383-417.

200. **Z. Hashin**, "Fatigue Failure Criteria for Unidirectional Fiber Composites," Journal of Applied Mechanics, Vol. 48, (Dec. 1981), pp. 846-852.

201. **Z. Hashin**, "Fatigue Failure Criteria for Combined Cyclic Stress," International Journal of Fracture, Vol. 17, No. 2, (April 1981), pp. 101-109.

202. **A. Rotem and Z. Hashin**, "Fatigue Failure of Angle Ply Laminates," AIAA Journal, Vol. 14, No. 7, (July 1976), pp. 868-872.

203. **A. Rotem**, "Fatigue Failure Mechanism of Composite Laminates," IUTAM Symposium on Mechanics of Composite Materials, Mechanics of Composite Materials, Recent Advances, Z. Hashin and C. T. Herakovich, Eds., Blacksburg, Va., (1982), pp. 421-435.

204. **A. Rotem and H. G. Nelson**, "Fatigue Behavior of Graphite-Epoxy Laminates at Elevated Temperatures," Fatigue of Fibrous Composite Materials, ASTM STP 723, (1981), pp. 152-173.

205. **F. Ellyin and H. El-Kadi**, "A Fatigue Failure Criterion for Fiber Reinforced Composite Laminae," Composite Structures, No. 15, (1990), pp. 61-74.

206. **R. C. Tennyson, J. S. Hansen, G. R. Heppler, G. Mabson, G. Wharram and K. N. Street**, "Computation of Influence of Defects on Static and Fatigue Strength of Composites," AGARD-CP-355, (1983), pp. 14-1 - 14-17.

207. **R. C. Tennyson, M. Tratt, G. Mabson and G. Wharram**, "Development of General Failure Model for CF-18 Graphite/Epoxy Laminates," Proc. DND Composite Workshop, Victoria, B. C., (July 1983), pp. 13-1 - 13-35.

208. **C. M. L. Wu**, "Thermal and Mechanical Fatigue Analysis of Angle-Ply CFRP Laminates," Second International Composites Conference and Exhibition, Ottawa, Ontario, Canada, (1993), pp. 631-638.

209. **A. Rotem and H. G. Nelson**, "Fatigue Behavior of Graphite-Epoxy Laminates at Elevated Temperatures," Fatigue of Fibrous Composite Materials, ASTM STP 723, (1981), pp. 152-173.

210. **J. T. Ryder and F. W. Crossman**, "A Study of Stiffness, Residual Strength and Fatigue Life Relationships for Composite Laminates," NASA Contract Report CR-172211, 1983.

211. **P. C. Chou and R. Croman**, "Residual Strength in Fatigue Based on the Strength-Life Equal Rank Assumption," Journal of Composite Materials, Vol. 12, (1978), pp. 177-194.

212. **P. C. Chou and R. Croman**, "Degradation and Sudden-Death Models of Fatigue of Graphite/Epoxy Composites," Composite Materials: Testing and Design (Fifth Conference), ASTM STP 674, S. W. Tsai, Ed., (1979), pp. 431-454.

213. **J. C. Halpin, T. A. Johnson and M. E. Waddups**, "Kinetic Fracture Models and Structural Reliability," International Journal of Fracture Mechanics, Vol. 8, 1972, pp. 465-468.

214. **L. J. Broutman and S. Sahu**, "A New Theory to Predict Cumulative Fatigue Damage in Fiberglass Reinforced Plastics," Composite Materials, Testing and Design (Second Conference), ASTM STP 497, (1972), pp. 170-188.

215. **H. T. Hahn and R. Y. Kim**, "Proof Testing of Composite Materials," Journal of Composite Materials, Vol. 9, July 1975, pp. 297-312.

216. **J. M. Whitney**, "Fatigue Characterization of Composite Materials," Fatigue of Fibrous Composite Materials, ASTM STP 723, (1981), pp. 133-151.

217. **G. P. Sendeckyj**, "Fitting Models to Composite Materials Fatigue Data," Test Methods and Design Allowable for Fibrous Composites, ASTM STP 734, C. C. Chamis, Ed., (1981), pp. 245-260.

218. **K. Radhakrishnan**, "Fatigue and Reliability Evaluation of Unnotched Carbon Epoxy Laminates," Journal of Composite Materials, Vol. 18, (1984), pp. 21-31.

219. **J. N. Yang and M. D. Liu**, "Residual Strength Degradation Model and Theory of Periodic Proof Tests for Graphite/Epoxy Laminates," Journal of Composite Materials, Vol. 11, (1977), pp. 176-202.

220. **J. N. Yang**, "Reliability Prediction for Composites Under Periodic Proof Tests in Service," Composite Materials: Testing and Design (Fourth Conference), ASTM STP 617, (1977), pp. 272-295.

221. **J. N. Yang**, "Fatigue and Residual Strength Degradation for Graphite/Epoxy Composites Under Tension-Compression Cyclic Loading," Journal of Composite Materials, Vol. 12, (1978), pp. 19-39.

222. **J. N. Yang and D. L. Jones**, "Statistical Fatigue of Graphite/Epoxy Angle-Ply Laminates in Shear," Journal of Composite materials, Vol. 12, (1978), pp. 371-289.

223. **J. N. Yang and C. T. Sun**, "Proof Test and Fatigue of Unnotched Composite Laminates," Journal of Composite Materials, Vol. 14, (1980), pp. 168-176.

224. **J. N. Yang, R. K. Miller and C. T. Sun**, "Effect of High Load on Statistical Fatigue of Unnotched Graphite/Epoxy Laminates," Journal of Composite Materials, Vol. 14, (1980), pp. 82-94.

225. **J. N. Yang and D. L. Jones**, "Load Sequence Effects on the Fatigue of Unnotched Composite Materials," Fatigue of Fibrous Composite Materials, ASTM STP 723, (1981), pp. 213-232.

226. **J. N. Yang and S. Du**, "An Exploratory Study into Fatigue of Composites Under Spectrum Loading," Journal of Composite Materials, Vol. 17, (1983), pp. 511-526.

227. **I. M. Daniel and A. Charewicz**, "Fatigue Damage Mechanisms and Residual Properties of Graphite/Epoxy Laminates," Engineering Fracture Mechanics, Vol. 25, Nos. 5/6, (1986), pp. 793-808.

228. **A. Charewicz and I. M. Daniel**, "Damage Mechanisms and Accumulation in Graphite/Epoxy Laminates," Composite Materials: Fatigue and Fracture, ASTM STP 907, H. T. Hahn, Ed., (1986), pp. 274-297.

229. **A. Rotem**, "Fatigue and Residual Strength of Composite Materials," Engineering Fracture Mechanics, Vol. 25, Nos. 5/6, (1986), pp. 819-827.

230. **H. W. Whitworth**, "Modeling Stiffness Reduction of Graphite/Epoxy Composite Laminates," Journal of Composite Materials, Vol. 21, (1987), pp. 2-13.

231. **T. Adam, R. F. Dickson, G. Fernando, B. Harris and H. Reiter**, "The Fatigue Behaviour of Kevlar/Carbon Hybrid Composites," IMechE Conference Publications (Institute of Mechanical Engineers), Vol. 2, (1986), pp. 329-335.

232. **T. Adam, R. F. Dickson, C. J. Jones, H. Reiter and B. Harris**, "A Power Law Fatigue Damage Model for Fiber-Reinforced Plastic Laminates," Proceedings of the Institution of Mechanical Engineers, Part C: Mechanical Engineering Science, V. 200, n C3, (1986), pp. 155-166.

233. **J. T. Fong**, "What is Fatigue Damage?," Damage in Composite Materials, ASTM STP 775, K. L. Reifsnider, Ed., (1982), pp. 243-266.

234. **W. Hwang and K. S. Han**, "Fatigue of Composites - Fatigue Modulus Concept and Life Prediction," Journal of Composite Materials, Vol. 20, 1986, pp. 154-165.

235. **A. Poursartip, M. F. Ashby and P. W. R. Beaumont**, "The Fatigue Damage Mechanics of a Carbon Fiber Composite Laminate: I-Development of the Model," Composites Science and Technology, Vol. 25, 1986, pp. 193-218.

236. **H. W. Whitworth**, "Modeling Stiffness Reduction of Graphite/Epoxy Composite Laminates," Journal of Composite Materials, Vol. 21, 1987, pp. 362-372.

237. **W. Hwang and K. S. Han**, "Fatigue of Composite Materials-Damage Model and Life Prediction," Composite Materials: Fatigue and Fracture, Second Volume, ASTM STP 1012, P. A. Lagace, Ed., (1989), pp. 87-102.

238. **J. J. Nevadunsky, J. J. Lucas and M. J. Salkind**, "Early Fatigue Damage Detection in Composite Materials," Journal of Composite Materials, Vol. 9, (1975), pp. 394-408.

239. **A. Poursartip and P. W. R. Beaumont**, "A Damage Approach to the Fatigue of Composite Materials," IUTAM Symposium on Mechanics of Composite Materials, Mechanics of Composite Materials, Recent Advances, Z. Hashin and C. T. Herakovich, Eds., Blacksburg, Va., (1982), pp. 449-456.

240. **A. L. Highsmith and K. L. Reifsnider**, "Stiffness-Reduction Mechanisms in Composite Laminates," Damage in Composite Materials, ASTM STP 775, K. L. Reifsnider, Ed., (1982), pp. 103-117.

241. **A. L. Highsmith, W. W. Stinchcomb and K. L. Reifsnider**, "Effect of Fatigue-Induced Defects on the Residual Response of Composite Laminates," Effects of Defects in Composite Materials, ASTM STP 836, (1984), pp. 194-216.

242. **M. H. R. Jen, J. M. Hsu and D. G. Hwang**, "Fatigue Degradation in Centrally Notched Quasi-Isotropic Laminates," Journal of Composite Materials, (1990), pp. 823-837.

243. **L. J. Lee, J. N. Yang and D. Y. Sheu**, "Prediction of Fatigue Life for Matrix Dominated Composite Laminates," ICCM/VIII, International Conference on Composite Materials, Honolulu, Hawaii, (1991), pp. 38-L-1--38-L-9.

244. **J. N. Yang, L. J. Lee and D. Y. Sheu**, "Modulus Reduction and Fatigue Damage of Matrix Dominated Composite Laminates," Composite Structures, No. 21, (1992), pp. 91-100.

245. **D. L. Jones, S. H. Yang, J. H. Lee and H. A. Withworth**, "Development of a Stiffness Degradation Model for Graphite Epoxy Laminates under Fatigue Loading," Proceedings of International Conference on Composite Engineering ICCE/1, Ed. D. Hui, (1994), pp. 243-244.

246. **D. Schutz and J. J. Gerharz**, "Fatigue Strength of a Fiber Reinforced Material," Composites, (Oct. 1977), pp. 245-250.

247. **K. H. Boller**, "Fatigue Properties of Fibrous Glass-Reinforced Plastics Laminates Subjected to Various Conditions," Modern Plastics, (June 1957), pp. 163-293.

248. **T. Adam, G. Fernando, R. F. Dickson, H. Reiter and B. Harris**, "Fatigue Life Prediction for Hybrid Composites," Int. J. Fatigue, Vol. 11, No. 4, (1989), pp. 233-237.

249. **B. Harris, H. Reiter, R. Adam, R. F. Dickson and G. Fernando**, "Fatigue Behaviour of Carbon Fibre Reinforced Plastics," Composites, Vol. 21, No. 3, (May 1990), pp. 232-242.

250. **N. Gathercole, T. Adam, B. Harris and H. Reiter**, "An Unified Model for Fatigue Life Prediction of Carbon Fibre/Resin Composites," Developments in the Science and Technology of Composite Materials, ECCM 5th. European Conference on Composite Materials, Bordeaux, France, June 9-12, (1992), pp. 89-94.

251. **T. Adam, N. Gathercole, H. Reiter and B. Harris**, "Fatigue Life Prediction for Carbon Fibre Composites" Advanced Composites Letters, 1, (1992), pp. 23-26.

252. **N. Gathercole, H. Reiter, T. Adam and B. Harris**, "Life Prediction for Fatigue of T800/524 Carbon-Fibre Composites: I Constant-Amplitude Loading," International Journal of Fatigue, Vol. 16, (November 1994), pp. 523-532.

253. **S. C. Chou, O. Orringer and J. H. Rainey**, "Post-Failure Behavior of Laminates I - No Stress Concentration," Journal of Composite Materials, Vol. 10, (1976), pp. 371-381.

254. **S. C. Chou, O. Orringer and J. H. Rainey**, "Post-Failure Behavior of Laminates II - Stress Concentration," Journal of Composite Materials, Vol. 11, (1976), pp. 71-78.

255. **B. D. Agarwal and L. J. Broutman**, *Analysis and Performance of Fiber Composites*, Second Edition, John Wiley and Sons, Inc., 1990.

256. **J. M. Whitney**, "Reflections on the Development of Test Methods for Advanced Composites," Composite Materials: Testing and Design (Tenth Volume), ASTM STP 1120, G. C. Crimes, Ed., (1992), pp. 7-16.

257. **J. Awerbuch and H. T. Hahn**, "Fatigue and Proof-Testing of Unidirectional Graphite/Epoxy Composites," Fatigue of Filamentary Materials, ASTM STP 636, K. L. Reifsnider and K. N. Lauraitis, Eds., (1977), pp. 248-266.

258. **ASTM D 3039-76** (Reapproved 1989), *Standard Test Method for Tensile Properties of Fiber-Resin Composites*, ASTM Designation, pp. 118-122, (1989).

259. **ASTM D 3479-76** (Reapproved 1990), *Standard Test Methods for Tension-Tension Fatigue of Oriented Fiber-Resin Matrix Composites*, ASTM Designation, pp. 142-144, (1990).

260. **ASTM D 3410-87**, *Standard Test Method for Compressive Properties of Unidirectional or Crossply Fiber-Resin Composites*, ASTM Designation, pp. 132-141, (1987).

261. **ASTM D 4255-83**, *Standard Guide for Testing In-Plane Shear Properties of Composite Laminates, ASTM Designation*, pp. 195-204, (1983).

262. **ASTM D 2733-70**, *Standard Methods of Test for Interlaminar Shear Strength of Structural Reinforced Plastics at Elevated Temperatures*, ASTM Designation, pp. 773-776, (1970).

263. **ASTM D 3846-93**, *Standard Test Method for In-Plane Shear Strength of Reinforced Plastics*, ASTM Designation, pp. 435-437, (1993).

264. **ASTM D 695-89**, *Standard Test Method for Compressive Properties of Rigid Plastics*, ASTM Designation, pp. 197-201, (1989).

265. **D. C. Curtis, M. Davis, D. R. Moore and B. Slater**, "Fatigue Behavior of Continuous Carbon-Fiber-Reinforced Peek," Composite Materials: Fatigue and Fracture (Third Volume), ASTM STP 1110, T. K. O'Brien, Ed., (1991), pp. 581-595.

266. **D. H. Woolstencroft, A. R. Curtis and R. L. Haresceugh**, "A Comparison of Test Techniques Used for the Evaluation of the Unidirectional Compressive Strength of Carbon Fibre-Reinforced Plastic," Composites, Vol. 12, No. 4, (Oct., 1981), pp. 275-280.

267. *Composite Test Methods*, Delaware Composite Design Encyclopedia, Vol. 6, Technomic Publishing Co. Inc., Pennsylvania, (1990), pp. 29-37.

268. **D. F. Adams and E. M. Odom**, "Influence of Test Fixture Configuration on the Measured Compressive Strength of a Composite Material," Journal of Composites and Technology, Vol. 13, No. 1, (1992), pp. 36-40.

269. **D. Lefebvre, S. Archambault, T. Vu Khan and Y. Simarf**, "Compressive Strength of Unidirectional CFRP Composites," Second International Composites Conference and Exhibition, Ottawa, Ontario, Canada, (1993), pp. 659-666.

270. **J. F. Milette, M. M. Shokrieh and L. B. Lessard**, "Static and Fatigue Behaviour of Unidirectional Composites in Compression," ICCM-10 International Conference on Composite Materials, Whistler, B. C., Canada, (1995), pp. I-617 - I-624.

271. **J. F. Milette**, *Static and Fatigue Behaviour of Unidirectional Composites in Compression*, Masters Thesis, Department of Mechanical Engineering, McGill University, Montreal, Canada, 1995.

272. **G. C. Grimes**, "Structural Design Significance of Tension-Tension Fatigue Data on Composites," Composite Materials: Testing and Design (Fourth Conference), ASTM STP 617, (1977), pp. 106-119.

273. **J. G. Haberle and F. L. Matthews**, "An Improved Technique for Compression Testing of Unidirectional Fiber-Reinforced Plastics; Development and Results," Composite, Vol. 25, No. 5, (1994), pp. 358-371.

274. **P. T. Curtis, J. Gates and C. G. Molyneux**, "An Improved Engineering Test Method for Measurement of the Compressive Strength of Unidirectional Carbon Fibre Composites," Composites, Vol. 22, No. 5, (Sept. 1991), pp. 363-368.

275. **A. S. Crasto and R. Y. Kim**, "An Improved Test Specimen to Determine Composite Compression Strength," ICCM, Ninth International Conference on Composite Materials, Madrid, Spain, 12-16 July 1993, pp. 621-630.

276. **L. B. Lessard and M. M. Shokrieh**, *Fatigue Behaviour of Composite Pinned/Bolted Joints*, Final Report, NRC #32171 and IAR-CR-29, Structure and Material Laboratory, Institute for Aerospace Research, National research Council, Canada, 1995.

277. **B. Harris**, *Private Communication*, 1995.

278. **D. Purslow**, "The Shear Properties of Unidirectional Carbon Fibre Reinforced Plastics and Their Experimental Determination," Aeronautical Research Council, Current Papers 1381, 1977.

279. **L. B. Lessard, O. P. Eilers and M. M. Shokrieh**, "Testing of In-Plane Shear Properties under Fatigue Loading," Journal of Reinforced Plastics and Composites, Vol. 14, No. 9, (Sept. 1995), pp. 965-987.

280. **M. M. Shokrieh, O. P. Eilers and L. B. Lessard** "Characterization of a Graphite/Epoxy Composite under In-Plane Shear Fatigue Laoding," High Temperature and Environmental Effects on Polymeric Composites: Second Symposium, ASTM STP 1302, Submitted and Accepted, 1995.

281. **M. M. Shokrieh, O. P. Eilers, P. Kotsiopriftis and L. B. Lessard**, "Determination of Interlaminar Shear Strength of Graphite/Epoxy Composite Materials in Static and Fatigue Loading ," ICCM-10 International Conference on Composite Materials, Whistler, B. C., Canada, (1995), pp. IV-81 - IV-88.

282. **P. H. Francis, D. E. Walrath, D. F. Sims and D. N. Weed**, "Biaxial Fatigue Loading of Notched Composites," Journal of Composite Materials, (1977), pp. 488-501.

283. **K. L. Reifsnider, W. W. Stinchcomb and T. K. O'Brien**, "Frequency Effects on a Stiffness-Based Fatigue Failure Criterion in Flawed Composite Specimens," Fatigue of Filamentary Composite Materials, ASTM STP 636, K. L. Reifsnider and K. N. Lauraitis, Eds., (1977), pp. 171-184.

284. **G. R. Kress and W. W. Stinchcomb**, "Fatigue Response of Notched Graphite/Epoxy Laminates," Recent Advances in Composites in United States and Japan, ASTM STP 864, J. R. Vinson and M. Taya, Eds., (1985), pp. 173-196.

285. **P. A. Lagace and S. C. Nolet**, "Effect of Ply Thickness on Longitudinal Splitting and Delamination in Graphite/Epoxy Under Compressive Cyclic Load," Composite Materials, Fatigue and Fracture, ASTM STP 907, H. T. Hahn, Ed., (1986), pp. 335-360.

286. **C. E. Bakis, H. R. Yih, W. W. Stinchcomb and K. L. Reifsnider**, "Damage Initiation and Growth in Notched Laminates Under Reversed Cycling Loading," Composite Materials: Fatigue and Fracture, Second Volume, ASTM STP 1012, P. A. Lagace, Ed., (1989), pp. 66-83.

287. **C. Soutis, N. A. Fleck and P. A. Smith**, "Compression Fatigue Behaviour of Notched Carbon Fibre-Epoxy Laminates," International Journal of Fatigue, Vol. 13, No. 4, (1991), pp. 303-312.

288. **G. J. Schneider**, "Evaluation of Lamina Strength Criteria by Off-Axis Tensile Coupon Tests," Fibre Science and Technology, 5, (1972), pp. 29-35.

289. **E. M. Wu**, "Optimal Experimental Measurements of Anisotropic Failure Tensors," Journal of Composite Materials, Vol. 6, (1972), pp. 472-489.

290. **R. B. Pipes and B. W. Cole**, "On the Off-Axis Strength Test for Anisotropic Materials," Journal of Composite Materials, Vol. 7, (1973), pp. 246-256.

291. **M. J. Owen and M. S. Found**, "The Fatigue Behaviour of a Glass-Fabric-Reinforced Polyester Resin Under Off-Axis Loading," J. Phys. D: Appl. Phys., Vol. 8, (1975), pp. 480-4978.

292. **M. J. Owen and J. R. Griffiths**, "Evaluation of Biaxial Stress Failure Surfaces for a Glass Fabric Reinforced Polyester Resign Under Static and Fatigue Loading," Journal of Material Science, 13, (1978), pp. 1521-1537.

293. **P. S. Theocaris and T. P. Phillippidis**, "On the Validity of the Tensor Polynomial Failure Theory with Stress Interaction Terms Omitted," Composites Science and Technology, 40, (1991), pp. 181-191.

294. **S. C. Tan and S. Cheng**, "Failure Criteria for Fibrous Anisotropic Materials," Materials in Civil Engineering, Vol. 5, No. 2, (May 1993), pp. 198-211.

295. **B. W. Rosen**, "A Simple Procedure for Experimental Determination of the Longitudinal Shear Modulus of Unidirectional Composites," Journal of Composite Materials, Vol. 6, (1972), pp. 552-554.

296. **M. -J. Pindera and C. T. Herakovich**, "Shear Characterization of Unidirectional Composites with the Off-Axis Tension Test," Experimental Mechanics, (1986), pp. 103-112.

297. **C. M. Browne**, "Alternative Methods for the Determination of Shear Modulus in a Composite Material," Composite Materials: Testing Technology of Metal Matrix Composites, ASTM STP 964, ASTM, P. R. Digovanni and N. R. Adist, Eds., (1988), pp. 259-274.

298. **J. Awerbuch and H. T. Hahn**, " Off-axis Fatigue of Graphite/Epoxy Composite," Fatigue of Fibrous Composite Materials, ASTM STP 723, ASTM, (1981), pp. 243-273.

299. **N. J. Pagano and J. G. Halpin**, "Influence of End Constraint in the Testing of Anisotropic Bodies," Journal of Composite Materials, Vol. 2, (1968), pp. 18-31.

300. **E. Wu and R. L. Thomas**, "Off-Axis Test of a Composite," Journal of Composite Materials, Vol. 2, (1968), pp. 523-526.

301. **C. C. Chamis and J. H. Sinclair**, "Ten-deg Off-axis Test for Shear Properties in Fiber Composites," Experimental Mechanics, (1977), pp. 339-346.

302. **B. W. Chang, P. H. Huang and D. G. Smith**, "A Pinned-End Fixture for Off-Axis Testing," Experimental Techniques, (June 1984), pp. 28-30.

303. **R. R. Rizzo**, "More on the Influence of End Constraints on Off-Axis Tensile Tests," Journal of Composite Materials, Vol. 3, (1969), pp. 202-219.

304. **R. B. Pipes and B. W. Cole**, "On the Off-Axis Strength Test for Anisotropic Materials," Journal of Composite Materials, Vol. 7, (1973), pp. 246-256.

305. **G. L. Richards, T. P. Airhart and J. E. Ashton**, "Off-Axis Tensile Coupon Testing," Journal of Composite Materials, Vol. 3, (1969), pp. 586-589.

306. **C. T. Sun and S. P. Berreth**, "A New End Tab Design for Off-Axis Tension Test of Composite Materials," Journal of Composite Materials, Vol. 22, (1988), pp. 766-779.

307. **C. T. Sun and I. Chungh**, "An Oblique End Tab Design For Testing Off-Axis Composite Specimens," Composite Materials Structures, ASME, Aerospace Division (Publication) A. D., ASME, NY, NSA, Vol. 19, (1991), pp. 7-11.

308. **S. W. Tsai,** *Introduction to Composite Materials*, Technomic Publication Company, Westport, Connecticut, 1980.

309. **M. M. Shokrieh and L. B. Lessard,** "Multiaxial Fatigue Behaviour of Unidirectional Plies Based on Uniaxial Fatigue Experiments: I. Modeling," Submitted to International Journal of Fatigue, 1995.

310. **M. M. Shokrieh and L. B. Lessard,** "Multiaxial Fatigue Behaviour of Unidirectional Plies Based on Uniaxial Fatigue Experiments: I. Experimental Evaluation," Submitted to International Journal of Fatigue, 1995.

311. **M. A. Miner and S. M. Calif,** "Cumulative Damage in Fatigue," Journal of Applied Mechanics, (Sept. 1945), pp. A-159 - A-164.

312. **Z. Hashin and A. Rotem,** "A Cumulative Damage Theory of Fatigue Failure," Materials Science and Engineering, Vol. 34, (1978), pp. 147-160.

313. **Z. Hashin,** "A Reinterpration of the Palmgren-Miner Rule for Fatigue Life Prediction," Journal of Applied Mechanics, Vol. 47, (June 1980), pp. 324-328.

314. **Z. Hashin,** "A Reinterpration of the Palmgren-Miner Rule for Fatigue Life Prediction," Journal of Applied Mechanics, Disscussion, Vol. 48, June (1981), pp. 446-448.

315. **K. Golos and F. Ellyin,** "Generalization of Cumulative Damage Criterion to Multilevel Cyclic Loading," Theoretical and Applied Fracture Mechanics, 7, (1987), pp. 169-176.

316. **A. Buch,** *Fatigue Strength Calculation*, Materials Science Surveys No. 6, Trans Tech. Publications, Switzerland, 1988.